Understanding the mechanisms underlying force transmission during epithelial cell division

Diana Pinheiro

Université Pierre et Marie Curie

Universidade do Porto

Ecole Doctorale Complexité du Vivant

Institut Curie, Unité Génétique Biologie du Développement

Equipe de Polarité, Division et Morphogenèse

Understanding the mechanisms underlying force transmission during epithelial cell division

Diana Pinheiro

Thèse de doctorat de Biologie Cellulaire et Moléculaire

Dirigée par Yohanns Bellaïche

Présentée et soutenue publiquement le 19/09/2016

Devant un jury composé de:

Dr. Yohanns Bellaïche	Directeur de Thèse
Dr. Claudio E. Sunkel	Co-Directeur de Thèse
Dr. Carl-Philipp Heisenberg	Rapporteur
Dr. Magali Suzanne	Rapporteur
Dr. Raphaël Voituriez	Examinateur
Dr. René-Marc Mège	Examinateur
Dr. Michel Gho	Examinateur

Para ser grande, sê inteiro: nada
Teu exagera ou exclui.
Sê todo em cada coisa. Põe tudo o que és no
Mínimo que fazes.
Assim em cada lago a lua toda
Brilha, porque alta ela vive.

Fernando Pessoa em "Ode de Ricardo Reis", 1933

ACKNOWLEDGEMENTS:

The last fours years have been a thrilling and demanding journey and, despite the difficulties, my PhD genuinely exceeded all my expectations! Moving to France, discovering a new culture and language and learning how to do science on a new model system and field were a truly exhilarating challenge that helped me grow immensely both from a personal and scientific standpoint. Since I was incredibly lucky with the people I encountered, now I would like to acknowledge them for sharing with me this incredible rollercoaster ride!

I have to start by thanking Professor Claudio, who gave me the first opportunity to work in the lab and to drive, along with Bernardo and his support, my first project during my master's internship. Still within the University of Porto, I must thank my PhD program – GABBA for making everything possible for me! Thanks to the mentors and their absolute commitment to make students ask questions and propose ideas, GABBA greatly enriched me and prepared me for a PhD better than I could have ever anticipated! The imperative that students must work together on all tasks had the wonderful side-effect of introducing me to a new group of friends! In particular, I want to thank Mafalda, Joana, Arezes and Gonçalo for all the GOT screenings, the dinners and parties at the Kittie Castle, the 5-way skype calls across an astounding 4 time zones, the weekend visits, the summer trips and the *what's app*-ing conversations that eased me through my PhD blues! I can't wait to see what is coming next for us!

Next, I would like to thank Yohanns for his contagious passion for science, constant motivation and his mentoring! I learned immensely and, it has been truly inspiring to work with you! For all my exhaustion, stress and anxiety, I hope I didn't make it too hard! ☺ I would also like to thank the Bellaiche Team, their enthusiasm, their crazy and innovative ideas, their drive and constant support throughout my PhD was a truly unique source of motivation! Another big thank you to Floriane, Olga, Stéphane, Isabelle, Maria and Zhimin that directly contributed for this project with reagents, codes and ideas. In particular, I want to thank my super talented and incredibly smart co-second authors – Sophie and Edouard that not only greatly contributed to this project, but helped me gave life to it! Sophie, you taught everything about flies, epithelia and cell division and learning from you was not only easy and natural, but a truly humbling experience! You are an incredibly talented scientist, your passion for science is almost palpable and your kindness as a teacher is just endearing…so I don't think I can ever thank you enough for letting me take over this project! Edouard, with your creative ideas and almost infinite patience your crash course on theoretical modelling and cytoskeleton mechanics truly challenged me and broaden my horizons! You made me a better biologist and a better scientist, so I cannot ever thank you enough!

Finally, I want to thank Floris for your invaluable help and support with the revision experiments! You are not the magic elf from my imagination, but not far from it! ☺

I would also want to thank all the crazy fly room people, which made my adaptation to flies, Curie and Paris so easy!! Your crazy talks and laughter were the constant in the 4th floor! In particular, a big thanks to Sophie, Neuza, Anahi, Ana Maria, Kasia and Mahevinha for all the fly room fun, for your constant belief in me and endless care!! You are the best! ☺ I must extend another big thanks to the rest of the BDD family for there is a true aura here!! The Friday beers, the crazy parties and the long working hours really made this building feel like home! Thank you all, it was a true pleasure to have worked with you for the last four years!

I must now address my very very special thanks for the ones that are always there! Neuza, Sophie, Inês, Rafael, Simão and Sylvie, our little Portuguese-speaking community was the rock for these crazy four years! I am lost for words to thank you for all the memorable fun and serious moments we shared! Neuza, thank you for welcoming me in Paris and for always putting a smile in my face! Inês and Raquel, you may not have been in Paris from day one, but now I can't imagine Paris without you! Raquel, your gentle heart, kindness and constant encouragement through these incredible hard two years was my shelter! Thank you so much! Jorgito, although you only joined the house in these last months, your easy smile and delicious dishes were a great source of sanity to both mind and body! Clotilde, my French friend with a Portuguese rib thank you for the lunches and endless talks about science and life! Um obrigado à Gui, porque me recebeste nesta cidade estranha e me fizeste sempre sentir em casa! Um enorme obrigado Ana, porque és e serás sempre a minha marida! Apesar de estares longe, conheces-me melhor do que eu mesma e sabes sempre como me dar força! Obrigado por aturares os meus dramas com a paciência que só tu consegues! ☺ Finalmente...Edouard! Obrigado pelo teu carinho, pela tua alegria e entusiasmo contagiantes, pelo teu apoio (e paciência) constante e pela tua fé inabalável em mim! É um orgulho enorme fazer parte da tua vida!

Por ultimo, quero agradecer à minha família, em especial aos meus pais por todo o apoio, confiança e oportunidades que me proporcionaram! É pelo vosso carinho, segurança e inesgotável firmeza que eu ganho a força e independência necessárias para enfrentar os desafios a que me proponho! Vocês são a minha base e o meu âmago! Obrigado por tudo! Não poderia ter mais orgulho em ser vossa filha!

TABLE OF CONTENTS:

ABSTRACT:

Epithelial tissue cohesiveness is ensured through cell-cell junctions that maintain both adhesion and mechanical coupling between neighbouring cells. Both during development and adult life, epithelial tissues undergo intensive cell proliferation. Cell division, and particularly cytokinesis, is coupled to the formation of new adhesive contacts between the future daughter cells, thereby preserving tissue integrity and propagating cell adhesion and polarity. In both Vertebrate and Invertebrate epithelial tissues, upon contractile ring constriction, the dividing cell and the neighbouring cell membranes co-ingress, thus maintaining epithelia integrity[1–6]. The dramatic deformation imposed by the contractile ring leads to the remodelling of the junctions assembled between the dividing cell and its neighbours. Concomitantly, non-muscle myosin II (MyoII) accumulates at the base of the ingressing AJ in the neighbouring cells[1,2,5], where it provides the force required for membrane juxtaposition to occur in the dividing cell[1], thereby defining the length of the new cell-cell contact formed between the daughters[1,4,5]. These findings support that epithelial cells maintain cohesiveness while dividing and highlight a remarkable cooperation between the dividing cell and its neighbours that is required to both remodel their contacts and to assemble a new AJ between the daughter cells after division. Thus, for my thesis work, we aimed to understand the molecular mechanisms underlying the interplay between epithelial during cell division.

I found that, each epithelial cell division is associated with a mechanotransduction event controlling MyoII dynamics in the neighbours. The contractile ring pulling forces locally elongate the neighbouring cells membrane, thereby diluting E-Cadherin (E-Cad) levels at the ingressing junction. In turn, local reduction of E-Cad concentration along with the neighbouring cells contractility promotes self-organized actomyosin flows, which ultimately lead to MyoII accumulation in the neighbours. By establishing epithelial cell cytokinesis as an endogenous source of mechanical stress, this work uncovered a novel mechanotransduction mechanism that coordinates actomyosin dynamics between epithelial cells and is compatible with AJ remodelling. These findings extend the current understanding of mechanotransduction that was so far based on junction reinforcement, and was therefore intrinsically unable to sustain cell-cell contact remodelling[6,7]. Finally, these findings also emphasize a novel role for actomyosin flows in force sensing and transmission and provide a general framework to understand how mechanical forces can coordinate epithelial cell dynamics.

RESUME:

Au sein d'un tissu épithélial, la cohésion des cellules est assurée par des jonctions adhérentes intercellulaires sur lesquelles reposent l'adhésion, le couplage mécanique et la polarité des cellules. Lors du développement et de la vie adulte, les tissues épithéliaux croissent et se renouvellent par prolifération cellulaire. La division cellulaire, et en particulier sa cytocinèse, doit être couplée à la formation de nouvelles jonctions intercellulaires entre les futures cellules-filles, afin de préserver l'intégrité du tissu et maintenir son adhésion, ses propriétés mécaniques et sa polarité. Chez les vertébrés et les invertébrés, lors de la constriction de l'anneau contractile, les membranes de la cellule en division et de ses cellules voisines se déforment de concert maintenant l'intégrité épithéliale[1–6]. La déformation imposée par l'anneau contractile conduit à un remodelage des jonctions intercellulaires entre la cellule en division et ses voisines. Concomitamment, la myosine non-musculaire II (MyoII) s'accumule dans les cellules voisines, à la base de la jonction adhérente déformée lors de la division[1,2,5]. La MyoII y produit une force nécessaire pour juxtaposer les membranes de la cellule en division[1], définissant ainsi la longueur de la future jonction formée entre les cellules-filles[1,4,5]. Ces résultats illustrent que les cellules épithéliales maintiennent leur cohésion lors de la division et soulignent l'existence d'un dialogue fascinant entre la cellule en division et ses voisines, qui est nécessaire pour le remodelage de leur contacts et l'assemblage d'une nouvelle jonction entre les cellules-filles. Dans le cadre de mes travaux de doctorat, j'ai cherché à comprendre les mécanismes moléculaires sous-jacents à ce dialogue.

J'ai notamment montré que chaque division cellulaire est associée à un processus de mécano-transduction qui contrôle la dynamique de la MyoII dans les cellules voisines. Les forces produites par l'anneau contractile allongent localement la membrane des voisines diluant ainsi localement la concentration de E-Cadhérine (E-Cad). En retour, cette réduction locale de la concentration d'E-Cad, couplée à la contractilité intrinsèque des cellules voisines, génère des flux auto-organisés d'actine et myosine, qui conduisent à l'accumulation de MyoII dans les cellules voisines. En montrant que la cytocinèse épithéliale est une source endogène de contraintes mécaniques, mon travail définit un nouveau mécanisme de mécano-transduction qui coordonne les dynamiques d'actine et myosine dans les cellules en division et leurs voisines, et qui permet de plus le remodelage des jonctions adhérentes. En conclusion, nous améliorons notre compréhension de la mécano-transduction, qui était jusqu'à présent surtout basée sur le renforcement des jonctions, sans pouvoir expliquer leur remodellage[6,7]. Enfin, nous démontrons un rôle nouveau des flux d'actomyosine dans la détection et la transmission des forces mécaniques, et définissions un cadre général pour comprendre comment les forces mécaniques peuvent coordonner la dynamique des cellules épithéliales.

RESUMO:

A estabilidade das junções intercelulares é essencial para manter a coesão dos tecidos epiteliais, bem como a sua polaridade e propriedades mecânicas. Tanto durante o desenvolvimento, como na vida adulta, os epitélios são tecidos particularmente proliferativos. A divisão celular e, em particular o processo de citocinese, está intimamente ligado à formação de um novo conjunto de junções entre as futuras células-filhas, o que permite preservar tanto a integridade, como a polaridade do tecido. Recentemente foi demonstrado, tanto em vertebrados como em invertebrados, que as membranas da célula em divisão e das suas células vizinhas se mantêm em contacto durante a citocinese[1–6]. Isto implica que, durante a constrição do anel contráctil, as junções estabelecidas entre a célula em divisão e as células vizinhas são remodeladas. Em simultâneo, motores de Miosina não-muscular do tipo II acumulam nas células vizinhas junto à base da junção deformada[1,2,5], onde exercem as forças necessárias para justapor as membranas da célula em divisão, o que constitui o primeiro passo para a formação de uma nova junção intercelular[1]. Estas observações implicam que a ação da Miosina nas células vizinhas contribui tanto a formação, como para a geometria da nova junção formada entre as células-filhas[1,4,5]. Como tal, o objetivo do meu projeto de doutoramento era de compreender os mecanismos moleculares que medeiam a colaboração entre as células epiteliais durante a divisão celular.

Com base num conjunto de experiências genéticas e de ablação a laser, o meu trabalho de doutoramento mostra que, durante a citocinese, a acumulação de Miosina nas células vizinhas é desencadeada pelas forças produzidas pelo anel contráctil. A força gerada na célula em divisão deforma as membranas das células vizinhas e dilui a concentração da molécula de adesão E-Caderina. Esta redução dos níveis de E-Caderina na membrana, bem como a contractilidade das células vizinhas, promove a formação de fluxos de Actina e Miosina, que eventualmente se acumulam na base da junção deformada. Ao demonstrar que a citocinese produz forças endógenas, este trabalho expõe um novo mecanismo de mecano-transdução que coordena a dinâmica do citoesqueleto entre células epiteliais e que permite a simultânea reorganização das junções intercelulares. Como tal, este estudo indica que a mecano-transdução não se limita a reforçar as junções intercelulares, mas pode também promover a sua remodelação[6,7]. Finalmente, o meu trabalho também destaca o papel dos fluxos de Actina e Miosina na deteção e transmissão de forças no epitélio, o que pode contribuir para uma melhor compreensão de como as forças coordenam a dinâmica das células epiteliais.

LIST OF ABBREVIATIONS:

wt: wild-type
ECM: Extracellular Matrix
AJs: Adherens Junctions
(or **ZAs:** Zonula Adherens)
TJs: Tight Junctions
STs: Septate Junctions
TCJs: Tricellular Junctions
FAs: Focal Adhesions
Cad: Cadherins
E-Cad: E-Cadherins
EC domain: Extracellular domain
Cat: Catenins
β-Cat: β-Catenin
α-Cat: α-Catenin
p120-Cat: p120-Catenin
ZO-1: Zonula Occludens 1
ER: Endoplasmic Reticulum
EPLIN: Epithelial Protein Lost In Neoplasm
Actomyosin: Actin-Myosin
ABPs: Actin Binding Proteins
MyoII: Non-muscle Myosin II
MyoI: Myosin I
pMyoII: Phosphorylated Non-Muscle Myosin II
MyoVI: Myosin VI
L_p: Persistence Length
L_c: Contour Length
ATP: Adenosine triphosphate
ADP: Adenosine diphosphate
Pi: Inorganic Phosphate
ROCK: Rho Associated Protein Kinase
WH2 domain: WASP Homology 2 domain
NPFs: Nucleation-Promoting Factors
FH: Formin Homology
DFRs: Diaphanous-related Formins
Dia: Diaphanous
VASP: Vasodilator-Stimulated Phosphoprotein
MTs: Microtubules
BAR domain: Bin/Amphiphysin/Rvs domain
Zyxin: Zyx
ERM: Ezrin-Radixin-Moesin
GEFs: Guanine Nucleotide Exchange Factors
GAPs: GTPase Activating Proteins
Abl: Abelson Kinase
PIP2: Phosphatidylinositol(4,5)-bisphosphate
Mist: Mesoderm Invagination Signal Transducer
GBE: Germ-Band Extension
YAP: Yes-Associated Protein
TAZ: Transcriptional Co-activator with PDZ-binding motif
Wts: Warts
Exp: Expanded
MSCs: Mechanosensitive Channels
CS: Centralspindlin Complex
ESCRT-III: Endosomal Sorting Complex Required for Transport-III
MDCK: Madin Darby canine kidney
FRET: Fluorescence Resonance Energy Transfer
MTC: Magnetic Twisting Cytometry
GUVs: Giant Unilamellar Vesicles

INTRODUCTION:

Epithelial tissues have as main function to physically separate body compartments, thereby allowing the coexistence of distinct biochemical and mechanical microenvironments. Epithelial architecture is dictated by the assembly of specialized junctions along the apical-basal axis of cells, including the Tight Junctions (TJ) and the Adherens Junctions (AJs). Such adhesive structures are connected to the underlying actomyosin cytoskeleton to ensure not only tissue cohesiveness, but also mechanical coupling between neighbouring cells. In this context, epithelial proliferation is a particularly challenging task, as the dividing cell must preserve tissue integrity, while undergoing dramatic cell shape changes to divide its components into two equal halves. Yet, epithelia are among the most proliferative tissues not just during development, but also in adulthood.

This apparent conundrum was partially solved by in vivo studies of epithelial cell division. Concurrent live imaging of the adhesion and the cytokinetic machineries showed that cells preserve both epithelial polarity and the attachment to their immediate neighbours during division. These findings supported that epithelial cells sustain tissue integrity during proliferation and preserve the epithelia's barrier function. The most striking finding of these studies was that, in a tissue, division involves a tight interplay between the dividing cell and its neighbours[1–6]. In both Vertebrate and Drosophila epithelial tissues, constriction of the contractile ring deforms both the dividing and the neighbouring cell membranes, thereby preserving tight membrane apposition throughout cell division. Concomitantly, the junctions assembled between these cells are remodelled and a pool of MyoII accumulates at the base of the ingressing AJ in the neighbouring cells[1,2,5]. MyoII activity in the neighbours provides the force for membrane juxtaposition in the dividing cell and, sets the final length of the new cell-cell contact[1]. This remarkable collaboration suggests that epithelial cell division is rather a multicellular process, where the neighbouring cells take an active role in sensing and responding to the dividing cell behaviour. Since understanding how junctional remodelling and actomyosin dynamics are coordinated across epithelial cells is likely to be critical to uncover the mechanisms underlying epithelial tissue cohesiveness, we aimed to dissect the molecular mechanism coupling epithelial cells behaviour during cytokinesis.

By combining fly genetics, live imaging and theoretical modelling I found that, each epithelial cell division is associated with a mechanotransduction event controlling MyoII dynamics in the neighbouring cells. By establishing epithelial cell cytokinesis as an endogenous source of mechanical stress, this work uncovers a novel mechanotransduction mechanism that can both coordinate actomyosin dynamics between neighbouring cells and allow AJ remodelling. As will be discussed later one, this study challenges the current understanding of mechanotransduction that is based on junction reinforcement[6,7] and highlights a novel role for actomyosin flows in force

sensing and transmission.

This thesis will be organized into three main sections. In the Introduction, I will discuss key concepts used in this work, namely: (1) the architecture and function of epithelial tissues with a particular focus on the AJs and the E-Cadherin-Catenins complexes; (2) the regulation of the actomyosin cytoskeleton and its ability to produce forces; (3) how mechanical forces act to remodel cell-cell contacts, as well as the mechanisms mediating force sensing and transduction at E-Cad-based junctions; and, finally (4) describe cytokinesis and our current understanding of epithelial cell division. Then, I will report the findings I obtained during my thesis work by including the manuscript we recently submitted (currently in revision), as well as two review articles I worked on during my PhD. To conclude, I will outline the main findings and their implications, as well as provide future directions and perspectives of this work.

I. Epithelial Tissue Architecture and Organization

Epithelial cells are the defining cell type of metazoans, as they are the first cell type to arise during development and probably were the first tissue type to arise with multicellularity. Epithelial tissues function as dynamic barriers to separate body compartments and organize into sheets or tubular tissues via the assembly of specialized cell-cell junctions along the apical-basal axis of cells, namely the TJs and the AJs[8,9]. In this Chapter, I will describe the architecture of epithelia with a particular focus on the AJs, their attachment to the cytoskeleton and the mechanisms regulating AJ formation and maturation.

A. Organization of Epithelial Tissues

Epithelial cells are polarized along their apical-basal axis into, at least, four distinct membrane domains: supra-apical, apical, lateral and basal. Each epithelial domain has distinct protein and lipid composition, cytoskeletal organization and function (Table 5). The apical most part of the cells, also known as the supra-apical domain, faces either the exterior of the tissue or luminal spaces of internal organs and can harbour specialized structures, such as microvilli and cilia. These structures are composed of a dense array of highly cross-linked Actin filaments and are particularly prominent in absorptive and secretory epithelia, such as the intestinal epithelium. Conversely, the basal side of epithelial cells is directly attached to the extracellular matrix (ECM), via adhesive structures termed the Focal adhesions (FAs, additional information regarding their composition and properties is provided in Chapter III). The apical and lateral domains contain specialised adhesive structures that mediate cell-cell adhesion and mechanically couple neighbouring cells, via their attachment to the underlying actomyosin cytoskeleton (Fig. 1)[9–13]. Finally, microtubules (MTs) usually adopt a non-centrosomal organization into three distinct arrays, namely: (i) an apical meshwork of short MTs of mixed polarity; (ii) a linear array of MTs running along the lateral membranes with their minus ends oriented apically and their plus ends pointing towards the basal domain; and, (iii) an additional basal meshwork of MTs of mixed polarity (Fig. 1)[14,15].

I will now briefly detail the different types of intercellular junctions present in epithelia, as well as their contributions to epithelial adhesion and function.

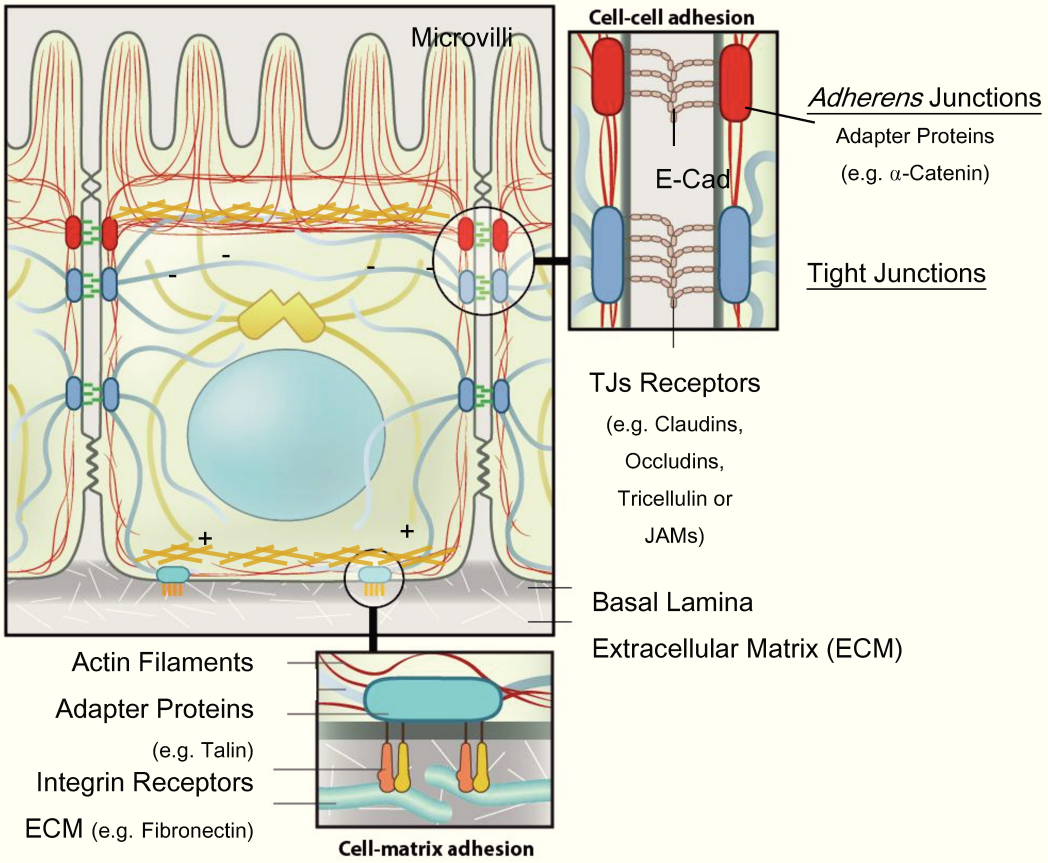

Figure 1: The organization intercellular junction and the cytoskeleton in invertebrate epithelial cells. The microvilli sit at the apical most part of epithelial cells and are composed of a dense array of Actin filaments (shown in red). The microtubule cytoskeleton is outlined in yellow, with long MT arrays running along the lateral membranes, with their minus ends (-) localized apically and their plus-ends (+) enriched basally. MT networks of mixed polarity are present both at the apical and basal domains. The intercellular adhesion junctions are highlighted in the insets, with the AJs shown in red and localized more apically than the TJs, which are shown in blue. Both the AJs and the TJs are directly linked to the Actin cytoskeleton; in blue, the Actin filaments connected to the TJs and in red, the F-Actin connected to the AJs. Cell-matrix adhesion is mediated by the FAs, which are composed of Integrin receptors and are also linked to the Actin cytoskeleton (in blue in the inset; adapted from: https://www.mechanobio.info/).

(i) Types of Intercellular Junctions:

The intercellular junctions were initially described in electron microscopy studies in mammalian tissues and classified as: (i) Zonula Occludens (or Tight Junctions), (ii) Zonula Adherens (or Adherens Junctions), and, (iii) Macula Adherens (or Desmossomes). The cell-cell junctions are electron dense structures associated with more or less dense cytoplasmic plaques found in regions where the plasma membranes of neighbouring cells are closely apposed. The TJs

are characterized by particularly tight membrane apposition, in agreement with its role as a semipermeable paracellular barrier, while the AJs bridge a distance of over ~200A and are associated with a thicker band of cytoplasmic material. In turn, the Macula Adherens are composed of Desmosomes and bridge a distance of ~240A. Importantly, Desmosomes localize more basally relative to both the TJs and AJs[16].

Tight Junctions act as a paracellular permeability barrier and are based on a set of transmembrane proteins, namely: (i) Claudins; (ii) Occludins; (iii) Tricellulin; and, (iv) Junction Adhesion Molecules (JAMs, proteins containing immunoglobulin-like domains). The TJs components interact loosely with the cytoskeleton via scaffolding proteins, such as Zonula Occludens-1 and -2 (ZO1-2) and act as signaling platforms for Guanine Nucleotide Exchange Factors (GEFs) and GTPase Activating Proteins (GAPs) that regulate the activity of small GTPases, namely Rho, Cdc42 and Rac (Box 1)[17]. The assembly of the TJs is facilitated by prior AJ formation, as several core components of the Adherens and Tight junctions interact, such as ZO-1 and α-Catenin or Afadin. TJ positioning along the apical-basal domain is defined by the polarity machinery (Table 5), but the TJs do not participate in the segregation of apical nor basal-lateral determinants, as in the absence of TJs apical-basal polarity is not disturbed[18]. In vertebrates, the TJs are localized more apical than the AJs; while in flies, the functional homologue of the TJs, termed the Septate Junctions (SJs) are almost always localized more basally (Fig. 1)[19].

The Adherens Junctions are mainly composed of the classical Cadherin-Catenins complexes and are closely connected to the Actin cytoskeleton, thereby sustaining strong cell-cell adhesion and mechanically coupling neighbouring cells. Similar to the TJs, AJ positioning is defined by the the polarity machinery, particularly via Par-3 function (Bazooka in flies; Table 5). During development, the AJs are highly dynamic structures that are extensively remodelled to produce tissue folding, extension or bending. Such processes typically involve changes in cell number, size, shape and position and are often regulated at the level of the AJs. Importantly, in flies, the AJs are restricted to the apical domain, while, in mammals these junctions spread more along the lateral domain[9,20].

Finally, Desmosomes are intercellular junctional complexes that strengthen cell-cell adhesion in tissues under extensive mechanical strain, such as the heart or skin epithelia. Desmosomes are, like the AJs, Ca^{2+}-dependent junctions composed of Cadherins and Plakin proteins that act as anchors to link the intermediate filaments of neighbouring cells, thus forming an integrated, mechanically resistant unit throughout the tissue[21]. Notably, Drosophila epithelial cells do not harbour Desmosomes, nor intermediate filaments[22].

Overall, despite the differences briefly highlighted here, intercellular junctions share similar composition and function across evolution. In the next section, I will focus on the key molecular players underlying AJs function and regulation.

B. Adherens Junction Composition and Attachment to the Cytoskeleton

The AJs can adopt different morphologies: (i) the Zonula Adherens (ZA, also known as linear AJ or simply as AJ) are present in virtually all mature epithelia (Fig.2A); (ii) the Spot AJ (SAJ, also called punctate or focal AJ) are generally observed in stratified epithelium-derived cells, fibroblastic cells and in immature epithelia; SAJs are visible during AJ assembly and initial steps of maturation (Fig. 2B); and, (iii) Tricellular AJ, which assemble at cell vertices, bridge three or more cells and their composition and mode of assembly is still poorly understood (Fig 2C). Linear AJs and Spot AJs adopt different organization of the Cad complexes and the actomyosin cytoskeleton; mature junctions are connected to parallel bundles of actomyosin running along the adhesion belt, while the Spot AJs are characterized by the assembly of nanometric Cad clusters connected to actomyosin bundles oriented perpendicular to the apposing cell membranes (Fig. 2)[23,24]. I will now describe the core AJ components and how the adhesion complexes are connected to the underlying actomyosin network and to microtubules.

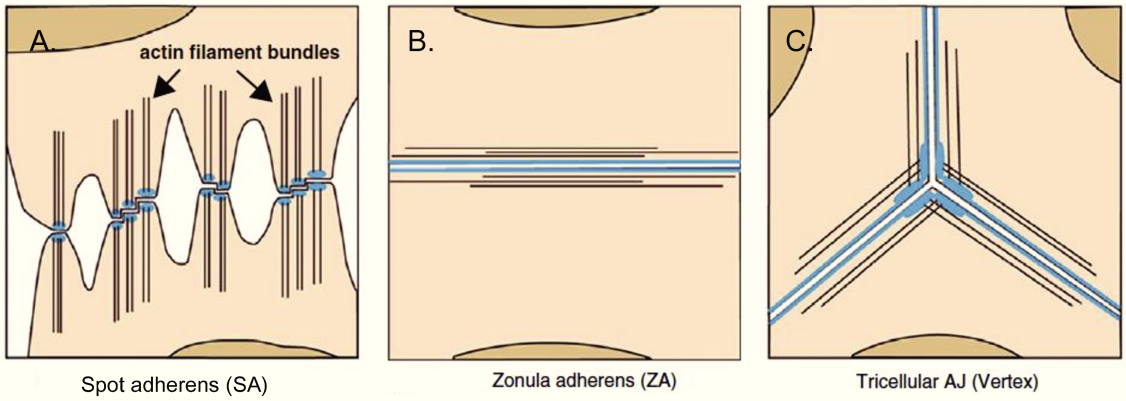

Figure 2: Different morphologies adopted by the Adherens Junctions.
(A-C) Schematic view of the different morphologies adopted by the AJs (highlighted in blue), as well as their mode of association to Actin filaments (adapted from[23]).

(i) Cadherin-Catenins Complexes:

Epithelial Cadherin (CDH1 in humans and Shotgun, or DE-Cad, in flies) is a member of the classical Cadherin family, together with a number of other Cadherins, such as Neural Cadherin (N-Cad) and Vascular Endothelial Cadherin (VE-Cad). Importantly, both E-Cadherin and N-Cadherin preferentially establish homophilic interactions; although both adhesion receptors can

also interact heterophilically. E-Cad harbours extracellular repeats with Ca^{2+} binding sites, which mediate homophilic interactions between Cadherin molecules expressed on neighbouring cells – trans engagement[25,26]. At the structural level, trans engagement can be mediated by E-Cad extracellular domain (EC) 1 that inserts a conserved tryptophan (Trp) residue into the hydrophobic pocket of their interacting neighbour or by extensive N-terminus interactions established along all the E-Cad EC domains near the Ca^{2+} binding sites. The binding interface adopted by the Cad molecules will force the dimers to adopt different 3D conformations, respectively the strand-swap or the X-dimer conformation (Fig. 3)[7,27]. Mutating the residues that mediate the interaction between the EC1 domains, namely the conserved Trp residue mentioned above, or residues along the N-terminus stretch abolishes the adhesive function of Cadherins. A subsequent study with type I/II Cadherins, E-Cad and Cadherin-6 respectively, revealed that both proteins adopt a strand-swap dimer conformation and proposed that X-dimer formation is rather an intermediate state (Fig. 3)[28–30]. In contrast to this, the X-dimer conformation may be primarily adopted by non-classical and invertebrate Cadherins, which lack the sequence signatures for the strand-swap conformation. Such behaviour was already reported for T-Cadherin, which forms non-strand-swapped dimers at the interface between the EC1-2 domains, close to the Ca^{2+} binding sites. Remarkably, the binding affinity of T-Cad dimers is similar to the one reported for classical Cadherins, such as E-Cad and C-Cad[31], suggesting that the 3D conformation of Cad dimers may not affect its binding affinity.

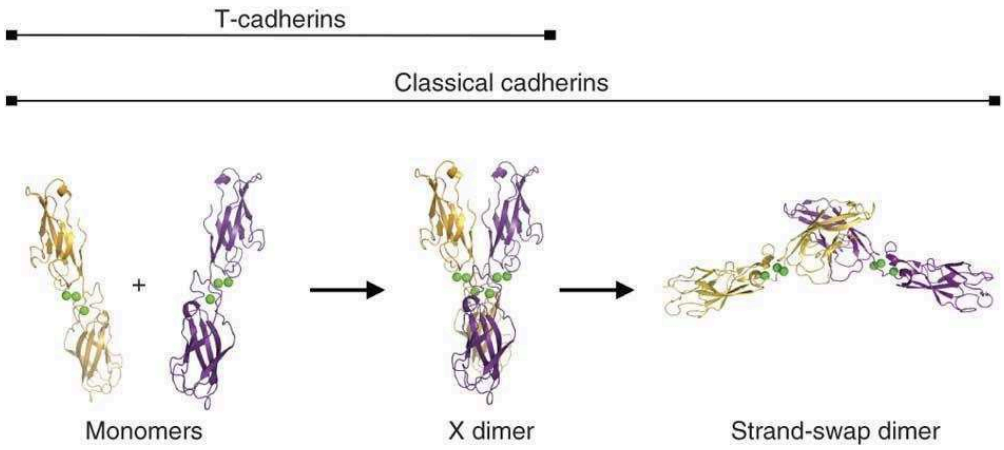

Figure 3: 3D conformation of Cadherin dimers.

Upon initial association, Classical Cadherin dimers can adopt either an X dimer or a strand-swap conformation. X dimer formation is mediated by residues near the EC1-EC2 Ca^{2+} binding sites, and the N-terminal β-strands of partner EC1 domains; while strand-swap assembly relies on the exchange of EC1 domains between partner Cadherin molecules. The X-dimer conformation was proposed to be an intermediate state towards the formation of strand-swapped dimers. Importantly, Non-Classical Cadherins, such as T-Cad can only adopt an X-dimer conformation (adapted from[28]).

Importantly, E-Cadherin molecules also associate laterally with neighbouring Cad molecules at the cell surface – termed cis engagement, a feature of Cadherins that further strengthens intercellular adhesion. The cis interaction is mediated by an interface between the EC1-EC2 domains and is stabilized by a hydrophobic interaction between residues Valine 81 and 175. As the cis and trans interfaces are distinct, a single cadherin can, in principle, be simultaneously engaged in one trans interaction and two cis interactions[32,33].

Intracellularly, the highly conserved cytosolic tail of Cadherin associates with the Catenins, namely β-, α- and p120-Catenin (Fig. 4). Once fully incorporated into the Cad complex, the three Catenins associate stoichiometrically with Cad molecules. The Catenins regulate E-Cad adhesion strength and its association with the cytoskeleton. I will now discuss how each Catenins contributes to E-Cad mediated adhesion, as well as their respective role in mediating the association of E-Cad with the cytoskeleton. β-Catenin (β-Cat) binds directly to the cytoplasmic tail of classical Cadherins and their association starts already in the endoplasmic reticulum (ER) for effective transport of Cadherin to the plasma membrane[34]. Once the β-Catenin-E-Cad complex reaches the plasma membrane, it recruits α-Catenin (α-Cat) which is essential for AJ integrity[35]. It is currently unclear whether β-Cat plays any additional function in epithelia other than escorting E-Cad to the plasma membrane, since expressing E-Cad-α-Cat fusions, in the background of β-Cat mutants, can restore epithelia integrity and function in many Drosophila tissues[36–39]. However, this is not the case during dorsal closure in flies, arguing that β-Catenin may play a particularly important role during processes that involve extensive AJ remodelling[40]. In MCF10a monolayers, β-Catenin recruits Vinculin to the AJs and this interaction was proposed to stabilize E-Cadherin at the cell surface (discussed in detail in Chapter III)[41]. Moreover, β-Cat phosphorylation by the Abelson (Abl) kinase was proposed to favour N-Cadherin-Catenins dissociation and, subsequent, N-Cad endocytosis[42]. Whether a similar mechanism regulates E-Cad levels at the plasma membrane remains unclear. In flies, β-Cat forms a complex with Rab11 and the Exocyst components, Sec15 and Sec10, to regulate E-Cad trafficking to the plasma membrane[43]. Finally, β-Cat bridges the Cad-Cat complex and the microtubule network, as it can both bind and recruit Dynein to the AJs[44,45].

Classical Cadherins also interact with p120-Catenin (p120-Cat) at their juxtamembrane region (Fig. 4)[46]. Follow-up studies showed that p120-Cat binding to E-Cad masks a dileucine motif that is recognized for Clathrin-mediated endocytosis[47–53], thus p120-Cat acts as a positive regulator of E-Cad mediated adhesion. Recent data also implicated another Cat, α-Catenin in stabilizing the p120-Catenin-E-Cad interaction[54]. p120-Catenin also mediates the linkage between Cadherins and microtubules, either through its direct interaction with the Kinesin heavy chain or its association with microtubule-binding proteins, such as PLEKHA7 (Pleckstrin Homology Domain-

Containing, Family A Member 7) and CLASP2 (CLIP-Associated Protein 2)[55–57]. The role of p120-Cat in connecting E-Cad to the actomyosin cytoskeleton remains unclear. Although p120-Cat can bind Rho1 directly, at least in flies, the functional relevance of this interaction is context-dependent[58–61]. Other report proposed an indirect link between p120-Cat and Rho signalling mediated by the recruitment of a Rho GAP, p190A-RhoGAP to the junctions, thereby locally down-regulating Rho signalling and strengthening the AJs (Box 1)[62,63]. Thus, whether the effect of p120-Catenin on Rho signalling is direct or just a consequence of p120-Cat's role in adhesion remains unclear. Importantly, p120-Catenin is not an essential gene in C. elegans nor in Drosophila[64–66]. Accordingly, in flies, an E-Cadherin mutant unable to bind p120-Cat fully rescues E-Cad loss-of-function, suggesting that the p120-Catenin-E-Cad association is not strictly required to regulate AJ stability[65]. A more recent report re-analysed p120-Catenin mutant flies and showed that loss of p120-Cat does have a minor impact in E-Cad levels. However, instead of acting as a positive regulator of adhesion, p120-Cat rather promotes E-Cad endocytosis, leading the authors to propose that the ancient role of p120-Catenin is to promote E-Cad endocytosis, a function that diverged in vertebrates[67].

Finally, α-Catenin is essential for AJ formation and function by mediating the interaction between the classical Cadherins and the actomyosin cytoskeleton[25]. Accordingly, α-Catenin can bind both the β-Catenin-E-Cadherin complex and F-Actin, but it was shown that, at least in vitro, the binding is mutually exclusive. Mammalian α-Catenin exists in both a monomeric and a homodimeric form; the α-Cat monomer preferentially binds β-Catenin, whereas the dimeric form has a higher affinity for F-Actin. In line with this, biochemical studies showed that an E-Cad-β-Cat-α-Cat complex is no longer able to bind F-Actin[68,69]. Thus, these studies suggested a revised model for how α-Catenin mediates the interaction between the junctional complexes and the actomyosin cytoskeleton where the binding was proposed to be only transient and highly dynamic. A more recent study solved this conundrum by showing that, under tension, α-Catenin undergoes a conformational change allowing it to bind simultaneously to β-Catenin and F-Actin (Fig. 4; discussed in-depth in Chapter III)[70]. These findings support an overwhelming amount of in vivo data showing that the physical connection between E-Cad and F-Actin is essential to support AJ integrity[36–39].

α-Cat also interacts with a number of ABPs and Actin regulators, namely EPLIN, Vinculin, α-Actinin, Formin1 and Afadin, thereby providing additional cascades for the regulation of the actomyosin network organization at the AJs, as well as its attachment to the Cad complexes (Fig. 4)[27]. Notably, ZO-1 also binds the C-terminal domain of α-Cat and F-Actin filaments, thereby providing additional links with the actomyosin cytoskeleton. Accordingly, α-Cat mutant cells, expressing an E-Cad-α-Cat fusion lacking the ZO-1 binding domain, were unable to establish strong adhesion[71]. α-Actinin, an Actin crosslinker (Table 1), was recently implicated along with the

Arp2/3 complex in de novo Actin assembly at apical E-Cad/α-Cat puncta, thereby regulating AJ integrity and stability[72]. Likewise, EPLIN contributes for integrity of the actin belt at the AJs and it is recruited to the junctions in an α-Cat and tension-dependent manner (discussed in detail in Chapter III)[73,74]. Finally, in vitro studies reported that α-Cat homodimers can inhibit filament nucleation by the Arp2/3 complex[68]. In agreement with an in vivo role for this inhibition, E-Cad-α-Cat fusions designed to adopt a constitutively monomeric form sustain cell-cell adhesion, but weaker than α-Cat heterodimers[39]. Thus, in the future, it will be important to discriminate the contribution of α-Cat monomers and cytosolic homodimers for strong cell-cell adhesion, as well as the functional relevance of these cascades in mediating indirect α-Catenin-F-Actin interactions, as well as their role in modulating the adhesion strength.

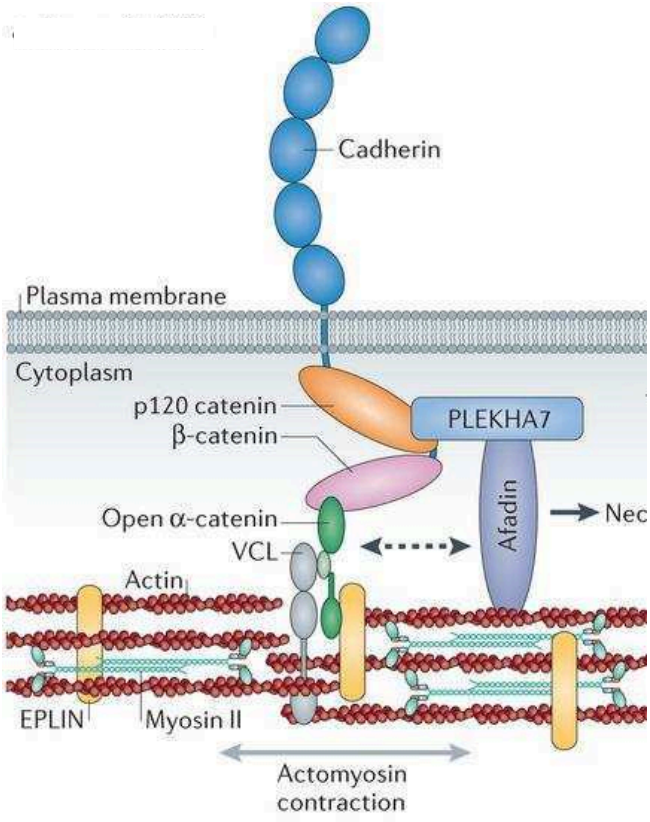

Figure 4: Molecular composition of the Adherens Junctions.

Schematic representation of the E-Cadherin-Catenins complexes, with a focus on the intracellular interactions of the E-Cadherin receptor (shown in blue) and its intracellular partners, where β-Catenin is shown in pink, p120-Catenin is shown in orange and α-Catenin is shown in green. α-Catenin is represented in its open conformation, able to bind both the F-Actin cytoskeleton and the Cadherin complexes. α-Catenin also interacts with Vinculin (VCL; shown in grey) and Afadin (shown in purple), providing additional F-Actin binding sites at E-Cadherin junctions. Finally, PLEKHA7 (shown in light blue) binds directly to the Cadherin-Catenins complex, via p120-Catenin, thereby providing a link for the MT cytoskeleton to be anchored at the AJs (adapted from[25]).

(ii) Nectin-Afadin Complexes:

Nectins and Nectin-like molecules (Necls) are the second class of adhesion receptors found at the AJs. Both Nectins and Necls are Ca^{2+}-independent transmembrane receptors belonging to the immunoglobulin superfamily, which contain three extracellular immunoglobulin-like domains and a cytoplasmic tail. Members of the Nectin and Necl families can interact both homophilically and heterophilically with each other[75,76]. In contrast to classical Cadherins, Nectins tend to adopt heterophilic rather than homophilic interactions, presumably because heterophilic binding produces stronger cell–cell adhesion[15]. Nectins bind AF6/Afadin (Canoe in flies), an Actin-binding protein shown to contribute to the connection between the AJs and the Actin cytoskeleton. AF6/Afadin binds along the sides of Actin filaments and shows Actin crosslinking activity, albeit to a lesser extent than α-Actinin (Table 1). AF6/Afadin also interacts with other adhesion receptors beyond Nectins, such as: (i) JAMs and ZO-1, both TJs components; and, (ii) AJs components, α-Cat and p120-Catenin (indirect interaction), thereby contributing to stabilize E-Cad at the membrane[75,76]. Importantly, in vertebrates, Nectins and AF6/Afadin localize strictly at the AJs, whereas the classical Cadherin-Catenins complexes are more spread along the lateral membranes[75].

In mammalian tissue culture models, Nectins are required to initiate cell-cell adhesion, followed by the recruitment of the E-Cad-β-Cat-α-Cat complexes via AF6/Afadin. It was also reported that heterotypic Nectin engagement per se is sufficient to promote E-Cadherin enrichment at nascent sites of cell-cell contacts[77]. Subsequently, the recruited E-cadherin molecules trans-interact with each other to form the AJs[77,78]. The interplay between Nectins and intracellular signalling generates a positive feedback loop that promotes efficient AJ formation[79] and facilitating the rapid reorganization of the Actin cytoskeleton. In line with an essential contribution of the Nectin-Afadin complexes for E-Cad-based adhesion, Afadin-deficient mice are embryonic lethal, exhibiting various developmental defects during and after gastrulation, including disorganized AJs and TJs and loss of cell polarity of epithelial cells in the ectoderm. These mice also display impaired migration and defective differentiation of the mesoderm cells[80,81].

A cooperative relationship between Nectin- and Cad-mediated adhesion was also uncovered in flies. Although flies do not possess a Nectin orthologue, Echinoid (Ed) a member of the immunoglobulin family acts as its functional homologue, since it localizes at the AJs and interacts with Canoe (Cno), the Drosophila orthologue of AF6/Afadin[82]. Similar to Nectin receptors, Ed can also establish both homophilic and heterophilic interactions with Neuroglian[83]. In flies, Cno also interacts physically with many proteins other than Ed, including: (i) DE-Cad; (ii) Polychaetoid (Drosophila ZO-1); (ii); (iv) signalling molecules, such as the small GTPase Rap1 (Box 1); and, (v) F-Actin, through its C-terminus[75,76]. Importantly, in flies, F-actin and Rap1 cooperate to recruit Cno to the AJs[84]. Upon Ed or Cno loss-of-function, although the AJs are still

present, their connection with the actomyosin cytoskeleton is impaired[82,84,85]; suggesting that, in flies, the main function of the Echinoid-Canoe complex is to attach the adhesion machinery to the cytoskeleton, rather than in AJ assembly as observed in mammalian cell lines. This function is particularly important in morphogenetically active tissues, such as the mesoderm during invagination, where the presumptive mesoderm undergoes dramatic apical constriction, and germ-band extension, where planar polarized actomyosin drives cell intercalation to extend the tissue along the anterior-posterior axis by several-fold (discussed in detail in Chapter III). Sawyer and colleagues reported that, upon Canoe loss-of-function, both in mesoderm and in germ-band cells, the actomyosin network can still constrict, but it is unable to power cell shape changes. This uncoupling between cytoskeleton-generated forces and cell shape results from the detachment of the actomyosin network from the AJs[84,86]. At the extreme, the actomyosin meshwork completely collapses in the centre of the cells, a phenotype that is reminiscent of α-Catenin mutants[37,38,84,86]. Finally, Canoe interaction with Drosophila ZO-1 is essential during dorsal closure, another well-studied model of epithelial morphogenesis[87,88].

Finally, it was shown that, similarly to p120-Catenin, AF6/Afadin also interacts with PLEKHA7, a microtubule minus-end binding protein. Accordingly, PLEKHA7 is recruited to sites of Nectin-based adhesion in an Afadin-dependent manner, but independent of p120-Cat. In mammary gland epithelial cells, this interaction is required for proper AJ assembly, but dispensable for TJs formation[89]. These findings highlight a role for the Nectin-Afadin complex in the organization of the microtubule network at the AJs and its role in cell-cell contact formation. This is in agreement with a previous study reporting that an array of microtubule minus-ends is anchored at the AJs, in a PLEKHA7/Nezha-dependent manner, where they contribute to junction integrity and organization[56]. Thus, it would be interesting to find whether a similar interaction is conserved in flies and whether it also impacts AJ assembly.

(iii) Non-Classical Cadherin Complexes:

Non-classical Cadherins share the conserved EC domains, but possess a divergent cytoplasmic tail. These include: Desmosomal Cadherins, Protocadherins, Fat and Dachsous Cadherins and Flamingo/CELSER. Desmosomal Cadherins are the most similar to Classical Cadherins and also interact homophilically to form cell-cell contacts (discussed above). Conversely, other non-classical Cadherins do not organize into specialized junctions, although they can establish homophilic interactions at the cell-cell interfaces. Accordingly, many non-classical Cadherins acquired unique molecular roles. For example, Fat and Flamingo are well-known regulators of planar cellular polarity and Fat also regulates tissue growth, via the Hippo pathway. Finally, other non-classical Cadherins, such as Protocadherins modulate Cadherin-based

adhesion[15,90].

More than 70 different genes encode Protocadherins, which differ from classical Cadherins both at their cytosolic tails, since Protocadherins lack the Catenin-binding domains and at their EC domains, as Protocadherins also lack the critical Trp residue required for strand-dimer formation. In line with this, Protocadherins exhibit only weak or no homophilic cell adhesion activity[91,92]. In the Xenopus embryo, Paraxial Protocadherin (PAPC), a Protocadherin with no adhesion capacity, is required for blastomere sorting and convergence-extension of the paraxial mesoderm. Chen and colleagues reported that PAPC function in morphogenesis relies on its ability to down-regulate C-Cadherin adhesive activity (C-Cad, main adhesion receptor in Xenopus). Accordingly, PAPC loss-of-function results in higher C-Cad-mediated adhesion in the dorsal mesoderm; conversely, exogenous C-Cad expression can rescue PAPC-induced cell sorting and gastrulation defects[93]. Interestingly, Arcadlin, the mammalian homolog of PAPC, also down-regulates another classical Cadherin, N-Cadherin[94]. Finally, in the Zebrafish embryo, another Protocadherin, Protocadherin 19 (Pcdh19) acts synergistically with N-Cadherin to control convergent cell movements in the anterior neural plate. Pcdh19-N-Cad complexes exhibit robust adhesion in bead aggregation assays, mostly due to Pcdh19 homophilic engagement. Such strong adhesion, however requires the presence of N-Cad, as Pcdh19 alone is only weakly adhesive[95].

Altogether, adhesion at the AJs relies mainly on the Cadherin and Nectin complexes with a potential, yet mostly unexplored, contribution from non-classical Cadherins, such as Protocadherins. Both Cadherin-Catenins and Nectin-Afadin complexes are connected to the actomyosin meshwork and the microtubule network. The main links between the adhesion machinery and the actomyosin cytoskeleton are α-Catenin and AF6/Afadin, which bind Actin filaments directly, and indirectly. Finally, p120-catenin, a member of the Cad-Cat complex and Afadin bridge the junctional complexes and the microtubule network, which is likely to be important for junctional integrity (although more work is required to clearly demonstrate this relationship).

C. E-Cadherin Cluster Organization and Regulation

A basic property of E-Cadherin is its ability into assemble nanometric clusters at the AJs. E-cadherin clusters were initially described during initial cell-cell contact formation and in lateral cell-cell junctions[96–98]. Using 3D super-resolution imaging, both in flies and in mammalian cell line models, E-Cad clusters were detected and characterised in detail. Although, E-Cad clusters display a preferred size[98], so far a preference for the number of molecules in each cluster was not detected[98,99]. The size, spatial distribution, and lateral dynamics of E-cadherin clusters are likely to

impact the adhesive forces acting at the AJs. In mature AJs where E-Cad molecules are tightly packed at the plasma membrane, the clusters remain distinct entities[98–100]. Surprisingly, in Eph4 mammary epithelial cells, loosely organized clusters composed of a few E-Cad molecules (up to 5) form independently of both cis or trans interactions with other E-Cad molecules. Wu and colleagues found that a cortical F-Actin meshwork surrounds E-Cad clusters, suggesting that Actin may act as a fence trapping E-Cad molecules in loosely, non-adhesive clusters – such "diffusion trap" was predicted by Hong and colleagues from theoretical work studying the partitioning of E-Cadherin into pre-adhesion clusters[98,101]. These findings suggest a model whereby the basic unit of adhesion is a loose E-Cadherin cluster that forms independently of actual cell-cell contact. As only abolishing both cis and trans interactions in a tailless E-Cadherin mutant completely impaired cluster formation, a cooperative model was proposed whereby cis and trans interactions cooperate with the E-Cad cytosolic tail to efficiently form adhesive clusters[33,98].

F-Actin and endocytosis are the key factors setting the E-Cadherin cluster size in vivo. An E-Cad mutant version lacking its cytosolic tail, therefore unable to bind F-Actin, still sustains cluster formation, although the clusters are smaller and more transient. Cluster stability can be rescued by fusing this Cadherin mutants with the F-Actin binding domains of α-Cat or Utrophin, supporting that Actin-binding is dispensable for cluster formation, but it is required to set its size and stability[102]. A similar stabilizing effect for F-Actin in setting E-Cad cluster size was reported in the Drosophila embryonic ectoderm, where F-Actin binding was shown to prevent cluster fission[99]. In line with this, previous findings showed that a small stable population of F-Actin filaments contact highly stable E-Cad clusters, while the remaining F-Actin meshwork exhibited a much more dynamic behaviour[103]. In contrast with these findings, in A431D cells, F-Actin rather limits the cluster size, as inducing F-Actin depolymerization enlarged E-Cad clusters and tail-deleted E-cadherin mutants formed substantially larger clusters than the full-length protein[98]. Thus, additional studies are required to clarify the exact role of F-Actin in setting the E-Cad cluster size. Importantly, cis interactions also regulate the lateral mobility of E-Cad molecules, as E-Cad mutants unable to establish such interactions exhibit a higher mobile fraction of both E-Cad and α-Cat, consistent with lower F-Actin anchoring[100]. Finally, MyoII activity at the AJs may coalesce F-Actin networks, thereby reorganizing F-Actin and associated proteins at the cell cortex[104]. Accordingly, local contractile pulses were reported at lateral junctions, resulting in the fusion of lateral Cadherin puncta[105]. High-resolution analysis will be required to determine the role of MyoII contractility in regulating the assembly and stability of E-Cad clusters.

In flies, endocytosis contributes to E-Cad turnover within the clusters, as clustering Cadherin using antibodies directed against its EC domains promoted receptor endocytosis[106]. Moreover, Dynamin-dependent endocytosis controls the cluster size, by limiting the maximum growth of the cluster through targeted removal of E-Cad molecules[99]. These findings suggest that

E-Cad clustering ultimately promotes its endocytosis, thereby intrinsically setting the maximal cluster size. However, rather surprisingly, in mammalian cell line models, a mutant version of E-Cad lacking all endocytic elements can still be removed from the membrane, albeit with much slower kinetics and in an ATP-independent manner[97]. A recent report helped clarifying these observations by showing that, in A431 epithelial cells, AF6/Afadin controls Cadherin cluster stability, via a Clathrin-independent mechanism[107]. These studies paved the way for a better understanding of E-Cad-based adhesion and additional work will now be required to understand the impact of the cluster properties for adhesion and whether these properties are modulated during morphogenesis.

D. Adherens Junction Regulation

The AJs are highly dynamic and plastic structures and as such they are regulated by a myriad of mechanisms. Most regulators act on the Cadherin-Catenins complexes, consistent with their pivotal role for AJ assembly, maturation and function. In this section, I will discuss the role of small GTPases, polarity complexes, microtubule network and endocytosis on de novo AJ assembly and maturation.

(i) The role of small GTPases:

Small GTPases, particularly from the Rho family, as well as their regulators GEFs/GAPs play a crucial in establishing and maintaining the AJs, by modulating Actin assembly and organization, as well as by regulating E-Cad trafficking at the cell-cell contacts (Box 1)[108,109]. Accordingly, Rho, Rac, Cdc42 and Rap1 accumulate at cell-cell junctions in their GTP-bound, active forms[110–113].

Box 1: Regulation of the small Rho GTPases.

In humans, ~20 Rho GTPases exist, of which RhoA (Ras homologue gene family member A), Rac and Cdc42 (Cell division cycle 42) remain the best studied[108,109]. In the figure below, a generic scheme of GTPase regulation is represented, where the Rho GTPase is anchored to the plasma membrane by a prenyl group. GEFs catalyse the release of GDP from the GTPase, allowing GTP to bind, thereby promoting GTPase activation. Conversely, GAPs increase the intrinsic GTPase activity of the Rho proteins, causing GTP to be hydrolysed to GDP and phosphate (Pi), resulting in its inactivation. GDP-bound Rho proteins can be sequestered by Rho guanine nucleotide dissociation inhibitors (GDIs), which bind to the prenyl group and

inhibit the GTPase association with the membrane (adapted from[108]). The main effectors of small Rho GTPase signalling are highly conserved. RhoA activates ROCK (RHO-associated coiled-coil-containing protein kinase; Rok in flies), which in turn promotes MyoII light chain phosphorylation both by directly phosphorylating MyoII and by inhibiting the Myo phosphatase. MyoII phosphorylation increases its ability to associate with Actin filaments. RhoA also activates unbranched Actin polymerization by Formins. Both Cdc42 and Rac1 activate the Arp2/3 protein complex, thereby promoting the polymerization of branched actin networks. Moreover, the PAK family kinases are another essential effector of Cdc42 and Rac1, which phosphorylates and activates the LIM domain kinase (LIMK). In turn, LIMK phosphorylates and inhibits Cofilin, an F-Actin severing enzyme, thus stabilizing the polymerized Actin[108,109].

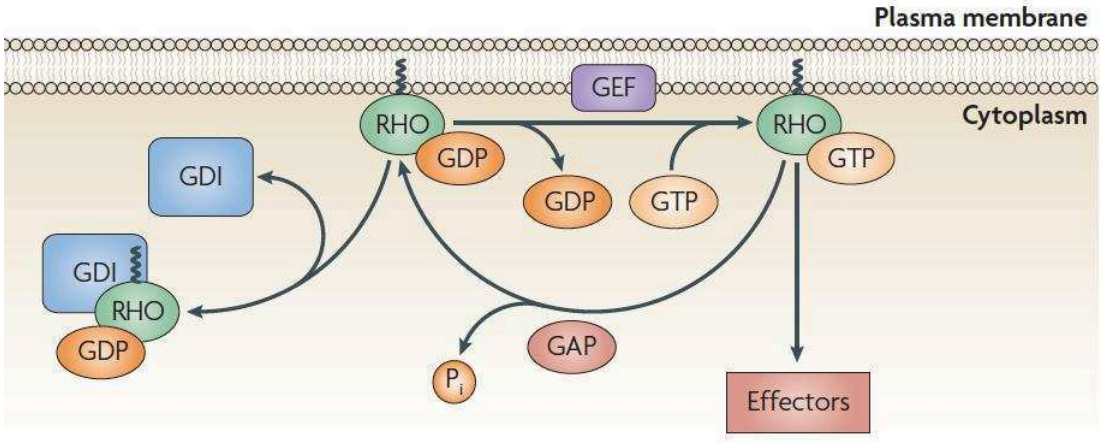

The involvement of both Rac and Rho in de novo AJ assembly was established in in vitro models of mesenchymal-epithelial transition, where exploratory lamellipodia contact each other and immobilize diffusive E-Cad molecules at the sites of cell-cell contact. While Rac activation is associated with nascent junctions, Rho activity is more associated with AJ maturation[114]. Importantly, constitutive Rac or Rho activation disrupts AJ integrity[115,116], supporting that their activities must be tightly regulated to ensure functional cell-cell contacts (Fig. 5). As briefly discussed in Box 1, Rac activates the Arp2/3 complex, via the WAVE complex to promote branched Actin polymerization and power membrane protrusion (Fig. 5; discussed in more detail in Chapter II)[117]. Importantly, initial E-Cad homophilic engagement feedbacks on Rac activity by recruiting the GEF Tiam1 to nascent sites of cell-cell contact[118,119]. E-Cad homophilic engagement per se can also activate Rac, in a Tiam1-independent manner, reaching a peak of activation after adhesive engagement that declines thereafter[110,120,121]. These findings suggest a model whereby the initial peak of Rac activity is likely to be triggered by E-Cad engagement and then sustained by subsequent Tiam1 recruitment. Importantly, Nectin ligation also activates Rac signalling and with similar kinetics than E-Cad, thereby providing an additional mechanism for initial Rac activation[121]. Moreover, the Actin-binding protein Ajuba, which is recruited to the AJs in an α-Cat-

dependent manner, also modulates Rac activity. Ajuba binds Rac, regardless of its nucleotide status and its depletion reduced Rac activation during contact formation and maturation, suggesting that a complex regulatory network fine-tunes Rac activation during AJ assembly and maturation[122,123]. Concomitantly, p120-Catenin binds p190A-RhoGAP, a GAP that prevents Rho activity at immature junctions. This interaction requires Rac activation, which initially recruits p190RhoGAP to nascent AJs. Thus, this regulatory loop prevents excessive Actin polymerization and contractile forces at immature cell-cell contacts[62]. Once junctions have expanded to a certain degree, α-Catenin and PAR-3 presumably inhibit the Arp2/3 complex and Tiam1 respectively, thereby inhibiting Rac signalling at the cell-cell contacts[68,124].

Upon initial cell-cell contact formation, Rho-dependent contractile forces power junction extension and stabilize the newly formed AJ. This requires the recruitment of RhoGEFs to the AJs, namely p114RhoGEF and Ect2[111,112]. p114RhoGEF is recruited to the cell-cell contacts by GEF-H1, a RhoA activator and it forms a complex with ROCK, MyoII and Cingulin[112]. Ect2 junctional localization and activation requires both α-Catenin and the Centralspindlin complex (composition and function described in Chapter IV). Once at the AJs, Centralspindlin also inhibits p190A-RhoGAP, thereby maximizing Rho activation[111]. Interestingly, there are two isoforms of p190RhoGAP, A and B and while p190A-RhoGAP is predominantly regulated by p120-Cat and Centralspindlin binding, p190B-RhoGAP binds Rac directly[125], providing a direct link for crosstalk between Rac and Rho signalling. Active Rho then activates Formin-dependent polymerization of unbranched Actin filaments and acts via ROCK to activate myosin II contractility (Box 1; Fig. 5). Accordingly, actomyosin contractility was shown in many contexts to be required for correct AJ assembly, organization and stability[71,126–134].

Figure 5: The role of the small GTPases, Rho and Rac in de novo AJ formation and maturation.
(1) Initial cell-cell contact is mediated by protrusive activity in the cells, resulting in initial E-Cadherin engagement. (2) E-Cadherin homophilic binding activates the GTPase Rac by the recruitment of its GEF Tiam1 to the sites of cell-cell contact. Rac activates the Arp2/3 complex, via the WAVE complex, promoting additional F-Actin polymerization and expanding the nascent sites of intercellular adhesion by recruiting additional E-Cadherin molecules. To avoid the generation of contractile forces at initial sites of cell-cell contact, Rac and 120-Catenin recruit the Rho GAP, p190A-RhoGAP. (3) Cluster expansion and Actin remodelling requires α-Catenin and Par-3-dependent inhibition of Tiam1 and Arp2/3, thus blocking Rac activation and, simultaneously, releasing Rho inhibition. (4) Contact maturation requires Rho, which is activated at the cell-cell contacts by several Rho GEFs, such as Ect2. Ect2 is recruited to the cell-cell contacts by α-Catenin and the Centralspindlin Complex, which also prevents p190A-RhoGAP junctional localization. In turn, Rho activates MyoII, by the ROCK kinase and F-Actin polymerization by Formins, thereby promoting the reorganization of the actomyosin network into the circumferential belt, typical of mature epithelia (adapted from[114]).

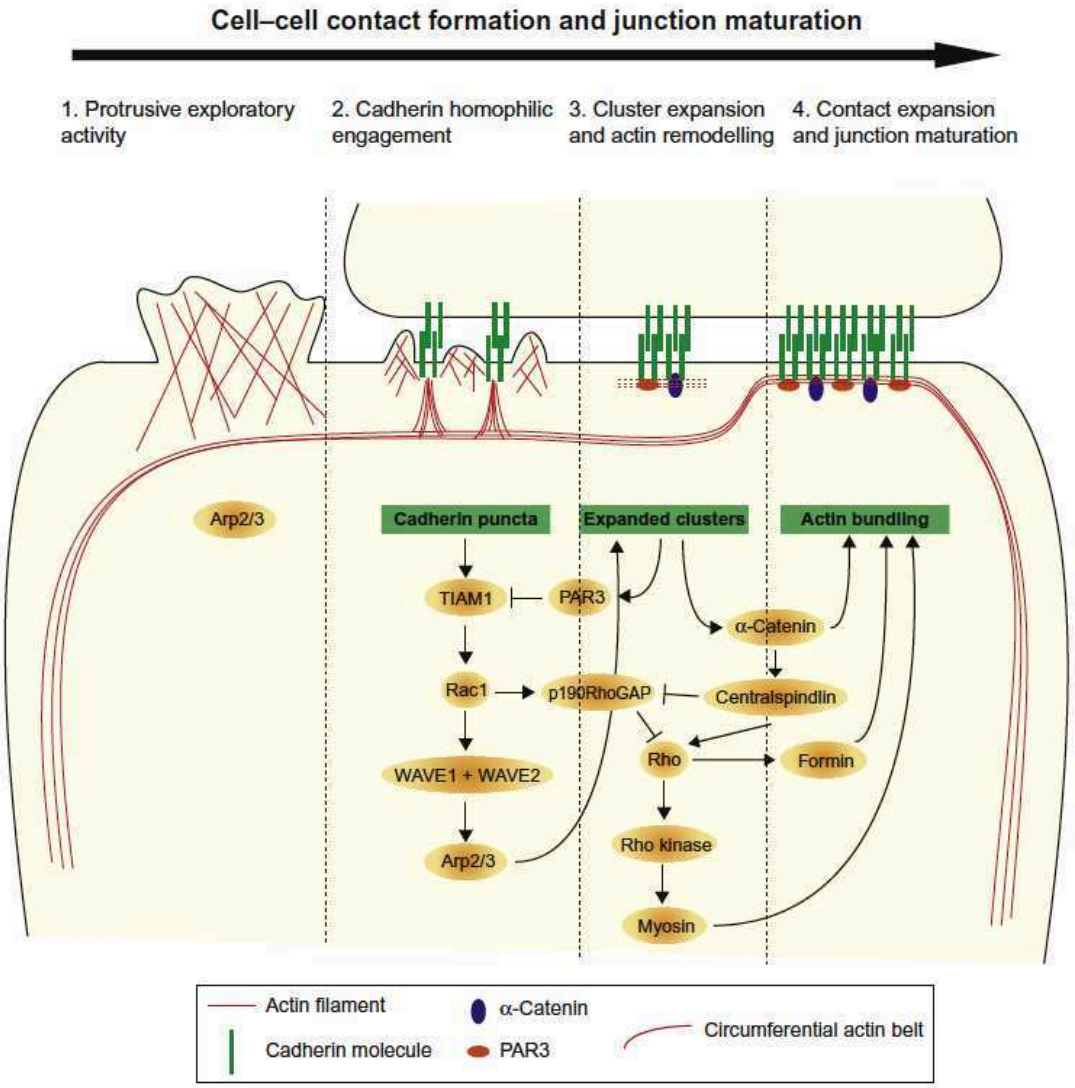

The GTPases Cdc42 and Rac1 are also involved in the regulation of E-Cadherin based adhesion, by regulating E-Cad trafficking and stability at the cell membrane. Early reports by Kim and colleagues showed that, in MCF-7 cells, initiation of E-Cadherin-mediated adhesion increases with the dose of active Cdc42[135]. Moreover, in MCDK cells, upon expression of a Cdc42 or a Rac1 dominant-negative mutant, E-Cad accumulates in punctate vesicles inside the cell[136], highlighting a role for both Rho GTPases in regulating E-Cad trafficking, which is also likely to contribute to Rac's function at nascent sites of cell-cell contact. In line with this, in a subsequent study both GTPases were found to be activated by trans-interacting E-Cadherin or trans-interacting Nectins[110,120,121,137]. In turn, activation of Rac and Cdc42 promotes the reorganization of the Actin cytoskeleton, via the Actin-binding protein IQGAP1, resulting in E-Cad stabilization at the cell membrane by blocking its endocytosis[137,138]. These findings highlight the crucial role of the signalling axis Rac/Cdc42-IQGAP1 in the dynamic organization and maintenance of E-cadherin-

based AJs (Box 1). Moreover, a novel Rac effector, Armus was recently described to act as a Rab7 GAP. Armus supported Rac-induced downregulation of E-cadherin by inhibiting Rab7. Thus, the integration of Rac1 and Rab7 activities by Armus provides an important regulatory node for E-Cadherin stability at cell-cell contacts[139]. In flies, Rac, Cdc42 and the Arp2/3 complex are also involved in endocytosis by promoting membrane invagination and scission. Rac, Cdc42 and the Arp2/3 complex mutant cells accumulate cytoplasmic E-Cad-positive vesicles, indicative of a role in E-Cad trafficking and turnover[1,140,141]. For Cdc42 the molecular mechanism was clarified in the Drosophila pupal notum, where it was shown to act via its effector CIP4 (Cdc42-interacting protein 4) and the polarity proteins Par6-aPKC (Table 5). CIP4 cooperates with WASP to activate the Arp2/3 complex and induce branched Actin polymerization at internalization sites (Table 1, 3), whereas Par6 targets CIP4 to the AJs, where it also binds Dynamin. These findings highlighted a role for Cdc42 and the epithelial polarity machinery, Par6-aPKC in E-Cadherin endocytosis (Fig. 6)[140,141]. The role of Cdc42 on AJ integrity is not restricted to E-cadherin endocytosis, but also to the trafficking of other apical components, such as the apical determinant, Crumbs (Table 5)[141,142]. Altogether, this data supports that Cdc42 and Rac function to regulate the turnover of apical proteins both by decreasing their endocytic uptake, and by accelerating the processing of apical cargo from the early to the late endosome.

Finally, the small GTPase Rap1 is enriched at the AJs in flies and in Rap1 mutant clones, E-Cad accumulates in patches[113]. A similar function for Rap1 was reported in mammalian cell culture models. Accordingly, three Rap1 GEFs, C3G, PDZ-GEF2 and Epac1 (Exchange Protein Directly Activated by cAMP 1) are recruited to the AJs and modulate E-Cadherin-based adhesion[143–145]. A follow-up study reported that Rap1 is essential to mediate the positive effect of Nectin-Afadin complexes in promoting E-Cad-mediated adhesion. Using a cell-free assay, the authors showed that Afadin associates with active Rap1 bound to Nectin and this complex is, in turn, able to bind p120-Catenin and strengthen its interaction with E-Cad, thereby stabilizing the adhesion receptor at the membrane[146]. The reverse relationship was however reported in GD25 cells, where Rap1 is activated at the cell contacts upon E-Cad internalization[147]. The potential roles of Rap1 in regulating E-Cadherin junctions, its connection with the Nectin-Afadin complexes, interactions with other GTPases and its role in dynamic morphogenetic systems remains to be investigated.

In summary, small GTPases are important regulators of adherens junction assembly, remodelling and stabilization, by regulating actomyosin organization at the AJs and the trafficking of junctional components. Rac and Rho are the main GTPases involved in de novo AJ assembly and cell-cell contact expansion, while Cdc42, and to a certain extent Rac, regulate E-Cad turnover. Finally, Rap1 was also proposed to modulate E-Cad stability at the plasma membrane, although its function is much less well understood.

(ii) The role of the Polarity Complexes:

As briefly mentioned in the previous section, the apical polarity complexes, particularly Par-3 (Bazooka in flies) are essential to position the AJs (Table 5). Accordingly, Par-3 and E-Cad co-localize in a number of epithelial models. Baz/Par-3 associates directly with a number of components of the adhesion machinery, namely: (i) Nectin1/3 (Echinoid in flies) and JAM1-3 in mammals; and, (ii) Armadillo in Drosophila (Arm; β-Catenin in vertebrates), thereby promoting their junctional recruitment. Since in mammalian cells, TJ assembly precedes AJ formation, the interaction between Par-3 and both Nectins and JAMs is the initial trigger for AJ assembly. Once enriched at the sites of initial cell-cell contact, Par-3 also recruits Afadin, thereby generating a feedback loop essential for both AJs and TJs formation[148]. Par-3 also regulates Rac activity, via Tiam1 recruitment to the TJs, which also contributes to TJ formation probably by promoting F-Actin polymerization[124].

In flies, de novo AJ formation occurs during cellularization, a process by which the membrane furrows are pulled towards the interior of the syncytial embryo to individualize the cortical nuclei into separate cells. In this system, Baz interacts with a myriad of factors to assemble spot AJs that will eventually mature and expand to form classical linear AJs. Baz apical recruitment is independent of its usual partners, Par-6 and aPKC and rather relies on cytoskeletal cues, namely the apical Actin meshwork and microtubule-dependent transport along the apical-basal axis. Baz apical accumulation also requires its interaction with phosphoinositides in order to facilitate its membrane association[149,150] and subsequent recruitment of the Cad-Cat complexes, most likely via Arm binding, thereby defining the spot AJs[151]. Moreover, Baz binding to Echinoid also promotes its recruitment to the membrane[82]. Baz apical anchoring at the Spot AJs localizes aPKC and Par-6, slightly above its own domain[152], where they contribute to the reorganization of the microtubule network, an essential aspect for AJ integrity[153]. Finally, Bitesize, a synaptotagmin-like PIP2-binding protein, is also recruited to the AJs by Bazooka, promoting the subsequent localization of the ERM protein, Moesin at the cell-cell contacts. Such mechanism stabilizes the junctions and contributes directly to the formation of a continuous belt of Actin around the apical cell cortex, a classical feature of linear AJs[154]. Overall, these findings support a pivotal role for Baz/Par-3 in directing AJ assembly.

The polarity complexes not only position the AJs, but also regulate AJ stability and integrity. This is well illustrated for the Par6-aPKC complex, which cooperate with Cdc42, to regulate E-Cad endocytosis in flies[140–142]. Beyond its role in E-Cad trafficking and microtubule organization at the cell-cell contacts, aPKC also regulates formation and stability of the apical actomyosin network. Accordingly, in mammalian cell models, expression of a dominant-negative form of aPKC blocks the transition from spot to mature AJs upon wound healing. Similar findings

were reported in a conditional aPKCλ knockout mice[155], suggesting that Actin reorganization into a belt-like structure regulates the transition from spot to mature AJs[156]. Kishikawa and colleagues later proposed that aPKC contributes to AJ integrity by antagonizing MyoII-driven centripetal contraction of the circumferential Actin cables[157]. How exactly aPKC functions in regulating apical belt organization is still unclear. One possible model would be that aPKC inhibits MyoII activity directly, as PKC can phosphorylate MHC, thereby inhibiting minifilament assembly and contractility (Table 2; discussed in detail in Chapter II)[10]. However, this effect may also be indirect, as aPKC can phosphorylate ROCK directly and prevent its junctional localization[158]. Since an aPKC isoform, aPKCζ cooperates with PAK1 to promote minifilament assembly and MyoII contractility[159], these findings argue for a more complex or context-dependent model. An alternative would be that aPKC regulates E-Cad levels at the cell membrane, thereby allowing the cell-cell contacts to resist contractile forces, which is compatible with the role of aPKC-Par6 in regulating E-Cad endocytosis[140–142]. Further studies will allow us to discriminate between these possibilities.

Finally, ROCK (Rok in flies) also phosphorylates Baz/Par-3[160,161], providing an additional link between the contractile network and the polarity machinery. In the fly embryonic epithelium, this phosphorylation is sufficient to inhibit Baz cortical association. This antagonism ensures that Rok/MyoII adopt a complementary localization to that of Baz/E-Cad, which is essential to direct cell intercalation events and consequently power tissue extension in vivo (discussed in Chapter III)[161]. In migrating cells, ROCK-dependent Par-3 phosphorylation, downstream of Rho, separates the Par complex, but does not prevent Par-3 interaction with the RacGEF, Tiam2. Nevertheless, Par-3 phophosmimic mutants are unable to rescue the migration defects observed in Par-3 mutants with cells exhibiting strong polarization defects, suggesting that Rho/ROCK-mediated inhibition of the Par complex by phosphorylation impairs its ability to activate Rac1. Moreover, Par-6 was also involved in regulating Rho signalling at dendritic spines, via p190RhoGAP recruitment[162]. The relationship between the polarity complexes and the contractile apparatus has been implicated in a wide range of morphogenetic processes, namely: dorsal closure[163], tubulogenesis of the salivary placodes[164], cyst growth[165] and germ-band extension[161] in flies and C. elegans zygote polarization[166]. Altogether, these findings support that the polarity complexes, particularly the Par complex are deeply involved in the regulation of AJ formation, expansion and maturation via a multitude of complex and not fully understood mechanisms.

(iii) The role of the Microtubule Cytoskeleton:

Although much less studied than the actomyosin network, microtubules (MTs) also contribute to AJ stability and organization. Accordingly, upon nocodazole treatment, a

microtubule-depolymerizing drug[167], E-Cad and MyoII accumulation and distribution at the AJs is affected[168–170]. Conversely, stabilizing the microtubule network with docetaxel or paclitaxel treatment attenuated the internalization of junctional proteins, such as E-Cadherin and Occludin[170]. Moreover, the number of MTs projecting to nascent contacts is greatly increased when cells lines are induced to form junctions, suggesting that the MTs may be anchored to the adhesive machinery[45]. In agreement with this, junctional components, such as β-Catenin, p120-Catenin and Afadin interact directly with microtubule-associated proteins, namely dynein[44], Kif3[55], CLASP2[57] and PLEKHA7[56,89]. Microtubules can interact with the AJs through their minus or plus ends; the minus-end array is anchored by Nehza/ PLEKHA7[56], whereas the plus-end population, is decorated by EB1[171], CLIP-170[169] and/or CLAPS2[57] and it is anchored at the AJs by dynein[44,45]. I will now discuss the state-of-the-art knowledge for the role of the MT network at the AJs, starting with plus-end MTs and then the minus-end MT population.

Stehbens and colleagues showed that, in MCF-7 cells, a pool of radial MTs is localized apically, with their plus-ends (CLIP-170 positive) facing the AJs. In CLIP-170 mutants or upon low doses of nocodazole treatment[167], E-Cad accumulates at the membrane in puncta and at lower levels, adopting an organization reminiscent of spot AJs. These findings suggest that this MT population may contribute to AJ maturation[169]. Moreover, Dynein, a minus-end directed motor was also found to anchor MT plus-ends at the AJs and its inhibition also affects AJ formation, suggesting that the tethered microtubules at the cell-cell contact may serve as tracks for Kinesin motors to delivery junctional components, such as α-Catenin, β-Catenin and p120-Catenin to the cell-cell contacts[45]. Dynein itself localizes at the AJs in a β-Catenin and PLAC-24-dependent manner, a relatively unknown junctional component that co-localizes with the E-Cad at the AJs[44,172]. More recently, CLASP2, yet another plus-tip protein, was found to localize at cell-cell contacts in a p120-Cat-dependent manner. According with previous findings, CLASP2 depletion delays AJ formation and impairs junction stability. These effects result, at least, partially from the reduction of p120-Catenin junctional levels[57]. Altogether these studies support that MTs interacting with AJs through their plus-ends stabilize the cell-cell contacts, although the exact mechanisms underlying this effect will require further investigation.

A subsequent study identified a population of minus-ends also anchored at the AJs, also by p120-Catening and its binding partner, PLEKHA7. Meng and colleagues showed that PLEKHA7 overexpression results in higher E-cadherin and Catenins accumulation at the AJs, while its depletion decreases E-Cad-Cat complexes also exclusively at this region (although the total levels at the cell-cell contacts are not affected). PLEKHA7's function at the AJ also requires its binding partner Nezha, a minus-end binding protein able to anchor non-centrosomal MTs at the AJs. PLEKHA7/Nezha-anchored MTs serve as tracks for the minus-end directed motor KifC3 and together these proteins contribute to AJ integrity[56]. Beyond p120-Catenin, PLEKHA7 also binds

Afadin, which provides an additional binding site for PLEKHA7 at the AJs[89]. Accordingly, in Drosophila, the microtubule network is essential to position the spot AJs during cellularization (discussed above)[173]. Although it remains unclear how exactly the minus-end MTs anchored at the AJs contribute to regulate their integrity, it is clear that different minus- and plus-end MT tracks co-exist at the AJs and that they contribute to junctional organization and stability. Another important aspect that is even less well characterized is how the microtubule network modulates the organization and contractility of the actomyosin cytoskeleton at the AJs, a feature that would certainly impact the organization and stability of E-Cad-Cat complexes. In agreement with this, dynamic MTs are proposed to inhibit contractility during cytokinesis[174] and during GBE[175], as well as to regulate the polarized distribution of RhoGEFs during apoptotic cell extrusion[176]. Moreover, it was shown during cell migration, that Rho and its effector mDia cooperate to stabilize the MT network, potentially by forming a complex with EB1 and APC at stable MT ends[177].

(iv) The role of Endocytosis and Trafficking:

E-Cad turnover must be fine-tuned to ensure junction integrity and stability and various mechanisms were already implicated in regulating E-Cad trafficking. Once at the cell membrane, E-Cad can be internalized by Dynamin- and Clathrin-mediated endocytosis. The small GTPases, Cdc42 and Rac regulate E-Cadherin levels at the plasma membrane, by regulating Dynamin-dependent E-Cadherin endocytosis (Fig. 6)[120,140–142]. Two other small GTPases, namely Rap1 and Arf6 (ADP-Ribosylation Factor 6) were also implicated in regulating E-Cad endocytosis, although additional studies are required to clarify their exact contribution for E-Cad stabilization at the membrane (Fig. 6)[113,143–146,173]. In contrast, p120-Catenin stabilizes E-Cad at the plasma membrane, by masking a dileucine motif in the E-Cad juxtamembrane domain required for Clathrin-dependent endocytosis of E-Cadherin (Fig. 6)[47–53]. However, in flies and C. elegans, p120-Catenin does not play an essential role in regulating E-Cad internalization[64–66]. Using a yeast 2-hybrid system, a novel E-Cadherin binding protein was identified and named Hakai (Fig. 6). Hakai is an E3 ubiquitin-ligase and it promotes ubiquitination of the E-Cad complexes, in a tyrosine phosphorylation-dependent manner[178]. Hakai is a highly conserved protein and its interaction with E-Cad and ubiquitination activities are also conserved in flies. The functional relevance of Hakai-dependent ubiquitination is unclear, as Hakai mutant embryos exhibit only mild defects in AJ and F-Actin organization[179]. Since the effect of these pathways seems to be mild, other mechanisms regulating Cadherin endocytosis must exist. Finally, transcriptional and posttranscriptional regulators also control Cadherin levels at the cell surface, as observed for the transcription factor Snail during mesoderm invagination in Drosophila (discussed in Chapter III)[15].

Internalized E-Cad molecules are transported to Rab11-positive endosomes or trafficked to late endosomes and lysosomes for degradation[43,51,106,114,180]. Rab11 associates with the Exocyst complex, via the Sec5 and Sec10 components to regulate E-Cad targeting back to the cell surface[43], as well as to deliver newly synthetized E-Cadherin molecules at the plasma membrane[181]. Another pathway transports endocytosed E-Cad molecules along the lateral membrane towards the apical junctions, a phenomenon termed Cadherin flow. Both in mammalian cell lines and in flies, Actin filaments are required to transport E-Cad along the lateral membranes[181,182]. Finally, Woichansky and colleagues recently identified a novel pathway involved in the recycling of endocytosed E-Cad molecules. RabX1 is essential for this pathway as it provides a link between early and recycling endosomes. Since the Exocyst mutants combine defects in apical-lateral trafficking and in the Rab11-pathway, it is likely that the Exocyst targets both Rab11- and RabX1-positive vesicles to the cell membrane[181]. How the different pathways regulating E-Cad endocytosis and trafficking are integrated and activated in the cell is an open avenue of research and it will be interesting to find whether differential activation of these pathways can be exploited to achieve asymmetric junctional remodelling during tissue morphogenesis.

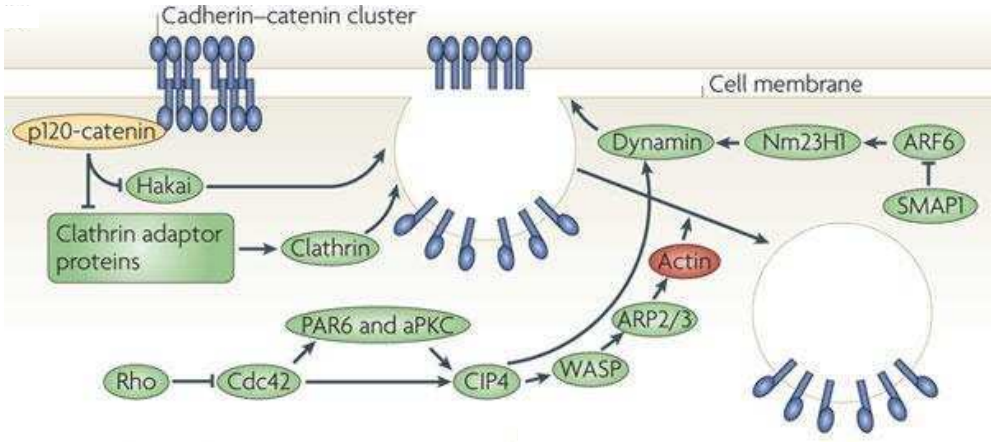

Figure 6: Regulation of E-Cadherin-mediated junctions by endocytosis.

The small GTPases, Cdc42 and Arf6 regulate E-Cadherin levels at the plasma membrane, by promoting Dynamin-dependent endocytosis. In turn, p120-Catenin binds the juxtamembrane region of E-Cadherin, thus blocking Clathrin-mediated endocytosis. Finally, Hakai, a E3 ubiquitin-ligase, promotes the ubiquitination of E-Cadherin complexes (adapted from[173]).

II. The Actomyosin Cytoskeleton: Regulation and Force Production

The actomyosin cytoskeleton is an essential cellular scaffold and force-generating machine. In agreement with its ancient function, Actin is among the ~400 ancestral genes present in the last common ancestor and its high cellular concentration makes it one of the most abundant proteins on earth[183,184]. Actin is essential for cell survival, as it provides mechanical support, tracks to move intracellular cargo and forces to power cell shape changes and movement. Myosins (Myo) are also highly conserved and almost all eukaryotes possess genes encoding similar motor proteins that can move Actin filaments[183]. The actomyosin cytoskeleton can produce both pushing and pulling forces, as observed during cell migration. A striking feature of the actomyosin cytoskeleton is its ability to regulate processes at all scales: (i) at the sub-cellular level, actomyosin regulates organelle transport; (ii) at the cell-scale it determines cell shape in processes as diverse and fundamental as cell division and cell intercalation; and, (iii) at the tissue-scale, it powers tissue morphogenesis in virtually all studied organisms[11,12]. In the present section, I will describe the composition, regulation and mechanics of the actomyosin network and then focus on how such networks generate forces in vivo. Finally, I will discuss the self-organizing properties of the cytoskeleton underlying complex network behaviours, such as actomyosin flows.

A. Actomyosin Cytoskeleton: Main Components

In the present introductory section, I will describe the basic properties of Actin filaments, Myosin motors, as well as their key regulators along with a brief description of their mechanism of action (provided in the form of Tables – Annexes).

(i) Actin Filaments:

Actin is the building block of the actomyosin cytoskeleton, mainly due to its ability to polymerize into double-stranded helical filaments, in an ATP-dependent manner. F-Actin polymerization is rate-limited by the nucleation step, which consists of the formation of Actin dimers/trimmers. To accelerate polymerization in vivo, Actin nucleators, i.e. Formins and the Arp2/3 complex, catalyse monomer addition, followed by ATP hydrolysis and subsequent Pi (Inorganic Phosphate) dissociation. This intrinsic property of the polymerization reaction, along with an array of G-Actin binding proteins, prevent spontaneous F-Actin polymerization in vivo and maintain a pool of unassembled Actin monomers, thereby ensuring quick remodelling of the Actin

network in vivo. F-Actin filaments are intrinsically asymmetric structures, with a fast-growing end – barbed end, which elongates up to 10 times faster than the slower growing end – pointed end. Therefore, at the steady-state, Actin monomers are then continuously polymerized at the barbed end and depolymerized at the pointed ends, a phenomenon termed treadmilling[185]. An impressive number of Actin binding proteins (ABPs) were described during the past decades and were shown to modulate Actin filament nucleation, elongation, as well as the overall higher-order network organization, contractility, degree of cross-linking and disassembly dynamics (Table 1).

(ii) Myosin Motors:

Myosins are motor proteins that bind and slide Actin filaments at the expense of ATP. Members of the muscle and non-muscle Myosin II families (MyoII) form hexamers, consisting of two heavy chains (MHCs), two essential light chains (ELCs) and two regulatory light chains (RLCs). The MHCs fold into a N-terminal globular head and mediate the motor activity, while the C-terminal domains fold into a tail and promote homodimer formation. Next to the motor domain sit two IQ motifs, which bind both the ELCs and RLCs, connecting the head and tail domains at the neck region (Fig. 7). Conformational changes associated with the ATPase cycle set the binding affinity of myosin motors to the Actin tracks. In the absence of nucleotide or in the ADP-bound state, the head strongly interacts with Actin; while, in the ATP- or ADP-Pi-bound states, the binding affinity for Actin is dramatically reduced, due to conformational changes that disrupt the Actin-binding site. Thus, upon ATP binding, Myo affinity for Actin is low and the motor is released, allowing the myosin head to hydrolyse ATP, thereby promoting a conformation change in the head domain that allows the motor to rebind Actin. As the Pi group dissociates from the ATP-binding pocket, the head domain undergoes a second conformational change – termed the power stroke. Since Myo is strongly bound to Actin, the exerted force is transmitted to the filament and drags it. The repetition of this cycle allows myosin motors to slide relative to an Actin filament. An essential parameter of myosin motors is the rate at which it hydrolyses ATP and how much time per cycle it remains in the ADP-bound state – the duty ratio[10,186–188].

MyoII motors are only processive upon minifilament assembly, which is mediated by the tail-to-tail association of several MyoII hexamers (Fig. 7). Hence, MyoII motors undergo dynamic assembly and disassembly cycles, which are regulated by rounds of phosphorylation and dephosphorylation, allowing tight spatial and temporal regulation (Table 2). Phosphorylated MyoII minifilaments generate contractility by pulling on antiparallel Actin filaments at the expense of ATP, thereby generating network contraction or extension. The classical example of MyoII-dependent forces occurs in the striated muscle. Here, in contrast to most cell types, the actomyosin network is orderly packed, with the Actin filaments' barbed ends oriented at the Z line and the

MyoII motors segregated towards the pointed ends of the Actin filaments. As the motors pull the antiparallel filaments together, they increase the overlap of myosins and F-Actin, and consequently reduce the sarcomere length[10,187].

In mammals, three genes encode different MCHs – IIA, IIB and IIC, thereby determining the MyoII isoform – MyoIIA, IIB and IIC, respectively. Despite high sequence similarity, the three isoforms have different duty ratios, exhibit distinct expression patterns and play mostly non-redundant functions in vivo. MyoIIA has the highest rate of ATP hydrolysis and it propels Actin filaments more rapidly than MyoIIB or IIC[189]. Conversely, MyoIIB has a higher duty ratio than MyoIIA with particularly high affinity for ADP binding[190–192]. Although MyoIIA and IIB colocalize at the apical belt and are both required for AJ integrity, the function of MyoIIC at cell-cell contacts does not seem essential[130,193]. In agreement with their non-overlapping functions in vivo, MyoIIA junctional localization requires E-Cad engagement and Rho/ROCK/MLCK activity, while MyoIIB targeting to cell-cell contacts requires the small GTPase Rap1. Selective depletion of MyoIIA affects E-Cad accumulation at the apical junctions, decreases Cadherin homophilic engagement and clustering, while MyoIIB knockdown decreases F-Actin content and increases lateral movements of the perijunctional Actin ring. Importantly, ectopic expression of MyoIIA, upon MyoIIB RNAi, cannot rescue normal actomyosin organization at the AJs. Altogether these findings support that the contribution of MyoII isoforms for AJ integrity is complementary, rather than redundant. Thus, MyoIIA acts more as a cortical organizer setting E-Cad junctional organization, while MyoIIB controls apical belt integrity and strengthens the junctions under tension[130,194]. Since flies only possess one MHC – Zipper[10], other regulatory mechanisms must exist to allow for a dynamic, yet stable, actomyosin network.

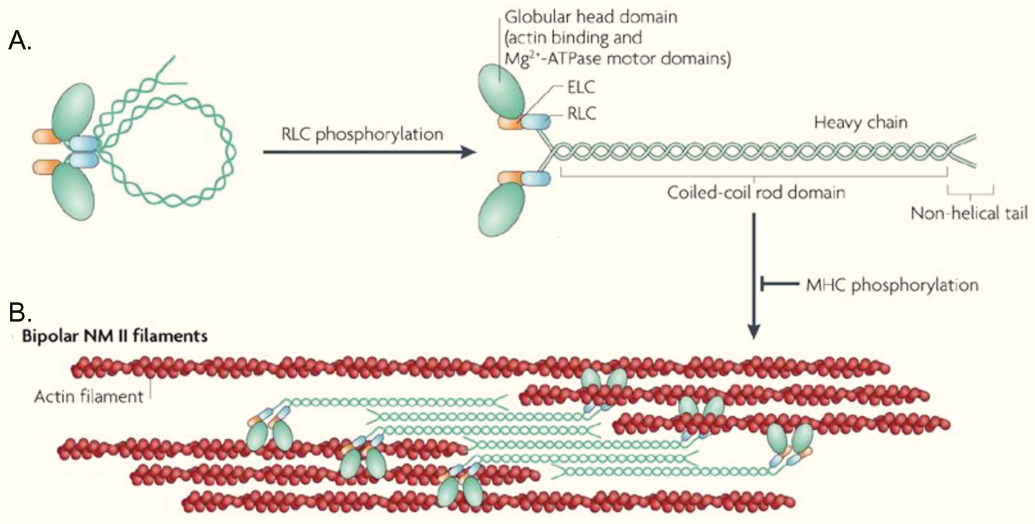

Figure 7: Myosin II organization and assembly into mini-filaments.

(A) Upon phosphorylation of the RLC, MyoII forms a dimer through interactions between the coiled-coil tail

domains. The globular head domain contains both the Actin-binding regions and the enzymatic Mg^{2+}-ATPase motor domains. The ELCs and the RLCs bind the heavy chains, linking the head and the tail domains. In the absence of RLC phosphorylation, MyoII forms a compact molecule through a head to tail association, which is unable to associate with other MyoII dimers. MyoII molecules assemble into bipolar filaments through interactions between their rod, or tail, domains. (B) Bipolar filaments are competent for F-Actin binding and ATPase activity, via their head domains, thereby enabling a conformational change that allows MyoII to slide Actin filaments (adapted from[10]).

B. Mechanical Properties of the Actomyosin Network

Cells can be defined as complex active soft materials and their mechanical properties are set by the longest, most abundant and most cross-linked polymers. Assuming this is indeed the case, F-Actin polymers are expected to dominate cell mechanics. An essential feature of any polymer is the persistence length (L_p), which is defined as the average length of straight filament fragments and it is proportional to the intrinsic polymer stiffness[195]. Actin filaments exhibit an L_p of 10-15μm, while microtubules are much more rigid polymers with an L_p of ~1mm, consistent with their preferred function as the cell's transporting tracks. To understand the mechanics of a polymer, it is useful to compare the L_p and the contour length (L_c); flexible polymers exhibit $L_c >> L_p$, i.e. thermal fluctuations induce strong filament distortions, as observed for intermediate filaments (L_p of 200nm-1μm), while stiff polymers show $L_c << L_p$, as observed for microtubules. According with this, Actin filaments can be defined as semi-flexible polymers with $L_c \approx L_p$. At the cell scale, Actin filaments shorter than 10μm will act as stiff rods, while longer filaments will tend to bend, due to mechanical constraints imposed by confinement/geometry and/or by motor protein activity[185,195,196]. The bending force required to curve Actin filaments is a way to determine how much force Actin can exert when growing against a load, e.g. plasma membrane. For shorter filaments, the buckling force is greater since it scales inversely proportional to the square of the filament length. The buckling force can be measured when Actin filaments are constrained on one end by Formins and on the other end by an inactivated Myosin; such setup showed that filaments shorter than 0.5μm elongate via monomer incorporation and can produce forces of up to 10pN without buckling, supporting that single filaments growing against a load exert can indeed exert considerable forces before buckling[197]. However above a critical curvature threshold, F-Actin buckling results in mechanically-induced severing of filaments. Arai and colleagues used optical tweezers to manipulate the ends of Actin filaments and induced buckling by tying a knot on the filament; under these conditions, mechanically induced severing occurs when the knot diameter falls below 0.4μm[198] (critical radius of curvature below 300-400nm)[199].

A generic property of semi-flexible polymers, like Actin filaments, is the increase in their elastic modulus upon stretching – strain stiffening[200–202]. For Actin filaments, strain stiffening can be observed at low-intermediate strains (~20%)[202]. The mesh size (average distance between adjacent filaments in the network), the average L_p and the concentration and dynamical properties of Actin crosslinkers will determine the stress required to produce network stiffening (Box 2). Longer filaments show stronger elastic behaviour, thus simply modulating filament length in vivo can profoundly affect the network rheology at the mesoscopic scale (Box 2). Notably, Formin-nucleated filaments are up to 10 times longer than Arp2/3-polymerized filaments. Although only up to ~10% of the total cortical Actin pool is nucleated by Formins, these filaments still contribute strongly to determine network elasticity[203]. As mentioned above, network crosslinking, as well as the crosslinking distance strongly impacts strain hardening – highly cross-linked networks exhibit higher elastic moduli[195,200–202,204,205]. In line with this, both α-Actinin or Filamin cross-linked Actin networks exhibit stronger strain stiffening at short timescales, yet these networks also soften more prominently at long timescales (Table 1; discussed below)[204,205]. Importantly, MyoII motor activity produces internal stress within cross-linked networks that further contribute to stiffening. Since this response is greatly affected by motor processivity[205], one can assume that the two MyoII isoforms will impact differently on F-Actin strain-stiffening. In Dictyostelium amoeba, MyoII was shown to contribute to cortical integrity via its crosslinking, rather than its not motor activity, suggesting that, at least, under certain conditions MyoII may not necessarily slide Actin filaments, but rather contribute to network rheology by modulating filament connectivity[206]. Overall these findings support that, at intermediate strains, the actomyosin network adopts an elastic behaviour mostly due to filament entanglement and crosslinking.

At large deformations, Actin networks adopt the reverse behaviour – termed strain softening. This behaviour results partly from mechanically induced filament disassembly, but mostly from F-Actin turnover and crosslinker unbinding or detachment, resulting in local filament rearrangements and stress dissipation – a viscous-like behaviour. Once the local stress is relaxed, the crosslinkers can rebind F-Actin and the network can recover its elasticity. As Actin filament severing increases the number of barbed ends, it can promote further F-Actin assembly or disassembly via the activity of the available Actin-binding proteins[195,198,199].

Another important parameter defining the rheology of actomyosin networks is the frequency of the applied stress. Elasticity is only observed for high stress/strain rates, i.e. rapid deformations (Box 2). Thus, actomyosin networks behave as a viscoelastic material; at short timescales, lower than turnover, cross-linked actomyosin networks will tend to adopt an elastic behaviour, but a more viscous behaviour will unavoidably ensue at longer timescales, due to F-Actin turnover, crosslinker unbinding and subsequent filament reorganization that strongly dissipate stress[187,195]. Importantly, in low cross-linked networks, MyoII motor activity has the

opposite effect than what was previously discussed, as active filament sliding will actually fluidize the network[205,207], supporting that the network organization will greatly impact its mechanical response. To get an approximation of the viscoelastic timescales at play here, one can compare the turnover time of Actin filaments and crosslinkers at the actomyosin cortex. The entire Actin network at the cortex turns over within approximately 1min, while Actin crosslinkers and myosin motors usually turnover 5-10 times faster than Actin, suggesting that, in response to any deformation applied, the timescale of viscoelastic relaxation of the cortex is dominated by the turnover of crosslinks, rather than of the Actin filaments themselves (6-12 sec)[196].

Finally, network mechanics also depends on its boundary conditions – attachment to the plasma membrane and/or the adhesion machinery, FAs and AJs. These boundary conditions define how much force is transmitted to the extracellular matrix (ECM) and/or the neighbouring cells, as well as the resisting force acting on the actomyosin network[199,208]. This point is well illustrated by studies showing that the velocity of retrograde Actin flows is ten-fold lower in the presence of integrin-based adhesions[209–211]. In agreement with this, in vitro studies where actomyosin networks are cross-linked to a lipid bilayer showed that strong adhesion constrains the transverse motions of F-Actin and prevents filament buckling. Additionally, the rate of F-Actin severing is dramatically enhanced under these conditions[208]. The build-up of internal stress by network anchoring also affects the behaviour of MyoII motors and Actin filaments themselves, which show, as discussed above, a highly nonlinear response to the applied load.

Altogether, one can conclude that the mechanics of the actomyosin network is determined by contributions from active stresses (contractility) and passive stresses (elastic and viscous) that depend on the network organization and connectivity, as well as on the magnitude and timescale of the applied forces.

Box 2: Definition of tension, stress, strain, rheology and stiffness.

Tension: considering the actomyosin network, one can define tension as the pulling force exerted by Myo motors on Actin filaments.

Stress: describes the internal force an object is experiencing, per unit cross sectional area. For example, MyoII motors generate stress by pulling on Actin filaments in the network.

Strain: describes how much an object is deformed by stress.

Rheology: study of the deformability of soft materials, such as gels or polymer solutions, under conditions of mechanical stress, deformation, or flow. Typically, materials are characterized by their response to small sinusoidal deformations at a given frequency. For example, the shear modulus of normal solids is independent of frequency, whereas that of liquids is proportional to frequency. Materials with complex microstructure (including cells) often display viscoelasticity, which describes any frequency-dependent

response between solid-like and liquid-like behaviour.

Stiffness: defined as the ratio between the force exerted on the object and the deformation induced by this force and it is an effective property of an object (adapted from[196,212–214]).

C. Cytoskeleton-generated Mechanical Forces

The actomyosin cytoskeleton generates two main types of forces: (i) protrusive or pushing forces, mediated by branched or unbranched Actin polymerization, push the plasma membrane or intracellular structures, and, (ii) contractile or pulling forces are mediated by MyoII motors and Actin crosslinking proteins. To elucidate how the cytoskeleton generates mechanical forces, I will focus on cell migration and cell division.

(i) Protrusive Forces:

Nucleation of Actin filaments from their monomeric subunits is sufficient to change cell shape and produce a protrusion, which is often the first step in cell locomotion. Each Actin filament produces picoNewton forces (pN) and together they push the plasma membrane at a rate of ~1μm/second[183]. Two main classes of proteins catalyse filament polymerization, namely: the Arp2/3 complex that nucleates dense, branched Actin networks and Formins that nucleate linear unbranched filaments (Table 1). Notably, recent studies identified a novel mechanism of Actin polymerization based on tandem clusters of G-Actin-binding motifs that can also assemble Actin seeds (Table 1). Since their cellular functions are less well described, I will focus exclusively on the two main nucleator classes. To facilitate the description of how Actin polymerization can generate protrusive forces, I will first describe the characteristics of the Actin networks polymerized by these two nucleators, their respective mechanical properties and illustrate how these networks generate protrusive forces in the context of cell locomotion.

- Protrusive forces generated by branched Actin networks:

Branched Actin networks participate in a myriad of cellular functions, namely in Clathrin-mediated endocytosis, phagocytosis, intracellular trafficking, meiotic spindle positioning, AJ assembly and integrity, motility of some bacteria and viruses in the host cell cytoplasm and they propel the leading edge of migrating cells[185]. A very illustrative example of how protrusive forces generated by branched networks power movement is the in vitro propelling of micrometre-sized beads and oil drops by Arp2/3-dependent F-Actin polymerization[215,216]. The Arp2/3 complex

initiates Actin filament nucleation on the side of existing filaments, with the free barbed end growing away from the mother filament and the pointed end anchored to the complex (Table 1 and Fig. 8).

The Arp2/3 complex is composed of seven subunits, of which two key Actin-related proteins Arp2 and Arp3 are stabilized in an inactive state by five other subunits – Arpc1-5. Arp2/3 activation requires collaboration between nucleation-promoting factors (NPFs), pre-existing F-Actin and Actin monomers (Fig. 8). Most NPFs activate the Arp2/3 via the WCA domain, which is comprised of one or more WASP homology 2 (WH2; also called a V motif standing for Verprolin Homology) domains that bind Actin monomers, plus an amphipathic connector region and an acidic peptide that collectively bind the Arp2/3. Among the most important NPFs are: WASP, Scar/WAVE complex, WHAMM, JMY and Cortactin (Table 3)[217,218]. Conversely, Arp2/3 activity is inhibited directly, via ATP hydrolysis and Coronin binding (Table 3), and, indirectly by debranching enzymes, like: ADF/Cofilin, which was proposed to compete with Arp2/3 for F-Actin binding, and the Protein Glia Maturation Factor (GMF), which binds to Arp2/3 and prevents branch nucleation (Table 1)[218,219]. Finally, in mammals, Arpc1 and Arpc5 subunits are each encoded by two isoforms and their differential inclusion in the Arp2/3 complex modulates its F-Actin nucleation ability and intrinsic resistance to debranching, supporting that isoform diversity provides an additional layer of Arp2/3 regulation[220].

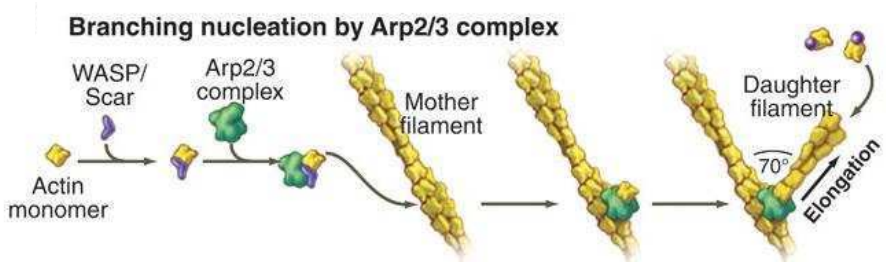

Figure 8: Branched F-Actin polymerization by the Arp2/3 complex.
Nucleation-promoting factors such as WASP bind simultaneously an Actin monomer and the Arp2/3 complex. Binding to the side of a filament completes activation, and the barbed end of the daughter filament grows away from the Arp2/3 complex (adapted from[183]).

To generate strong pushing forces able to power cell protrusions, branched networks must be kept short to prevent Actin filaments from buckling under stress. Capping proteins perform this essential function, as they bind to the barbed ends with high affinity and preclude continuous F-Actin elongation by the Arp2/3 complex. Accordingly, in the absence of Capping Proteins (CPs) F-

Actin branches are long and eventually turn into an array of parallel bundles growing away from the Arp2/3 anchoring points[221,222]. Since CPs divert Actin monomers from elongation towards polymerization, they promote the nucleation of multiple Arp2/3 seeds, giving rise to the polymerization of a number of parallel and independent branched sub-networks that can merge or repulse, depending of whether the individual branches are or not sufficiently long to interact. Such system generates a very dense network of short filaments[223,224]. Another important component of branched network mechanics is the degree of branching, which cooperates with CPs and Actin monomer concentration to define the mesh size. As discussed above, decreasing the mesh size (high filament density) dramatically increases network stiffness, which is essential for effective force production[185].

One of the best-characterized examples of Arp2/3-dependent protrusive forces is the formation of lamellipodia during cell migration (although other Actin nucleators, such as Formins and Spire can cooperate with the Arp2/3 complex). Many extracellular stimuli induce lamellipodia formation, including growth factors, cytokines and cell adhesion receptors that eventually converge downstream to ensure the activation of Rho GTPases (Box 1). Accordingly, Rac activation is sufficient to drive lamellipodia extension[225], although both RhoA and Cdc42 also localize at the lamellipodia. In migrating cells, Rac and Cdc42 cooperate to recruit both the WAVE complex and Arp2/3 to the lamellipodium, which is a wide sheet-like membrane protrusion observed at the leading edge of cultured cells migrating in a 2D substrate[226]. Incorporation of the Arp2/3 complex occurs exclusively at the tip of the lamellipodium, similarly to the WAVE complex, CPs and Actin[227], thereby providing directionality to Actin polymerization and allowing a directed pushing of the membrane (Fig. 9). Somehow paradoxically, not all branches are positioned toward the leading edge membrane in vivo, although the angle distribution does narrow in fast moving cells (Fig. 9)[228,229]. Thus, whether oblique oriented branches can still contribute to lamellipodia protrusion is not clear. Importantly, behind the lamellipodium sits the lamella, a region of F-Actin depolymerization that recycles Actin monomers to fuel more Actin nucleation at the front, thereby facilitating a phenomenon termed Actin treadmilling (more detailed in section D)[226].

Finally, the plasma membrane was recently reported to be much less passive than initially anticipated. Membrane tension was shown to direct cell migration by restricting the spread of the leading edge[230–232]. Interestingly, the F-Actin polymerization rates follow the same trend; increasing membrane tension reduces lateral protrusions with longer and more oriented F-Actin filaments towards the direction of movement[231]. To explain these findings a theoretical model considering the impact of plasma membrane tension on the actomyosin cytoskeleton was proposed. The key assumption is that, although local increases in membrane tension are rapidly propagated to the rest of the cell, the transmitted tension is inversely correlated with the local filament density. Thus, at the leading edge, where F-Actin density is high, membrane resistance per filament is

small, allowing filaments to grow rapidly and generate protrusion; conversely, at the rear and the sides of the leading edge, filament density gradually decreases, resulting in increased resistance to polymerization, thereby stalling membrane protrusion[233]. Overall, the role of the plasma membrane as an active player in organizing protrusive forces is an exciting open field.

Altogether, these findings support that localized F-Actin polymerization coupled with constant monomer recycling is sufficient to generate pushing forces able to power cell locomotion. Furthermore, recent findings implicate membrane tension in regulating cell migration directionality[230–232], suggesting that the plasma membrane may not be simply pushed.

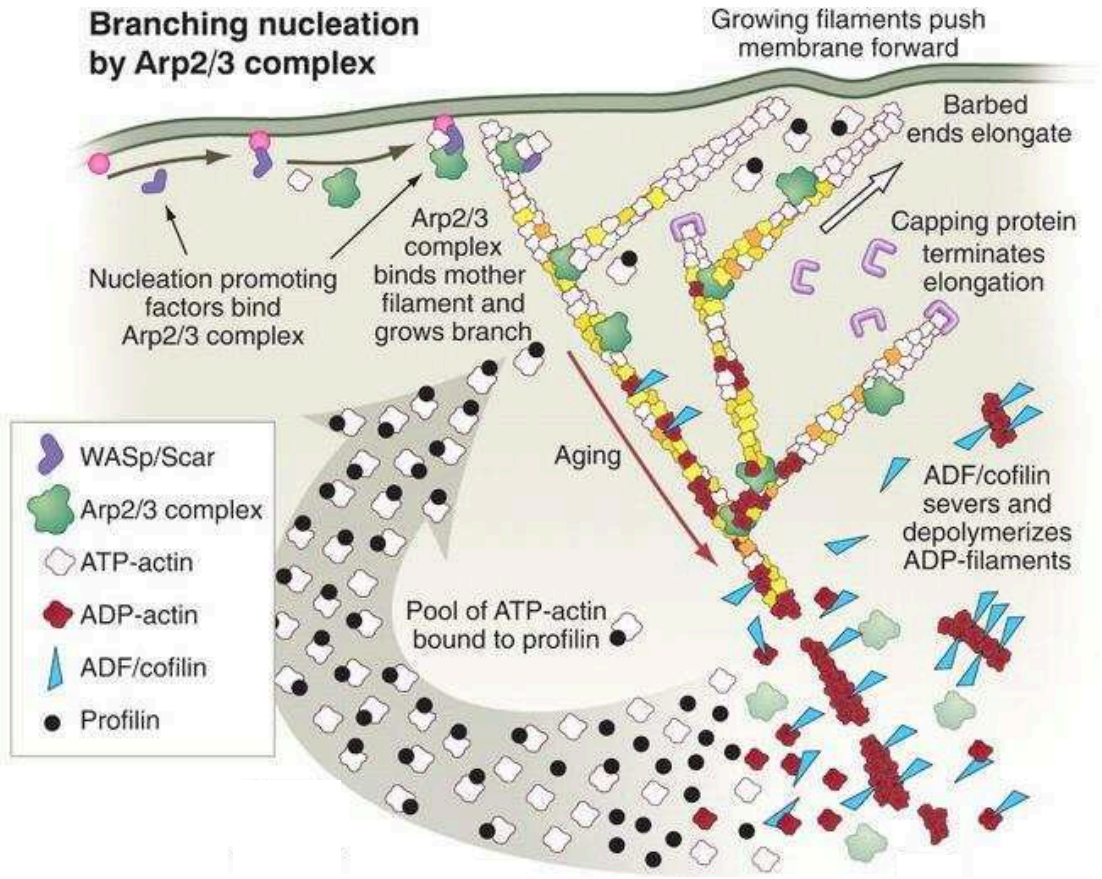

Figure 9: Schematic representation of events at the leading edge of a migrating cell.

The branched Actin network, nucleated by the Arp2/3 complex produces protrusive forces at the cell front, due to massive and fast F-Actin assembly underneath the plasma membrane. This wave of F-Actin assembly is finely balanced by continuous ADF/Cofilin-mediated fragmentation, thereby recycling Actin monomers and contributing for the formation of Actin retrograde flows toward the leading edge (not shown; adapted from[183]).

- Protrusive forces generated by unbranched Actin networks:

Unbranched (or linear) Actin networks are involved in contractile ring constriction during cytokinesis, in preserving AJ and FA integrity, in microvilli formation and powering cellular protrusions, such as filopodia. Unbranched networks are polymerized and elongated by Formin homodimers, via the Formin Homology 1 and 2 (FH1-FH2) domains that mediate the formation of an Actin seed and bind Profilin-bound Actin, respectively (Table 1 and Fig. 10A; note that some Formins also possess crosslinking activity)[217,218]. Since most Formins remain processively bound to the barbed ends during filament elongation, Formin-nucleated filaments tend to be longer than Arp2/3-polymerized F-Actin[203].

There are up to seven classes of Formins and their ability to nucleate filaments, associate with the barbed ends and cooperate with Profilin can vary dramatically. Not surprisingly, their activity is also regulated by a myriad of distinct regulators (Table 4). So far, the best understood regulatory mechanisms are those of Diaphanous-related Formins (DFRs). DFRs are autoinhibited by intramolecular associations between the Diaphanous (Dia) auto-regulatory domain (DAD) and the Dia inhibitory domain (DID), thereby preventing new monomer incorporation. A well-characterized DRFs activator is the GTPase RhoA that binds Dia in a partially overlapping site with the DAD domain, thereby partly releasing the inhibitory DID-DAD association. SH3 domain-containing proteins, such as Src family kinases also interact with DRFs, suggesting a potential cooperation with RhoA to promote DRFs activation in vivo[217,218]. Dia-interacting protein/WASP interacting SH3 protein (DIP/WISH), Spire and Tropomyosin inhibit or attenuate Formin-mediated F-Actin elongation by promoting their displacement from the barbed ends (Table 1)[219]. The biological function of such interactions is still unclear, as Spire was actually shown to cooperate with Dia in Drosophila oocytes[234]. Finally, DRFs were also implicated in microtubule binding directly, and, indirectly, via interactions with plus-tip proteins. Thus, DRFs were proposed to stabilize the microtubule network, although more studies are required to understand the functional relevance of this crosstalk[218].

Formin-nucleated filaments tend to associate in bundled structures, due to lateral interactions and the action of Actin crosslinkers, such as Fascin and α-Actinin (Table 1 and Fig. 10B). The crosslinker properties will greatly affect the bundle density, motor accessibility and filament orientation – parallel and antiparallel. A key property of each crosslinking protein is the distance by which it can bridge two Actin filaments; tightly packed bundles rely on crosslinkers with short crosslinking distances, such as Fascin and loosely packed bundles rely on long crosslinking distances, such as networks cross-linked by α-Actinin (Fig. 10B)[185]. Additionally, bundle formation requires a fluid-like environment to facilitate rotational and translational diffusion of filaments. In line with this, increasing the rate of Actin assembly abolishes the

formation of Actin bundles generated by α-Actinin, since fast Actin assembly generates long filaments that have limited mobility, preventing their alignment into bundles. This implies that as Actin polymerization and filament elongation proceeds, bundle formation is concomitantly stalled, suggesting a kinetic window for bundle formation that is in constant competition with filament polymerization/elongation (or, in other words, network densification). In this sense, F-Actin turnover due to motor and severing activity is likely to be critical to fluidize the network[235]. These features determine the bundles' mechanical properties and cellular functions. Importantly, bundled networks can also arise from branched networks. Accordingly, in in vitro reconstitution studies using giant unilamellar vesicles (GUVs) that nucleate branched Actin networks, the authors were surprised to find the formation of thin protrusions similar to filopodia, rather than dendritic networks. Thus, it was proposed that a deformable membrane can overcome the bending rigidity of Actin filaments to both gather and bundle nearby filaments into a single tubular protrusion[236].

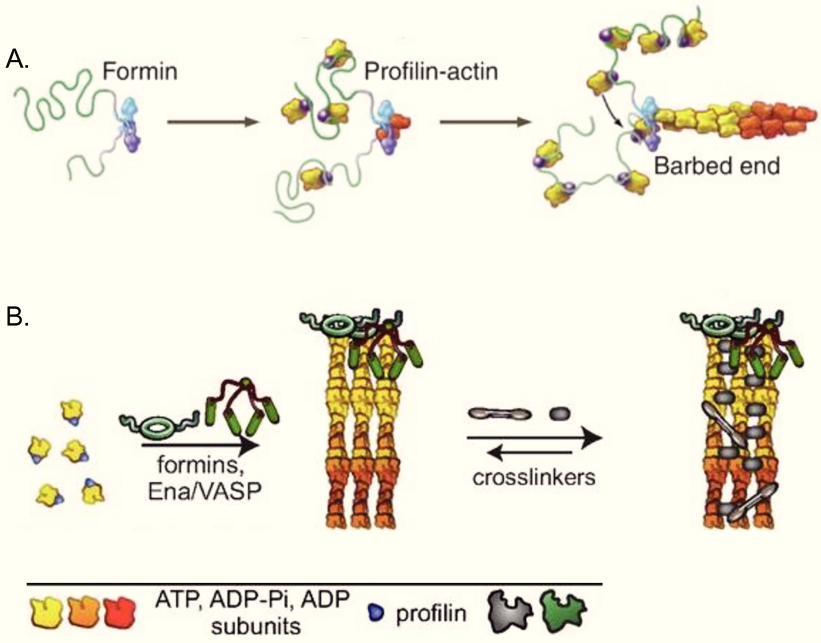

Figure 10: Unbranched F-Actin nucleation and elongation by Formins.
(A) Formins initiate polymerization from free Actin monomers and remain processively associated with the growing barbed end. Profilin-bound Actin binds to Formin and transfers the monomer onto the barbed end of the filament. (B) The action of short distance Actin crosslinkers (e.g. Fascin) tightly packs unbranched filaments, such as those generated by Formins or Ena/VASP proteins, into stiff, straight bundles (adapted from[183,185]).

To illustrate how unbranched networks can produce protrusive forces, I will now focus on the mechanisms underlying Filopodia formation. Filopodia are finger-like projections, composed of

unbranched, bundled Actin filaments oriented with their growing ends toward the membrane (10-30 Actin filaments). The function of filopodia goes beyond cell migration, as they also participate in sensing the cell environment, initiating cell contacts and transmitting cell-cell signals. Filopodia formation requires the Rho GTPase Cdc42 and encompasses three basic steps: filament nucleation, sustained barbed-end elongation and filament bundling (Fig. 11). It remains unclear whether filopodia formation requires exclusive Formin-dependent F-Actin polymerization or whether Arp2/3 also plays a role in this process. Since N-WASP and the Arp2/3 complex are required for filopodia formation in some conditions, it was proposed that filopodia assembly may also emerge from the Arp2/3-polymerized filaments that are elongated and bundled by Ena/VASP proteins and Fascin – the convergent extension model[237]. In line with this, it was recently shown that low levels of CPs localize throughout the filopodia and their depletion decreased filopodia length, altered filopodia shape and dynamics[238,239]. Nevertheless, Arp2/3 mutant cells still form filopodia[240,241], suggesting that, at most, the Arp2/3 complex may collaborate with Formins during filopodia initiation. Importantly, during filopodia formation, proteins containing I-BAR domains (Bin/Amphiphysin/Rvs), which are plasma membrane curvature-sensing and stabilizing domains, such as IRSp53, are also recruited and are proposed to bend the plasma membrane outwards, thereby facilitating membrane protrusion. Notably, both mDia2 and IRSp53 are recruited to initial sites of filopodium formation by Cdc42, the master regulator of filopodia formation (Fig. 11)[226].

Protrusive forces stem from filament polymerization and elongation at the tip of the filopodia, mediated by Formins and Ena/VASP (Table 1 and Fig. 11). Ena/VASP proteins play a dual function in filopodia elongation, since they act both as anti-capping proteins and F-Actin elongation machines. Actin filaments are tightly packed into bundles via the action of Actin crosslinkers, such as Fascin, α-Actinin and Fimbrin that undergo highly dynamic (order of seconds) cycles of binding/unbinding, thereby stiffening the network for membrane pushing (Fig. 11)[226,242]. Tight Actin bundling ensures that the buckling force exerted by a given number of filaments scales with the bundle radius to the power four. Bundle stiffening stems from the force required to break the bond between crosslinkers and F-Actin; the rupture force can range from 30pN for α-Actinin to 50pN for Filamin[185]. Similarly to protrusive forces driving lamellipodium extension, it remains unclear how many filaments are perfectly oriented with the plasma membrane and actually drive extension. Using optical traps to directly measure the forces generated by parallel bundles of elongating Actin filaments growing against a rigid barrier, showed that relatively low forces, on the order of 1pN, are sufficient to stall elongation. This is consistent with the load required to stall the elongation of a single Actin filament, suggesting at, any given time, only the longest filament is in contact with the barrier[243]. Whether a similar mechanism occurs in vivo is unclear, however this data argues that only a few filaments may actually push the plasma membrane forward. Importantly, filopodia elongation is mostly independent of MyoII motor activity (filament bundles

have parallel orientation), supporting that polarized Actin assembly at the membrane tip is indeed sufficient to drive membrane protrusion.

In summary, both branched and unbranched Actin networks can generate protrusive forces that power cell locomotion. Both in lamellipodia and filopodia, polarized Actin nucleation in the proximity of the plasma membrane coupled with a fine-tuning of network connectivity, disassembly and mechanics are sufficient to push the plasma membrane forward.

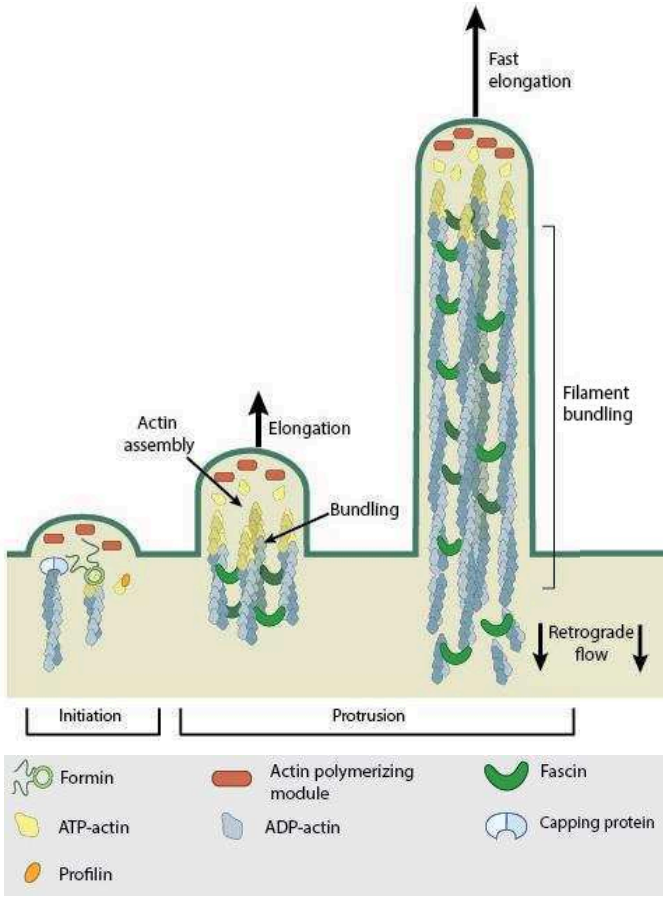

Figure 11: Filopodia formation and elongation.
Filopodia assembly can be initiated by uncapping of pre-formed Actin filaments or by de novo F-Actin nucleation. The filaments are then tightly packed into bundles, via the action of crosslinkers, such as Fascin. Finally, progressive F-actin elongation under the plasma membrane drives filopodia extension (adapted from: https://www.mechanobio.info/).

(ii) Contractile Forces:

MyoII isoforms are the main source of cellular contractility. Although we now understand how MyoII slides antiparallel Actin filaments, it remains puzzling how the motor can generate

predominantly contractile stresses in disordered networks such as those present in non-muscle cells. Since Myosin translocate towards the barbed ends with no intrinsic preference for generating contractile or extensile forces, symmetry breaking must rely on the intrinsic organization and architecture of the Actin network, rather than on the motor itself[196,199]. Accordingly, in vitro studies with polymerized Actin networks of defined geometries showed that network architecture sets the ability of MyoVI to induce contraction. Although MyoVI binding is homogenous along the network, its ability to induce contraction is restricted to antiparallel bundles and branched networks. Importantly, networks of mixed architectures showed faster contraction of the antiparallel bundles than of the branched regions, and no contraction of parallel bundles. These findings demonstrate that myosin motors intrinsically exhibit "orientation selectivity" and suggest a model where myosins can generate contraction even in disordered networks[244]. Importantly, differential contraction speeds can arise even within the same network architecture, as filament length scales with the number of myosin heads per unit and the tension is proportional to the number of myosin heads[245].

Another important parameter determining Myosin-generated contractility is the degree of network connectivity. In vitro studies showed that buckling effects dominate MyoII-induced contraction of cross-linked networks, as the filament strains correspond exactly to the extent of mesoscopic network contraction[208,246]. Highly cross-linked networks are intrinsically more resistant to individual filament motion (rotation, pivoting or sliding), thereby favouring buckling effects[205,208,247,248]. These findings support a model where the degree of network crosslinking must be tightly regulated to avoid "freezing" the network or, alternatively, crosslinking must be actively balanced with filament turnover. In agreement with this, the authors were able to restore contractility by adding ADF/Cofilin to highly cross-linked networks[248]. Since filaments break above a critical bending threshold, the build-up of MyoII compressive stresses is ideally placed to couple contraction and disassembly. Accordingly, it was reported in the same studies that portions of F-Actin bent to high curvature are more prone to severing[208,249]. Thus, compressive stresses induced by MyoII motor activity can couple network contraction to F-Actin severing, which, in turn, relieves stress by changing the filament length distribution (longer filaments are more prone to go beyond the buckling threshold and disassemble), generating new barbed ends available for polymerization and changing F-Actin density. Therefore, the intrinsic filament properties coupled with motor and crosslinking activities can generate asymmetric contractility of disordered actomyosin networks. Additionally, the extent of crosslinking strongly influences the transmission of contractile stresses within the actomyosin network, as a minimal degree of network connectivity is required to produce myosin-mediated contractility at large length scales[208]. Finally, not all crosslinking proteins promote contraction to the same extent. Crosslinking proteins vary in their size, affinity and compliance. Crosslinking proteins such as Fascin, which bind to polar, parallel F-

Actin, do not support contraction as α-Actinin and Fimbrin, which bind to filaments in a polarity-independent fashion (Table 1). Increased levels of polar crosslinking proteins might even give rise to non-contractile, dynamic states of Actin networks[244,247].

Additionally, Actin crosslinkers per se can generate contractile forces independently of Myo motor activity. Theoretically, binding of crosslinkers to the Actin network increases filament density; if the filaments are connected to an external load, i.e. adhesion complexes or the plasma membrane, the density increase will slowly produce network contraction (Fig. 12A). Also, filament disassembly can further enhance crosslinker-dependent contraction; if an intermediary filament bound to each of the grafted polymers undergoes disassembly, it may allow the two remaining polymers to bind, generating contraction (Fig. 12B)[250]. Such a mechanism of force generation could be involved in cleavage furrow ingression since it was reported that, in Dictostilium, MyoII-null cells undergo the mitotic cleavage stages with a speed comparable to wt cells[251]. Since MyoII also possesses crosslinking activity, it is possible that it may also generate contractility without using its motor domain. Accordingly, COS-7 cells expressing a motor-impaired version of MyoII, in a MyoII-null background, restored contractile ring constriction and at normal speed[252]. Similarly, it was proposed that the stabilizing effect of MyoII on the integrity of the Actin cortex relies, not on its motor domain, but in its ability to crosslink F-Actin[206].

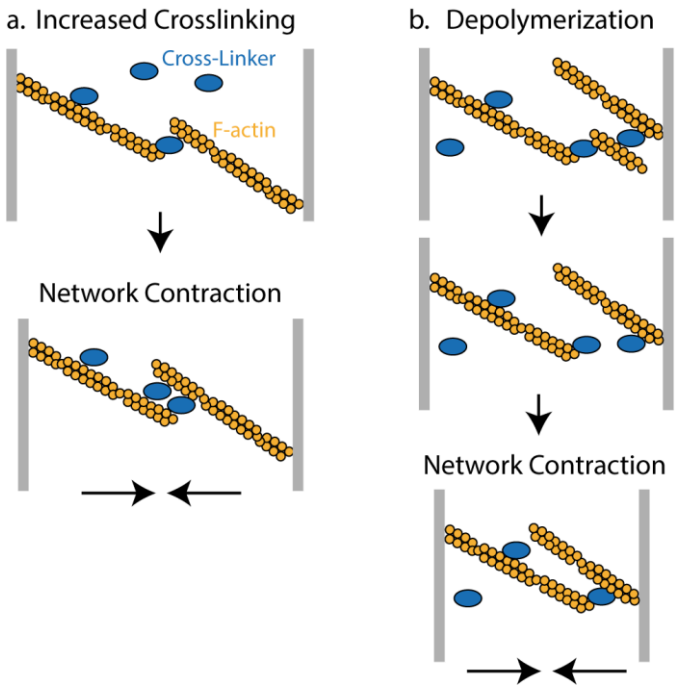

Figure 12: Production of contractile forces by Actin cross-linkers and depolymerization.
(A) Consider two Actin filaments attached at each side of a movable boundary, e.g. plasma membrane and a solution of Actin cross-linkers; when there is overlap between two filaments, the cross-linker can bind the

filaments together. The size of overlap can be increased by the binding of additional cross-linkers, an energetically favoured reaction that produces network contraction. Higher densities of cross-linking proteins produce larger, but slower, contractions. (B) In the presence of F-Actin depolymerization agents, an intermediary filament bound to each of the grafted filaments may be disassembled, allowing the two remaining polymers to bind each other via Actin cross-linkers, thus ratcheting the system in a contracted state (adapted from[250]).

Overall, symmetry breaking at the network level towards contractile forces mostly results from buckling of Actin filaments. Contractile forces are greatly affected by network connectivity, which is mediated by several Actin crosslinkers and MyoII itself. Network connectivity determines not only the length scale of contraction, but also the intrinsic network resistance to deformation. Accordingly, mechanically induced Actin severing is essential to prevent "freezing" of the actomyosin network, by releasing crosslinks, changing the length distribution of filaments and generating new barbed ends for growth. To illustrate how cells use contractile stresses to drive cell shape changes, I will briefly describe the example of cytokinesis.

- Contractile Forces during Cytokinesis:

Cytokinesis occurs just after chromosome segregation to the poles and it is required to partition the dividing cell's cytoplasm to the future daughter cells. Cytokinesis proceeds through the formation of an actomyosin contractile ring at the cell equator that is directly attached to the underlying plasma membrane. As the contractile ring constricts, it progressively closes the connection between the future daughter cells, until the midbody is formed (in-depth description in Chapter IV)[253]. To describe how contractile stresses drive cell shape in vivo, I will focus on contractile ring constriction.

Contractile rings form around the cell equator beneath the plasma membrane upon activation of the GTPase RhoA and are composed mostly of Actin filaments and myosin motors[253,254]. As visualized in a number of electron microscopy studies, the Actin filaments within the contractile ring are not orderly packed[255–258]. The mechanism driving contractile ring constriction is not fully understood. However two non-exclusive models for how contractile forces drive constriction have been proposed: (i) the more classical view is that myosin motors pull antiparallel Actin filaments to drive constriction; and, (ii) an alternative model suggests that depolymerization of cross-linked Actin filaments is the main driver of contractile ring constriction[259]. In both models, Myosin takes centre stage either by directly sliding Actin filaments or/and by triggering mechanically induced Actin disassembly. Although MyoII activity is essential for cytokinesis in most cell types, its exact contribution remains largely unclear. A recent study

showed that MyoII mutants unable to slide Actin filaments can still sustain tension and are able to rescue cytokinesis in myosin II–depleted cells both in culture and in myosin-mutant cells in mice[252]. These findings suggested that MyoII crosslinking activity might play an essential role during cytokinesis. Accordingly, in budding yeast, MyoII-induced Actin disassembly was shownt o be essential for contractile ring constriction[260]. Accordingly, both in vivo and in vitro studies showed that F-Actin turnover in the contractile ring is indeed decreased upon MyoII inhibition[261–263]. These studies highlight other relevant functions of MyoII for cytokinesis beyond its ability to slide Actin filaments.

To integrate all these aspects, physical models of contractile ring constriction were developed. Importantly, the proposed models must satisfy a key non-trivial prediction – that the rate of contractile ring constriction is constant throughout cytokinesis[264]. A model considering that contraction of a ring composed of parallel filaments is resisted by substrate adhesion, cell surface elasticity and cytoplasmic viscosity highlighted the importance of Actin polymerization and depolymerization throughout cytokinesis, suggesting that viscous dissipation is essential for the dynamics of contraction. Importantly, such model predicts that Actin concentration within the ring and consequently its power to drive contraction increases during constriction[265]. In line with this, Actin depolymerization was shown to be critical to set the rate of constriction in budding yeast, as Cofilin mutants or chemically stabilized Actin filaments exhibited delayed contractile ring constriction[260]. Another model predicted that tight cross-linking of individual Actin filaments into larger bundles, as well as filament turnover, would be essential for efficient contraction. In this model, the rate of ring constriction was limited by the F-Actin treadmilling rate[266]. In agreement with the importance of high-order Actin organization, Septins were shown to play an essential role in setting the rate of contractile ring constriction in Drosophila embryos and pupae[2,3,267]. Moreover, in vitro experiments showed that both Drosophila and mammalian Septins promote high-order organization of Actin filament into bundles and can even generate rings in the absence of MyoII[267].

Finally, following the observation that the rate of constriction scales with the initial ring diameter, it was proposed that the ring is composed of ‘‘contractile units’’, so that larger rings contain more units than smaller rings and thus constrict faster[264]. No evidence for the organization of filaments into contractile units was found, however more recent studies with in vitro polymerized Actin networks showed that the rate of MyoII contraction depends on the proportion of antiparallel filament bundles. Thus, by modulating the proportion of antiparallel and branched networks the authors were able to change the rate of network constriction, suggesting an alternative mechanism by which ring scalability could be achieved[244]. To further understand the contribution of MyoII and other crosslinkers to constriction, more careful experimental manipulations are required along with a general theoretical framework that can account for filament and motor properties as well as describe mesoscopically the network behaviour.

D. Actomyosin Flows: a dynamic behaviour of the actomyosin network

Actomyosin networks exhibit complex behaviours, such as flows and pulses. In this context, the distribution of MyoII motors and Actin is highly dynamic, generating deformations and stresses that evolve extremely fast in time and space, travelling the cell distance within seconds-minutes. These behaviours rely on the intrinsic properties of the actomyosin networks and have been implicated in an impressive number of force-generating processes. In this section, I will focus on how actomyosin flows are generated and regulated during cell migration and cytokinesis. Actomyosin pulses will be discussed in detail in the next Chapter, as this network behaviour is observed in epithelia and requires the integration of both actomyosin and AJ dynamics.

Actomyosin flows have been observed in a wide range of cellular processes, namely at the lamella during cell migration[268] and amoeboid migration[211,269], in cytokinesis[270] and upon antero-posterior axis polarization in the C. elegans zygote[166]. Actomyosin flows were also reported to contribute to tissue morphogenesis, as observed during germ-band extension in Drosophila[271], enveloping layer spreading in the Zebrafish embryo[272] and during wound closure in Xenopus[273]. Actomyosin flows were reported to be driven by: (i) polarized regulation of Actin polymerization/depolymerization, as observed at the leading edge during cell migration for example; and, (ii) contractility gradients, as observed during contractile ring assembly in cytokinesis.

(i) Actin Polymerization/Depolymerization-driven Flows:

To illustrate how cycles of assembly and disassembly of Actin networks can produce actomyosin flows, I will re-focus on lamellipodia-driven cell migration. As mentioned above, at the leading edge, Arp2/3-polymerized branched networks exert protrusive forces on the plasma membrane; however, for continuous Actin polymerization to occur, cells must mobilize a massive amount of Actin monomers to the vicinity of the lamellipodium. This is achieved via dramatic severing of F-Actin by the actomyosin network siting at the rear of the cell, coupled to the FAs and the region just behind the lamellipodia termed the lamella. Thus, a retrograde flow is formed from the leading edge towards the lamella, which predominantly involves Actin treadmilling, i.e. barbed end elongation balances pointed end depolymerization, so that on average the filament moves forward and keeps the same length. Concomitantly, an anterograde flow arises from the rear towards the lamella, resulting from stress fibre contraction. The convergence of both flows generates a zone of accumulation of G-Actin just a few micrometres away from the leading edge, termed the ‘convergence zone’ (Fig. 13)[187,226,274].

Since Actin treadmilling is an intrinsically slow process to account for the speed of cell locomotion, Actin severing and debranching enzymes are essential to accelerate the treadmilling phenomenon. ADF/Cofilin is enriched at the lamellipodium, where its activity is regulated by a balance between the activity of the LIM kinase and the Cofilin Phosphatase (Slingshot in flies)[227,275]. An homologue of Cofilin – Glia Maturation Factor (GMF), shown to prevent de novo Arp2/3-dependent polymerization and stimulate F-Actin debranching[276], was recently implicated, in both cultured $S2R^+$ cells and Drosophila egg chambers, in regulating the dynamics of the lamellipodia during migration[277]. Concomitantly, MyoII, which is associated with the FAs, drives, albeit to less extent, F-Actin disassembly at the rear, thereby generating an anterograde flow towards the lamellum (Table 1)[278,279]. The strength of adhesion to the substrate regulates the flow velocity, probably through its indirect effect on contractility. Accordingly, low adhesion accelerates the velocity of the Actin flows[209,210]. Importantly, a retrograde flow of MyoII was also characterized in the lamellipodium and proposed to participate in organizing the Actin filaments within the lamellipodium, leading to the formation of large actomyosin bundles[279]. Finally, Thymosin β4-bound G-Actin, that localizes to the leading edge in an Arp2/3-independent manner, also contributes to maintain a high G/F-Actin ratio at the lamellipodium by mobilizing additional G-Actin monomers from the cytosol to the leading edge (Table 1)[280]. Thus, lamellipodium retrograde flow relies on controlled assembly and disassembly of F-Actin, whereas Actin flows towards the lamellum are produced by the fluid-like properties of actomyosin and contractility (Fig. 13). The combined action of these mechanisms ensures a constant disassembly rate, thereby efficiently mobilizing G-Actin to the leading edge and fuelling Arp2/3-dependent Actin polymerization under the plasma membrane. Productive displacement also requires effective contraction at the lamellum, through a combination of contractile activity and attachment to the substrate[279].

Several questions regarding the mechanisms protecting the lamellipodia from full disassembly and how F-Actin polymerization/depolymerization coupling is achieved during migration still remain. Hsiao and colleagues recently reported, at least, a partial answer for the first question. The authors showed that a balance between the activities of ADF/Cofilin and Arp2/3 regulates Tropomyosin's binding to the branched network. Tropomyosin intrinsic ability to bind preferentially to ADP-Actin filaments near the pointed ends stabilizes the filaments upon ADF/Cofilin severing, thereby partially insulating the lamellipodial filaments from full disassembly[281]. These are particularly important findings, as it had been previously shown that Cofilin is able to displace the Arp2/3 complex from filament branches, thereby promoting disassembly throughout the leading edge[282]. Regarding the polymerization/depolymerization timer, MyoII would be an ideal candidate, as its accumulation in the lamellum is tightly coupled to the flow and it also modulates the rearward pulling forces[279].

Actomyosin flows are self-sustained in nature, as they are expected to passively affect the concentration profile of molecules interacting, even indirectly, with Actin via advection: faster retrograde Actin flows result in steeper concentration gradients, with higher concentrations at the rear and lower concentrations at the front[283]. This was recently demonstrated in bone marrow dendritic cells (BMDCs), whereby the authors modulated the velocity of actomyosin flows, as well as the concentration gradients of strong Actin binders. Such positive feedback enhances long-term cell polarization along the direction of movement, or in other words, cell persistence[284]. Since the speed and persistence of cell migration are generally correlated, this simple first-order principle could explain the mechanism underlying this coupling[284,285]. Since cells use many different modes of migration, it is possible that the molecular players underlying this coupling may vary. Nevertheless, good candidates for this role are proteins that both bind strongly to Actin, as its concentration gradient along the direction of flow will be steeper, and that modulate flow velocity. In line with this, the authors of the previous study showed that, at least for BMDCs, MyoII is likely to play this role, as motility strongly relies on the extent of MyoII activity[284]. Accordingly, in liver epithelial cells, inhibiting MyoII activity by blebbistatin treatment[286] or by MyoIIB RNAi, resulted in dramatic cell shape reorganization and a spontaneous switch towards migration. The molecular basis for this switch lies in the release of actomyosin bundles upon MyoII inhibition, suggesting that cells have a reserved pool of Actin and while it is "locked" in bundled networks, it is unavailable for dendritic growth normally driving cell motility[287]. Since Actin retrograde flows transport MyoII to the rear, motor activity in the back of the cell can locally 'lock' Actin in contractile bundles further polarizing the cell towards migration.

The dynamic reorganization of the lamellipodium through a combined effect of Actin polymerization/depolymerization and MyoII motor activity at the lamellum results in a very robust structure that can efficiently push the plasma membrane and power cell locomotion. In light of the recent findings regarding the importance of MyoII contractility during cell migration, it became clear that actomyosin flows are more dependent on contractility than previously anticipated. Thus, to address experimentally the relative contribution of F-Actin assembly and disassembly vs. MyoII motor activity, it would be important to compare cell migration speed and persistence in MyoII mutants lacking the motor domain or ATPase activity, as well as modulate the stability of Actin filaments and their ability to incorporate new Actin monomers.

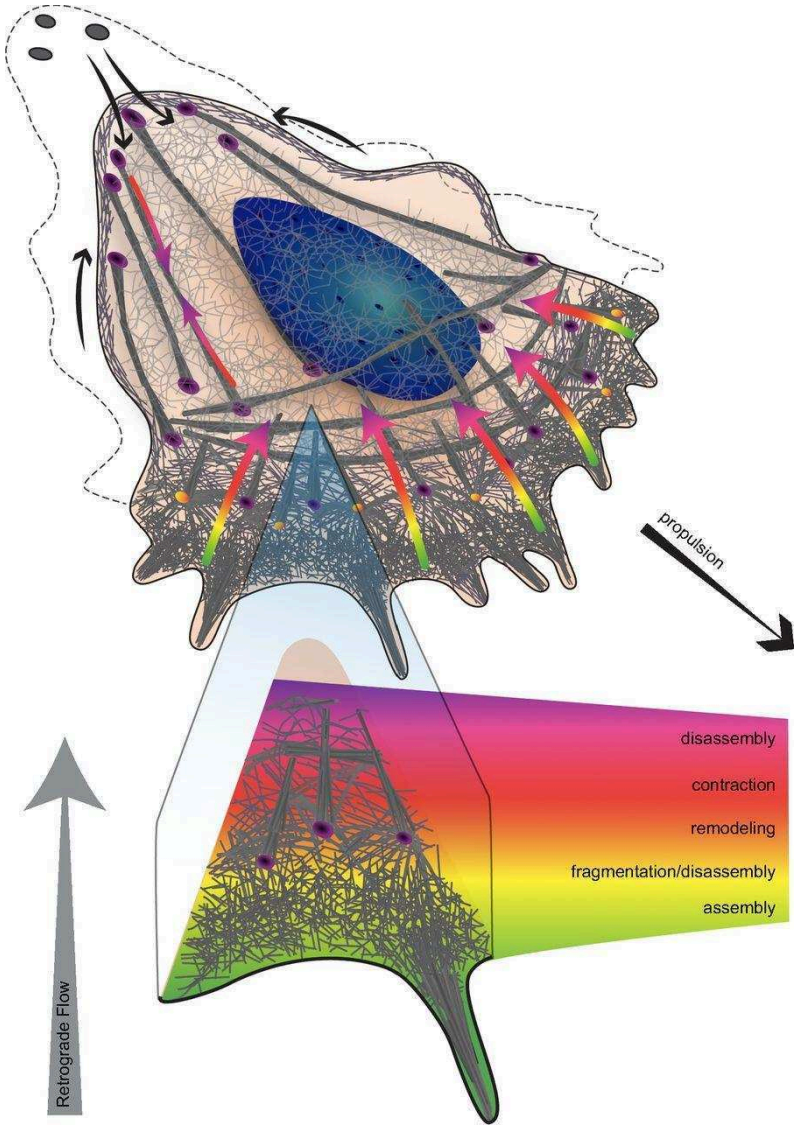

Figure 13: Actomyosin flows at the leading edge of a migrating cell.

The tight spatiotemporal coordination of F-Actin assembly and disassembly gives rise to the retrograde flows of actomyosin toward the cell centre. The colour code in the zoom region corresponds to the different mechanisms controlling Actin dynamics (assembly, fragmentation/disassembly, remodelling, contraction, and disassembly). This colour code is used also in the large arrows in the cell to illustrate where these different mechanisms occur during cell motility and the purple circles represent the FAs (adapted from[185]).

(ii) Contractility-driven Actomyosin Flows:

During contractile ring assembly, cortical actomyosin flows from the cell poles towards the equator. In contrast to the actomyosin flows observed in cell migration, during cytokinesis the cortical flows require MyoII ATPase and motor activities[288–290], supporting that they are indeed

contractility driven. Two partially redundant mechanisms contribute to support the cortical actomyosin flows, namely: (i) relaxation of the polar cortex of the dividing cell; and, (ii) MyoII activation at the cell equator, establishing high contractility at the equator and low contractility in the poles[288–293]. Pole relaxation is triggered by the asters that prevent the accumulation of contractile ring proteins in their vicinity; since the density of astral microtubules is higher at the polar cortex than at the equatorial cortex, this results in increased equatorial contractility relative to the poles[174,289,291]. Importantly, some actomyosin still remains at the poles, where it contributes to position the furrow and slow down constriction[294]. Concomitantly, the Centralspindlin complex, via MgcRacGAP, recruits Ect2, a Rho GEF, to the equator, which, in turn, locally activates RhoA and the subsequent cascade required for ring assembly[295–297] (Fig. 14; further discussed in Chapter IV).

Similarly to what was extensively described above, once the actomyosin flows form they can be sustained by positive feedback, as the flow accentuates the gradients of its own regulators, such as MyoII[187,269,284]. A coarse-grained model of cortical flows suggests that actomyosin flows arise from an increase in MyoII density and they also contributes to align the Actin filaments at the equator[298]. The role of MyoII in organizing and locking Actin bundles was recently demonstrated to be relevant for cell migration[287]. Importantly, MyoII also increases Actin turnover at the equator, suggesting that a gradient of MyoII concentration is also likely to establish a gradient of F-Actin turnover[261,262]. Theoretical studies and work done in budding yeast support that such feedback loop is also likely to be important for efficient contractile ring constriction during cytokinesis[260,265,266]. Together, these mechanisms reinforce the flow through polarized polymerization/depolymerization of Actin and Actin treadmilling, as observed in cell migration.

Since the cortical actomyosin flows occur on a sufficiently long timescale (seconds-minutes) to allow for stress dissipation by actomyosin remodelling and turnover, they rely on the fluid-like properties of actomyosin[299]. An important question is how a contractility gradient can impact the directionality and intensity of actomyosin flows. This question was addressed in the C. elegans zygote where it was shown that the gradient of contractility is transformed into a grade of anisotropic tension that pulls the actomyosin towards the strongest pulling area. The length scale of the flows are, in turn, set by a balance between Actin meshwork viscosity and attachement[299]. Presumably such model could also be valid for cytokinesis, as a similar contractility gradient is established from the poles to the equator. Accordingly, a recent theoretical work showed that such gradient is sufficient to drive cytokinesis and to reproduce its main features: contractile ring formation, cortical flow towards the equator and furrow constriction. Such model also highlights the critical influence of Actin turnover[300].

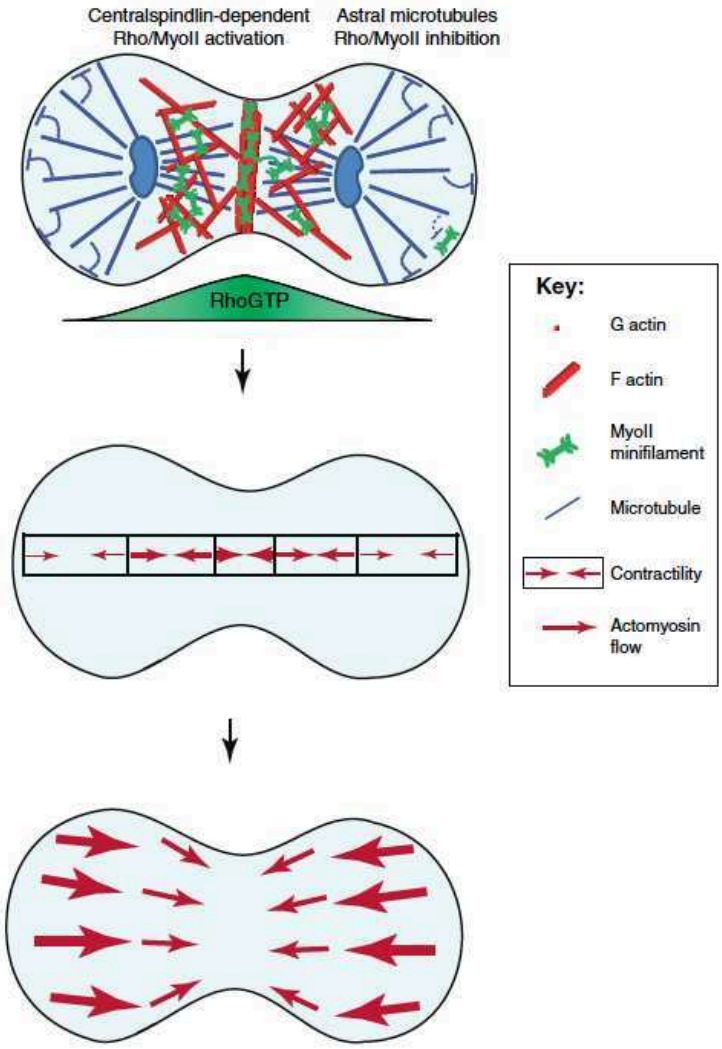

Figure 14: A gradient of contractility drives actomyosin flows during cytokinesis.

The spindle midzone promotes MyoII recruitment at the dividing cell's equator, while astral microtubules at the poles act to inhibit MyoII recruitment. The gradient of cortical RhoA activity is shown in the middle panel and the resulting contractility gradient is highlighted below (red arrows; adapted from[187]).

III. Interplay between Mechanical Forces and the Adherens Junction

"Cell and tissue, shell and bone, leaf and flower, are so many portions of matter, and it is in obedience to the *laws of physics that their particles have been moved, moulded and conformed. (...)* Their problems of form are in the first instance mathematical problems, their problems of growth are essentially physical problems, and the morphologist is, ipso facto, a student of physical science."

D'Arcy Thompson on "Growth and Form", 1917

An increasing body of evidence gathered over the past decades has placed mechanical forces on the centre stage as key regulators of cell dynamics and tissue morphogenesis[11]. Although the concept that biological systems must generate forces to move, divide or acquire shapes dates back to the 19th century, the advent of: (i) new microscopy techniques allowing scientists to record cell dynamics in vivo; (ii) the ability to estimate the forces produced by cells, using new biophysical approaches (Box 3); and, (iii) the combined power of experimental manipulation and theoretical models contributed to major advances in the understanding of how cells produce mechanical forces, as well as on the mechanisms used to convert a mechanical signal into a biochemical response, termed mechanotransduction[11,301,302]. Mechanical forces produced externally or endogenously, by the cytoskeleton, are transmitted to the neighbouring cells and the extracellular environment, via Cadherins (Cad) and Integrins respectively, thereby defining the adhesive contacts as essential mechanotransduction platforms. In this Chapter, I will first focus on how mechanical forces drive cell-cell contact remodelling and power tissue deformation in vivo and then discuss the mechanotransduction mechanisms operating at E-Cadherin-based junctions. Finally, I will compare mechanotransduction at the AJs with the classical Integrin-based pathways and briefly describe other modes of mechanotransduction.

A. Adherens Junction Remodelling by Mechanical Forces

Cellular processes, such as cell shape changes, cell division, cell intercalation or cell delamination events add, remove or exchange cell junctions and their integration in time and space regulates the final size and shape of epithelial tissues[303,304]. Junction remodelling is powered by contractile forces generated by the actomyosin cytoskeleton, which pull and deform the AJs. In turn, E-Cadherin junctions both resist deformation and transmit subcellular stresses to the neighbouring cells. Thus, I will briefly discuss how contractile forces regulate AJ organization and

remodelling in vivo and how this interplay can be used to power tissue morphogenesis. Since epithelial cell division is the focus of this work, I will not discuss this cellular behaviour in the present section and rather dedicate Chapter IV to review state-of-the-art knowledge in this field and outline the aims of my PhD project.

(i) Cell Shape Changes - Apical Constriction

Dramatic cells shape changes, such as apical constriction are observed during mesoderm invagination[305] and dorsal closure[163] in Drosophila, convergent extension of the dorsal and paraxial mesoderm of vertebrates[306,307] and neural tube closure in chicken[308]. To illustrate how mechanical forces act at E-Cad-based contacts to drive apical constriction and power tissue deformation in vivo, I will briefly describe mesoderm invagination in flies.

The first movement of Drosophila gastrulation is the segregation of the presumptive mesoderm towards the inside of the embryo, forming the ventral furrow (Fig. 15C). Mesoderm specification relies on two transcription factors – Twist and Snail, whose expression is activated by zygotic factors. Twist drives the expression of T48, a transmembrane protein that contributes for RhoGEF2 and Folded Gastrulation (Fog) apical enrichment. Fog is an apically secreted ligand that binds G-protein-coupled receptors (GPCRs) – Mist[309] (expressed in a Snail dependent-manner) and Smog[310], resulting in the activation of the heterotrimeric G proteins – Gα12/13 (known as Concertina in flies) and Gβ13F/Gγ1[12,310–313]. While Gα12/13 activates the medial-apical pool of MyoII, via its effector RhoGEF2[312,314], Gβ13F/Gγ1 activates MyoII both at cell junctions and at the medial-apical domain[310].

Apical recruitment of RhoGEF2 activates Rho1, which, in turn, promotes the subsequent activation of both ROCK (Rok in flies) and Diaphanous (Dia). This actomyosin meshwork adopts two behaviours: (i) a pulsatile medial-apical pool[305] and, (ii) supracellular cables of MyoII that accumulate at the cell-cell contacts (Fig. 15A,B)[315]. Actomyosin pulses, i.e. transient accumulations of Actin and MyoII, require a combined feed forward loop that orients MyoII motors, as well as a delayed negative feedback that eventually leads to the collapse of the network and allows a new cycle to start[187]. The pulsatile actomyosin network exerts transient traction forces on the cell-cell contacts, producing incremental reductions of cell perimeter – a ratchet-like mechanism (Fig. 15A,B)[305,316]. The regulation of MyoII phosphorylation status in the presumptive mesodermal cells is essential to drive pulsatilility, as expressing phosphomimetic and non-phosphorylatable forms of MyoII affects the dynamics of foci assembly and disassembly. Accordingly, both Rok and Myosin phosphatase localize dynamically with MyoII in these foci[317]. It was recently shown in germ-band cells that actomyosin oscillations are an emerging property of the network and arise from a combined effect of the molecular cascade regulating MyoII activity

and advection that concentrates Myo and its upstream regulators in the apical cortex. The progressive densification of the network locally increases friction at the cortex, thereby reducing the advection and providing a negative feedback[318]. This work provided a paradigm to understand actomyosin oscillatory behaviours and it would be interesting to test whether similar mechanisms operate in mesoderm cells. The magnitude of MyoII pulses, as well as the transitions from unratcheted-to-ratcheted pulses increases in a Twist-dependent manner. Additionally, cells undergoing ratcheted pulses have higher probability of having neighbouring contractile pulses than expected by chance, suggesting a mechanosensitive process[315,319]. An important aspect that remains poorly explored is how Actin dynamics is regulated during actomyosin pulses. The assumption is that MyoII determines F-Actin turnover and accumulation, however it was shown that when Rok is inhibited, F-Actin cables continue to assemble and disassemble, showing that Myosin is to some extent dispensable for medial apical F-Actin organization[320].

To ensure the irreversibility of each step of contraction, Twist also promotes the accumulation of actomyosin at the cell-cell contacts in supracellular cables, thereby preventing cell relaxation in between each pulse. The coupling between such structures and the AJs is essential to organize the actomyosin network and to couple neighbouring cells[315]. Accordingly, integrity of the E-Cad junctions and their attachment to the actomyosin cytoskeleton are essential during ventral furrow formation, since E-Cad, β-Cat, α-Cat or Afadin (Canoe in flies) depletion results in tears in the normally intact supracellular myosin meshwork that spans the ventral tissue (Fig. 15A)[84,315]. Recently it was proposed that stable attachment between the contractile machine and AJs during apical constriction also requires rapid turnover of the apical F-Actin meshwork[321].

Altogether, these findings support that apical constriction requires concerted activation of actomyosin-generated mechanical forces, which are resisted and integrated by E-Cad junctions, thus allowing long-range force transmission, an essential feature to achieve coordinated tissue invagination.

(ii) Cell Intercalation

Cell intercalation involves an initial step of junction contraction, where four or more cells are brought into contact and a subsequent step of junction growth, orthogonal to the original cell-cell contact, thereby generating new adhering neighbours (Fig. 15F). Oriented cell intercalation events power tissue extension in vivo, namely convergence-extension movements during germ-band extension[271] in flies and in the Xenopus mesoderm[322], as well as scutellum contraction in the Drosophila pupal notum[323]. To illustrate how mechanical forces promote polarized cell intercalations and drive tissue extension in vivo, I will briefly describe germ-band extension (GBE) in Drosophila.

In flies, the pair-rule transcription factors Eve and Runt provide the instructive polarity cues for GBE, a process by which the germ-band doubles its length along the anterior-posterior axis and shrinks along the dorsal-ventral axis (~2 hours; Fig. 15F)[324]. Downstream of the pair-rule genes, a spatial code of Toll receptors (2/6/8) regulates polarized tissue extension[325]. Such dramatic tissue extension arises mostly from the intercalation of cells along the dorsal-ventral axis[324,326], with contributions from cell shape changes[327] and oriented cell divisions[328]. Planar polarized cell intercalation is driven by the complementary localization of RhoGEF2, MyoII, Rok, Shroom (an activator of Rok) and F-Actin, which are enriched in anterior-posterior or vertical junctions and E-Cad, β-Cat and Par3 (Bazooka in flies) accumulation at dorsal-ventral or horizontal junctions (Fig. 15D)[106,161,326,329–331]. The opposed distribution of the actomyosin cytoskeleton and the adhesion machinery suggests that upon anterior-posterior junctions shrinkage, a new junction will then be added along the dorsal-ventral axis (Fig. 15D,F)[326,332].

MyoII and F-Actin do not statically accumulate at the AJs, but rather exhibit medial actomyosin flows (Fig. 15E). Such medial flows of actomyosin contribute for oriented junction shrinkage, as laser ablating of this medial pool affects junction contraction. Nevertheless, junctional actomyosin accumulation is also required to stabilize the contraction produced by the actomyosin flows, much like the previous ratchet model[271]. E-Cad and α-Cat are required to physically stabilize actomyosin at the junctions and to orient the actomyosin flows, as their depletion results in continuous centripetal flows[271,333]. Accordingly, upon vertical edge shrinkage, MyoII flows in between the junctions with lower E-Cad levels. In line with a role for E-Cad levels in polarizing the actomyosin medial pool, the authors showed that by modulating E-Cad endocytosis, which decreases the extent of E-Cad planar polarization, affects both the magnitude and the speed of the medial actomyosin flows[106,333]. Thus, the authors proposed that planar polarization of the medial actomyosin flows emerges from transient fluctuations in E-Cad levels at the vertical junctions, which generates fluctuating asymmetries in actomyosin coupling to the AJs[333]. Beyond the classical intercalation events described, a more regional mechanism of junction remodelling is also observed – termed rosettes, which also resolves in the direction of tissue extension[330,334]. Rosette formation results from the simultaneous shrinkage of several junctions, thereby bringing together more than 3 cells. In rosettes, junction shrinkage also requires MyoII activity, as MyoII mutants show defects in rosette formation[161].

Recent work showed that polarized addition of a new junction following junction shrinkage contributes dramatically to tissue extension. In contrary to the previous notion, polarized addition of a new junction does not reflect passive stress relaxation, but rather results from active junction growth. Strikingly, junction elongation requires MyoII flows in the cells neighbouring the intercalating cells, thereby generating anisotropic anterior-posterior pulling forces that contribute to new junction elongation[335]. The molecular mechanism regulating these MyoII-dependent forces is

not yet clear. Previous work, in the Drosophila pupal wing, reported that junction elongation requires a specific down-regulation of MyoII activity at the growing junction, downstream of the lipid phosphatase PTEN (Phosphatase and Tensin Homolog), which converts PIP3 into PIP2. Since the levels of both PIP3 and MyoII are anti-correlated with junction elongation, the authors proposed that PTEN activity promotes PIP2 accumulation at the elongating junction, leading (by an unknown mechanism) to a subsequent decrease of MyoII, thereby allowing the new AJ to grow[336]. It will be interesting to test whether both mechanisms cooperate to promote junction growth or whether they represent different strategies to promote junction elongation following an intercalation event. Overall, GBE results from two successive planar polarized and active processes; initially, anisotropic stresses drive irreversible junction shrinkage and eventually, a new junction is added by active growth.

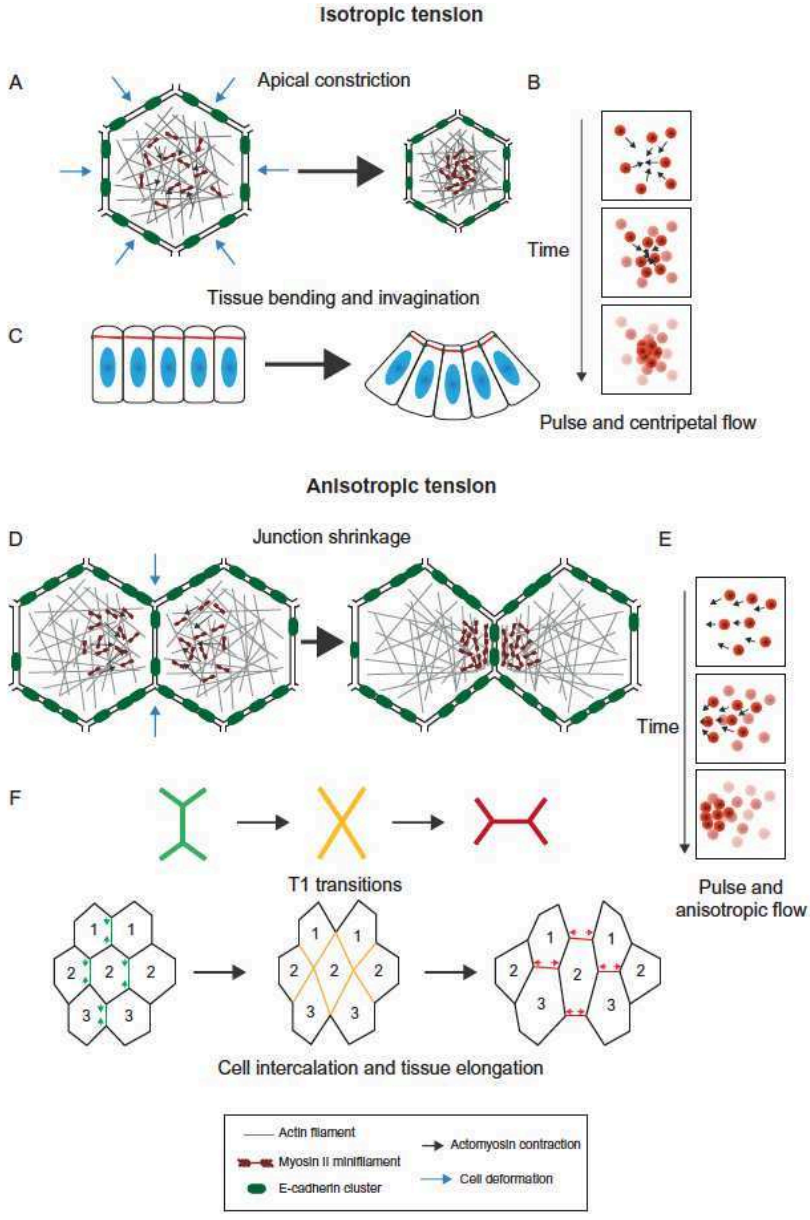

Figure 15: Mechanical forces power isotropic or anisotropic junction remodelling and drive epithelial tissue morphogenesis.

(A) In Drosophila mesodermal cells, apical constriction is mediated by isotropic actomyosin pulling forces that constrict the apical cell surface. (B) During apical constriction, the actomyosin networks adopt a pulsatile behaviour; actomyosin flows in a centripetal fashion, accumulating in foci that eventually coalesce (red dots; shaded dots correspond to the previous position of MyoII molecules during the pulse). (C) Apical constriction across a cohesive sheet of epithelial cells powers tissue bending and invagination. (D) In Drosophila germ-band cells, E-Cadherin clusters and the actomyosin distribution is anisotropic and complementary, resulting in polarized shrinkage of vertical junctions. (E) In germ-band cells, actomyosin flows toward vertical junctions, thereby promoting junction shrinkage (red dots; shaded dots represent the previous position of MyoII during the emergence of the flows). (F) Vertical junction shrinkage is followed by the formation and extension of a new junction in the perpendicular direction (T1 transition), resulting in cell intercalation and tissue extension (adapted from[114]).

(iii) Cell Delamination

Cell delamination is the process by which cells are eliminated from epithelial sheets. Cell delamination can occur as a consequence of apoptosis, but live cells were also reported to be able to delaminate, usually in regions where the tissue is under compression[176,337–340]. However, in the Drosophila pupal notum, the observation that live cell delamination can actually occur in the tissue midline was recently disputed by the observation that Caspase 3 activation both precedes and is strictly required for cell delamination to occur[338,340]. Thus, subsequent studies are required to clarify whether epithelial tissues must reach a given threshold of compression to trigger live cell delamination or whether that is a specific property of some epithelia. Importantly, apoptotic cell delamination was shown to promote tissue bending in the Drosophila leg epithelium[341], highlighting a more active role for cell delamination in shaping epithelial tissues.

Cell delamination follows a stereotyped sequence of events that culminates with extrusion from the epithelial layer; if delamination is triggered as a consequence of apoptosis, then it culminates with fragmentation of the cell into apoptotic bodies[342]. In vertebrates, epithelial cells delaminate apically, while, in flies, delamination occurs from the basal side of the epithelium[338,339]. This different behaviour may reflect the differential positioning of the TJs and SJs in these two models. However a general description of events at the TJs/SPs during cell delamination is still lacking, as all the studies have so far focused on the role of the AJs and the contractile apparatus acting at the apical domain. Thus, the initial step of delamination is an initial reduction of the apex size of the extruding cell and, subsequent dismantling of the AJs established with its neighbouring cells. Importantly, E-Cadherin is itself a Caspase substrate, thus, in apoptosis-induced

delamination, progressive junctional dismantling is likely to be a direct consequence of Caspase activation[343]. In live cell delamination, junction remodelling is powered by local intercalation events, resulting in a progressive loss of cell-cell contacts with the delaminating cell[338]. Concomitantly, an actomyosin cable is formed initially exclusively in the delaminating cell and subsequently also in the neighbours[344]. Importantly, apoptosis-induced delamination, at least in MDCK monolayers, relies solely on actomyosin activity in the neighbouring cells, rather than on the delaminating cell itself[337]. Thus, it would be important to test whether this is also the case in live-cell delamination events. Actomyosin cable formation was proposed to rely on a signal sent by the delaminating cell, namely the levels of sphingosine-1-phosphate (S1P). Accordingly, in MDCK monolayers, extracellular S1P is sufficient to activate cell extrusion and Zebrafish mutants lacking the S1P receptor, S1P2, no longer show cell delamination events in highly crowded tissue regions[345]. However, this is unlikely to be the only signal, as laser-induced delamination also results in the formation of an actomyosin cable[346]. Finally, after full constriction of the extruding cell apex, a new AJ is then assembled between the neighbouring cells[176,337,338,341]. The mechanisms underlying junctional and actomyosin remodelling in both the delaminating cell and its neighbours are still under intense investigation.

E-Cadherin-mediated adhesion is essential for cell delamination, as cells expressing low levels of E-Cad show defective apoptotic extrusion. Moreover, the usual elongation observed in the neighbouring cells during delamination is lost, indicating that tissue integrity is impaired[347]. These findings support an important role for E-Cadherin in mediating actomyosin anchorage to the AJs during rosette formation and in maintaining tissue cohesiveness during delamination. Although this may sound slightly in opposition with previous reports, it is likely that adhesion remodelling occurs progressively during apical surface constriction in the delaminating cell. Accordingly, studies in the Drosophila leg epithelium indeed reported such two-step mechanism. Initially, the delaminating cell constricts its apical surface, without loss of adhesion, thereby dragging the neighbouring cells and likely maintaining tissue cohesion. Subsequently, a peak-like structure enriched for adhesion molecules, such as E-Cad, β- and α-Catenin forms within the delaminating cell and an actomyosin cable arises from this structure. The actomyosin cable produces pulling forces that drag both the delaminating cell and its immediate neighbours more basally, transiently deforming the epithelium apical surface[341]. Although many questions remain, these findings highlight a tight interplay between the actomyosin cytoskeleton and the adhesion machinery during cell delamination, as well as a remarkable collaboration between the delaminating cell and its neighbours.

In summary, these studies highlighted how mechanical forces act at cell-cell contacts to induce localized or global junction remodelling, powering tissue deformation in vivo. For the next section, I will focus on how the E-Cad-based junctions can sense and respond to mechanical forces.

B. Mechanotransduction at E-Cadherin-based Junctions

E-Cadherin molecules can bear force, as evidenced mesoscopically by the recoil observed upon AJ laser ablation[103,111,299,332,334,348]. Using an E-Cad FRET (Förster resonance energy transfer) sensor designed to be tension-sensitive (Box 3B), it was demonstrated, first in MDCK monolayers[349] and later in the Drosophila ovary[350], that E-Cad is constitutively under tension, due to the activity of the actomyosin cytoskeleton[349,350]. Externally applied forces also increase tension across E-Cadherin molecules, since applying uniaxial stretch to pairs of contacting cells further decreased the FRET index[349]. In agreement with this, magnetic twisting cytometry assays using E-Cad-coated beads (MTC; Box 3D) showed that the relative stiffness of E-Cad bond scales with the magnitude of the applied shear[129]. Similarly to E-Cad, MTC assays and traction force microscopy (Box 3C,D) were employed to show that both VE-Cadherin and N-Cadherin bonds are also mechanosensitive[351–355]. Altogether these findings supported that force-sensing mechanisms operate at Cadherin-based junctions and that Cad molecules can respond to both exogenous and endogenous forces, generated by the actomyosin cytoskeleton. In the present section, I will describe the molecular mechanisms underlying force sensing/transmission at E-Cad junctions, followed by the cellular consequences of Cad mechanotransduction.

Box 3: Approaches to test intercellular forces and mechanosensing through adhesion receptors.

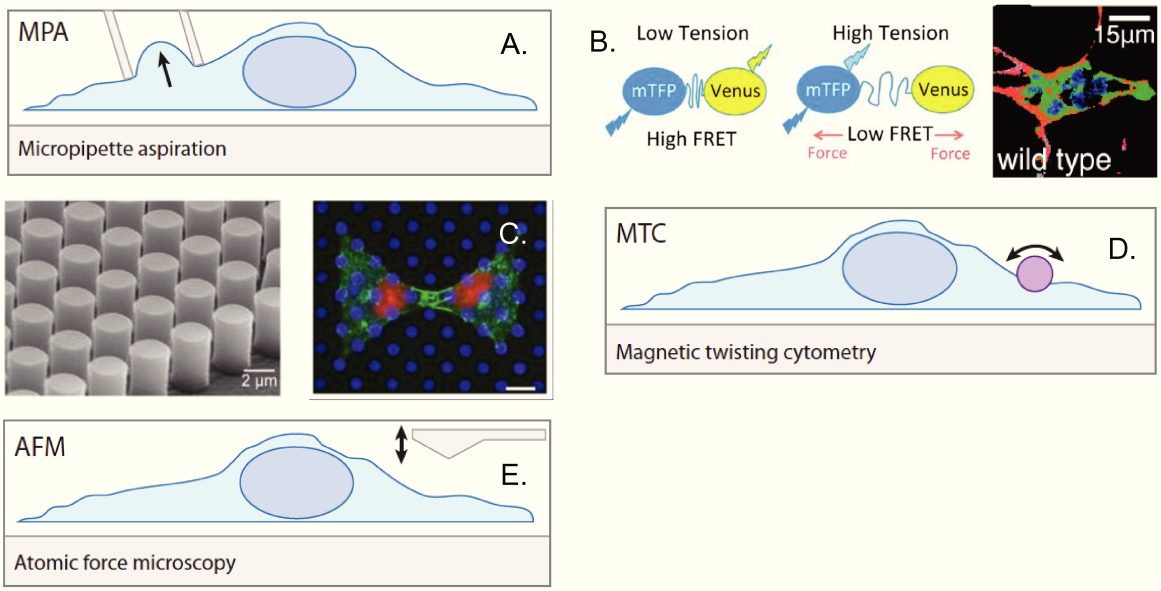

(A) Micropipette Aspiration Assays involve partial suction of single cells or cell droplets into the pipette using a negative pressure and it can be used to measure the tensile and shear stresses[356,357]. (B) Tension-sensitive FRET sensors are composed of two fluorophores, in this example the Teal fluorescent protein (mTFP) and Venus separated by a nanospring protein domain from spider silk. In the relaxed state, the two

fluorophores are close enough to allow FRET (left); while in response to pN forces, the domain stretches and FRET is reduced (right)[350,358]. The FRET image on the right shows a border cell in the Drosophila ovary expressing a tension-sensitive FRET of E-Cad (high FRET ratio in red and low in blue)[350]. (C) Traction Force Microscopy uses beads embedded in a soft gel (not shown) or elastomeric pillars (left) to infer the traction forces exerted by cells on a substrate on in a cell-cell contact. Mechanical forces are inferred from the deflection patterns of the pillars, which act independently and allow the detection forces of the order of 1 nN. Between cell doublets constrained to such array (right), the net force at the cell-cell contact correlates with an increase in the size of the intercellular junction, indicated by β-Cat (green)[359–361]. (D) Magnetic Twisting Cytometry uses magnetic beads functionalized with adhesion receptors at its surface, as well as an oscillating magnetic field. The coated beads are brought into contact with the cell surface and subjected to an orthogonal magnetic field, which induces a torque on the bead. The amplitude of the resulting bead displacement reflects the stiffness of the attachment between the adhesion receptors. (E) Atomic Force Microscopy uses a cantilever (can also be functionalised with adhesion receptors) to map the topology and stiffness of the cell surface and the cellular adhesion forces. AFM probes very local properties at the subcellular scale, providing a map of the cell mechanical properties[360].

(i) Sensing and Transmitting Mechanical Forces via E-Cadherin

Mechanical forces affect E-Cad adhesion by modulating its affinity, as well as its interaction with the cytoskeleton, via α-Catenin (α-Cat). A tension-induced conformational change of the α-Cat molecule is another key mechanism providing mechanosensitivity to the AJs. Finally, tension also modulates the dynamics of the actomyosin network, which, in turn, regulates E-Cad stability at the membrane.

- Catch Bond Behaviour:

Applying a mechanical load to interacting biomolecules can result either in: bond detachment and/or a more short-lived bond – slip bond; or bond reinforcement, due to increased affinity and/or a more long-lived bond – catch bond; or no bond change – ideal bond. Catch bonds are particularly relevant for mechanotransduction, as they stabilize attachment under tension usually by inducing conformational changes in the interacting proteins[7,362]. Examples of such behaviour were described for several proteins involved in mechanotransduction cascades, such as: (i) Myosin[363]; (ii) Selectins[364–366], which are expressed by many white blood cells and are sensitive to shear stress; (iii) FimH, an Escheria Coli protein that promotes shear-enhanced adhesion[367]; and, (iv) Integrins[368,369]. For Cadherins such behaviour, as well as its molecular basis, was more recently demonstrated. Using single-molecule AFM force clamp spectroscopy (Box 3E), in which

immobilized E-Cadherins are allowed to interact under a clamping force, it was shown that E-Cadherin homophilic bonds respond to mechanical stimulation[370,371]. Similar observations were reported for Xenopus Laevis C-Cadherin[372–374]. These studies demonstrated that Cad-Cad interactions behave like a catch bond under tension. Furthermore, this behaviour was shown to be independent of the Cad cytosolic tail, suggesting that catch bond stabilization occurs at the level of the extracellular (EC) domains[370–374].

The molecular basis for the catch-bond behaviour of Cadherins came from crystallographic studies describing two possible conformations for Cad dimers, either the strand-swap or the X-dimer conformation (Fig. 3; in-depth description in Chapter I). E-Cad mutants "locked" in the X-dimer conformation exhibit catch-bond behaviour, as the bond lifetime increased with the applied force (until the critical value of ~30pN). Conversely, mutants "locked" in the strand-swap conformation behaved like a traditional slip bond. Interestingly, at very fast interacting times (0.001-0.05s), wt Cad dimers are insensitive to force, a feature of ideal bonds. Thus, the authors hypothesized that, at these timescales, Cad dimers are transitioning from the X-dimer to the strand-swap conformation[371]. Since all Cadherins tested can form X-dimers (although this may not be the preferred conformation for classical vertebrate Cad), it is tempting to speculate that the force-dependent reinforcement of Cad homophilic engagement is a major mechanotransduction mechanism.

Many open questions remain, for example, it is unclear what is the prevalent conformation of Cad molecules at nascent vs. mature AJs. In line with this, it was shown that although both Cad dimer conformations can cluster at the AJs, the strand-swap dimers are more stable, leading the authors to propose that adhesion is based on strand-swap interactions[29]. Another open question is how Cadherin cis associations and clustering modulates single-dimer conformation, and vice-versa. The role of Cad EC domains in lateral associations is still a matter of debate, as biophysical measurements of the E-Cad full EC1-5 domains detected three distinct bonds, while only two bonds were identified with the EC1-2 fragment (presumably corresponding to the X-dimer/strand-swap conformations), suggesting that the additional bond could result from lateral association with neighbouring Cad molecules[101,370,372,374,375]. Yet, Cad double mutants unable to adopt X-dimer/strand-swap conformations cannot be recruited to the AJs, not even in the presence of endogenous wt Cad, supporting that the putative "third interface" is unable to establish cis interactions with other Cad molecules in the absence of the EC1-2 interactions[29]. An alternative model would be that proximity between Cad molecules in the membrane facilitates the formation of weaker cis interactions, mediated by the full Cad ectodomains[27]. Finally, it is important to determine how the catch/slip bonds behave at endogenous forces, as even E-Cad X-dimers act as slip bonds above a critical force (30pN)[371].

Catch bond behaviour was also recently described for α-Catenin, enhancing its ability to bind simultaneously Actin filaments and the adhesive complex E-Cad-β-Cat. Using a single-molecule optical-trap-based assay, the authors showed that the application of pN forces on the Cadherin-Catenins complexes increased the lifetime of its bond with Actin, such that at intermediate forces (~8 pN) the lifetime of the bonds dramatically increased relative to those observed at lower forces. α-Cat was proposed to adopt a two-state catch-bond, in which mechanical loads both accelerate the transition to the strongly bound state and "lock" the molecule in this conformation. Conversely, above a critical level of force (~10 pN) the dissociation of Cad-Cat complexes from Actin filaments is accelerated[70]. In agreement with other studies, the dissociation events observed in this setup resulted from the unbinding between the intact Cadherin-Catenins complex and the Actin filaments, rather than from the dissociation of the E-Cad-β-Cat-α-Cat complex[37,38,70]. The challenges now are to determine the molecular basis for the α-Cat catch bond, as well as to understand the relative contribution of E-Cad and α-Cat catch bonds to mechanotransduction. Altogether, tension-dependent reinforcement of E-Cad homophilic engagement, as well as its interaction with Actin filaments, via α-Cat, is likely to constitute an essential feedback loop to strengthen the link between the adhesion complexes and the underlying actomyosin cytoskeleton under tension.

- Tension-dependent Conformational Switches:

A detailed structure-function analysis of α-Cat showed that, unlike wt cells where Vinculin is only detected at nascent contacts, in cells expressing an α-Cat mutant version lacking a sequence in its central domain, Vinculin becomes constitutively localized at the AJs. These findings suggested that this α-Catenin sequence usually prevents Vinculin recruitment to mature AJs, possibly by mediating intramolecular associations that mask the Vinculin binding site (VBS)[131,376]. In agreement with this, α-Cat mutants lacking this inhibitory region are the only α-Cat fragments able to efficiently bind Vinculin in vitro at ~1:1 ratio[131,377]. As a key demonstration that α-Cat can indeed coexist at the AJs in two conformational states, an epitope-specific antibody was able to detect exclusively the "open" conformation of α-Cat – competent for Vinculin binding[131,376]. Importantly, upon blebbistatin treatment (which inhibits MyoII activity)[286], α-Cat remained "closed" and Vinculin was no longer recruited to the junctions[129,131,132]. Thus, a model was proposed whereby α-Cat intramolecular interactions are released under tension, thereby exposing cryptic binding sites for Vinculin and recruiting it to the AJs (Fig. 16)[131]. In agreement with this, MTC assays in cells expressing an α-Cat FRET sensor (Box 3B,D) showed that α-Cat can indeed undergo a rapid, yet reversible, conformational switch upon mechanical stimulation at Cad bonds. Both β-Catenin and F-Actin binding domains are essential for α-Cat unfurling, while, Vinculin

binding is dispensable[378,379]. Nevertheless, Vinculin binding does stabilize α-Cat in the ”open” conformation, which is likely to prolong tension-dependent AJ reinforcement[380].

The mechanism of Vinculin recruitment to the AJs by α-Cat is still unclear. Vinculin itself is an auto-inhibited molecule, thus it requires an activation step previous to its AJ recruitment to release intramolecular interactions that maintain it in a “closed” conformation[377,381,382]. Crystallographic studies showed that the head and tail domains of Vinculin bind each other with high affinity and proposed that Vinculin is likely to be activated in a cooperative manner requiring at least two binding partners[382,383]. Although it was shown that α-Catenin can bind and activate Vinculin even in the absence of a second ligand, the efficiency of activation is much lower than in the presence of Actin[377,383,384]. In line with this, it was proposed that rather than a direct α-Cat-dependent Vinculin activation, F-Actin binding initially unfurls Vinculin, which then allows for α-Catenin binding[384]. Since Vinculin also binds β-Catenin, an alternative model would then be that Vinculin is initially recruited to the AJs in a β-Cat-dependent manner[41]. In line with this, Abelson kinase (Abl) tension-dependent phosphorylation of Vinculin is required for β-Cat binding and its recruitment to the junctions[385]. However, the general relevance of such pathway remains uncertain, as it was shown that in, α-Cat mutant cells, Vinculin is lost from the AJs[354,376,386,387] and that α-Cat, but not β-Cat, binding can activate Vinculin[383]. Furthermore, E-Cad-α-Cat fusions can rescue α-Cat loss of function in many systems[36–39,376]. Finally, Myosin VI, a minus-end directed myosin motor, was also implicated in Vinculin recruitment to the AJs[388]. This Myo motor contributes to the transition between nascent to mature AJs, at least partially via Vinculin function[388].

Although the exact nature of Vinculin recruitment to the AJs remains elusive, in a wide range of cultured cells, its function at the junctions is essential for force-dependent E-Cadherin stiffening, as Vinculin knockout cells showed reduced spreading on E-Cad-coated substrates, indicative of lower adhesion[129,354]. This was confirmed by MTC assays (Box 3D), which showed that force-dependent E-Cad stiffening was up to 50% lower in cells lacking Vinculin expression[129]. Moreover, Vinculin-mediated E-Cad mechanosensing regulates efficient epithelial barrier formation in MDCK monolayers[132]. Similarly, in endothelial cells Vinculin associates with VE-Cad and powers force-dependent AJ remodelling[129,376,386,388–390].

Vinculin-dependent reinforcement of the AJs is proposed to result from increased attachment of the actomyosin network to the cell-cell contacts by establishing additional bonds between α-Cat and the actomyosin cytoskeleton[129,376]. Upon activation, Vinculin exposes cryptic binding sites for a number of binding partners, namely: α-Actinin, VASP, Arp2/3 complex, Vinexin, Ponsin, Talin, Paxilin, PIP2 and F-Actin[391]. In line with this, Vinculin not only increases the number of attached filaments at the AJs, but also promotes additional F-Actin nucleation/elongation, via the Arp2/3 complex and/or VASP (Table 1)[392,393]. Since Vinculin can also recruit monomeric G-Actin and form a new seed for Actin polymerization, it is possible that it

can also promote Arp2/3-independent Actin polymerization[394]. Moreover, the combined effect of increased α-Actinin recruitment to the AJs and Vinculin's intrinsic bundling activity could also result in a dramatic remodelling of the actomyosin network at the cell-cell contacts and potentially contribute to junction reinforcement[274]. Finally, it was shown that Vinculin is itself under tension at the AJs, which correlates with the molecule adopting an "open" conformation; nevertheless Vinculin conformation does not change upon tension release, due to Y-27632 treatment (a ROCK inhibitor)[392,395,396]. Thus, it is unclear whether tension affects Vinculin directly, or indirectly by modulating α-Cat conformation. Therefore, the exact contribution of each of these mechanisms for Vinculin-dependent AJ reinforcement is still unclear. Remarkably, Vinculin is a non-essential gene in Drosophila[397]. This apparent conundrum challenges the idea that Vinculin recruitment to the AJs is decisive for mechanotransduction in flies. Thus, it is possible that other proteins that can be recruited in a tension-dependent manner to the AJ, such as Formins[398–400] and/or VASP[401], can compensate for loss of Vinculin. Alternatively, catch bond behaviour at the level of the E-Cad molecules could be more relevant in invertebrates, rendering the AJs intrinsically more resistant to force[31,402].

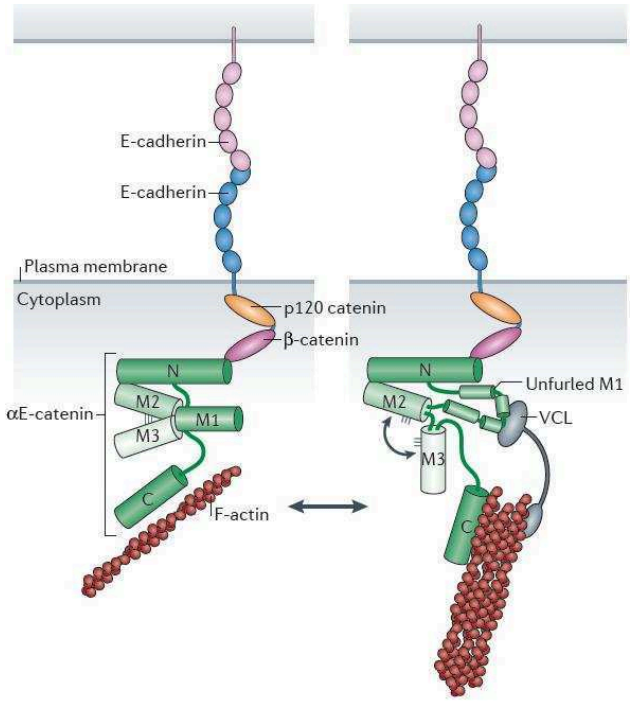

Figure 16: Tension-dependent α-Catenin conformational switch.

Crystal structures of mammalian αE-Catenin, where the Modulatory domains 1-3 (M1-M3) adopt an auto-inhibited conformation, preventing its interaction with Vinculin (VCL; shown on the left). The grey lines highlight additional interactions required to maintain the closed conformation. On the right, the open state of αE-Catenin is illustrated, in which the M2-M3 interface is disrupted, exposing the VCL binding site (adapted from[25]).

Importantly, unfolded α-Cat can also interact with other ABPs beyond Vinculin, such as α-Actinin, Formin1 and Afadin, thereby providing additional cascades for the regulation of tension-dependent AJ remodelling[27]. α-Actinin, an Actin crosslinker cooperates with the Arp2/3 complex for de novo Actin assembly at apical E-Cad/α-Cat puncta[72]. Using a hydraulic apparatus to apply load to intercellular junctions in a confluent monolayer it was shown that both α-Actinin-4 and Actin rapidly accumulate at the AJs and this is required for junction stiffening. α-Actinin-4 tension-sensitive recruitment to the AJs is mediated by Synaptopodin, which also binds β-Cat and MyoII. Synaptopodin depletion prevents junctional accumulation of α-Actinin-4, Vinculin and Actin, thereby decreasing the junction strength, cellular contractility and increasing the monolayer permeability[403]. α-Actinin also binds Vinculin, providing additional routes for its tension-dependent recruitment to the AJs. However, since the binding sites for Vinculin and α-Actinin in α-Cat are partially overlapping, Vinculin and Synaptopodin are the main candidates to recruit α-Actinin to the AJs in a tension-dependent manner[404]. As discussed in Chapter I, ZO-1 also binds the C-terminal domain of α-Cat and F-Actin filaments and it reinforces cell-cell contacts under tension in both epithelial and endothelial cells[71,405]. Interestingly, a recent report showed that, in MDCK monolayers, ZO-1 or ZO-2 knockdown increases contractility at the AJs, in a Shroom3/ROCK-dependent manner. Accordingly, initial junction recoil upon laser ablation is significantly increased in the absence of ZO proteins, indicative of higher tension at the AJs. This increase in junction tension and actomyosin at the cell-cell contacts enhances Afadin junctional localization, particularly at Tricellular junctions[134]. These findings suggest that Afadin may be required to remodel the junctions under tension, in particular by anchoring additional actomyosin cables at the Tricellular AJs. Likewise, EPLIN also binds α-Cat and it is recruited to the junctions in a tension-dependent manner (discussed in detail below)[74]. Finally, at least in vitro, α-Cat homodimers adopt a conformation compatible with F-Actin binding and inhibit filament nucleation by the Arp2/3 complex[68]. Thus, in the future, it will be important to test the functional relevance of α-Cat dimers in vivo and to dissect how all these potential cascades cooperate, or not, with Vinculin to promote tension-dependent AJ strengthening.

- Tension Modulates Actomyosin Dynamics:

Mechanical forces affect the duty ratio of Myosin, essentially transforming the motor into an Actin anchor. Such behaviour was already reported for MyoI, II, V and VI[406–409]. With the exception of MyoVI, the applied mechanical load limits ADP release, thereby increasing the lifetime of the high affinity state for Actin filament binding (discussed in detail in Chapter II)[406,407,409]. Additionally, MyoII isoforms, A and B, respond differently to mechanical stimulation. Although both isoforms show load-dependent changes in ADP release, this rate is considerably

lower for MyoIIB than for MyoIIA (12-fold vs. 5-fold)[409]. Thus, MyoIIB exhibits especially striking mechanosensitivity. In agreement with this, MyoII isoforms contribute to junction integrity by different mechanisms. MyoIIA regulates E-Cad clustering at the AJs, while MyoIIB supports the integrity of the Actin belt lining the cell-cell contacts, mainly by strengthening the AJs to resist disruptive orthogonal forces[130]. Altogether these findings support that, under tensile forces, MyoII and Actin filaments interact more strongly, which is likely to result in the stabilization of actomyosin at the network level.

Somehow paradoxically to the previous notion, application of an external force, by micropipette aspiration, is sufficient to locally recruit MyoII[334,410–412], suggesting that the actomyosin network not only generates tension, but that tension can also regulate actomyosin dynamics. In line with this, actomyosin contractility is required for AJ assembly, yet junctional remodelling under tension also requires actomyosin reorganization[71,126–134]. Accordingly, Actin turnover directly modulates E-Cad recruitment/organization at the AJs, thus establishing an alternative mechanotransduction cascade. Using doublet assays, where a single cell-cell contact is formed in the absence of ECM adhesion, it was shown that lower filament turnover restricts E-Cad movements along the membrane[413], which is in agreement with previous reports showing that F-Actin anchoring contributes to cluster stability[99,102]. Since MyoII contractility affects cortical Actin turnover, it is expected that this mechanotransduction mechanism will indirectly regulate the adhesion strength[413]. Accordingly, MyoII activity is required for E-Cad-Cat complexes, ZO-1 and Vinculin recruitment to the AJs[127–132,414].

In addition to the dynamic properties of the actomyosin meshwork, its structural properties, namely meshwork density, degree of branching or bundling are also likely to be important parameters for mechanotransduction. In agreement with this, several ABPs were reported to be tension-sensitive, such as EPLIN[74], Ena/VASP[401] and Formins[398–400]. Thus, I will now discuss in more detail the mechanosensitive behaviour of the ABPS. EPLIN is an ABP that blocks Arp2/3-dependent branching, enhances filament bundling and stabilizes the actomyosin network by suppressing F-Actin depolymerization[415]. EPLIN depletion disrupts apical Actin organization, as well as the integrity of the adhesion belt, with E-Cad accumulating in puncta. Furthermore, EPLIN mediates the formation of a ternary complex with E-Cad-bound-α-Cat and F-Actin, suggesting that it may regulate the integrity of the apical belt by providing additional bonds between the adhesive complex and the actomyosin cytoskeleton, as well as by organizing Actin filaments along the junction[73]. The key finding underlying EPLIN mechanosensitivity came from a study describing its differential recruitment to linear junctions, which are assembled at cell-cell contacts vs. spot junctions, which assemble at the cell-free edge of cultured monolayers (Fig. 2). Differential mechanical tension across the two types of junction was proposed to be the trigger for EPLIN recruitment, since: (i) laser ablation of Actin filaments, which converts punctate into linear

junctions, induced EPLIN accumulation; (ii) uniaxial stretch increased EPLIN levels at the AJs; and, (iii) inhibiting ROCK activity, by Y-27632 treatment[395,396], or performing MyoIIB RNAi, which converts linear to spots junctions, completely abolished EPLIN recruitment. In agreement with a function of EPLIN at mature contacts, expressing an α-Cat-EPLIN fusion in α-Cat mutant cells, rescues linear junction formation. For this, EPLIN also requires Vinculin[74]. Altogether these findings support a model where EPLIN establishes additional bonds between the actomyosin network and the Cad-Cat complexes and where tension-sensitive EPLIN localization is involved in the conversion of nascent to mature AJs.

Ena/VASP is a family of Actin regulatory proteins found at both FAs and cell–cell junctions (Table 1). At the AJs, Ena/VASP is recruited upon homophilic E-Cad engagement, where it contributes both to F-Actin accumulation and organization[416]. In endothelial cells, Ena/VASP also regulates F-Actin content, contractility and response to shear stress[417]. Accordingly, when VE-Cad-coated beads are brought into contact with endothelial cells under a clamping force, VASP is required for adhesion strengthening[401]. More recently, VASP and Mena were implicated in tension-sensitive Actin assembly at the AJs downstream of Vinculin. The authors showed that, at least in Caco-2 cells, Vinculin binding is the predominant mechanism mediating Mena and VASP recruitment to the AJs[392], thereby questioning the role of other VASP binding proteins, such as Zyxin (Zyx), in regulating its tension-sensitive junctional recruitment. Zyx is an auto-inhibited LIM protein with no ability to bind F-Actin that also localizes to cell-cell contacts, where it contributes to junction establishment/strengethening[418–420]. At the FAs, it was proposed that Zyx phosphorylation, as well as tension-dependent unfurling releases its auto-inhibition, thereby exposing the VASP binding site[418,421,422]. Therefore, it would be important to understand whether Zyx unfolding at the AJs can also be tension-sensitive and whether Zyx and Vinculin cooperate or compete to recruit VASP to the junctions. Finally, Ena/VASP proteins were shown to both inhibit, and promote, Arp2/3-dependent Actin branching[423–425]. In flies, Ena inhibits Dia-mediated Actin polymerization[426,427]. These interactions with the two main Actin nucleators at the cortex are likely to be important for Ena/VASP's role in tension-dependent AJ reinforcement.

As discussed in Chapter II, Formins are a family of auto-inhibited Actin nucleators, which are activated upon Rho binding (Table 1). Using a stretch chamber, it was shown that cells overexpressing mDia1 showed transient increases in the amount of F-Actin after tension release, suggesting that mDia1, and potentially other Formins, increase filament nucleation upon mechanical stimulation. Notably, mechanosensitive Actin nucleation by mDia1 depends on a combined effect of Rho and Actin filament disassembly, i.e. the G-Actin content. Upon mechanical stimulation, G-Actin content increases, possibly due to mechanically-induced disassembly and increased AIP1 (Actin Interacting Protein 1, a cofactor of Cofilin.) levels, thereby providing a direct route for mechanosensitive filament nucleation[399]. Using a microfluidics setup to apply pN

forces to single filaments elongated by mDia1, it was further shown that the rate of filament elongation increases up to 2-fold under tension. The authors proposed that tension favours a conformation where the FH1 and FH2 domains are localized in close proximity, promoting a rapid transfer of Actin monomers to the barbed end. Surprisingly, these authors also showed that mDia1 also remains processively bound to the barbed-end of a depolymerizing filament, thereby delaying depolymerization and placing the Actin filaments themselves under tension[400]. Similar tension-dependent Actin assembly was reported for the yeast formin Bni1p. In this single molecule study, Bni1p mechanosensitive nucleation depends on the presence of Profilin-bound Actin. The authors proposed that Profilin-Actin biases Bni1p towards the "open" conformation, favouring Actin polymerization[398]. Overall these findings support that the actomyosin network is intrinsically sensitive to mechanical forces, an effect that is greatly amplified by tension-sensitive ABPs. A general picture of how all of these mechanisms coexist and cooperate to elicit coherent mechanotransduction responses is however still lacking.

Finally, mechanical forces were also proposed to regulate endocytosis. In MCDK monolayers, micropipette aspiration assays at the AJs showed that mechanical stimulation, increases E-Cad turnover. These findings were further supported by the observation that E-Cad turnover also increases at junctions shared with a "super" contractile neighbour, due to constitutively active RhoA expression[428]. This mechanosensitive adaptation of E-Cad levels is likely to control the adhesion force at cell-cell contacts, as endocytosis has been directly implicated in regulating the size of E-Cad clusters[99]. Unlike all the mechanisms described above, mechanosensitive turnover of E-Cad could potentially offer a negative feedback loop for cells to respond to large stresses.

(ii) E-Cadherin-dependent Mechanoresponses

The short-term effect of mechanically stimulating Cadherin complexes is a positive feedback that remodels the cell-cell junctions, promoting adhesion strengthening[129,376] and junction growth[357,389]. As described above, under tension, macroscopic junctional remodelling results from the combined effect of several parallel pathways, of which α-Catenin unfurling is the most extensively studied. α-Cat acts as an essential signalling axis mediating the attachment of adhesion complexes to the actomyosin cytoskeleton, partly by direct F-Actin binding and partly by promoting the recruitment of additional ABPs to the AJs, such as Vinculin, EPLIN, Formins, α-Actinin and Afadin. Although α-Cat unfurling under tension is rapid, the subsequent recruitment of Vinculin occurs up to 6-fold slower[379], suggesting that, at the cellular level, mechanoresponses are likely to result from the sum of successive reinforcement mechanisms. In such model, the fastest mechanoresponses (sec-few mins) are the stabilization of E-Cad/α-Cat catch bonds, α-Cat

unfolding and the stabilization of Myo binding to Actin, providing an almost immediate mechanism to resist mechanical stress. On a slightly longer timescale (tens of secs-tens of mins), additional ABPs can then be recruited to the junctions, thereby establishing additional links between the adhesion machinery and the cytoskeleton, and promoting actomyosin reorganization at the cell-cell contacts, which ultimately impacts on the stability/organization of E-Cad molecules.

On longer timescales (hours), mechanotransduction at the cell-cell contacts not only preserves tissue integrity and cohesiveness, but it also impacts on the regulatory gene networks controlling cell proliferation, stemness and differentiation, such as the Wnt/β-Catenin and the Hippo pathways[359]. The Hippo pathway is a kinase cascade that phosphorylates and inhibits the nuclear localization of transcriptional co-activators, YAP (Yes-Associated Protein) and TAZ (Transcriptional Co-activator with PDZ-binding motif). Once in the nucleus, YAP/TAZ associate with transcription factors, such as the TEAD1–4 and drive the expression of genes controlling cell proliferation, cell death and differentiation. Whether mechanical forces acting at the cell-cell contacts can also impact Hippo signalling is still an open question. In fact, many components of the Hippo pathway localize at the cell-cell contacts (both the AJs and the TJs) and disrupting junctional integrity induces nuclear localization of YAP/TAZ[429,430]. In line with this, α-Catenin can form a trimeric complex with YAP and 14-3-3, thereby sequestering it at the cell junctions and preventing its activation by phosphorylation[429]. Recent work in flies showed that Ajuda, a Zyx-related protein is recruited to the AJs in a tension-dependent manner, where it binds α-Cat. Once at the AJs, Ajuba recruits and inhibits Warts, one of the central kinases in the Hippo pathway, resulting in increased Yorkie activity (YAP/TAZ in mammals) and ectopic organ growth[431]. Zyxin itself was also implicated as a positive regulator of the Hippo pathway in an RNAi screen, as its depletion reduced Yorkie activity and, consequently, organ growth. Using epistasis tests, Zyx was placed on the Fat/Dachous branch of this signalling pathway and shown to bind the atypical Myosin, Dachs and the Warts kinase[432]. This was later challenged by the observation that Zyx null flies had, at most, a very modest effect on the growth phenotype of Fat mutants. These authors rather showed that Zyx, and its binding partner Ena, were implicated in antagonizing Expanded (Ex) function at the apical cortex[433]. Ex is known to promote cytoplasmic sequestration of Yorkie by direct binding and by promoting Hippo-Warts kinase activity[434,435]. Since there is no clear evidence of a direct interplay between Zyx and Ex, an alternative model was proposed whereby their roles in organ growth are mediated by antagonistic effects on the F-Actin network, which, in turn, affects Yorkie localization[433,436]. Altogether, these findings link cytoskeletal tension at the cell-cell contacts to the regulation of the Hippo pathway activity, although how exactly junctional components regulate YAP/TAZ localization/activity in a tension-dependent manner is still not fully understood.

β-Catenin is a core component of the adhesive complex, but it also acts as a transcription factor downstream of the Wnt signalling pathway. Evidence for force-sensitivity of the Wnt/β-Cat

pathway was initially provided in gastrulating fly embryos. Imposing uniaxial mechanical deformations to fly embryos induces nuclear re-localization of β-Cat and, subsequent, ectopic Twist expression. Since Twist expression is also increased in other tissues under active deformation (e.g. mesoderm cells during invagination and stomodeal primordium during GBE) and its expression could be induced in these contexts by simply mechanically compressing embryos, it was proposed that the Wnt/β-Cat pathway is mechanosensitive[437]. More recently, it was reported that applying mechanical loads on the Frizzled receptor, part of the canonical Wnt signalling, was sufficient to activate the expression of Wnt targets by promoting the nuclear translocation of β-Cat[438]. Whether and how β-Cat contributes for mechanosensitivity at the AJs and whether and how mechanical tension acting at the junctions feeds back onto β-Cat localization is still unclear.

Overall, the interplay between mechanical forces and E-Cad-mediated adhesion is essential to regulate junction remodelling/integrity, as well as the transcriptional landscape. An important question that remains is what determines if an applied load results in reinforcement or disassembly of the cell-cell contacts. Finally, it is unclear what defines the timescale of the mechanoresponses, or in other words, how do cells turn off the signal. On one hand, above a critical threshold of force, both E-Cad and α-Cat bonds behave as slip bonds[70,371], suggesting that mechanotransduction may be restricted to an optimal (intermediate) force regime. On the other hand, mechanical forces themselves limit mechanotransduction by inducing the disassembly of the actomyosin network[185].

C. Mechanotransduction at Integrin Adhesion Sites

Integrin complexes mediate the anchorage of the cell surface to the ECM (Fig. 1), thereby providing a substrate for cell migration and driving the reorganization of the extracellular environment during morphogenesis. Integrins cluster in punctate structures, termed Focal Adhesions (FAs) that are directly connected to perpendicular F-Actin fibres. Tension sensitivity was initially reported at Integrin complexes and the advances in this field guided research on E-Cad mechanotransduction. It has become increasingly clear that, not only similar molecular mechanisms operate at both Cad and Integrin complexes, but also that there is a significant overlap in their networks of interacting proteins (Fig. 17)[404]. I will therefore compare and contrast mechanotransduction at Integrin adhesion sites with the mechanotransduction mechanisms operating at cell-cell contacts.

Integrin complexes are composed of α/β subunits forming an extracellular ligand-binding headpiece that rests on a cytosolic tail extending from each subunit. Integrin complexes come in all flavours, as they are composed of a variety of Integrin subunits (up to 24), which determine their

ligand specificity. Similarly to E-Cad, Integrins exhibit catch-bond behaviour, as single molecule force-clamp experiments showed that the bond lifetime rises upon mechanical stimulation (10-30 pN). Above the critical force of ~30 pN, Integrin bonds behave as slip bonds[368,369]. Strikingly, both E-Cad and Integrin catch bonds operate at very similar force regimes and both are independent of their respective cytosolic tails[368,369,371]. Integrin bonds stiffen even further over repeated cycles of force application, a feature that was so far not reported for E-Cad catch bonds. Such behaviour was termed "cyclic mechanical reinforcement" and it is likely to be much more efficient than catch bonds at prolonging the bond lifetimes under load[439].

As for E-Cad, the cytosolic tails of Integrins are the major signalling platforms for mechanotransduction, as they interact with a number of adaptor proteins, namely Paxilin and Talin. α-Catenin and Talin play analogous functions in E-Cad and Integrin adhesion sites respectively, as both proteins link the adhesive complexes to the underlying actomyosin cytoskeleton and undergo tension-dependent unfurling, thereby exposing cryptic binding sites for additional ABPs, namely Vinculin[440–442]. Remarkably, Talin is able to discriminate between parallel vs. perpendicular forces, due to its different arrangements relative to the Integrin receptors[443]. It would very interesting to perform a similar dissection of the α-Cat molecule and its binding to E-Cad in pursuit of such mechanism. Under tension, Talin unfolds from 50-400 nm in three successive steps. The first unfolding step is sufficient to recruit Vinculin, which locks Talin in an open conformation[444]. The mechanism underlying Vinculin recruitment to the FAs is still a matter of debate. Talin and α-Cat bind Vinculin with similar affinity, although they interact with slightly different Vinculin helices[383,445]. Bois and colleagues showed that short Talin peptides are sufficient to bind/activate Vinculin in the absence of a second ligand[446]. However, in agreement with structural data available for Vinculin, other authors showed that Talin only releases Vinculin's intramolecular interaction in the presence of F-Actin or PIP2[382,445,447]. Thus, it is unclear whether full-length Talin, as well as α-Cat, binding to Vinculin is sufficient for its activation in vivo.

Vinculin recruitment to the Integrin-adhesion sites reinforces the attachment between the Integrin complexes and the actomyosin cytoskeleton, resulting in FA enlargement[358]. Vinculin recruits additional ABPs to the FAs, such as the Arp2/3 complex, VASP and α-Actinin[404,448]. A recent study challenged this notion and showed that when cells expressing constitutively active (CA) Vinculin are treated with Cytochalasin D, which binds to F-Actin barbed ends and prevents Actin polymerization[449,450], both VASP and α-Actinin are lost from the FAs, suggesting that although Vinculin can interact with these proteins it may not do so in vivo. Using the same assay, the authors implicated the Vinculin neck domain in recruiting α/β-Vinexin and Ponsin to the FAs; while, Vinculin CA stabilizes Paxilin, Zyxin, Tensin and Focal Adhesion Kinase at FAs most likely indirectly, via Talin unfolding[451]. These and other findings suggested that Vinculin works like an ON/OFF switch, as its activation/inactivation results in the recruitment/loss of a substantial number

of proteins from the FAs. Although the role of Vinculin in ECM adhesion formation and stability has been extensively studied in cultured cells[451,452], its impact in tissue behaviour is not so far not clear. In fact, as mentioned above, Vinculin-deficient fruit flies[397] are viable and fertile and even Vinculin-knockout mice only die late in development[453], suggesting that there may be redundant mechanisms underlying tension-sensitive FA enlargement.

Other ABPs beyond Vinculin are present at FAs as well as the AJs, namely α-Actinin, Filamins and Zyxin, suggesting that the actomyosin organization at both junctions is likely to be similar. I will now discuss in more detail each of these components, as well as their roles in the FAs and AJs. α-Actinin is required for adhesion maturation in both the AJs and the FAs[404]. At the FAs, α-Actinin is itself under tension, as visualized by a tension-sensitive FRET sensor (Box 3B)[454,455]. Tension across α-Actinin is correlated with FA enlargement, likely due to increased recruitment of α-Actinin and Paxilin to the adhesion sites. These findings suggested that α-Actinin not only serves as a physical linker between the Integrin complexes and the cytoskeleton, but also participates in force transmission to facilitate FA growth. Thus, it would be interesting to test whether a similar mechanotransduction mechanism operates at the cell-cell contacts. Filamins are a family of Actin crosslinking proteins able to bind Integrins (Table 1). Using AFM (Box 3E), it was shown that single Filamin molecules also unfold and stretch in response to external force, however it is unclear whether specific Filamin-ligand or Filamin-Actin interactions are preserved and/or added under tension. Filamins bind to: (i) several GTPases, namely Rho, Rac, Cdc42 and Ral; (ii) GEFs/GAPs, such as Trio; and, (iii) ROCK, suggesting it may play a general role in regulating cellular contractility[456]. Although Filamins were implicated already in adhesion stiffening under tension[404], the underlying mechanism remains unclear. Although Filamins are required for efficient assembly of the AJs upon Ca^{2+} switch, it is not known whether it also contributes for mechanotransduction. Also, the binding partner of Filamins at the AJs is currently unknown. Finally, Zyxin (Zyx) is recruited to the FAs in a tension-dependent manner, where it recruits Ena/VASP proteins and contributes for Actin assembly[418,421,422]. Zyxin accumulation at the FAs is observed when cells are cultured in stiff substrates and is lost upon actomyosin inhibition[457]. Although the mechanism promoting Zyxin/VASP recruitment to the FAs is likely to be different than its targeting to the AJs, in both cases, they contribute to tension-sensitive F-Actin assembly[392,401,416,421,458,459].

Altogether these findings support that Integrin and Cadherin adhesion complexes employ similar strategies and effectors to transform a mechanical input into a biochemical signal. Catch-bound behaviour, the Talin/α-Cat tension-dependent unfurling and Vinculin recruitment are the key mechanisms for junction remodelling under tension. Now, it is important to understand how other mechanosensitive pathways contribute to adhesion strengthening, as well as the significance of these mechanotransduction mechanisms at adhesion sites in vivo. Similarly to mechanotransduction

at the AJs, long-term mechanoresponses at the FAs also affect transcription, for example, via the Hippo and the β-Cat/Wnt signalling pathways. Accordingly, YAP/TAZ were implicated in mechanotransduction at the FAs in the context of contact inhibition[460], sensing cell geometry[461] and ECM rigidity[462]. More recently, Merlin (NF2), a member of the Hippo pathway, was shown to coordinate collective cell migration due to its action as a mechanotransducer, although the underlying molecular mechanism remains unclear[463]. Moreover, Zyx was also implicated in transcription regulation, as it was observed that, upon cyclic stretch, it translocates from the FAs to the nucleus[464,465]. Moeover, several F-Actin capping/severing proteins, such as Cofilin, CapZ, and Gelsolin (Table 1) limit YAP/TAZ activity under low mechanical stresses, including contact inhibition of proliferation[466], suggesting another possible mechanosensitive cascade that potentially regulates the Hippo pathway. Finally, ECM rigidity also impacts β-Cat/Wnt signalling pathway, which, in turn, controls stem cell differentiation[467,468]. Thus, it is important to find which mechanosensitive proteins actually relay mechanical signals to the nucleus and whether the same players convey the signal from the FAs and the AJs.

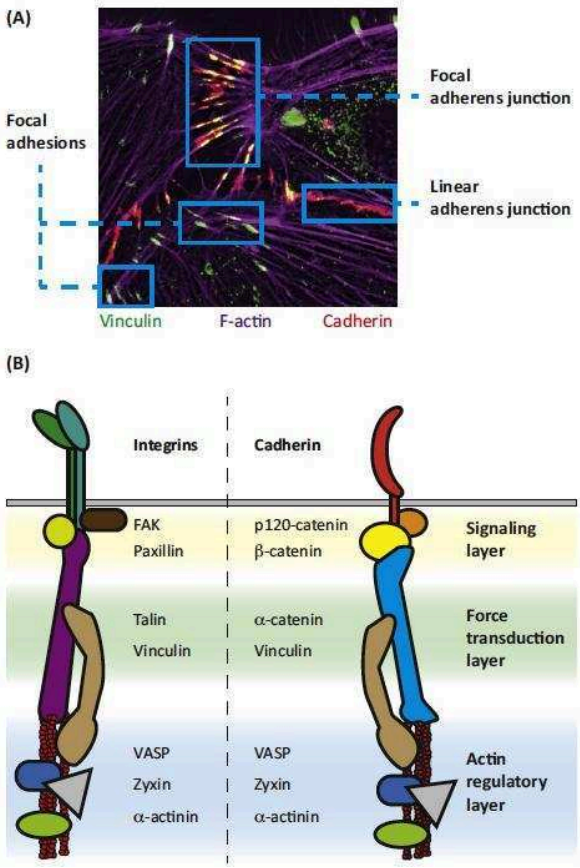

Figure 17: Molecular composition of Integrin and Cadherin Adhesion Complexes.

(A) Immunofluorescence image of thrombin-stimulated HUVEC cells. FAs are marked by Vinculin staining (green); linear AJs are marked by VE-Cadherin staining (red) and Spot AJs are marked by colocalization of

Vinculin and VE-Cadherin (yellow). (B) Main molecular players acting at Integrin (green) and Cadherin (red) adhesion sites. These authors proposed that both junctions organize into: a signalling layer (SL), a force transduction layer (FTL) and an Actin regulatory layer (ARL). A key feature shared between Integrin and Cadherin complexes is the tension-dependent conformational switch in Talin (purple) and α-Catenin (blue), respectively, which mediates binding of Vinculin (light brown), thereby resulting in adhesion strengthening (adapted from[404]).

D. Other Mechanotransduction Mechanisms

Mechanotransduction is not restricted to the adhesion sites, as the plasma membrane itself also senses/responds to mechanical forces. The actomyosin cortex not only lines the plasma membrane, but is also attached to it, by linker proteins, namely by members of the Ezrin-Radixin-Moesin (ERM) family, Filamins and MyoI motors. The tight interplay between the cytoskeleton and the cell membrane suggests that cytoskeletal remodelling under tension impacts on plasma membrane dynamics and conversely, that increasing membrane tension is likely to impact on the actomyosin cytoskeleton. Membrane tension can thus be defined as the force per unit length acting on the membrane. Since cells possess membrane free folds and stable reservoirs, such as blebs, caveolae and microvilli (Fig. 18), which can store or release membrane to regulate surface area, it is quite challenging to measure membrane tension in vivo. Also, as mentioned above, the actomyosin cytoskeleton is attached to the membrane, raising further difficulties when determining the membrane, and not the cortical, tension[469–471].

Using laser tweezers to pull membrane tethers, it was shown that membrane tension progressively decreases during fibroblast spreading, suggesting that cells must employ a compensatory mechanism to increase their surface area. Accordingly, high membrane tension induces exocytosis, which acts to decrease tension; while low membrane tension promotes endocytosis, which acts to increase tension[230,472,473]. These findings suggest that there is an optimum regime of membrane tension, which is actively adjusted by the cell. Such reduction in membrane tension during spreading also relies on the flattening of membrane reservoirs, such as folds and/or caveolae, since preventing lipid mobilization from these compartments rather increases tension during cell spreading. Such tension increase is then partially compensated by exoctytosis and MyoII contraction[473–475]. Using a lipid bilayer, coupled to an elastic sheet, it was shown that, not only during stretching, but also during compression, cells reversibly regulate their surface area. As shown before, upon stretching, the bilayer laterally expands by fusing adhered lipid vesicles; upon compression, lipid tubes grow out of the membrane plane, thereby reducing its effective surface area[476]. These data implicate tension in coordinating membrane trafficking,

actomyosin contraction and plasma membrane surface area. In line with this, micropipette aspiration assays in Drosophila embryos, promoted MyoII apical localization, which, in turn, blocked Folded-gastrulation (Fog) endocytosis at the apical membrane of mesoderm cells[411]. Fog is a secreted protein that promotes coordinated apical constriction in mesoderm cells. The mechanism by which mechanical forces impede Fog endocytosis remains unclear, but, in agreement with the previous studies, it was proposed that it could result from direct membrane stretching[411].

In contrast with this, recent work in motile keratocytes proposed that cytoskeletal forces, rather than changes in the available surface area, determine membrane tension. Accordingly, artificially increasing membrane area, by fusion of GUVs with moving keratocytes, did not significantly change membrane tension; conversely, inhibiting Actin polymerization and/or MyoII contractility completely freezed the lamellipodia, resulting in a dramatic drop in membrane tension[477]. Another factor determining membrane tension is the different levels of adhesiveness to the susbtrate[471,477]. To reconcile these apparently conflicting data, one could envision a model whereby membrane tension is defined by two main components: the tension in the lipid bilayer, which is regulated by the surface area and a second component resulting from membrane-cytoskeleton attachment. The relevance of each contribution may be context-specific, in agreement with the wide range of membrane tension magnitudes observed in different cell types[469–471].

Membrane tension was proposed to direct cell migration by aligning F-Actin polymerization with the direction of movement[230–232] (see Chapter II). The current model is that membrane tension is transmitted to the underlying cytoskeleton in an Actin density-dependent manner; so that, at the leading edge (high F-Actin density), membrane resistance per filament is small, allowing filaments to grow rapidly and generate protrusion; conversely, at the rear and sides of the leading edge (intermediate-low filament density), membrane resistance to F-Actin polymerization is increased, thereby stalling membrane protrusions[233]. Accordingly, studies using GUVs that nucleate branched Actin networks showed that rather than dendritic networks, thin protrusions similar to filopodia are formed. The unexpected formation and stability of the filopodium-like protrusions in vitro demonstrates that the lipid bilayer per se is sufficient to facilitate free barbed-end clustering and alignment of filaments under the membrane load[236]. Finally, membrane tension also promotes E-Cad clustering, at least in vitro, suggesting that tension imposes membrane flattening and facilitates E-Cad aggregation, possibly by diffusion[126].

However, how cells sense membrane tension is still not fully understood. Several mechanisms are likely to participate, namely mechanosensitive channels (MSCs), curvature-sensing proteins and tension-sensitive linkers mediating membrane-cortex attachment. The best understood examples of eukaryotic mechanosensitive channels are stretch-activated ionic channels, such as: (i) TRP channels, which modulate intracellular Ca^{2+} levels and are activated by membrane stretch or osmotic forces; (ii) TREK channels, which are mechanosensitive K^+ channels activated

by stretch, temperature, phospholipids and acidosis; and, (iii) Piezo1/2, which are non-selective cation channels conducting Na^+, K^+, Ca^{2+} and Mg^{2+} ions. Note that these MSCs are particular, as they all require interactions with the actomyosin cytoskeleton. Thus, it is proposed that increased membrane tension promotes channel opening, resulting in a subsequent influx of ions and water[469,478]. Curvature-sensing proteins could potentially both detect and control membrane tension locally, as many of these proteins interact closely with GTPases and Actin regulators. Proteins containing BAR or ALPS (Amphipathic Lipid-Packing Sensor) domains, MyoII and the Septin cytoskeleton associate with curved membranes and can also limit membrane bending[469,479–482]. Finally, linkers mediating membrane-cortex attachment are put under tension when the membrane moves away from the cortex. Filamins, that bind both the actomyosin cytoskeleton and the Integrin receptors, are ideal candidates for this function, as they are reported to be mechanosensitive[456]. MyoI motors bridge membrane-cortex attachment and their affinity to bind Actin is also modulated by tension[406,407,409].

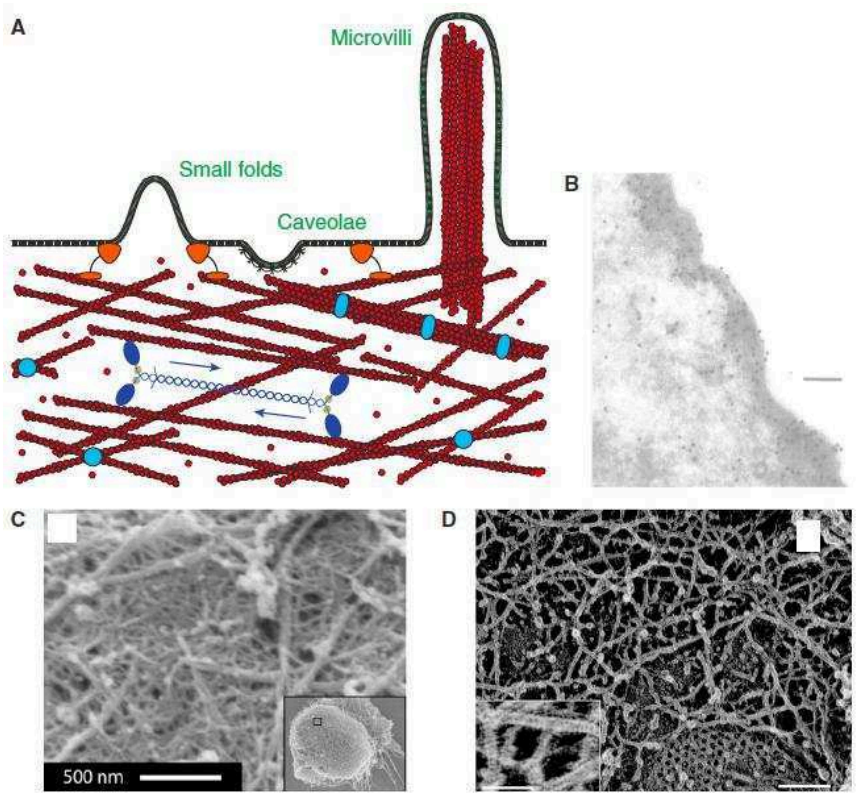

Figure 18: Plasma membrane structure and organization.

(A) Schematic representation of the plasma membrane (black) and the underlying actomyosin cortex (F-Actin: red; MyoII: dark blue; Crosslinking and Bundling Proteins: light blue; Linking proteins mediating membrane-cortex attachment: orange). Highlighted in green are small outward folds, caveolae and long, thin microvilli. (B) Transmission electron micrograph showing a cross-section of the cell periphery in

Dictyostelium discoideum labelled by immunogold staining with an anti-Actin antibody. (C) Scanning electron micrograph of the surface of a rounded HeLa cell showing the cortical network, without the plasma membrane. (D) Electron tomograph of the cytoplasmic surface of the plasma membrane and actomyosin cortex from fetal rat skin keratinocyte (FRSK) cells. Scale bars in main panel: 100 nm and scale bar in inset: 50 nm (adapted from[470]).

Altogether, these findings suggest that membrane tension can impact the surface area of the plasma membrane and vesicle trafficking, as well as the cytoskeleton organization and vice-versa. However, many open questions remain, namely whether cells maintain an optimum regime of membrane tension and if so, whether that is an active or mostly passive process. In addition, how exactly cytoskeletal tension impacts membrane tension and vice-versa is still not fully understood and to address such question new techniques to measure/perturb membrane tension will be required. Similarly, understanding how the lipid composition of the membrane sets its mechanical properties and interactions with the actomyosin cytoskeleton is likely to be another crucial aspect.

IV. Cytokinesis in Epithelial Tissues

Cytokinesis occurs after chromosome segregation and it partitions the dividing cell's cytoplasm into the future daughter cells. The mechanisms controlling cytokinesis were studied in-depth in individual cells, such as one-cell embryos and isolated cells in culture. Although the cytokinetic machinery operates similarly in tissues, questions remain regarding how cytokinesis impacts on the cells surrounding the dividing cell and how epithelial tissue integrity is maintained during proliferation. To address this question, a number of recent studies analysed cytokinesis in a number of epithelial tissues, namely the embryonic ectoderm, the pupal notum and the follicular epithelium in Drosophila, the gastrulating chick embryo and, more recently, in the Xenopus Laevis embryo. Overall, these studies highlighted that, in epithelia, cytokinesis is not a strictly autonomous process, as the neighbouring cells cooperate with the dividing cell and regulate both the dynamics of cytokinesis and the subsequent arrangement of the daughter cells in the tissue following division[1–6]. Thus, I will start by a brief description of the molecular mechanisms underlying cytokinesis, followed by a more extensive discussion on cytokinesis in multicellular systems.

A. Animal Cell Cytokinesis

As briefly mentioned in Chapter II, cytokinesis in animal cells proceeds through the formation and constriction of an actomyosin contractile ring at the cell equator (for symmetrically dividing cells; asymmetric cell division won't be discussed here), which is attached to the plasma membrane. Thus, as the contractile ring constricts, it progressively closes the connection between the future daughter cells. By the end of cytokinesis, the daughters remain connected by a narrow intercellular bridge, which is eventually cleaved by abscission (Fig. 19)[253]. Therefore, in the present section, I will discuss the molecular mechanisms involved in: (i) positioning the contractile ring; (ii) contractile ring assembly and constriction (briefly discussed as this was already addressed in Chapter II); and, finally (iii) abscission, the process by which the two daughter cells are finally individualized.

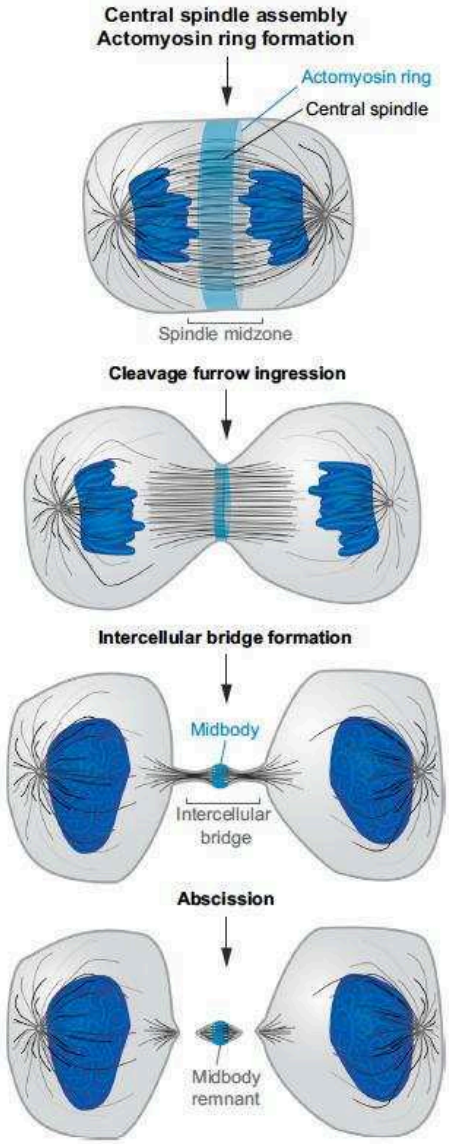

Figure 19: Schematic representation of Animal Cell Cytokinesis.

Following chromosome segregation during anaphase (not shown), MTs (in black) of the mitotic spindle reorganize to form the midzone. Signalling between the midzone and astral MTs positions the future contractile ring at the cell equator. Contractile ring constriction progressively ingresses the attached cell cortex to form the cleavage furrow, thereby partitioning the cytoplasm into two equal halves. Upon full constriction, the midbody is formed within intercellular bridge, that is eventually cleaved by abscission (adapted from[483]).

(i) Positioning the Contractile Ring

Contractile ring positioning occurs following chromosome segregation at early anaphase and it relies on an interplay between the mitotic spindle and the actomyosin cortex. The role of the

spindle in ring positioning was established in the 1980s by micromanipulation experiments in echinoderm eggs, where it was shown that moving the spindle during anaphase causes the furrow to regress and re-form at the spindle midzone, demonstrating a dynamic signalling between the spindle and the contractile ring machinery[484]. Two microtubule populations within the mitotic spindle cooperate to position the contractile ring, namely the midzone and the astral microtubules[253]. Midzone microtubules interdigitate at the equator with their plus ends facing the array from the opposite pole and their minus ends facing the pole; while, the astral microtubules are nucleated by the centrosomes, so their plus ends face the cell cortex. RhoA activation at the equator is achieved by a positive signal provided by the spindle midzone and suppressed at the cell poles by dynamic astral microtubules[174,291]. Importantly, a spindle-independent pathway also cooperates to position the contractile ring in Drosophila neuroblasts. This cortical polarity pathway positions the ring basally and it depends on the Pins complex (composed of Pins, Gαi and Discs large)[485]. In the next sub-sections, I will focus on the spindle-dependent pathway and discuss how the redundant signals from the spindle midzone and the astral MTs cooperate during cytokinesis to position the contractile ring at the equator.

- The role of Midzone Microtubules:

In vitro reconstitution assays recently showed that a combined action of the microtubule cross-linkers, PRC1 and the Kinesin-4 (KIF4) is sufficient to reconstitute the typical MT overlap found at the spindle midzone. In this assay, PRC1 was shown to be sufficient to bundle antiparallel MTs, which, in turn, recruit KIF4. Then, this Kinesin sets the size of the overlap region by limiting MT growth at the plus-ends[486]. KIF-4 activity is indirectly regulated by Polo-like Kinase 1 (Plk1), which inhibits KIF-4 and promotes bundle elongation[487]. In addition to PRC1 and KIF4, the Centralspindlin complex (CS) also localizes at the midzone and contributes both for midzone formation and contractile ring positioning. The CS complex is composed of two Mitotic Kinesin-Like Protein 1 (MKLP1; ZEN-4 in C. elegans and Pavarotti in Drosophila) proteins and two MgcRacGAP (CYK-4 in C. elegans and RacGAP50C in Drosophila) molecules, and its recruitment to the midzone requires multimerization, which in turn depends on two subsequent phosphorylation events by the Aurora kinase, a component of the Chromosomal Protein Complex (CPC)[488–492]. Moreover, PRC1 also interacts directly with the CS component, MgcRacGAP in a number of systems and further contributes to Centralspindlin recruitment to the spindle midzone[493,494]. Similarly to PRC1, the CS complex also shows bundling activity, thereby contributing to midzone formation[490].

Although PRC1, KIF4, CS complex and the CPC are essential for spindle midzone assembly, their roles in contractile ring positioning and assembly are still a matter of debate, as

removing each of these components does not fully prevent ring formation[253]. A possibility would be that these components act independently and, at least, partially redundantly to target contractile ring components to the spindle midzone. According with this, simultaneous inhibition of the CPC and CS complexes produces additive defects on contractile ring positioning and formation[495]. The CS complex recruits Ect2, a Rho GEF, to the equator, which, in turn, locally activates RhoA (Box 1, Fig. 14)[295,297,496]. Ect2 interacts directly with MgcRacGAP upon its phosphorylation by Plk1[295,297,497–500]. MgcRacGAP promotes contractile ring constriction via two mechanisms; on one hand, it contributes for Ect2 recruitment to the midzone and secondly, it activates Ect2 by relieving its autoinhibition[498,499]. Also, MgcRacGAP GAP activity was reported to be required for cytokinesis in some systems, although the identity of its targets is still unclear, it was proposed that it can either inhibit or promote Rho signalling at the spindle midzone. In Xenopus embryos, HeLa and hematopoietic cells, expression of a mutant version of MgcRacGAP with no GAP activity results in the formation of a broader zone of RhoA activation at the cell equator, consistent with the idea that MgcRacGAP acts as a Rho GAP during cytokinesis[501–503]. In contrast, in C. elegans, MgcRacGAP GAP activity rather promotes RhoA activation at the cell division plane[504]. Additional studies will now be required to dissect whether any GAP activity is retained towards RhoA, or Rac, since subsequent studies proposed that MgcRacGAP promotes Rho activity by inhibiting Rac activity locally[504,505]. Finally, the CPC complex acts both to: (i) activate the CS and promote its recruitment to the midzone; and; (ii) directly on MyoII[488,489,491,492,506].

In summary, the spindle midzone provides a platform for the assembly and the concentration of the Centralspindlin complex, which is essential for Rho activation at the cell division plane.

- The role of Astral Microtubules:

The asters prevent the accumulation of contractile ring proteins in their vicinity, which contributes for their relative enrichment at the cell equator. In agreement with this, Werner and colleagues reported that, in the C. elegans embryo, the formation of a small spindle is sufficient to restrict the accumulation of Myosin at the opposite polar cortex[291,293]. Similar observations were reported in grasshopper spermatocytes, where the positioning of the asters on one side of the cell, resulted in a cortical Actin flow towards the opposite pole[507]. In vertebrate cells, astral microtubules were also shown to contribute to contractile ring positioning, as selective disruption of the asters resulted in the formation of a wider ring[174]. A detailed analysis of MyoII dynamics at the polar cortex showed that net accumulation at these regions is prevented by a balance between phases of Myo recruitment and phases of motor loss from the poles[289]. Consistent with this, eliminating the astral microtubules in sea urchin embryos through laser ablation or other means led

to a broader zone of active RhoA and contractile ring proteins[508–510]. Since the total amount of RhoA did not change, the authors proposed that rather than directly inhibiting RhoA, the asters corral a fixed amount of active RhoA and prevent it from spreading from the cell equator[510]. Additionally, a pool of stable asters is also present at the spindle midzone and it is proposed to contribute to contractile ring assembly[509]. Nevertheless, it remains unclear exactly how this microtubule pool reaches the midzone and mechanistically how it contributes to ring positioning and assembly. As mentioned in Chapter II, relaxation of the polar cortex contributes for the formation of a contractility gradient along the cell, which is further amplified by additional MyoII activation at the cell equator[288–293]. Importantly, even without MyoII activation at the midzone, inhibition of contractility at the poles can still induce contractile ring constriction if the asters are sufficiently far apart[495,510–512].

(ii) Contractile Ring Assembly and Constriction

Contractile rings are composed of a thin (0.1-0.2µm) layer of cross-linked filaments that forms around the cell equator beneath the plasma membrane. The activation of the GTPase RhoA at the cell equator is sufficient to drive contractile ring assembly[254]. Once active, RhoA binds to effectors, including Dia to induce F-Actin assembly and Rho kinase to activate MyoII (Fig. 14). Moreover, cortical actomyosin flows from the cell poles towards the equator further contributes to the actomyosin accumulation at the equator (Fig. 14)[288–290]. A recent theoretical study showed that such a contractility gradient is sufficient to drive cortical flow towards the equator, contractile ring formation and furrow constriction[300]. In addition to Actin filaments and myosin motors, the contractile ring also contains Septin filaments[253]. In flies, Septins contribute to contractile ring constriction by organizing the Actin filaments within the ring[267]. Septins, in turn, are recruited to the contractile ring by Anillin, a filament cross-linker that can bind all filament types[513]. Finally, a number of Actin-binding proteins regulating Actin nucleation, capping, polymerization, disassembly, and cross-linking are also recruited to the contractile ring[253].

Contractile ring assembly occurs in two steps; initially, Ect2 and Rho are recruited and activated at the equator by a combined action of the spindle midzone and astral microtubules, followed by a subsequent step where the ring matures, producing a more condensed contractile band[487,514,515]. Contractile ring maturation was proposed to result from the alignment of the Actin filaments into highly compacted bundles[253]. Several mechanisms were proposed to contribute to filament alignment in the contractile ring. Based on theoretical modelling, the actomyosin flow itself was proposed to align the Actin filaments within the ring[298]. Additionally, in Drosophila, Septin filaments were shown to be important organizers of the filaments within the contractile ring, by generating curved and tightly packed Actin filament networks[267]. However, more work will be

required to understand how the contractile ring evolves during cytokinesis. An essential aspect will certainly be to develop an in vivo high-resolution imaging technique to carefully characterize filament alignment throughout cytokinesis, as well as in a series of mutant conditions.

To drive constriction of the dividing cell's membranes, the contractile ring must be strongly anchored to the plasma membrane. The Centralspindlin complex was recently implicated in mediating contractile ring tethering to the membrane, via its MgcRacGAP subunit which interacts with polyanionic phosphoinositide lipids. In agreement with an essential role for this interaction, cells expressing a mutant form of MgcRacGAP lacking its C1 domain, which is responsible for phosphoinosites binding, impaired cytokinesis[516]. Additionally, the lipid PIP2 was also implicated in contractile ring anchoring. PIP2 accumulates at the cytokinetic furrow and the lipid kinases generating this lipid, as well as the phosphatidylinositol lipid transfer proteins are required for cytokinesis in both flies and fission yeast[517]. Moreover, overexpressing PLCδ-PH or Tubby domains that bind specifically to PIP2 or the PIP2-Phosphatase Synaptojanin in mouse fibroblasts also results in a slight detachment of the contractile ring from the membrane[518]. Consistent with these findings, several cleavage furrow components bind PIP2 lipids, namely: (i) Septins[519]; (ii) Anillin[520]; and, (iii) Ect2[521].

As extensively discussed in Chapter II, contractile ring constriction is likely to result from a combined action of MyoII pulling forces and depolymerization of cross-linked Actin filaments[259]. Importantly, cortical pole relaxation also contributes to contractile ring positioning and constriction[174,289,291,294]. Sedzinski and colleagues showed that perturbing the polar cortex leads to cell shape oscillations, resulting in furrow displacement and aneuploidy. These authors proposed that a competition between cortex turnover and contraction accurately accounts for these shape oscillations, suggesting that the blebs normally formed at the poles during cytokinesis release cortical contractility and stabilize cell shape during cytokinesis[294]. Blebs are plasma membrane protrusions observed upon loss of actomyosin cortex attachment due to cytoplasmic pressure[522]. Interestingly, the polar relaxation model also provides an intuitive way to generate asymmetric daughter cells, as the stabilization of an unbalanced cell shape with one pole more constricted than other is, in principle, sufficient to destabilize the position of the contractile ring[294]. Accordingly, asymmetrically dividing cells, such as the Q neuroblasts in C. elegans[523] and larval neuroblasts in Drosophila[485], were reported to accumulate MyoII at one of the poles.

(iii) Abscission

The final stage of cytokinesis corresponds to abscission, the process by which the two daughter cells are finally individualized. As the ring constricts, the spindle midzone is remodelled to form the densely packed midbody, which, in turn, organizes the intracellular bridge. During this

process, the actomyosin ring is progressively replaced by a distinct membrane-associated filament system, termed the Endosomal Sorting Complex Required for Transport-III (ESCRT-III). ESCRT-III filaments are proposed to promote abscission by progressively narrowing the intercellular bridge and promoting MT disassembly[524].

- Midbody Formation and Maturation:

The midbody is an electron-dense organelle, composed of densely packed antiparallel bundles of very stable MTs. The midbody confers mechanical stability to the intracellular bridge, and provides a platform for the recruitment of vesicles and the abscission machinery to the intercellular bridge[524]. During maturation, the midbody organizes into three regions, namely: (i) the midbody core, which contains the MT overlap derived from the spindle midzone. This region contains both KIF4 and PRC1, whereas CENP-E, MKLP2, and Aurora B localize at microtubules adjacent to the midbody[525,526]; (ii) the midbody ring, which accumulates around the midbody core and is composed of the contractile ring remnant. This region is enriched for ring components, such as Anillin, Septins, Citron kinase, and RhoA[526–528]; and, (iii) the midbody flanks, contain MT bundles located at the vicinity of the midbody core. These regions are enriched in CENP-E, MKLP2 and Aurora B and terminate near the eventual abscission site (Fig. 20)[526]. The organization of the midbody in distinct regions depends on Plk1, as its inhibition or depletion affects midbody regionalization and leads to abscission failure[526].

In Drosophila S2 cells, Anillin and Septins are required to both transform the contractile ring into the midbody ring, as well as to anchor it to the plasma membrane. This anchoring function stabilizes the intercellular bridge and is therefore essential for abscission to occur[528]. Anillin is recruited and maintained at the intercellular bridge through binding to Citron kinase (Sticky, the Drosophila orthologue)[527,529]. Citron kinase also contributes to midbody stability by binding MKLP1, a CS component and KIF1[530–532]. In turn, MKLP1 contributes to midbody anchoring through the small GTPase Arf6, which binds the plasma membrane through its N-terminal myristorylated helix[533]. Arf6 also has an additional function in stabilizing cleavage furrow ingression, as it contributes to maintain the midbody core integrity by counteracting 14-3-3 protein, which sequesters the CS complex in an unclustered form[534]. Additionally, the other Centralspindlin subunit, MgcRacGAP tethers the midbody MTs to the plasma membrane via PI4P and PIP2 binding[516]. Moreover, PIP2 also specifies the localization of various cytokinesis proteins, such as Anillin, Septins, RhoA and MgcRacGAP[483,516,535,536]. Meanwhile, PIP3 lipids accumulate closer to the midbody, where it binds FYVE-CENT and TTC19, two factors mediating the recruitment of the abscission factor CHMP4B[537]. Thus, several redundant pathways cooperate to ensure the

mechanical stability of the intercellular bridge, by tethering the midbody and adjacent regions to the plasma membrane.

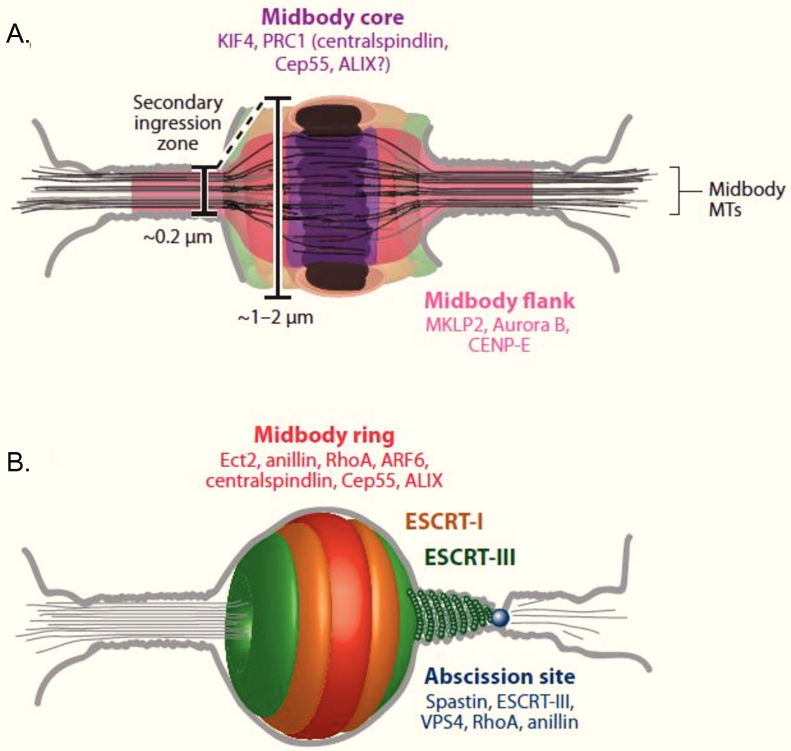

Figure 20: Organization and molecular composition of the midbody.
Following contractile ring constriction, the midbody organizes into three district regions: the midbody core (A; highlighted in purple), the midbody ring (A; highlighted in red) and the midbody flanks (B; shown in pink). In (B), an additional schematic representation of the molecular composition of the abscission site is shown in blue (adapted from[253]).

- Cytoskeleton Reorganization and Membrane Fission:

Upon full contractile ring constriction, the intercellular bridge forms and matures, thereby reducing its initial width by half. Intercellular bridge maturation results from cytoskeleton disassembly[538]. F-actin severing at the intercellular bridge depends on the inactivation of RhoA, which is mediated by a complex of PKCε kinase and 14-3-3 protein[539]. Actin disassembly in the bridge is further regulated by changes in the lipid composition of the plasma membrane. In particular, the GTPase Rab35 delivers the PIP2 5-Phosphatase Oculocerebrorenal Syndrome of Lowe 1 (OCRL) to the intercellular bridge, thereby reducing the levels of both PIP2 and actin filaments[540]. Moreover, Rab11 and FIP3 containing endosomal vesicles also contribute to the

depolymerization of cortical actin filaments in the intercellular bridge through the local delivery of p50RhoGAP[541]. The remodelling of the actin filaments contributes to a gradual narrowing of the intercellular bridge, which precedes the formation of ESCRT-III filaments at the future constriction zone[483]. Finally, the removal of MT bundles derived from the spindle midzone is mediated by Spastin, a MT-severing protein[542,543]. Spastin is targeted to the abscission site by its interaction with the ESCRT-III complex, supporting that MT clearance and membrane fission are coordinated during abscission (Fig. 21)[542].

Before abscission, the cortex adjacent to the midbody constricts and appears rippled in electron micrographs. In this region, membrane-associated filaments of 17nm diameter encircle the intercellular bridge as large helices (Fig. 21). The current model for abscission is that constriction of cortical filament helices progressively closes the plasma membrane tube by fission. Although the identity of the cortical filaments is currently unknown, the most prominent candidate is the ESCRT-III complex. Polymerization of ESCRT-III filaments into spirals, mediates membrane constriction and fission in a variety of cellular processes, including budding of endosomal vesicles and viruses[524]. Accordingly, ESCRT-III is essential for abscission and it accumulates at constriction zones within late-stage intercellular bridges[538,544]. Moreover, CHMP2A depletion, an ESCRT-III subunit, suppressed the formation of 17 nm diameter filaments and constriction of the intercellular bridge[538], suggesting that ESCRT-III may either directly polymerize into 17 nm filaments during abscission or regulate their assembly.

The timing of abscission is regulated by multiple kinases and by mechanical tension. Both Plk1 and Aurora B play additional functions in regulating ESCRT-III; while, Plk1 suppresses ESCRT-III accumulation by phosphorylating CEP55[545], Aurora B kinase phosphorylates ESCRT-III subunit CHMP4C and functions as a negative regulator of abscission[546–548]. In Drosophila egg chambers, abscission timing is regulated by positively by Cyclin B and negatively Aurora B. As Aurora B phosphorylates Cyclin B directly, these authors proposed a model whereby the mutual inhibition between Aurora B and Cyclin B regulates the duration of abscission[547]. Finally, in a tissue context, abscission may be further regulated by mechanical tension between the nascent sister cells, as severing the intercellular bridge by laser microsurgery triggered ESCRT-III accumulation and abscission. Thus, abscission was proposed to only occur upon the release of the tension on the intercellular bridge[549].

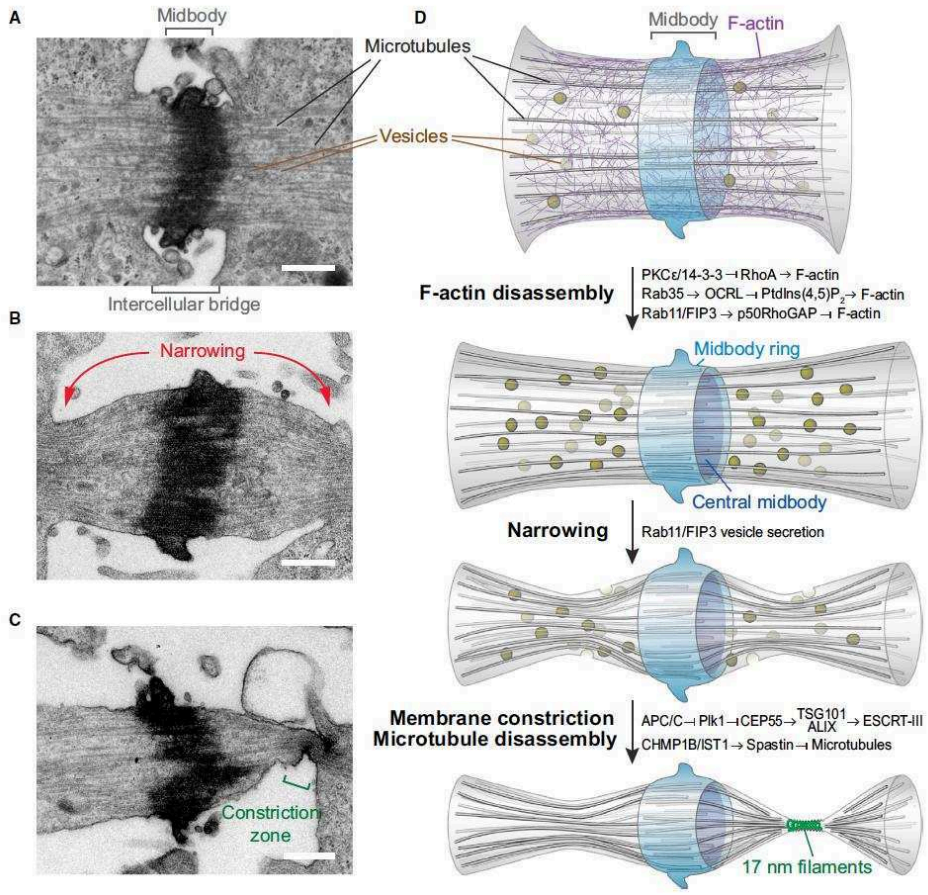

Figure 21: Maturation of the Intercellular Bridge.

(A–C) Transmission electron micrographs of intercellular bridges of HeLa cells at progressive stages of maturation. During early-stages, the intercellular bridge contains bundles of straight MTs, which will adopt an increasingly compressed appearance during maturation. Finally, the intercellular bridge becomes rippled and a constriction region appears, thus further enhancing MT compression. Scale bars, 500 nm. (D) Schematic representation of the events leading to intercellular bridge maturation. Upon full contractile ring constriction, F-Actin in the furrow region is disassembled. Finally, abscission proceeds by assembly and constriction of 17 nm filaments adjacent to the midbody and simultaneous disassembly of the microtubules lateral to the midbody (adapted from[483]).

B. Cytokinesis in a multicellular context

The molecular mechanisms underlying contractile ring positioning, assembly and constriction, as well as midbody formation and abscission were mostly dissected in cells growing in culture or in early embryonic stages. These studies now serve as a valuable basis for studying how cytokinesis proceeds in multicellular contexts. As briefly outlined in the Introduction, in a

tissue, the dividing cell must preserve cohesiveness with its neighbours, while undergoing dramatic cell shape changes to perform both contractile ring constriction and abscission. Moreover, for tissue polarity and adhesion to be maintained during proliferation, a new set of cell-cell contacts must be assembled between the daughter cells. In line with this, early reports published in the 1990s analysed cell division in the mouse small intestine epithelium and in MDCK monolayers by electron microscopy and by immunofluorescence, respectively. In both cases, the dividing epithelial cells were shown to maintain adhesion with their neighbours, supporting that epithelia integrity is indeed maintained throughout tissue proliferation[550,551]. Similar observations were reported soon after in cultured mouse hepatocytes[552]. More recently, a number of studied revisited this question and characterized cell division in vivo in a series of epithelial tissues both in vertebrates and invertebrates[1–6]. The increased temporal and spatial resolution employed allowed these authors to uncover novel aspects of cytokinesis in multicellular contexts. In this section, I will outline the general picture emerging from cell division in multicellular contexts, as well as discuss the main unresolved questions in the field. I will start by discussing junction remodelling between the dividing cell and its neighbours during contractile ring constriction, then I will shift gears to discuss how apical midbody positioning contributes for epithelial architecture and, finally, how new junctions assemble between the daughter cells upon cell division.

(i) Adherens Junction Remodelling during Cytokinesis

During cytokinesis, epithelial cells remain polarized and tightly attached to their neighbours. Accordingly, upon contractile ring constriction in the dividing cell, the neighbours progressively deform and eventually become interposed in between the daughter cells, thereby ensuring that tissue integrity is maintained during proliferation[1,2,4–6,550,551,553]. Thus, the dividing cell must overcome the resisting forces exerted by the neighbours in order to complete cytokinesis. In line with this, it was proposed that a local down-regulation of E-Cadherin at the ingressing AJ, termed adhesion disengagement, is required for the dividing cell to overcome the resisting forces exerted by the neighbouring cells[2,3]. Accordingly, reducing the rate of contractile ring constriction by Septin or Anillin RNAi, delays or impairs both junction disengagement and new junction formation. Moreover, when the dividing cell pulls too close to a vertex, where the resisting forces exerted by the neighbours are likely to be higher, junction disengagement is affected[2,3]. In line with this, lowering or increasing E-Cadherin dosage in the Drosophila embryonic ectoderm affects the timing of adhesion disengagement and new junction formation[3]. Altogether these findings suggest that a tug-of-war exists between the pulling forces produced in the dividing cell during contractile ring constriction and the resisting forces exerted by its neighbouring cells. These authors further

proposed that adhesion disengagement is required to allow efficient contractile ring constriction and new junction formation.

In agreement with their reported function in stabilizing the intercellular bridge[528], Septins or Anillins dividing cells tend to fail cytokinesis at later stages after full contractile ring constriction[2,3]. In those cases, contractile ring constriction in the dividing cell still proceeds even though adhesion disengagement is impaired[2,3], supporting that even under low contraction, the dividing cell can undergo cytokinesis without adhesion disengagement. Finally, it was recently shown in the Xenopus embryo that E-Cadherin levels at the ingressing junction are stabilized by Vinculin during cell division, arguing that the resisting forces imposed by the neighbours are unlikely to prevent cell division. Thus, several aspects of epithelial cell cytokinesis remain unclear, namely: (i) what drives adhesion disengagement at the ingressing junction; (ii) whether cytokinesis proceeds or not independently of its neighbours; and, (iii) what is the role of the resisting forces exerted by the neighbouring cells during cell division.

(ii) Apical Midbody Positioning: conserved feature of epithelial cell cytokinesis?

In monolayered epithelial tissues, the mitotic spindle is usually oriented parallel to the plane of the tissue, thereby ensuring that both daughter cells are integrated in the monolayer. Therefore, contractile ring constriction proceeds perpendicularly to the plane of the tissue and the dividing cell is cleaved along its apical-basal axis. Interestingly, in most epithelial tissues studied so far, furrowing is asymmetric, with contractile ring constriction occurring from the basal to the apical domain, thereby positioning the midbody apically (Fig. 22). Accordingly, asymmetric furrowing was observed in MDCK monolayers[550], in the mouse small intestine epithelium[551], in cultured mouse hepatocytes[552], in the Drosophila embryonic ectoderm[3], pupal notum[1,2] and follicular epithelium[4], as well as in the chicken[5] and Xenopus embryonic epithelia[6]. Notably, asymmetric furrowing is not a specific property of epithelial tissues, as in early C. elegans embryos and in the vertebrate neuroepithelium[554–556] furrow ingression is also asymmetric. In the vertebrate neuroepithelium furrowing proceeds in a stereotypical manner directed from the basal to apical plane[554–556], while in the C. elegans embryo the direction of ingression is random. In this system, polarized furrowing relies on the asymmetric distribution of MyoII within the contractile ring, which, in turn, depends on the distribution of both Anillin and Septins within the ring[557].

In the epithelial tissues studied so far, neither Anillin nor Septins are required for asymmetric furrow ingression[2–4]. Accordingly, in the Drosophila embryonic ectoderm and follicular epithelium, the distribution of Septins and MyoII in the contractile ring is fairly uniform. In these systems, apical positioning of the AJs was shown to drive asymmetric constriction of the contractile ring. In line with this, upon E-Cadherin, β-Catenin or α-Catenin depletion, asymmetric

furrow ingression is abolished[3,4]. Moreover, in a polarization assay in S2 cells, where E-Cadherin cytosolic tail was fused to the extracellular domain of Echinoid, promoting its recruitment to the sites of cell-cell contact, the midbody was efficiently recruited to sites of E-Cad enrichment[4]. In contrast with this, in the Drosophila pupal notum, asymmetric furrowing is still observed upon E-Cadherin, β-Catenin or α-Catenin RNAi, arguing against a role for the AJs in polarizing contractile ring constriction (our own unpublished findings). In agreement with an intrinsic asymmetry in the contractile ring, MyoII and Septins are enriched at the basal part of the ring, where the rate of constriction is higher[1,2]. However, how this asymmetry is regulated remains unclear.

Importantly, although asymmetric furrowing is prevalent in most epithelial tissues studied so far, a few examples of symmetric furrowing were also reported, namely in the wing epithelium[1] and, in some cases, in the follicular epithelium in Drosophila[4]. Despite the observation that contractile ring ingression proceeds in a symmetric fashion, in both cases the midbody is still apically positioned. The apical positioning of the midbody results either from partial apical cell extrusion, or by an AJ-dependent upward movement of the midbody following symmetric contractile ring constriction (Fig. 22). In both tissues the contractile ring is symmetric, with a uniform distribution of MyoII[1,4]. Interestingly, also in the follicular epithelium, the more the dividing cell extrudes from the epithelial layer, the more symmetric furrowing is observed[4].

In summary, regardless of the mode of furrowing, apical positioning of the midbody seems to be conserved in all studied epithelia. Work in the follicular, wing and dorsal thorax Drosophila epithelia showed that apically positioning of the midbody does not serve simply as a platform for abscission, but also act as a cue to control the propagation of apical-basal polarity during proliferation and preserving tissue architecture[1,4]. Accordingly, fusing the E-Cadherin intracellular domain to Dystroglican, a basal transmembrane protein, occasionally resulted in the formation of epithelial invaginations, characterized by a basal shift of the new interface between the daughter cells. This basal re-localization of the daughter cells interface resulted from the ectopic recruitment of AJ components basally. Interestingly, the authors also noted that upon expression of the E-Cad-Dystroglican protein fusion, both the midbody and its Arp2/3-dependent F-Actin polymerization wave were also shifted basally[4]. Similar results were reported in the pupal notum[1], supporting the direct involvement of the midbody in the generation of a wave of F-Actin polymerization.

In the Drosophila pupal notum, F-Actin polymerization at the midbody contributes to the formation of a long cell-cell contact between the daughters. During contractile ring constriction, the cells neighbouring the dividing cell are deformed and become interposed in between the future daughter cells, thereby preventing new junction formation. Live imaging analysis revealed that, as the midbody forms in the dividing cell and a wave of F-Actin appears around the midbody, the neighbouring cells membranes are pushed away, allowing the new AJ to expand. Accordingly, Rac, Arp2/3 and Scar/WAVE mutant dividing cells exhibit lower levels of F-Actin around the midbody

and, consequently, the new interface formed between the daughter cells is shorter than in wt cases[1](unpublished results). These findings support that Rac and Arp2/3 activities in the dividing cell push away the neighbouring cells and allow rapid expansion of the daughters interface. Altogether, these studies support a role for the midbody in providing a spatial cue for the formation of the apical daughter cell interface and preserving tissue architecture during proliferation.

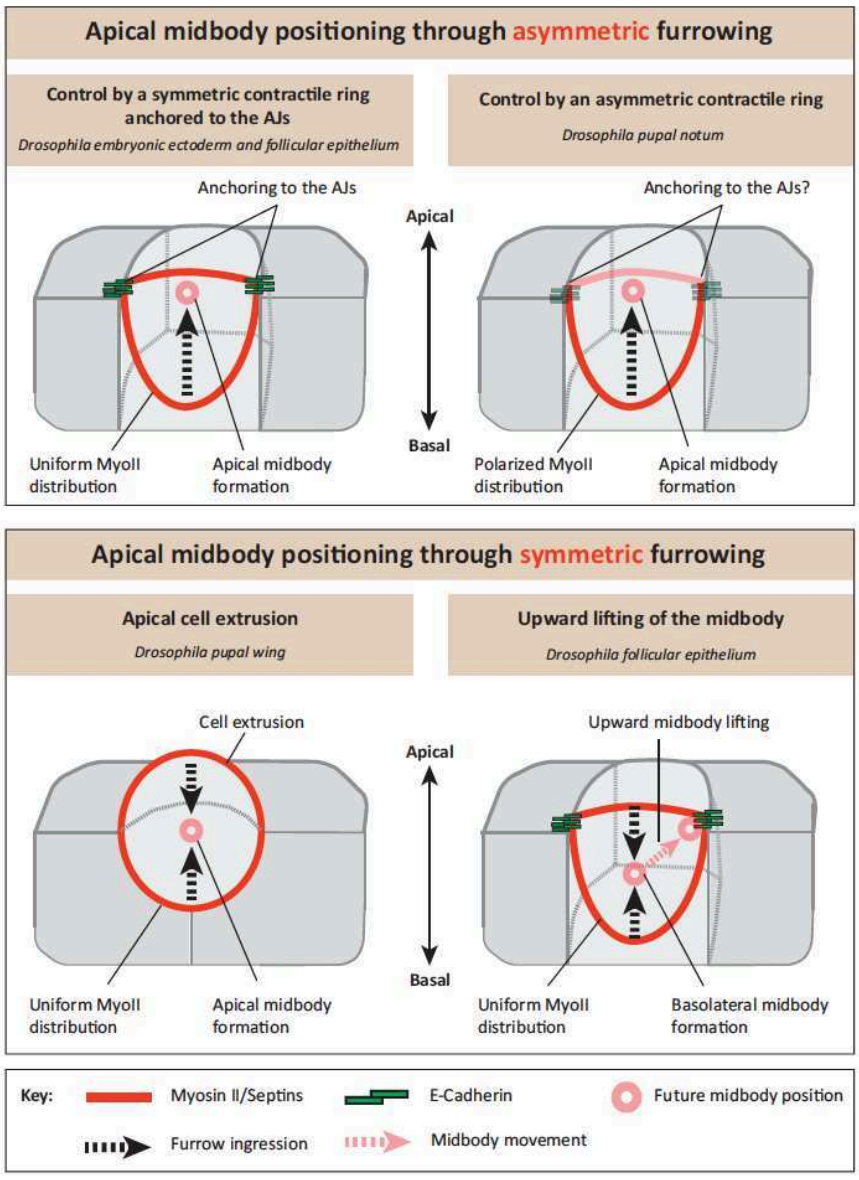

Figure 22: Different mechanisms ensure apical midbody positioning in epithelia.

In the examples highlighted in the top panel, apical midbody positioning results from asymmetric furrowing. Asymmetric furrowing can result from contractile ring anchoring to the AJs (left), or from an intrinsically asymmetric contractile ring, with MyoII enrichment at the basolateral domain of the ring (right). In the examples schemed in the lower panel, apical midbody positioning is achieved via symmetric furrowing, via

partial apical cell extrusion (left) or via the upward lifting of the midbody following symmetric constriction (right; adapted from[558]).

(iii) De Novo Cell-Cell Contact Formation

In order to preserve tissue polarity and adhesion during proliferation, a new set of cell-cell contacts must be assembled between the daughter cells after each round of cell division. In line with this, it is well-known that epithelial clones do not scatter and tend to form cohesive groups[553], indicating that at each round of cell division the daughter cells remain in contact. This was confirmed in the Drosophila wing epithelium, where the majority of the dividing cells form a new junction between the daughter cells (94%). Interestingly, in a small percentage of cases (6%), the authors reported that either a short contact assembles between the daughters or a cell intercalation event occurs and the neighbouring cells, rather than the daughters establish a new contact[559]. Similar results were subsequently reported in the embryonic ectoderm[3], follicular epithelium[4] and pupal notum[1,2]. Since daughter cell adhesion upon cell division was also reported in early studies in MDCK monolayers and mouse intestine epithelium[550,551], it was proposed that the formation of a long contact between the daughter cells after each round of division is likely to be a conserved feature of epithelia.

The mechanisms underlying new junction formation were dissected in the Drosophila pupal notum, where it was shown that an interplay between the dividing cell and its neighbours is required to set the geometry of the new cell-cell contacts. Accordingly, upon circular laser ablation, where the dividing cell is mechanically isolated from its direct neighbours, the new AJ formed between the daughter cells is short, reminiscent of the 6% cases detected in the wing epithelium. Herszterg and colleagues reported that, during contractile ring constriction in the dividing cell, the neighbouring cells become increasingly deformed and, eventually, accumulate MyoII. Importantly, MyoII accumulation in the neighbours is concomitant to membrane juxtaposition in the dividing cell. Consistent with an essential role for MyoII in promoting membrane juxtaposition, preventing MyoII accumulation in the neighbours genetically, or by laser ablation, affects membrane juxtaposition and shortens the final length of the junction formed between the daughter cells. During membrane juxtaposition, the neighbours remain interposed in between the daughters, thereby preventing de novo junction assembly. As mentioned above, this final step before new junction assembly requires a Rac- and Arp2/3-dependent wave of F-Actin polymerization in the dividing cell, thereby squeezing out the neighbours and allowing adhesion to be established in between the daughter cells (Fig. 23). Importantly, in some cases, Rac or Arp3 mutant dividing cells rather assemble a new cell-cell contact in between the two neighbouring cells, resulting in a

rearrangement[1]. In summary, these findings highlighted that in a tissue, cell division is not a strictly autonomous process and supported that cooperation between the dividing cell and its neighbours is essential to preserve tissue cohesiveness, adhesion and polarity during proliferation.

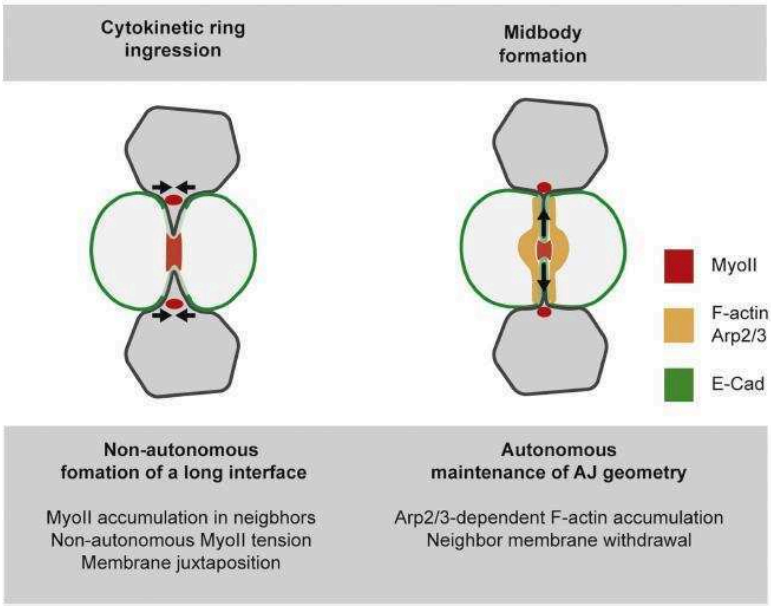

Figure 23: Interplay between the dividing cell and its neighbours regulates de novo AJ formation upon epithelial cytokinesis.

During contractile ring constriction, MyoII accumulates in the neighbours, thereby providing the cortical tension required for membrane juxtaposition in the dividing cell. Following midbody formation, a wave of F-Actin polymerization is observed in the dividing cell. Concomitantly, the neighbouring cell membranes withdraw, allowing the new junction to form in between the daughter cells (adapted from[1]).

A recent follow-up study extended these findings and highlighted an unexpected role for cell division in promoting tissue morphogenesis in the chick embryo. Using live imaging, Firmino and colleagues analysed epithelial proliferation and new junction formation throughout the early developmental stages of the chick embryo, both before and during the gastrulation movements[5]. In contrast to the generally accepted view that assembly of a cell-cell interface between daughter cells is a conserved feature among Metazoa, these authors reported that, depending on the developmental stage, the new junction formed upon cell division may be established either in between the daughter cells or in between the neighbours, giving rise to cell rearrangement events[5,559]. Importantly, it is the interplay between the tensile forces generated by the dividing cell and the dynamics of actomyosin in the neighbouring cells that prevents rearrangements before the onset of gastrulation, whereas it favours cell division-powered rearrangements as gastrulation

movements occur. During gastrulation, cell division-mediated intercalations represent the majority of cell intercalation events observed, as blocking cell division prevents rearrangements within the early embryo, resulting in defective morphogenetic movements (Fig. 24)[5]. These findings underscore that the interplay between the dividing cell and its neighbours is conserved and further suggest that simply altering the mechanics of the neighbouring cells can shift the balance towards adhesion between the daughters or power rearrangements. Importantly, cell division was also shown to power cell rearrangements during mouse limb ectoderm morphogenesis[560].

Finally, work published earlier this year in the epithelium of gastrula-stage Xenopus Laevis embryos analysed how the Tight Junctions and the Tricellular Tight Junctions are remodelled and re-formed after cell division, a question that had remained poorly explored in previous studies, which focused on the events at the level of the AJs. In agreement with previous findings, Higashi and colleagues found that, during constriction in the dividing cells, the neighbours are pulled and become interposed in between the daughter cells[6]. However, in this system, the neighbouring cells do not withdraw and remain inserted in between the daughters, consistent with the absence of the wave of F-Actin polymerization at the midbody observed in the follicular, wing and dorsal thorax epithelia in flies[1,4,6]. After cell division, adhesion is established between the neighbours and two new Tricellular Tight Junctions assemble at each side of the midbody, in a conformation similar to a rosette. Interestingly, within 1 hour, only ¼ of the neighbouring cells remained in contact giving rise to a rearrangement, while most cells re-established adhesion between the daughter cells[6]. Thus, now it would be interesting to characterize how adhesion is re-established between the daughter cells and whether this contributes to tissue morphogenesis.

In conclusion, these studies provided a wealth of knowledge into the mechanisms underlying epithelial cell cytokinesis in a variety of systems, from flies to chicken. The general picture emerging is that, in epithelial tissues, a crosstalk between the dividing cell and its neighbours is essential to regulate the formation of new cell-cell contacts between the daughter cells, as well as to determine their arrangement in the tissue. Thus, for my PhD, I aimed to understand how the dividing cell signals to its neighbours. By dissecting how epithelial cells couple their behaviours during cell division, this work is likely to provide valuable insights to understand how the integrity, the arrangement and morphogenesis of proliferative tissues is regulated.

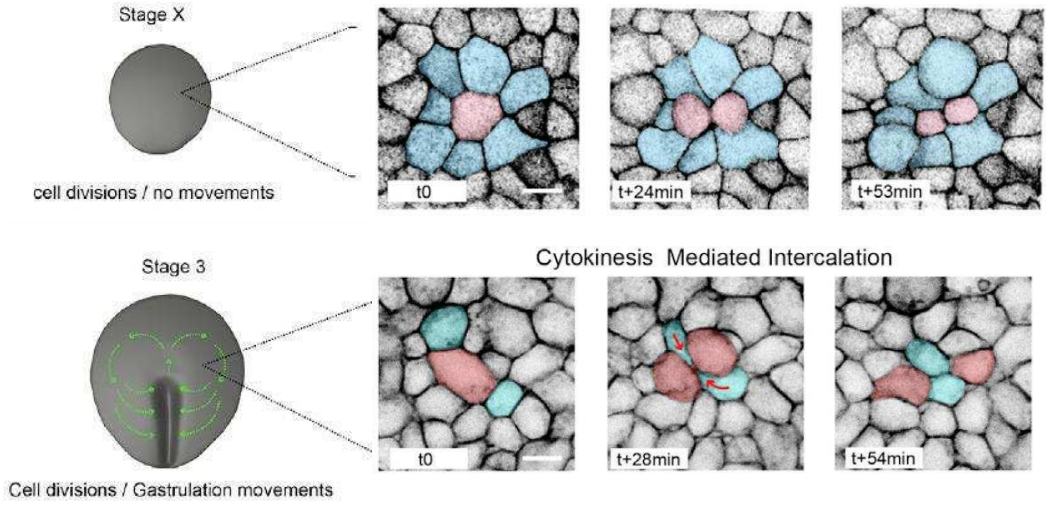

Figure 24: Cell division-mediated rearrangement contribute to chick gastrulation movements.

At stage X, before gastrulation movements initiate, epithelial cells divide (pink) and the new junction is formed between the daughter cells. In this stage, neighbouring cells (blue) accumulate actomyosin and seem to resist the deformation imposed by the dividing cell, thereby preventing a cell-cell rearrangement. At stage 3, as gastrulation movements are taking place, cell division promotes epithelial cell rearrangements. At this stage, the neighbouring cells exhibit lower actomyosin accumulation, thus the dividing cells displaces its neighbours, bringing them in between the future daughters (adapted from[5]).

RESULTS:

This Results section will be organized into three distinct parts corresponding to the publications I have worked on during my PhD, respectively:

- **Transmission of cytokinesis forces via E-Cadherin dilution and actomyosin flows** (in revision). This first section corresponds to the bulk of my experimental work and outlines our main findings.

- **Studying cytokinesis in Drosophila epithelial tissues** (in press). This is a technical paper, written as a Methods Chapter to be published in a special Cytokinesis edition of Methods in Cell Biology. The aim was to provide the scientific community with a detailed description of the methods available to perform live imaging of cell division in Drosophila epithelial tissues, to share useful reagents and techniques, as well as discuss some important aspects of image processing and analysis useful to the study cytokinesis.

- **A multicellular view of cytokinesis in epithelial tissues**. This review article was written in collaboration with a previous PhD student in the team, Sophie Herszterg and helped us to set the stage for my thesis work, as it involved an extensive review of the literature regarding epithelial cell cytokinesis. Since its publication however additional studies reported novel aspects of epithelial cell cytokinesis in vertebrates, therefore I provided and updated discussion in Chapter IV of Introduction.

Transmission of cytokinesis forces via E-Cadherin dilution and actomyosin flows

Diana Pinheiro[1,2,3], Edouard Hannezo[4,5,*], Sophie Herszterg[1,2,6,*], Floris Bosveld[1,2], Isabelle Gaugue[1,2], Maria Balakireva[1,2], Zhimin Wang[1,2], Stéphane Rigaud[1,2], Olga Markova[1,2] and Yohanns Bellaïche[1,2°]

1: Institut Curie, PSL Research University, CNRS UMR 3215, INSERM U934, F-75248 Paris Cedex 05, France.

2: Sorbonne Universités, UPMC Univ Paris 06, CNRS, CNRS UMR 3215, INSERM U934, F-75005, France.

3: Graduate Program in Areas of Basic and Applied Biology, Abel Salazar Biomedical Sciences Institute, University of Porto, Portugal.

4: Cavendish Laboratory, Department of Physics, J. J. Thomson Avenue, University of Cambridge, Cam ridge CB3 0HE, UK

5: The Wellcome Trust/Cancer Research UK Gurdon Institute, Tennis Court Rd, University of Cambridge, Cambridge CB2 1Q , United Kingdom.

6: Present address: The Francis Crick Institute, Mill Hill Laboratory, The Ridgeway, NW7 1AA, London UK

* these authors contributed equally to this work.

° Corresponding author: yohanns.bellaiche@curie.fr

Abstract:

During epithelial cytokinesis, the remodelling of adhesive cell-cell contacts between the dividing cell and its neighbours has profound roles in the integrity, the arrangement and morphogenesis of proliferative tissues[1-7]. In both vertebrates and invertebrates, this remodelling requires the activity of non-muscle Myosin II (MyoII) in the interphasic cells neighbouring the dividing cells[1,3,6]. However, the mechanisms coordinating cytokinesis and MyoII activity in the neighbours are unknown. Here, we found that, in the *Drosophila* notum epithelium, each cell division is associated with a mechano-sensing and transmission event controlling MyoII dynamics in the neighbours. We established that the ring pulling forces promote local junction elongation, resulting in a decrease of E-Cadherin (E-Cad) concentration at the ingressing *adherens* junction (AJ). In turn, the local reduction of E-Cad concentration and the contractility of the neighbouring cells promote self-organized actomyosin flows, ultimately leading to MyoII accumulation at the base of the ingressing AJ. While mechano-sensing has been extensively studied in the context of AJ reinforcement to stabilize the adhesive cell-cell contacts[8], we propose an alternative mechano-sensing mechanism able to coordinate actomyosin dynamics between epithelial cells and to sustain AJ remodelling in response to mechanical forces.

In both Vertebrate and *Drosophila* epithelial tissues, constriction of the contractile ring deforms the dividing cell as well as the neighbouring cell membranes, which co-ingress at the rim of the contractile ring and remain closely apposed[1,3-7] (Fig. 1a). Concomitantly, in the cells neighbouring the dividing cell, MyoII participates in the remodelling of the adhesive contacts formed between the dividing cell and its neighbours[1,6,7]. Accordingly, in several *Drosophila* epithelial tissues, MyoII accumulates near the base of the ingressing membrane in the neighbours, where it provides the tension required to juxtapose the dividing cell membranes[1,3,7](Fig. 1a). Since the remodelling of the adhesive contacts during cell division is critical for the integrity, the arrangement and morphogenesis of proliferative tissues[1-7], we analysed, in the *Drosophila* notum

epithelium, whether and how the dividing cell signals to its neighbours to regulate MyoII dynamics.

The contractile ring produces mechanical forces deforming the dividing cell and its neighbours (Fig. 1a). As MyoII accumulation in the neighbours is observed from mid-constriction onwards (Fig. 1b), we investigated the role of contractile ring pulling forces by analysing whether they increase during constriction and whether their magnitude is important for MyoII accumulation. To estimate the magnitude of these forces, we used laser ablation to sever the contractile ring, labelled by MyoII::mCherryFP (MyoII::mChFP), and measured the initial recoil velocity of the AJs, labelled by E-Cadherin::GFP (E-Cad::GFP). We found that the recoil velocity increases with the amount of ring constriction, indicating that the pulling forces build up during cytokinesis (Extended Data Fig. 1a,b). Furthermore, the ablation of the contractile ring prior to, or after mid-constriction, prevented or abolished MyoII accumulation in the neighbouring cells, respectively (Fig. 1c,d). These findings support the idea that the pulling forces exerted by the contractile ring are required to both trigger and sustain MyoII accumulation in the neighbours. To further probe the role of force in the neighbouring cells response, we tested whether a reduction of the pulling forces exerted by the dividing cell could affect MyoII accumulation. While *pnut (Drosophila Septin-7)*, *rok (Drosophila Rho-Kinase)* and *ani* (*anillin*) have distinct roles during cytokinesis[9], decreasing their function in the dividing cell reduced both the rate of contractile ring constriction and the AJ recoil velocities upon contractile ring laser ablation relative to wild-type (*wt*) dividing cells (Fig. 1e,g and Extended Data Fig. 1a-h). This supports that *pnut, rok* and *ani* dividing cells exert less force on the AJs during cytokinesis. Importantly, MyoII accumulation is reduced in cells neighbouring *pnut*, *rok* and *anillin* dividing cells (Fig. 1f,h and Extended Data Fig. 1i). Furthermore, the amount of MyoII accumulation in the neighbours' scales with the magnitude of the pulling forces produced in the dividing cells, as estimated by the average recoil velocities (Fig. 1i). Together, these findings indicate that MyoII accumulation in the neighbouring cells depends on the pulling forces generated by contractile ring constriction in the dividing cell. Cytokinesis therefore provides an endogenous and local mechanical force generator to study the mechanisms of force sensing and MyoII dynamics during AJ remodelling.

To begin deciphering how pulling forces can ultimately result in MyoII accumulation in the neighbouring cells, we performed higher spatio-temporal resolution analyses of E-Cad::GFP and cortical MyoII distributions during cytokinesis. Prior to constriction, E-Cad::GFP and cortical MyoII::mChFP signals colocalize (Fig. 2a, t=0s and Fig. 2b). As constriction proceeds, the AJ at the edges of the furrow locally elongates, becomes increasingly curved, and, as previously described, the E-Cad::GFP signal locally decreases[1,3] (Fig. 2a, insets and Fig. 2b). Concomitantly, the signals of E-Cad::GFP and MyoII::mChFP in the neighbouring cells separate and no longer colocalize (Fig. 2a, insets and Fig. 2b). The spatial separation of the E-Cad::GFP and MyoII::mChFP signals indicates a local cortex detachment from the AJ, since: (i) the

MyoII::mChFP cortical signal remains at a relatively fixed position away from the tip of the ingressing AJ, while the E-Cad::GFP signal keeps ingressing with the cell membranes (marked by CAAX::mOrg) (Fig. 2c), (ii) the cortical marker β_H-spectrin, which colocalizes with MyoII at the cell cortex prior to constriction, remains colocalized with MyoII away from the ingressing AJ (Fig. 2d). Soon after, and while the E-Cad::GFP signal remains low in the ingressing AJ, MyoII::mChFP accumulates at the base of the ingressing AJ (Fig. 2a, insets and Fig. 2b). The local E-Cad decrease is also accompanied by a decrease in α-catenin::GFP (α-Cat::GFP) signal, suggesting that the E-Cad-Catenins complex concentration decreases along the ingressing membrane (Extended Data Fig. 2a). The accumulation of MyoII in the neighbouring cells is therefore preceded by two events: a local detachment of the cortex and a local decrease of the E-Cad-Catenins complex concentration along the ingressing AJ. This contrasts with the previously described mechano-transduction pathways, known to rely on the attachment of the Cad-Catenins complex to the underlying cortex and to reinforce this attachment by promoting additional Actin and MyoII recruitment to the AJ[10-15]. Together, these findings lead us to investigate whether an uncharacterized mechano-sensing mechanism mediates the response to the endogenous pulling forces associated with contractile ring constriction.

Having observed that cortical MyoII locally detaches from the AJs prior to its accumulation, one possibility would be that MyoII accumulation arises from the contraction of the detached cortical MyoII. However, several lines of evidence argue against this simple model. First, in cells neighbouring *pnut* dividing cells, cortex detachment was observed in 50% of the cases in the absence of a marked E-Cad::GFP decrease (n=20 cells, Fig. 2e). Although weak and transient accumulations of MyoII could be observed in these neighbouring cells at the position of the detached cortex, MyoII failed to strongly and steadily accumulate (Fig. 2e). This shows that cortex detachment is not sufficient to drive persistent MyoII accumulation in the neighbours. Second, upon laser ablation of the detached cortex, MyoII re-accumulates at the base of the ingressing membranes in the neighbouring cells (Fig. 2f). Lastly, having analysed theoretically and experimentally that cortex detachment, in response to the contractile ring pulling forces, is determined by a balance between membrane curvature, membrane-cortex adhesion and contractility (Extended Data Fig. 3a-d and Supplementary Theory Note), we induced a precocious detachment of the cortex by reducing the function of Moesin (Moe), which promotes membrane-cortex adhesion[16] (Fig. 2g, Extended Data Fig. 3a-d and Supplementary Theory Note). In these conditions, the initially detached cortical MyoII is localized further away from the ingressing membrane during ring constriction (Fig. 2g, insets). While a transient accumulation of MyoII could be observed around the position of the detached cortex, MyoII becomes strongly enriched away from it, at the base of the ingressing AJ, nearby the boundary between low and high E-Cad::GFP signals (Fig. 2g, insets). Collectively, these data indicate that MyoII accumulation does not arise solely from the contraction of the detached cortex and further suggest that the position of

MyoII accumulation is determined by the boundary between the low and high E-Cad concentration domains.

We therefore analysed in detail the mechanisms underlying the decrease of E-Cad concentration at the ingressing AJ, as well as its role in the response of the neighbouring cells. By generating adjacent patches of cells expressing E-Cad::GFP or E-Cad::3XmTagRFP, we found that the decrease of E-Cad signal is concomitant in the dividing cell and its neighbours (Extended Data Fig. 4a, insets). Two distinct mechanisms can account for a local reduction in E-Cad::GFP concentration: (i) a local decrease in the total amount of E-Cad::GFP, or (ii) a local E-Cad::GFP dilution. Since blocking E-Cad trafficking, using Dynamin, Rab11 or Sec5 mutant conditions, does not prevent the reduction of E-Cad concentration at the ingressing AJ (Extended Data Fig. 4b-d) and since the total amount of E-Cad::GFP does not decrease during AJ ingression (Extended Data Fig. 4e), we examined whether the local reduction of E-Cad concentration could result from its local dilution due to junction elongation. Kymographs generated along the ingressing junction showed that the local E-Cad decrease is concomitant to junction elongation (Fig. 3a-c). To analyse whether junction elongation would be sufficient to reduce E-Cad concentration at the ingressing AJ, we modelled E-Cad dynamics on a locally elongating junction (Extended Data Fig. 5a,b and Supplementary Theory Note). We found that E-Cad concentration depends on the rate of local elongation, as well as on the E-Cad turnover, immobile fraction and diffusion, which we determined experimentally by FRAP (Supplementary Table 1 and Supplementary Theory Note). As E-Cad diffusion is low and its immobile fraction is large on the time scale of *wt* cytokinesis, our numerical simulations illustrate how local junction elongation is sufficient to locally reduce E-Cad concentration, and to maintain this decrease in time, similarly to the *wt* experimental conditions (Fig. 3d and Extended Data Fig. 5a-c). In agreement with the notion that local junction elongation would be sufficient to reduce E-Cad concentration, we found that: (i) in the absence of Rok activity in the neighbouring cells, which impairs MyoII accumulation[1], E-Cad signal still decreases, indicating that the decrease is not a consequence of MyoII accumulation (Fig. 3e-h, Extended Data Fig. 4f and Extended Data Fig. 5a,b,d-j); (ii) *pnut* dividing cells, which do not show a marked E-Cad decrease at the edges of the furrow[3], display significantly lower and less local junction elongation (Fig. 3i-k, Extended Data Fig. 5a,b,f and Extended Data Figure 4g) and; (iii) the lower and less local junction elongation measured in cells neighbouring a *pnut* dividing cell is sufficient to reproduce the impaired E-Cad concentration decrease in our numerical simulation (Fig. 3l and Extended Data Fig. 5k-m). Together these findings indicate that the pulling forces exerted by contractile ring constriction promote local AJ elongation, which can account for the local decrease in E-Cad concentration.

Next, we asked whether the decrease of E-Cad levels would be sufficient to drive MyoII accumulation in the neighbouring cells. We hypothesized that, if lowering E-Cad levels is pivotal for MyoII accumulation, reducing total E-Cad levels would rescue MyoII accumulation in cells

neighbouring a *pnut* dividing cell, which produce lower pulling forces and junction elongation. Although *pnut* dividing cells facing an *E-Cad* mutant neighbour (E-Cad^{JH}) still constrict at a lower rate and fail cytokinesis, MyoII accumulation in the neighbours is, nevertheless, restored (Fig. 3m,n, and Extended Data Fig. 6a-e). Therefore, reducing E-Cad levels is sufficient to rescue the neighbouring cells response upon reduced pulling forces, supporting that the decrease of E-Cad concentration mediates the neighbours' response to cytokinesis forces.

We then analysed the mechanisms by which a decrease of E-Cad concentration triggers MyoII accumulation. For that, we considered both the signalling and mechanical roles of the E-Cad adhesion receptor. Under force, α-Cat locally recruits Vinculin (Vinc) to stabilize the AJ, by strengthening the link between α-Cat and the actomyosin cortex and further recruiting MyoII[10-14]. In agreement with our observations that the cortex locally detaches and that the E-Cad and α-cat signals decrease along the ingressing membrane, Vinc function was not necessary for MyoII accumulation in the neighbours (Extended Data Fig. 7a-d). Furthermore, Vinc did not colocalize with the MyoII accumulation in the neighbours (Extended Data Fig. 7a,e). E-Cad/Catenins complexes are also known sites of Rho GTPase signalling and F-Actin polymerization[8,17-21]. In agreement with previous findings[22,23], we found that loss of Rho or Dia function in the dividing cell results in defective cytokinesis (Extended Data Fig. 7f). In sharp contrast, their loss of function in the neighbouring cells only delays MyoII accumulation, supporting that their activities have only a minor contribution for the neighbouring cells response (Extended Data Fig. 7g-k). Finally, the E-Cad/catenin complexes also regulate the activity of the branched Actin nucleator Arp2/3[17,19]. Yet, Arp3 loss of function in the neighbours does not significantly affect MyoII accumulation (Extended Data Fig. 7l-n). Altogether, these results led us to investigate whether changes in the core physical property of the E-Cad/Catenins complex, i.e. its interaction with the underlying actomyosin cortex[8,24,25], could be sufficient to promote MyoII accumulation. For that, we modelled the actomyosin cortex of neighbouring cells using the classical active gel theory[26-29], as a one-dimensional viscous and contractile gel, adhered to a plasma membrane (Supplementary Theory Note). Theoretically, it has been shown that when MyoII contractility exceeds a threshold, an otherwise uniform cortex destabilizes into a local accumulation[30-32].

Having shown that E-Cad decrease promotes the response of the neighbouring cells, we investigated its role in determining the cortex stability threshold. Since E-Cad, via the Catenins, is physically linked to the actomyosin cortex and can restrict its dynamics[8,24,25,33,34], we modelled its function as an effective friction. Strikingly, this minimal model suggests that locally lowering E-Cad concentration and/or the linkage between the actomyosin cortex and the membrane, i.e. lowering locally the effective friction, is sufficient to spontaneously generate actomyosin flows, and thus drive a local actomyosin accumulation, even for uniform and constant MyoII contractility and F-Actin polymerization (Extended Data Fig. 8a-e). More importantly, using a 2D model taking into account the geometry of the ingressed AJ, we found that the decrease of friction along

the AJ is sufficient to drive actomyosin flows towards the boundary between low and high E-Cad concentrations (Fig. 4a-c and Extended Data Fig. 8f-m).

Our theoretical model suggests that MyoII accumulation arises from retrograde actomyosin flows in the ingressing region (Fig. 4c and Extended Data Fig. 8h,i), that would be distinct from the medial pulsatile flows associated with apical constriction and cell intercalation[33,35-38]. To test the predictions of our model *in vivo*, we analysed the existence and the direction of the actomyosin flows, as well as their contribution for MyoII accumulation in the neighbouring cells. For that, we generated groups of cells expressing MyoII::GFP facing MyoII::RFP dividing cells and photobleached the MyoII::GFP accumulation in the neighbours. Remarkably, MyoII accumulation recovers mostly from the ingressing membrane, as revealed by MyoII speckles flowing along the neighbouring cell membranes and reaching a MyoII::GFP pool at the base of the ingressing membrane (Fig. 4d,e). In contrast, the mobilization of MyoII from the medial pool and from the attached cortex located on each side of the ingressing AJ was small (Fig. 4d,e). Expressing Lifeact::GFP, an F-Actin probe, in the neighbouring cells in a MyoII::3XmKate2 tissue allowed us to visualize F-Actin dynamics exclusively in cells neighbouring a dividing cell. This revealed F-Actin speckles moving along the ingressing cell membranes and accumulating at the base (Fig. 4f,g) supporting that MyoII accumulation is associated with F-Actin flows within the ingressing region. As stated above, Rok is essential for MyoII accumulation in the neighbours, while Dia loss of function only delays the accumulation (Extended Data Fig. 7i,j). Accordingly, loss of Rok activity drastically reduced Lifeact::GFP speckle velocity in the ingressing region (Fig.4h,i and Fig. 4l,m), whereas Dia loss of function induced only a weak decrease in speckle velocity (Fig. 4j-m). Together, our experimental data and theoretical analysis support that a local decrease of E-Cad concentration at the ingressing AJ, resulting from the pulling forces produced by contractile ring constriction, plays a major role in driving the actomyosin flows in the neighbouring cells.

Cell division and AJ dynamics have pivotal roles in epithelial tissue development, regeneration and homeostasis. Here, we provide evidence that, in epithelial tissues, each cell division is associated with a force sensing and transmission event at the AJ shared by the dividing cell and its neighbours. Under physiological forces, resulting from contractile ring constriction in the dividing cell, AJ mechano-sensitivity arises from the local decrease of E-Cad concentration and results in actomyosin flows in the neighbouring cells. This mechanism coordinates the actomyosin dynamics between neighbouring cells during the AJ remodelling event associated with cell division. Conversely, previously proposed mechano-transduction mechanisms function to stabilize cell-cell junctions under mechanical forces and involve increased binding of α-cat to E-Cad and F-Actin, reduced F-Actin turnover and recruitment of Vinc, as well as MyoII[10-12,15,25,39-41]. By showing that a local decrease of E-Cad/Catenins concentration coordinates the actomyosin dynamics of neighbouring epithelial cells, our work extends the previously described function of

this complex in coupling cell cortices[42]. Actomyosin flows produce mechanical forces to organize cell polarity, cell shape, cell movement, as well as junction remodelling[27,31,33,35,36,38,43]. Our work highlights an additional role of actomyosin flows in force sensing and transmission between epithelial cells. Since mechanical forces have emerged as a tissue-scale regulator of polarization and collective cell movements[44-46], the integration of the roles of actomyosin flows in force production, sensing and transmission should provide a general framework to understand the coordination of epithelial cell dynamics.

FIGURE LEGENDS

Figure 1. Contractile ring pulling forces trigger MyoII accumulation in the neighbouring cells.

(a) Schematic representation of MyoII (red circles) accumulation in the neighbouring cells upon contractile ring constriction. D: dividing cell (white). N: neighbouring cells (light grey). Dark grey: cell outlines. Solid and dashed lines: contractile ring. Black arrows: force generated by MyoII in the neighbouring cells required to promote membrane juxtaposition in the dividing cell[1].

(b) E-Cad::GFP and MyoII::mChFP distribution in the dividing cell (D) and its neighbours (N). White arrowheads: MyoII::mChFP accumulation in the neighbouring cells from mid-constriction onwards. *n*=21 cells.

(c,d) E-Cad::GFP and MyoII::mChFP localization in the dividing cell (D) and its neighbours (N) upon contractile ring laser ablation before (c, *n*=48 ablations), or after (d, *n*=32 ablations) MyoII::mChFP accumulation. Dashed box: ablated region. Time was set to 0s at the time of ablation. White open arrowheads: reduced MyoII::mChFP accumulation in the neighbours. White arrowheads: MyoII::mChFP accumulation in the neighbouring cells.

(e) Graph of the AJ recoil velocity upon contractile ring laser ablation in *wt*, $pnut^{RNAi}$, rok^{RNAi} and ani^{RNAi} dividing cells (mean±SEM). *n*: number of cells. Kruskal-Wallis test, **: $p<0.01$; ****:$p<0.0001$.

(f) E-Cad::GFP and MyoII::mChFP localization in cells neighbouring *wt*, $pnut^{RNAi}$, rok^{RNAi} and ani^{RNAi} dividing cells (D). White dots: $pnut^{RNAi}$, rok^{RNAi} or ani^{RNAi} cells in each panel. White arrowheads: MyoII::mChFP accumulation in the neighbouring cells. White open arrowheads: reduced MyoII::mChFP accumulation in the neighbours.

(g) Graph of the rate of contractile ring constriction (s^{-1}, mean±SEM) in *wt*, $pnut^{RNAi}$, rok^{RNAi} and ani^{RNAi} dividing cells. *n:* number of cells. Kruskal-Wallis test, ****:$p<0.0001$.

(h) Graph of the normalized MyoII accumulation at 80% of the initial cell diameter (mean±SEM) in cells neighbouring *wt*, $pnut^{RNAi}$, rok^{RNAi} and ani^{RNAi} dividing cells. For details on the quantification of normalized MyoII accumulation, see Extended Data Fig. 1i and the Methods section. *n*: number of cells. Kruskal-Wallis test, **: $p<0.01$; ****:$p<0.0001$.

(i) Graph of the normalized MyoII accumulation in the neighbouring cells (mean±SEM, plotted in h) versus the recoil velocity (mean±SEM, plotted in e) for *wt*, $pnut^{RNAi}$, rok^{RNAi} and ani^{RNAi} dividing cells.

Scale bars: 5µm (b,c,d,f)

Figure 1.

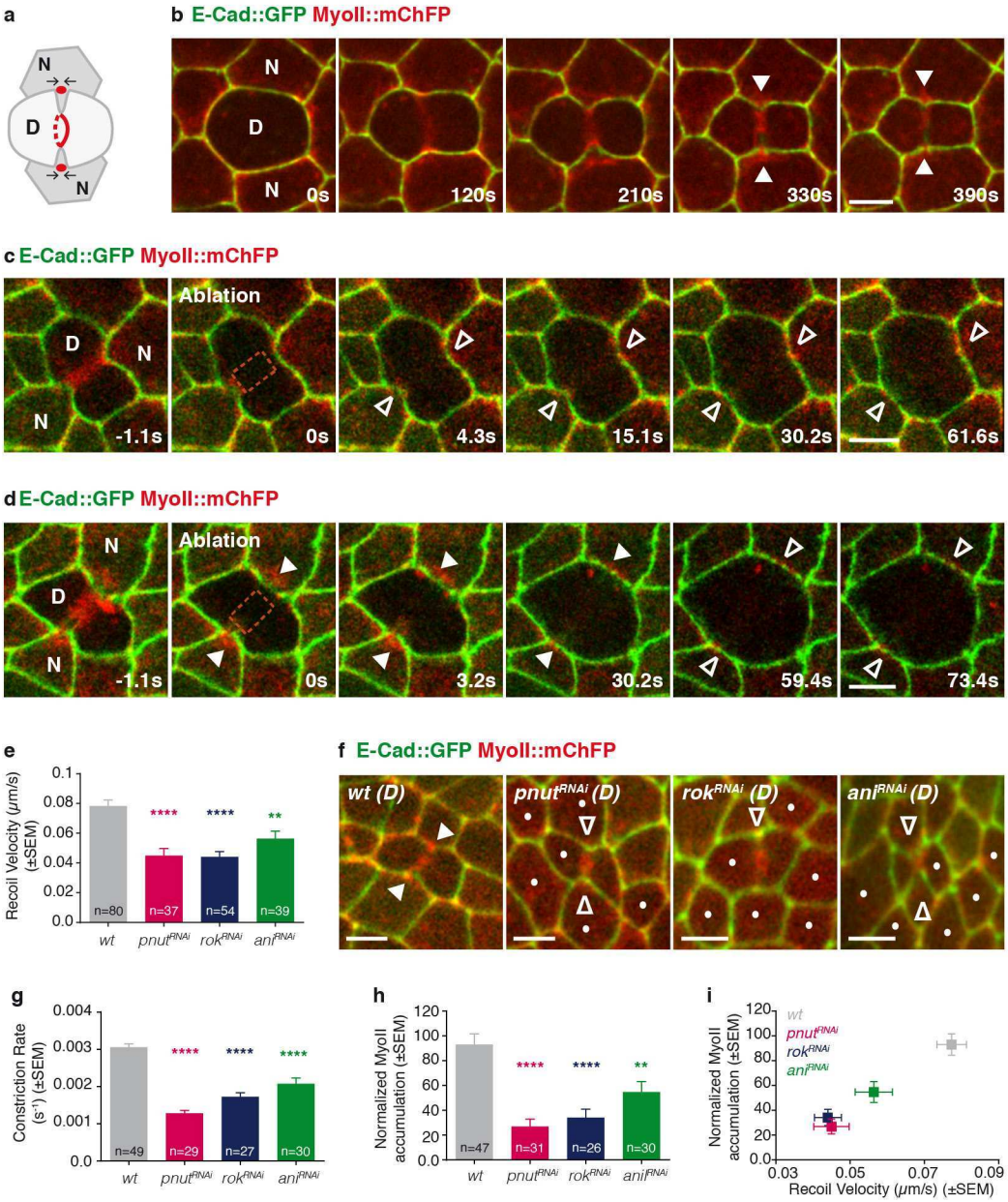
a
b E-Cad::GFP MyoII::mChFP
N
D
N
0s
120s
210s
330s
390s
c E-Cad::GFP MyoII::mChFP
Ablation
-1.1s
0s
4.3s
15.1s
30.2s
61.6s
d E-Cad::GFP MyoII::mChFP
Ablation
-1.1s
0s
3.2s
30.2s
59.4s
73.4s
e
Recoil Velocity (μm/s) (±SEM)
n=80
n=37
n=54
n=39
wt
pnut^RNAi
rok^RNAi
ani^RNAi
f E-Cad::GFP MyoII::mChFP
wt (D)
pnut^RNAi (D)
rok^RNAi (D)
ani^RNAi (D)
g
Constriction Rate (s⁻¹) (±SEM)
n=49
n=29
n=27
n=30
h
Normalized MyoII accumulation (±SEM)
n=47
n=31
n=26
n=30
i
Normalized MyoII accumulation (±SEM)
Recoil Velocity (μm/s) (±SEM)

Figure 2. Cortex detachment and decrease of E-Cad levels at the ingressing AJ precede MyoII accumulation in the neighbours.

(a,b) E-Cad::GFP and MyoII::mChFP localization in the dividing cell (D) and its neighbours (N). Yellow dashed box: region used to generate the kymograph in (b). White asterisk: separation of the MyoII::mChFP and the E-Cad::GFP signals at the ingressing AJ. Yellow open arrowheads: decrease of E-Cad::GFP signal at the ingressing AJ. White arrowheads: MyoII::mChFP accumulation in the neighbouring cells. *n*=23 cells.

(c) E-Cad::GFP, MyoII::3XmKate2 and CAAX::mOrg distribution in the dividing cell (D) and its neighbours (N). White asterisk: separation of the MyoII::3XmKate2 and the E-Cad::GFP and CAAX::mOrg signals at the ingressing AJ. White arrow: AJ ingression. Yellow open arrowheads: decrease of E-Cad::GFP signal at the ingressing AJ. *n*=24 cells

(d) β_H-Spectrin::GFP (β_H-Spec::GFP) and MyoII::3XmKate2 distribution in the dividing cell (D) and its neighbours (N). White asterisk: co-localization of MyoII::3XmKate2 and β_H-Spectrin::GFP away from the ingressing AJ. *n*=103 cells.

(e) E-Cad::GFP and MyoII::mChFP localization in a $pnut^{RNAi}$ dividing cell (D) and its neighbours (N). White dots: $pnut^{RNAi}$ cells. White asterisk: separation of the MyoII::mChFP and the E-Cad::GFP signals at the ingressing AJ. White arrowheads: transient MyoII::mChFP accumulation in the neighbouring cells. White open arrowheads: reduced MyoII::mChFP accumulation in the neighbouring cells. *n*=28 cells.

(f) E-Cad::GFP and MyoII::mChFP localization in the dividing cell (D) and its neighbours (N) upon laser ablation of the detached cortical MyoII. Time was set to 0s at the time of ablation. Dashed box: ablated region. Brackets: width of the ingressed AJ, indicating the relaxation of the neighbouring cell upon laser ablation. White arrowheads: MyoII::mChFP accumulation in the neighbouring cell upon laser ablation of the detached MyoII::mChFP. *n*=24 ablations.

(g) E-Cad::GFP and MyoII::mChFP localization in the dividing cell (D) and its moe^{RNAi} neighbour (N). White dots: moe^{RNAi} expressing cells, marked by the absence of cytosolic GFP. White asterisk: separation of the MyoII::mChFP and the E-Cad::GFP signals at the ingressing AJ. White arrowheads: at t=208s, it indicates the transient accumulation of MyoII::mChFP at the detached cortex; at t=340s and t=400s, it indicates the re-localization of the MyoII::mChFP accumulation near the boundary between high and low E-Cad::GFP. *n*=18 cells.

Scale bars: 5µm (a,c,d,e,f,g)

Figure 2.

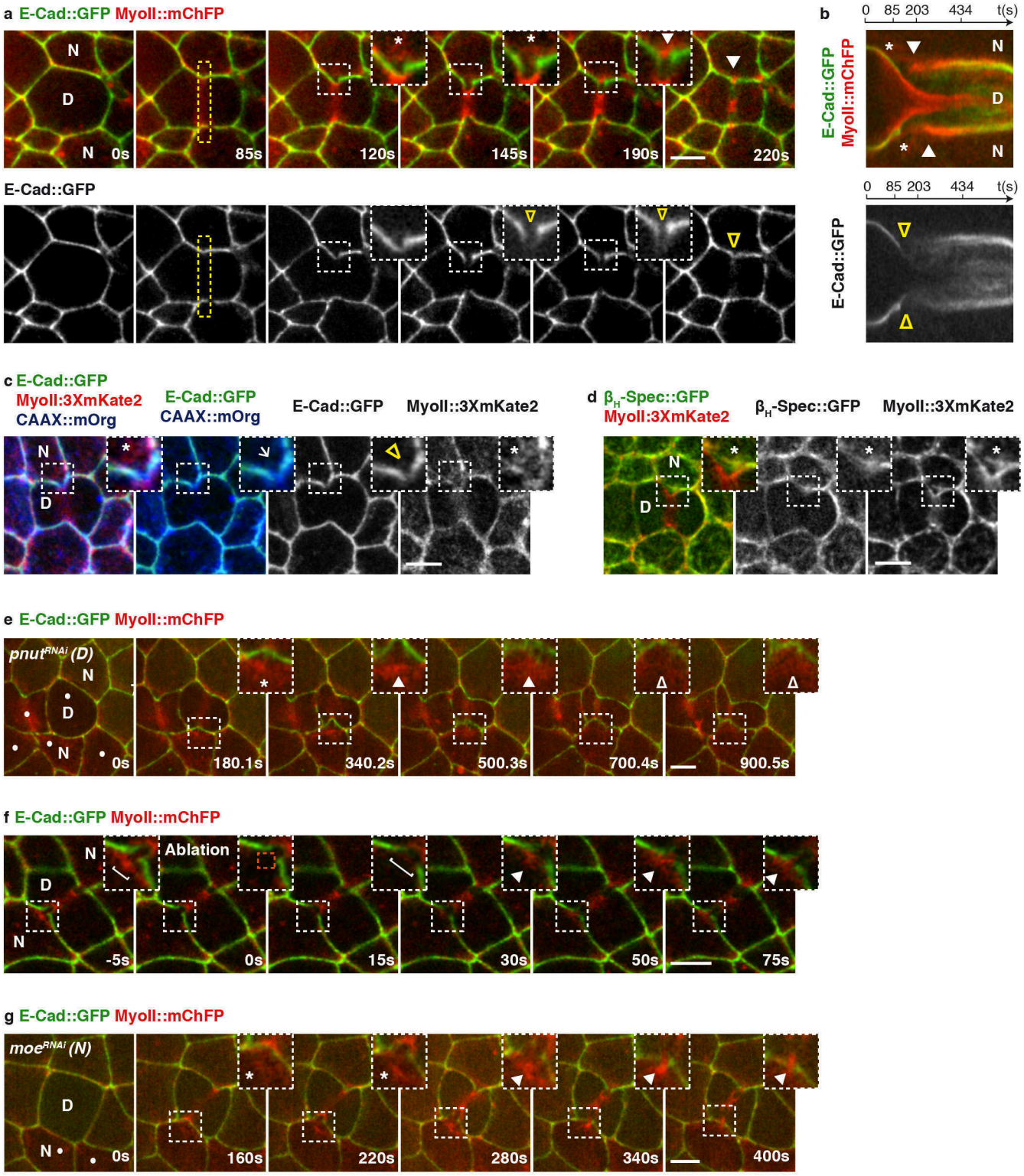
a E-Cad::GFP MyoII::mChFP
N
D
N
0s
85s
120s
145s
190s
220s
E-Cad::GFP
b
0 85 203 434 t(s)
E-Cad::GFP
MyoII::mChFP
N
D
N
0 85 203 434 t(s)
E-Cad::GFP
c E-Cad::GFP
MyoII:3XmKate2
CAAX::mOrg
E-Cad::GFP
CAAX::mOrg
E-Cad::GFP
MyoII::3XmKate2
d βH-Spec::GFP
MyoII:3XmKate2
βH-Spec::GFP
MyoII::3XmKate2
e E-Cad::GFP MyoII::mChFP
pnutRNAi (D)
N
D
N
0s
180.1s
340.2s
500.3s
700.4s
900.5s
f E-Cad::GFP MyoII::mChFP
N
Ablation
D
N
-5s
0s
15s
30s
50s
75s
g E-Cad::GFP MyoII::mChFP
moeRNAi (N)
D
N
0s
160s
220s
280s
340s
400s

Figure 3: Lowering E-Cad concentration at the ingressing AJ is required for MyoII accumulation in the neighbouring cells.

(a,b) E-Cad::GFP distribution in the dividing cell (D) and its neighbours (N). Yellow dashed line: junction used to generate the kymograph in (b). The remaining E-Cad::GFP signal and MyoII::mChFP signal labelling the contractile ring (not shown) were used to precisely determine the tip of the ingressing junction. Yellow open arrowheads: decrease of E-Cad::GFP signal at the ingressing AJ. *n*=20 cells.

(c) Graph of the normalized local E-Cad::GFP intensity at the ingressing AJ (solid line) and of the normalized total AJ elongation (dashed line) versus the amount of contractile ring constriction in *wt* dividing cells facing *wt* neighbours (mean±SEM). D: Dividing cell. The local E-Cad concentration at the ingressing AJ is defined as the mean E-Cad::GFP intensity at the tip of the ingressing AJ. For additional details on the quantification, see the Methods section. *n*: number of cells.

(d) Numerical integration of E-Cad levels on a locally elongating AJ up to 58% of its initial length, as measured in *wt* dividing cells facing *wt* neighbours (see Supplementary Theory Note).

(e,f) E-Cad::GFP distribution in the dividing cell (D) and its rok^{RNAi} neighbours (N). White dots: rok^{RNAi} cells. Yellow dashed line: junction used to generate the kymograph in (f). The remaining E-Cad::GFP signal and MyoII::mChFP signal of the contractile ring (not shown) were used to precisely determine the tip of the ingressing junction. Yellow open arrowheads: decrease of E-Cad::GFP signal at the ingressing AJ. *n*=20 cells.

(g) Graph of the normalized local E-Cad concentration at the ingressing AJ (solid line) and of the normalized total AJ elongation (dashed line) versus the amount of contractile ring constriction in *wt* dividing cells facing rok^{RNAi} neighbours (mean±SEM). N: neighbouring cell. The local E-Cad concentration at the ingressing AJ is defined as the mean E-Cad::GFP intensity at the tip of the ingressing AJ. For additional details on the quantification, see the Methods section. *n:* number of cells.

(h) Numerical integration of E-Cad levels on a locally elongating AJ up to 40% of its initial length, as measured in *wt* dividing cells facing rok^{RNAi} neighbours (see Supplementary Theory Note).

(i,j) E-Cad::GFP distribution in a $pnut^{RNAi}$ dividing cell (D) and its neighbouring cells (N). Yellow dashed line: junction used to generate the kymograph in (j). Yellow arrowheads: absence of a marked E-Cad::GFP signal decrease at the ingressing AJ. *n*=28 cells.

(k) Graph of the normalized total E-Cad::GFP intensity at the ingressing AJ (solid line) and of the normalized total AJ elongation (dashed line) versus the amount of contractile ring constriction in cells neighbouring $pnut^{RNAi}$ dividing cells (mean±SEM). D: dividing cell. The total E-Cad concentration at the ingressing AJ is defined as the mean E-Cad::GFP intensity at the ingressing AJ. *n:* number of cells.

(l) Numerical integration of E-Cad levels on a globally elongating AJ up to 25% of the initial length, as measured in cells neighbouring $pnut^{RNAi}$ dividing cells (see Supplementary Theory Note).

(m) E-Cad::GFP and MyoII::3XmKate2 distribution in a *pnut* dividing cell (D), marked by 2 copies of E-Cad::GFP, and its *E-Cad* mutant neighbour (N, white dots), marked by the absence of E-Cad::GFP. White arrowheads: MyoII::3XmKate2 accumulation in the neighbouring cells. Orange arrowhead: cytokinesis failure of the *pnut* dividing cell. *n*=19 cells.

(n) Graph of the normalized MyoII accumulation at 80% of the initial cell diameter (mean±SEM) in *wt* or *E-Cad* (shg^{JN}) mutant cells neighbouring a *wt* or a *pnut* dividing cell. D: Dividing cell. N: Neighbouring cell. *n:*

number of cells. Kruskal-Wallis test, ns: not significant, *:$p<0.05$, ****:$p<0.0001$.
Scale bars: 5µm (a,e,i,m)

Figure 3.

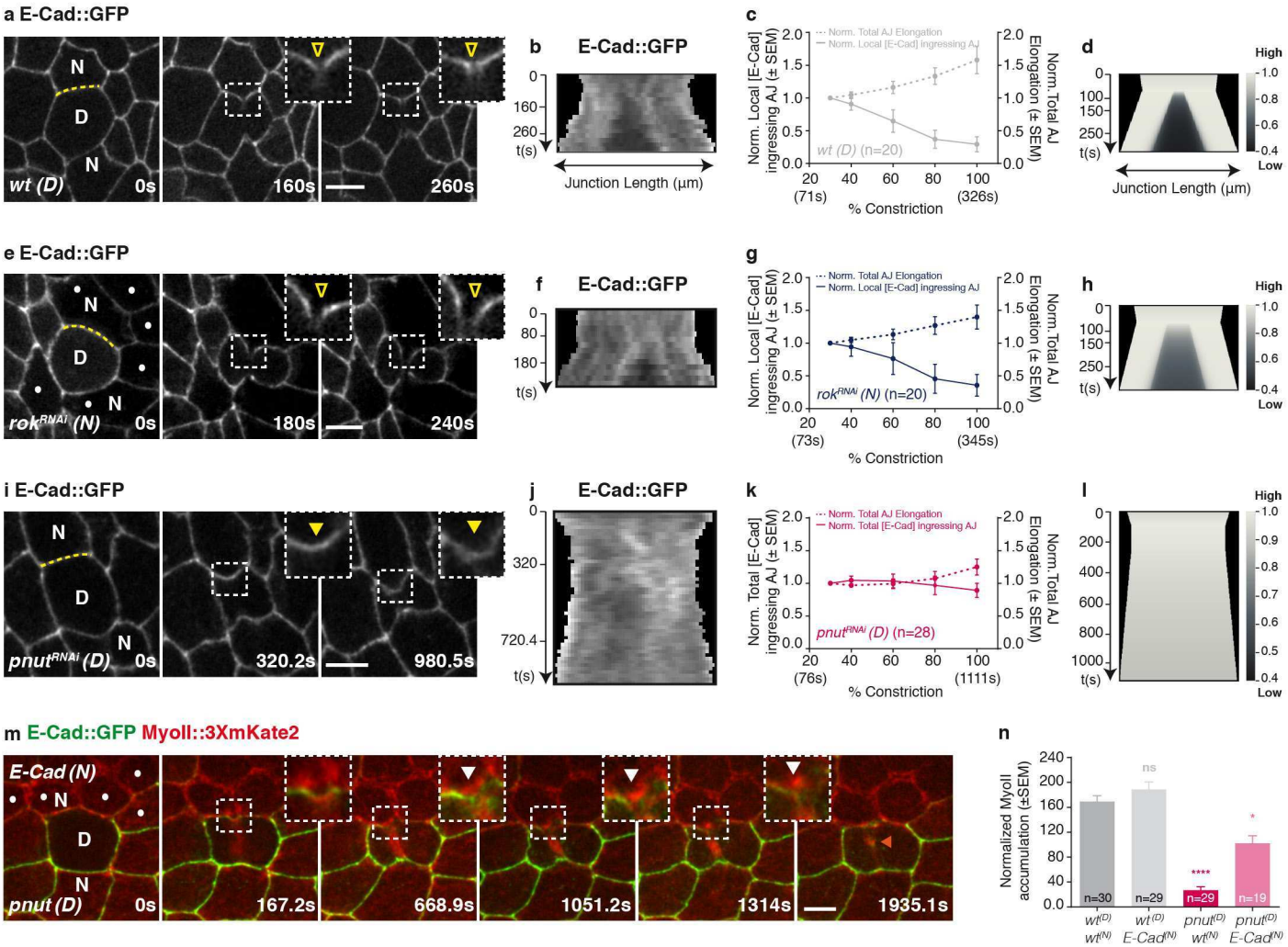
a E-Cad::GFP
N
D
N
wt (D)
0s
160s
260s
b
E-Cad::GFP
0
160
260
t(s)
Junction Length (μm)
c
Norm. Total AJ Elongation
Norm. Local [E-Cad] Ingressing AJ
Norm. Local [E-Cad] ingressing AJ (± SEM)
Norm. Total AJ Elongation (± SEM)
wt (D) (n=20)
(71s)
(326s)
% Constriction
d
High
Low
t(s)
Junction Length (μm)
e E-Cad::GFP
rokRNAi (N)
0s
180s
240s
f
E-Cad::GFP
0
80
180
t(s)
g
Norm. Total AJ Elongation
Norm. Local [E-Cad] ingressing AJ
rokRNAi (N) (n=20)
(73s)
(345s)
% Constriction
h
High
Low
t(s)
i E-Cad::GFP
pnutRNAi (D)
0s
320.2s
980.5s
j
E-Cad::GFP
0
320
720.4
t(s)
k
Norm. Total AJ Elongation
Norm. Total [E-Cad] ingressing AJ
Norm. Total [E-Cad] ingressing AJ (± SEM)
Norm. Total AJ Elongation (± SEM)
pnutRNAi (D) (n=28)
(76s)
(1111s)
% Constriction
l
High
Low
t(s)
m E-Cad::GFP MyoII::3XmKate2
E-Cad (N)
N
D
N
pnut (D)
0s
167.2s
668.9s
1051.2s
1314s
1935.1s
n
Normalized MyoII accumulation (±SEM)
ns
*
****
n=30
n=29
n=29
n=19
wt(D) wt(N)
wt(D) E-Cad(N)
pnut(D) wt(N)
pnut(D) E-Cad(N)

Figure 4: Actomyosin flows drive the neighbouring cells response.

(a) Geometry of the domain used for the numerical integration of the active gel equations, using a Finite Element method. The geometrical parameters are extracted from the experimental data (see Supplementary Theory Note). The assumption is that friction is low in the ingressing membrane (thick grey line) and high in the surrounding cortex (thick black line). All other parameters are constant in space and time. Thin Grey lines: initial mesh used for the numerical integration.

(b) Steady-state concentration of MyoII showing a MyoII depletion (green) in the ingressed region, and a MyoII accumulation at the base of the ingressing membrane (deep blue) (see Supplementary Theory Note). Scale: color-coded representation of MyoII concentration.

(c) Steady-state velocity field of the actomyosin gel (same numerical simulation as b). The size of the vector is proportional to the local velocity. Low velocities are color-coded in black and high velocities are color-coded in yellow. The horizontal velocity is consistently much lower than the vertical velocity (see Supplementary Theory Note). Scale: color-coded representation of actomyosin flow velocity.

(d,e) MyoII::GFP//MyoII::RFP patch during cytokinesis of a MyoII::RFP dividing cell (D) with a MyoII::GFP neighbouring cell (N). Orange dashed box: bleached region. Time was set to 0s at the time of photobleaching. Yellow dashed box: region used to generate the kymograph in (e). White arrowheads: MyoII::GFP localization in the neighbour both prior and upon photobleaching. *n*=18 cells.

(f,g) Lifeact::GFP neighbouring (N) cells facing a dividing cell (D) in a MyoII::3XmKate2 tissue. Yellow dashed box: region used to generate the kymograph in (g). White arrowheads: MyoII::3XmKate2 and Lifeact::GFP accumulation in the neighbouring cells. *n*=31 cells.

(h-k) *rok* (h,i) and *dia* (j,k) neighbouring cells (N), marked by Lifeact::GFP, facing *wt* dividing cells (D) in a MyoII::3XmKate2 tissue. White dots: *rok* (h) or *dia* (j) mutant cells. Yellow dashed boxes (h,j): regions used to generate the kymographs in (i) and (k), respectively. White open arrowhead (h): reduced MyoII::3XmKate2 and Lifeact::GFP accumulation in the *rok* neighbour. White arrowhead (j): MyoII::3XmKate2 and Lifeact::GFP accumulation in the *dia* neighbour. *n*=22 (h,i) and *n*=20 (j,k) cells.

(l) Graph of the percentage of *wt, rok* and *dia* neighbouring cells (N) exhibiting no flows, intermittent flows (1-3 detectable speckles throughout constriction), or sustained flows (>3 detectable speckles throughout constriction). *n:* number of cells.

(m) Graph of the velocity of Actin flows for *wt, rok* and *dia* neighbouring cells (N) facing *wt* dividing cells (mean±SEM). *n/n*: number of speckles quantified/corresponding number of cells measured. Kruskal-Wallis test, ****:$p<0.0001$.

Scale bars: 5µm (d,f,h,j)

Figure 4.

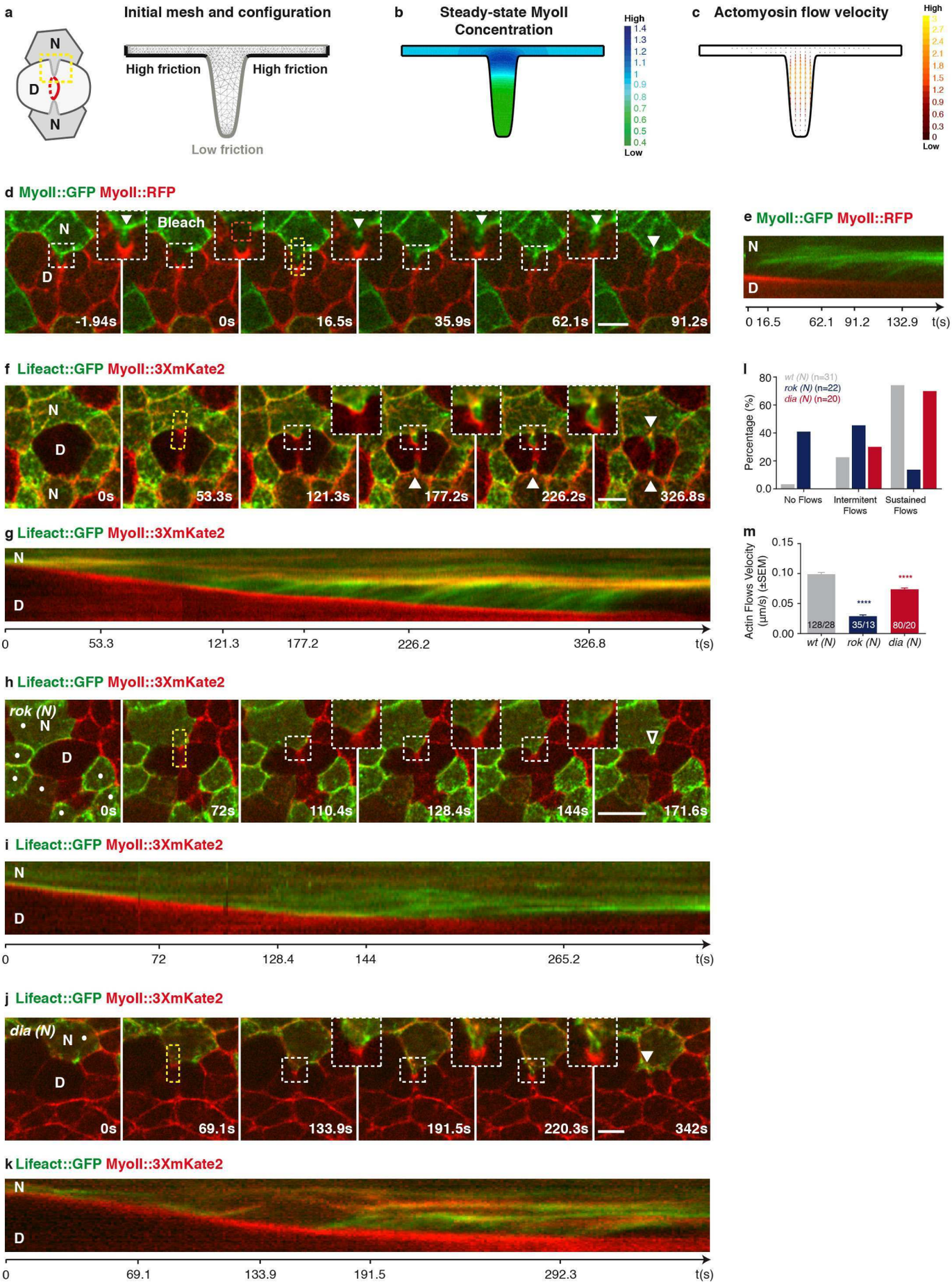
a
Initial mesh and configuration
N
D
N
High friction
High friction
Low friction
b
Steady-state MyoII Concentration
High
1.4
1.3
1.2
1.1
1
0.9
0.8
0.7
0.6
0.5
0.4
Low
c
Actomyosin flow velocity
High
3
2.7
2.4
2.1
1.8
1.5
1.2
0.9
0.6
0.3
0
Low
d MyoII::GFP MyoII::RFP
N
D
Bleach
-1.94s
0s
16.5s
35.9s
62.1s
91.2s
e MyoII::GFP MyoII::RFP
N
D
0 16.5
62.1
91.2
132.9
t(s)
f Lifeact::GFP MyoII::3XmKate2
N
D
N
0s
53.3s
121.3s
177.2s
226.2s
326.8s
g Lifeact::GFP MyoII::3XmKate2
N
D
0
53.3
121.3
177.2
226.2
326.8
t(s)
l
wt (N) (n=31)
rok (N) (n=22)
dia (N) (n=20)
Percentage (%)
80
60
40
20
0.0
No Flows
Intermitent Flows
Sustained Flows
m
Actin Flows Velocity (μm/s) (±SEM)
0.15
0.10
0.05
0.00
****
****
128/28
35/13
80/20
wt (N)
rok (N)
dia (N)
h Lifeact::GFP MyoII::3XmKate2
rok (N)
N
D
0s
72s
110.4s
128.4s
144s
171.6s
i Lifeact::GFP MyoII::3XmKate2
N
D
0
72
128.4
144
265.2
t(s)
j Lifeact::GFP MyoII::3XmKate2
dia (N)
N
D
0s
69.1s
133.9s
191.5s
220.3s
342s
k Lifeact::GFP MyoII::3XmKate2
N
D
0
69.1
133.9
191.5
292.3
t(s)

Acknowledgments

We thank M. Affolter, J. Großhans, H. Hong, A. Martin, H. Oda, B. Sanson, D. St Johnston, J. Zallen, the Bloomington Stock Centre and Developmental Studies Hybridoma Bank for reagents; J. Prost, M. Thery, L. Blanchoin and H. Ennomanix for input; the imaging facility platform of the Developmental Biology Unit, *Institut Curie*; F. Bosveld, J.-F. Joanny, F. Graner, A. Villedieu, R.-M. Mège, for comments; P. Recho for helpful discussions about the simulations; ANR-MaxForce, ANR-MorphoDro, ERC Advanced (TiMoprh, 340784), ARC (SL220130607097), ANR Labex DEEP (11-LBX-0044, ANR-10-IDEX-0001-02) and PSL grants for funding. D.P. acknowledges fellowships from FCT (SFRH/BD/51700/2011) and FRM (FDT20150531972). E.H. acknowledges fellowships from the Wellcome Trust (110326/Z/15/Z), Trinity College and the Bettencourt-Schueller Foundation.

Author contributions

D.P., E.H., S.H. and Y.B. designed the project. I.G., Z.W., M.B. produced reagents. D.P. and S.H. performed experiments. E.H. and S.R. developed methods and scripts for data analysis. D.P. and E.H. analysed the data. E.H. and O.M. developed theoretical models. E.H. performed simulations. D.P., E.H. and Y.B. wrote the manuscript.

Author Information

The authors declare no competing financial interests. Correspondence and requests for material should be addressed to Y.B. (yohanns.bellaiche@curie.fr).

References

1. Herszterg, S., Leibfried, A., Bosveld, F., Martin, C. & Bellaiche, Y. Interplay between the Dividing Cell and Its Neighbors Regulates Adherens Junction Formation during Cytokinesis in Epithelial Tissue. *Dev Cell* **24,** 256-270 (2013).

2. Guillot, C. & Lecuit, T. Adhesion disengagement uncouples intrinsic and extrinsic forces to drive cytokinesis in epithelial tissues. *Dev Cell* **24,** 227-241 (2013).

3. Founounou, N., Loyer, N. & Le Borgne, R. Septins regulate the contractility of the actomyosin ring to enable adherens junction remodeling during cytokinesis of epithelial cells. *Dev Cell* **24,** 242-255 (2013).

4. Lau, K., Tao, H., Liu, H., Wen, J., *et al.* Anisotropic stress orients remodelling of mammalian limb bud ectoderm. *Nat Cell Biol* **17,** 569-579 (2015).

5. Reinsch, S. & Karsenti, E. Orientation of spindle axis and distribution of plasma membrane proteins during cell division in polarized MDCKII cells. *J Cell Biol* **126,** 1509-1526 (1994).

6. Firmino, J., Rocancourt, D., Saadaoui, M., Moreau, C. & Gros, J. Cell Division Drives Epithelial Cell Rearrangements during Gastrulation in Chick. *Dev Cell* **36,** 249-261 (2016).

7. Morais-de-Sá, E. & Sunkel, C. Adherens junctions determine the apical position of the midbody during follicular epithelial cell division. *EMBO Rep* **14,** 696-703 (2013).

8. Hoffman, B. D. & Yap, A. S. Towards a Dynamic Understanding of Cadherin-Based Mechanobiology. *Trends Cell Biol* **25,** 803-814 (2015).

9. Green, R. A., Paluch, E. & Oegema, K. Cytokinesis in animal cells. *Annu Rev Cell Dev Biol* **28,** 29-58 (2012).

10. le Duc, Q., Shi, Q., Blonk, I., Sonnenberg, A., *et al.* Vinculin potentiates E-cadherin mechanosensing and is recruited to actin-anchored sites within adherens junctions in a myosin II-dependent manner. *J Cell Biol* **189,** 1107-1115 (2010).

11. Yonemura, S., Wada, Y., Watanabe, T., Nagafuchi, A. & Shibata, M. alpha-Catenin as a tension transducer that induces adherens junction development. *Nat Cell Biol* **12,** 533-542 (2010).

12. Yao, M., Qiu, W., Liu, R., Efremov, A. K., *et al.* Force-dependent conformational switch of α-catenin controls vinculin binding. *Nat Commun* **5,** 4525 (2014).

13. Choi, H. J., Pokutta, S., Cadwell, G. W., Bobkov, A. A., *et al.* αE-catenin is an autoinhibited molecule that coactivates vinculin. *Proc Natl Acad Sci U S A* **109,** 8576-8581 (2012).

14. Thomas, W. A., Boscher, C., Chu, Y. S., Cuvelier, D., *et al.* α-Catenin and vinculin cooperate to promote high E-cadherin-based adhesion strength. *J Biol Chem* **288,** 4957-4969 (2013).

15. Leerberg, J. M., Gomez, G. A., Verma, S., Moussa, E. J., *et al.* Tension-sensitive actin assembly supports contractility at the epithelial zonula adherens. *Curr Biol* **24,** 1689-1699 (2014).

16. Fehon, R. G., McClatchey, A. I. & Bretscher, A. Organizing the cell cortex: the role of ERM proteins. *Nat Rev Mol Cell Biol* **11,** 276-287 (2010).

17. Drees, F., Pokutta, S., Yamada, S., Nelson, W. J. & Weis, W. I. Alpha-catenin is a molecular switch that binds E-cadherin-beta-catenin and regulates actin-filament assembly. *Cell* **123,** 903-915 (2005).

18. Ratheesh, A., Gomez, G. A., Priya, R., Verma, S., *et al.* Centralspindlin and α-catenin regulate Rho signalling at the epithelial zonula adherens. *Nat Cell Biol* (2012).

19. Verma, S., Han, S. P., Michael, M., Gomez, G. A., *et al.* A WAVE2-Arp2/3 actin nucleator apparatus supports junctional tension at the epithelial zonula adherens. *Mol Biol Cell* **23,** 4601-4610 (2012).

20. Homem, C. C. & Peifer, M. Diaphanous regulates myosin and adherens junctions to control cell contractility and protrusive behavior during morphogenesis. *Development* **135,** 1005-1018 (2008).

21. Fox, D. T., Homem, C. C., Myster, S. H., Wang, F., *et al.* Rho1 regulates Drosophila adherens junctions independently of p120ctn. *Development* **132,** 4819-4831 (2005).

22. Prokopenko, S. N., Brumby, A., O'Keefe, L., Prior, L., *et al.* A putative exchange factor for Rho1 GTPase is required for initiation of cytokinesis in Drosophila. *Genes Dev* **13,** 2301-2314 (1999).

23. Castrillon, D. H. & Wasserman, S. A. Diaphanous is required for cytokinesis in Drosophila and shares domains of similarity with the products of the limb deformity gene. *Development* **120,** 3367-3377 (1994).

24. Desai, R., Sarpal, R., Ishiyama, N., Pellikka, M., *et al.* Monomeric α-catenin links cadherin to the actin cytoskeleton. *Nat Cell Biol* **15,** 261-273 (2013).

25. Buckley, C. D., Tan, J., Anderson, K. L., Hanein, D., *et al.* Cell adhesion. The minimal cadherin-catenin complex binds to actin filaments under force. *Science* **346,** 1254211 (2014).

26. Kruse, K., Joanny, J. -F., Jülicher, F., Prost, J. & Sekimoto, K. Generic theory of active polar gels: a paradigm for cytoskeletal dynamics. *The European Physical Journal E* **16,** 5-16 (2005).

27. Mayer, M., Depken, M., Bois, J. S., Jülicher, F. & Grill, S. W. Anisotropies in cortical tension reveal the physical basis of polarizing cortical flows. *Nature* **467,** 617-621 (2010).

28. Prost, J., Jülicher, F. & Joanny, J. F. Active gel physics. *Nature Physics* **11,** 111-117 (2015).

29. Bergert, M., Erzberger, A., Desai, R. A., Aspalter, I. M., *et al.* Force transmission during adhesion-independent migration. *Nat Cell Biol* **17,** 524-529 (2015).

30. Callan-Jones, A. C. & Voituriez, R. Active gel model of amoeboid cell motility. *New Journal of Physics* **15,** 025022 (2013).

31. Ruprecht, V., Wieser, S., Callan-Jones, A., Smutny, M., *et al.* Cortical contractility triggers a stochastic switch to fast amoeboid cell motility. *Cell* **160,** 673-685 (2015).

32. Recho, P., Putelat, T. & Truskinovsky, L. Contraction-driven cell motility. *Physical review letters* **111,** 108102 (2013).

33. Rauzi, M., Lenne, P. F. & Lecuit, T. Planar polarized actomyosin contractile flows control epithelial junction remodelling. *Nature* **468,** 1110-1114 (2010).

34. Levayer, R. & Lecuit, T. Oscillation and polarity of E-cadherin asymmetries control actomyosin flow patterns during morphogenesis. *Dev Cell* **26,** 162-175 (2013).

35. Martin, A. C., Kaschube, M. & Wieschaus, E. F. Pulsed contractions of an actin-myosin network drive apical constriction. *Nature* (2008).

36. Roh-Johnson, M., Shemer, G., Higgins, C. D., McClellan, J. H., *et al.* Triggering a cell shape change by exploiting preexisting actomyosin contractions. *Science* **335,** 1232-1235 (2012).

37. Solon, J., Kaya-Copur, A., Colombelli, J. & Brunner, D. Pulsed forces timed by a ratchet-like mechanism drive directed tissue movement during dorsal closure. *Cell* **137,** 1331-1342 (2009).

38. David, D. J., Tishkina, A. & Harris, T. J. The PAR complex regulates pulsed actomyosin contractions during amnioserosa apical constriction in Drosophila. *Development* **137,** 1645-1655 (2010).

39. Engl, W., Arasi, B., Yap, L. L., Thiery, J. P. & Viasnoff, V. Actin dynamics modulate mechanosensitive immobilization of E-cadherin at adherens junctions. *Nat Cell Biol* **16,** 587-594 (2014).

40. Rakshit, S., Zhang, Y., Manibog, K., Shafraz, O. & Sivasankar, S. Ideal, catch, and slip bonds in cadherin adhesion. *Proc Natl Acad Sci U S A* **109,** 18815-18820 (2012).

41. Taguchi, K., Ishiuchi, T. & Takeichi, M. Mechanosensitive EPLIN-dependent remodeling of adherens junctions regulates epithelial reshaping. *J Cell Biol* **194,** 643-656 (2011).

42. Maître, J. L., Berthoumieux, H., Krens, S. F., Salbreux, G., *et al.* Adhesion functions in cell sorting by mechanically coupling the cortices of adhering cells. *Science* **338,** 253-256 (2012).

43. Behrndt, M., Salbreux, G., Campinho, P., Hauschild, R., *et al.* Forces driving epithelial spreading in zebrafish gastrulation. *Science* **338,** 257-260 (2012).

44. Fernandez-Gonzalez, R., Simoes, S. d. e. . M., Röper, J. C., Eaton, S. & Zallen, J. A. Myosin II dynamics are regulated by tension in intercalating cells. *Dev Cell* **17,** 736-743 (2009).

45. Aigouy, B., Farhadifar, R., Staple, D. B., Sagner, A., *et al.* Cell flow reorients the axis of planar polarity in the wing epithelium of Drosophila. *Cell* **142,** 773-786 (2010).

46. Ladoux, B., Mège, R. M. & Trepat, X. Front-Rear Polarization by Mechanical Cues: From Single Cells to Tissues. *Trends Cell Biol* (2016).

METHODS

Fly stocks and genetics

Drosophila melanogaster stocks and associated references are listed in Supplementary Table 2. Flies were crossed and experiments were performed at 25°C (except for the rok^{RNAi} experiments, the shi^{ts} and their respective control experiments, which were conducted at 29°C). Loss of function, gain of function and dual-colour patch experiments were carried out using the FLP/FRT or the MARCM techniques[47-49]. Somatic clones were induced in the second instar larval stage by heat-shock (1 hour at 37°C, except for the Lifeact::GFP patches in Fig. 4f,g, for which the heat-shock was only 30min at 37°C) and analysed 3-4 days after clone induction in 15-18 hours after puparium formation (hAPF) pupae.

Molecular biology

The *vinc* ^{3}, GFP::Vinc, E-Cad::3XmTagRFP and E-Cad::3XmKate2 alleles were generated by CRISPR/Cas9-mediated homologous recombination at their respective endogenous loci, using the *vas-Cas9* line[50].

To generate the *vinc* ^{3} and GFP::Vinc alleles, the sgRNAs were cloned into the pU6B-sgRNA-vector[51]. For the *vinc* ^{3} allele, which deletes the *vinc* coding sequence, the oligonucleotides used were: 5'-ATGGTTTTTGTGTGAAAGACGGG-3' and 5'-CACTGACAATCGCCTAGTACTGG-3'; while for GFP::Vinc we used the following oligonucleotides: 5'-ATGGTTTTTGTGTGAAAGACGGG-3' and 5'-GATGGTTTTTGTGTGAAAGACGG-3'. Homology sequences were cloned into a homologous recombination vector harbouring a hs-*miniwhite* cassette flanked by *loxP* sites[52] and a GFP sequence for GFP tagging (vector and map available upon request). The two homologous regions (HR1 and HR2) flanking the site of CRISPR/Cas9 cuts were cloned using the following primers: (i) for *vinc* ^{3}: (HR1) 5'-CCGGGCTAATTATGGGGTGTCGCCCTTCGCTCTGTGCTCCCACTGGCTGGA-3' and 5'-CTTCGTATAGCATACATTATACGAAGTTATCATTTTGGCTGCGCTTTTCGTCTG-3'; (HR2) 5'-TCGTATAATGTATGCTATACGAAGTTATTGTAGGCGATTGTCAGTGCCTACGG-3' and 5'-AATTTTGTGTCGCCCTTGAACTCGATTGACCCCACTGAGGGCATTGCTCAAAC-3'; (ii) for GFP::Vinc: (HR1) 5'-CCCGGGCTAATTATGGGGTGTCGCCCTTCGTCTGTGCTCCCACTGGCTGGA-3' and 5'-CCCGGTGAACAGCTCCTCGCCCTTGCTCACCATTTTGGCTGCGCTTTTCGTCTGATT-3'; (HR2) 5'-AGTTCGGGGTCCAGCGGTTCTTCAGGCAGTCCAGTCTTTCACACAAAAACCATCGAGAGC-3' and 5'-GCCCTTGAACTCGATTGACGCTCTTCGACTCCTCTCGCTGACGCCGAATGT-3'.

The E-Cad::3XmTagRFP and E-Cad::3XmKate2 alleles were generated in two steps following the strategy used by[52,53]. First, an attP site was introduced along with a 4.8kb deletion of the *E-Cad (shg)* locus. The following CRISPR/Cas9 guides were used: 5'-AAGGTTTTCTGTATCGAACCGGG-3' and 5'-TTTGTGTTTCCCTAAATGTGTGG-3'. The HR1 and HR2 homology sequences were cloned into a vector harbouring an attP site and a white shRNA marker flanked by *loxP* sites, using the following primers: (HR1) 5'-CGCCAAGCTTGCATGCCTGCAGGTCGACTCTAGAGGATCCGCGGCCGCAAAGTGAACGAAAATATCAGCCAGAGCAGC-3' and 5'-AACTGAGAGAACTCAAAGGTTACCCCAGTTGGGGCACTACGCAATGAACCCAAAACCCGTCTCCAAGTGG-3'; (HR2) 5'-ATGCTATACGAAGTTATGCGGAGGATCCGGCGGCGGTGGGATTTAGGGAAACACAAATGGGGTAGAAATAAA-3' and 5'-AACGACGGCCAGTGAATTCGAGCTCGGTACCCGGGGATCCGCGGCCGCAACAACCAGCTAGACATACATACCATTAATC-3'. According to[52], *31*-mediated recombination was then used to complement the *E-Cad* locus with transgenes harbouring the E-Cad tagged-versions with either three mTagRFP or mKate2 sequences in tandem. The E-Cad::3XmTagRFP and E-Cad::3XmKate2 alleles are both homozygous viable.

To generate the MyoII::3XmKate2 P-element transgene, a C-terminal triple tandem repeat of the mKate2 sequence was cloned into the *spaghetti squash* (*sqh)* genomic rescue construct, which expressed the Myosin II regulatory light chain under the control of its endogenous promoter[54]. The functionality of the MyoII::3XmKate2 allele was verified by rescue of the sqh^{AX3} null allele. All injections were performed by Bestgene, except for *31*-mediated recombination.

Immunohistochemistry and fixed tissue imaging

Pupae were dissected and fixed as previously described[55]. The primary and secondary antibodies used were: rat anti-E-Cad[56] (1:300) and Cy5 donkey-anti-rat IgGs (1:300, Interchim), respectively. Images were collected with a confocal microscope - LSM880, Carl Zeiss, 63x NA 1.4 OIL DICII PL APO objective (optical zoom 2X). All images are sum projections of a *z*-stack (0.5µm step size; 7.5-10µm stack).

Live imaging microscopy

Live imaging

Pupae were prepared for live imaging as described previously[1]. Samples were imaged at 25°C or 29°C with an inverted confocal spinning disk microscope from Nikon or Zeiss, using either 60x NA1.4 OIL DIC N2 PL APO VC, 63x NA1.4 OIL DICII PL APO or 100x NA1.4 OIL DIC N2 PL APO VC objectives and either a CoolSNAP HQ2 (Photometrics) or a CMOS (Hamamtsu) camera. Live imaging of E-Cad::GFP, MyoII::3XmKate2 and CAAX::mOrg was performed using a confocal microscope (LSM880, Carl Zeiss) with a 63x NA 1.4 OIL DICII PL APO objective (optical zoom 2X). To improve signal-to-noise ratio, the CAXX::mOrg channel was denoised using the Feature J Derivatives, a Fiji plugin.

All experiments were performed during the first round of cell divisions in the anterior-central region of the notum tissue (15-18hAPF). In the analyses (unless mentioned otherwise), the time, t=0, was set at cytokinesis onset, identified by the initial cell constriction.

FRAP (Fluorescence Recovery After Photobleaching)

To determine E-Cad::GFP dynamics, FRAP experiments were performed in *wt* and $pnut^{RNAi}$ interphase cells in E-Cad::GFP expressing pupae. Regions, corresponding to approximately one-third of the AJ length, were bleached (491nm laser at 100% power, 40-50 iterations). Following photobleaching, confocal images were acquired at the level of the AJs every 5 seconds. In order to determine E-Cad::GFP dynamics in *wt* dividing cells, similar FRAP experiments were conducted in the AJs of cells undergoing cytokinesis. In this case images were acquired every second, to correct for *z*-drift.

To analyse the relative contribution of the medial pool versus the ingressing region for MyoII accumulation in the neighbouring cells, MyoII::GFP//MyoII::RFP adjacent cell patches were generated. MyoII::GFP accumulation was exclusively photobleached in the neighbouring cells at the clone boundary (491nm laser at 100% power, 40-50 iterations). Following photobleaching, confocal images were acquired every second at the plane of maximum MyoII::GFP intensity.

Laser ablations

Contractile ring laser ablations were performed in flies expressing E-Cad::GFP and MyoII::mChFP. Images were acquired using a confocal laser-scanning microscope (LSM710 NLO, Carl Zeiss) equipped with a 63x NA 1.4 OIL DICII PL APO objective (optical zoom 2X) in single-photon bidirectional scan mode. The contractile ring was severed, at the level of the AJs, using the two-photon Ti:Sapphire laser (Mai Tai DeepSee, Spectra Physics) at 800 nm with < 100 fs pulses with a 80 MHz repetition rate, typically set at 25% power. Following laser ablation, a confocal image was acquired every second at the level of the AJs.

To test the contribution of the detached cortex for MyoII accumulation in the neighbouring cells, the initially detached cortex, labelled by MyoII::mChFP, was severed before MyoII accumulation was detectable, using the Ti:Sapphire laser at 800 nm with < 100 fs pulses with a 80 MHz repetition rate, typically set at 25% power. Confocal images were then acquired at the level of the E-Cad::GFP labelled AJ every 5 seconds.

Quantifications

Recoil Velocity upon Contractile Ring Laser Ablation

To measure the recoil velocity upon contractile ring laser ablation, time-lapse movies were generated as described above. For the quantification, we generated kymographs along the contractile ring, encompassing both the dividing cell and its neighbours. Using the kymograph, the dividing cell diameter over time was measured using a custom made MATLAB code. The recoil velocity was then measured between t_0 and t_{20} (averaging the 2 time points closest to t_{20}).

The amount of constriction prior to contractile ring laser ablation was determined as the ratio of the difference in cell diameter prior to contractile ring laser ablation and upon full cell relaxation.

Rate of Contractile Ring Constriction

To determine the rate of contractile ring constriction, time-lapse movies of E-Cad::GFP and MyoII::mChFP or MyoII::3XmKate2 were generated. The contractile ring length from the onset of cytokinesis t_0 (t=0) to full constriction was manually measured using a Fiji macro. The rate of constriction was determined as the slope of the linear fit of the contractile ring length normalized to its length at the onset of cytokinesis (t_0) as a function of time[1]. For $pnut^{RNAi}$ (or *pnut* mutant cells), rok^{RNAi} and ani^{RNAi} dividing cells, which constrict very slowly, only the linear part of the curves was fitted to determine the constriction rate. A schematic representation of this quantification is provided in Extended Data Fig. 1i.

MyoII Accumulation in the Neighbouring Cells

MyoII accumulation in the neighbouring cells was determined in E-Cad::GFP and MyoII::mChFP or MyoII::3XmKate2 tissues. Since initial quantifications showed that the maximum of MyoII accumulation in *wt* cells is observed at 80% of the initial cell diameter, MyoII::mChFP or MyoII::3XmKate2 accumulation in the neighbouring cells was quantified at this time point in all experimental conditions (measured as described above).

Upon determination of the time-point corresponding to 80% of the initial cell diameter, MyoII::mChFP or MyoII::3XmKate2 accumulation was determined as the average of the 2 time points closest to 80% of the initial cell diameter. To quantify MyoII::mChFP or MyoII::3XmKate2 accumulation in an unbiased manner using Fiji, the mean MyoII intensity of the neighbouring cells in each frame was used to threshold the image and select pixels above the mean intensity and thus obtain a ROI of the regions of MyoII::mChFP or MyoII::3XmKate2 accumulation. The integrated density of the ROI at the base of the ingressing AJ was then determined. MyoII::mChFP or MyoII::3XmKate2 accumulation in the neighbouring cells was normalized by the mean MyoII::mChFP/MyoII::3XmKate2 cortical intensity in the neighbouring cells. A schematic representation of this quantification is provided in Extended Data Fig. 1i.

Angle Formed by the Ingressing AJ

To determine the angle formed by the ingressing AJ, E-Cad::GFP and MyoII::mChFP time-lapse movies were generated and the angles were measured manually using a Fiji Macro, as schematically represented in Extended Data Fig. 3a.

E-Cad::GFP Recovery upon Photobleaching

To analyse E-Cad::GFP dynamics, the FRAP time-lapse movies were first bleach-corrected (Histogram matching option) using Fiji. To determine E-Cad::GFP turnover, E-Cad::GFP mean intensity in the bleached region was then measured manually in Fiji, using a 3-pixel-wide box centred at the position of the AJs (pixel size: 0.13µmx0.13µm). To quantify the E-Cad coefficient of diffusion, E-Cad::GFP mean intensity across the entire AJ was measured, using a plot profile of a 3-pixel-wide line, again drawn manually using Fiji (pixel size: 0.13µmx0.13µm). The fitting strategies used to extract the turnover time, the mobile and the immobile fraction and the coefficient of diffusion are detailed in the Supplementary Theory Note.

E-Cad::GFP Intensity along the Ingressing AJ

Time-lapse imaging of E-Cad::GFP and MyoII::mChFP were acquired as a *z*-stack every 20 seconds (0.5µm step size; 7.5-10µm stack). The sum projection of the z-stack was corrected for photobleaching using Fiji (Histogram Matching option). Then, custom MATLAB codes were used to obtain the total AJ length, the E-Cad::GFP mean intensity at the AJ and a stretched kymograph.

First, a MATLAB code was used to segment the E-Cad::GFP cell contours[57]. Upon manual correction of the segmented contours, in particular at the position of the ingressing AJ, where the E-Cad::GFP signal is low (we used both the remaining E-Cad::GFP signal, as well as the MyoII::mChFP signal, which labels the contractile ring in the dividing cell, as an additional landmark), a second MATLAB code was used to track the cell junctions[58]. Finally, the pixel contour of the AJ was extracted at each time point and a stretched kymograph along the ingressing AJ was generated, using a 3-pixel-wide averaging box sliding along the pixel contour at each time point.

To measure the E-Cad::GFP integrated density along the ingressing AJ, we multiplied the mean E-Cad::GFP intensity at the ingressing AJ by the total AJ length before AJ elongation ($t_{30\%\ constriction}$) and upon full contractile ring constriction (t_{final}).

The kymographs along the ingressing junction were also used to quantify the local [E-Cad::GFP] at the ingressing AJ, by defining a 10-pixel-wide box centred at the tip of the ingressing AJ and measuring the mean E-Cad::GFP intensity as a function of time. Upon contractile ring constriction, the total AJ length slightly decreases and elongation starts on average at 30% of constriction, thus, we used this time point to normalize the total AJ length, the E-Cad::GFP integrated density at the AJ, the mean E-Cad::GFP intensity at the tip of the ingressing AJ and the total E-Cad::GFP intensity at the ingressing AJ. The mean GFP background intensity was determined at the centre of each quantified cell and subtracted to the average E-Cad::GFP intensity.

Width and Height of the Ingressing AJ

Using E-Cad::GFP and MyoII::mChFP time-lapse movies generated in different experimental conditions, we measured the width and height of the ingressing AJ, using Fiji. The width is defined as the distance between the inflection points at the base of the ingressing AJ, whereas the height corresponds to the distance between the tip and the base of the ingressing AJ, as represented in Extended Data Fig. 5a,b.

Velocity of the Actin Flows

To determine the velocity of the Actin flows in the neighbouring cells, we performed time-lapse confocal imaging of Lifeact::GFP expressing neighbours in a MyoII::3XmKate2 tissue at the rate of one image per second. Kymographs parallel to the ingressing membrane encompassing 10-20 pixels in width were then generated (see for example Fig. 4f,g). The velocity of the Actin speckles (defined as the boundary between high/low Lifeact::GFP signal) was manually determined, using Fiji, by fitting a line and determining its slope on each kymograph speckle trajectory. Similar analyses were performed for both *rok* and *dia* neighbouring cells, also marked by Lifeact::GFP.

Statistics

Sample sizes vary in each experiment. The experiments were repeated, at least, three independent times, except for the data shown in: Extended Data Fig. 2a, in which the experiment was performed once for 2 different pupae and Extended Data Fig. 7n, which was repeated twice. All samples sizes are reported in figure legends.

All error bars shown in the figures are standard error of the mean and the statistical test used to access significance is stated in the figure legends. Each test was chosen after the distribution normalities of each group were tested using the D'Agostino and Pearson omnibus normality test. To compare two groups, a t-test or a Mann-Whitney test were used for normal distribution and not normal distribution, respectively. When using the t-test, the variances were tested with the F-test. To compare more than 2 groups we used either an ANOVA or a Kruskal-Wallis test, depending on the whether the data set shows or not a normal distribution, respectively. In these cases, a correction was used to increase statistical power. All statistical analysis was performed with GraphPad.

Code availability

The MATLAB codes used to segment and track cells are already published[57]. The MATLAB code used to extract the kymographs along the neighbouring cell junction and the Fiji macros used to quantify the rate of contractile ring constriction, MyoII accumulation in the neighbouring cells and the angle formed by the ingressing AJ are available upon request.

Extended Data Figure 1: Estimation of the pulling forces produced during contractile ring constriction in *wt*, *pnut*, *rok* and *ani* dividing cells.

(a,c,e,g) Estimation of the pulling forces produced by the contractile ring (labelled by MyoII::mChFP) on the AJ (marked by E-Cad::GFP) by laser ablation in *wt* (a), $pnut^{RNAi}$ (c), rok^{RNAi} (e) and ani^{RNAi} (g) dividing cells (D). White dots: $pnut^{RNAi}$, rok^{RNAi} and ani^{RNAi} expressing cells, respectively. Dashed boxes: ablated regions. Time was set to 0s at the time of laser ablation. Dashed arrows: indicate the dividing cells relaxation upon contractile ring laser ablation.

(b,d,f,h) Graph of the recoil velocity upon contractile ring laser ablation versus the amount of ring constriction at the time of the ablation in *wt* (grey dots and linear fit in (b,d,f,h), $pnut^{RNAi}$ (pink dots and linear fit in d), rok^{RNAi} (blue dots and linear fit in f) and ani^{RNAi} (green dots and linear fit in h) dividing cells. In *pnut, rok* and *ani* dividing cells, the recoil velocity upon contractile ring laser ablation is on average lower than in *wt* dividing cells (see also Fig. 1e) and it scales less with the amount of contractile ring constriction at the time of the ablation. *n:* number of cells.

(i) Schematic representation of the method used in the quantification of MyoII accumulation at 80% of the initial cell diameter in the neighbouring cells (N). D: Dividing cell. Yellow double arrow segment: indicates 80% cell diameter. Dashed region: ROI corresponding to the outline of the neighbouring cells. Yellow regions: ROI's used in the quantification. As detailed in the Methods section, MyoII accumulation in the neighbouring cells was determined at 80% of the initial cell diameter. To obtain an ROI of the regions of MyoII accumulation in the neighbours, we used the mean MyoII intensity of the neighbours to threshold the image. Then, we determined MyoII accumulation as a ratio between the integrated density of the ROI at the base of the ingressing AJ and the average MyoII cortical intensity in the neighbouring cells.

Scale bars: 5μm (a,c,e,g,i)

Extended Data Figure 1.

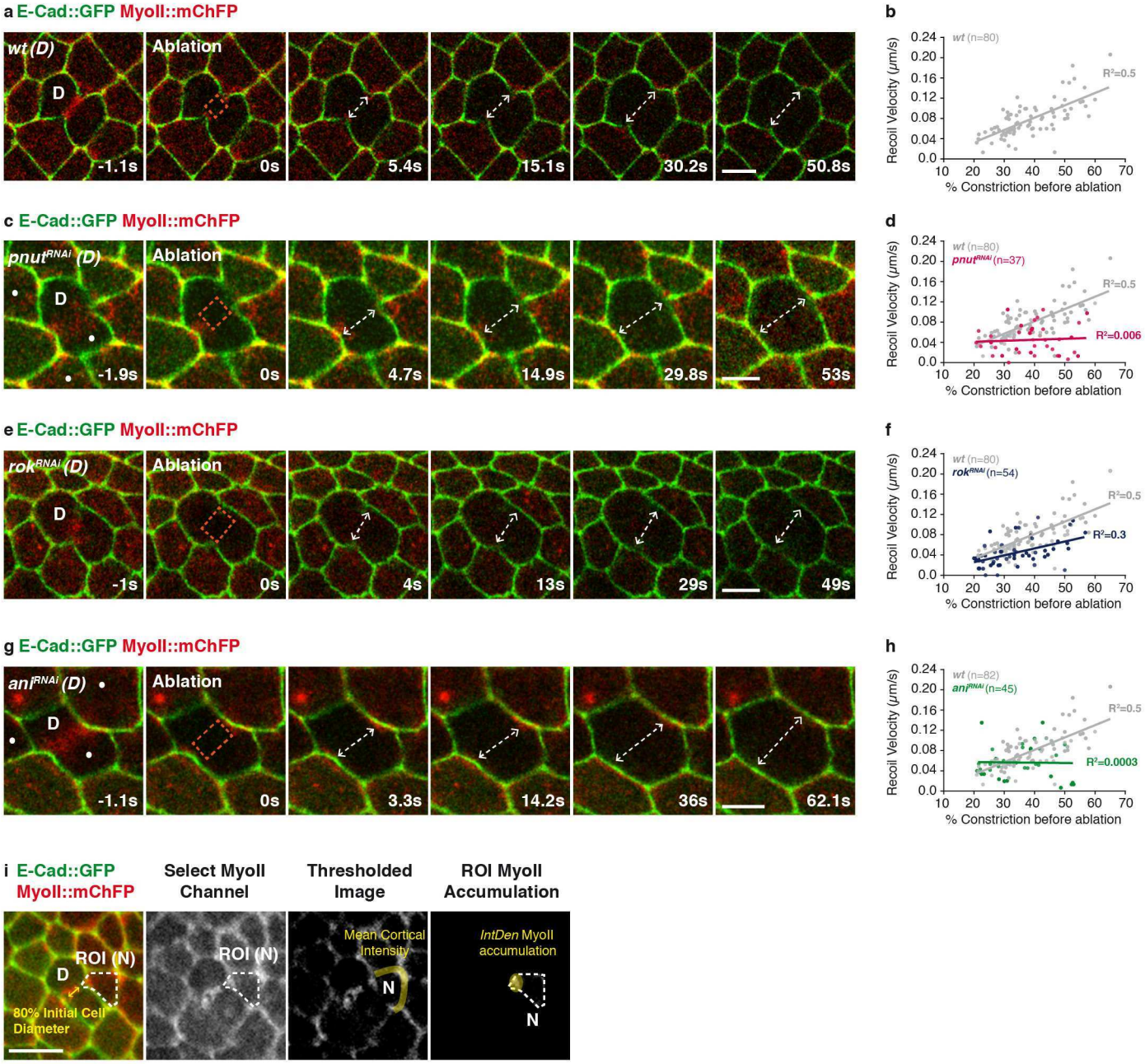

Extended Data Figure 2: α-Cat::GFP distribution during cytokinesis.

(a) α-Cat::GFP and E-Cad::3XmKate2 distribution in the dividing cell (D) and its neighbours (N) during cytokinesis. The insets highlight the progressive and concomitant decrease of E-Cad::3XmKate2 and α-Cat::GFP signals at the ingressing AJ. *n*=58 cells.

Scale bar: 5µm (a)

Extended Data Figure 2.

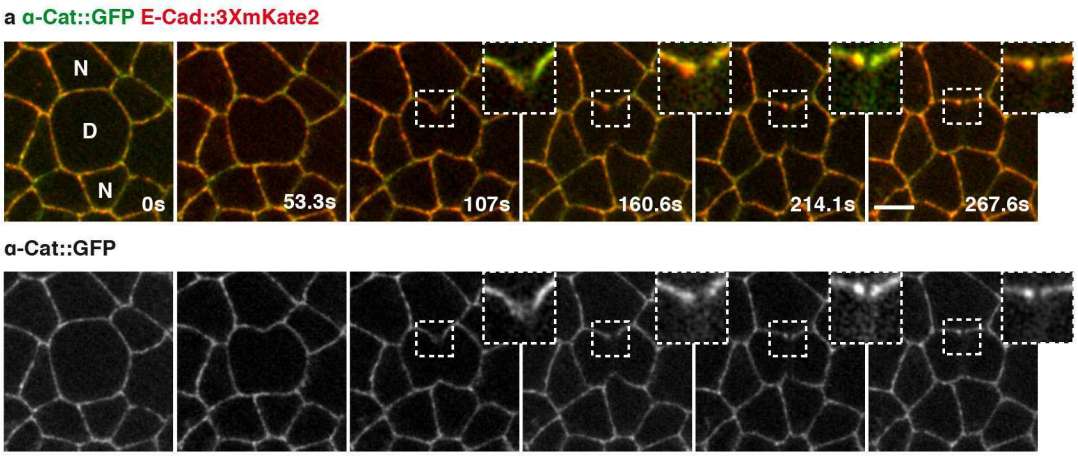

Extended Data Figure 3: A balance between membrane curvature, adhesion and contractility regulates cortex detachment in the neighbouring cells, in response to the contractile ring pulling forces.

(a) Schematic representation of the theoretical model describing cortex detachment in the neighbouring cells (see Supplementary Theory Note). D: Dividing cell (white). N: Neighbouring cell (light grey). The AJs are highlighted in green, while the actomyosin cortex is shown in the red dashed line and in further detail in the insets. CR: Contractile Ring (solid and dashed curved lines in red). Double Arrow: separation of the actomyosin cortex from the AJ – cortex detachment. Dashed black lines: indicate the angle formed by the ingressing AJ. The model assumes a membrane, which can be locally curved and an actomyosin cortex, modelled as a 1D contractile fibre. In such a curved geometry, there is a tug-of-war between membrane-cortex adhesion force and the normal forces arising from MyoII activity that tend to separate the cortex from the membrane (contractility). Detachment occurs when the normal forces resulting from MyoII activity overcome the adhesion force maintaining membrane-cortex attachment. Thus, the model predicts that increasing contractility, either by increasing MyoII activity or concentration, should accelerate cortex detachment; similarly, decreasing the adhesion force is predicted to result in precocious detachment. To test the model experimentally, we analysed the angle formed by the ingressing AJ, a proxy for the local membrane curvature (Supplementary Theory Note), in a set of conditions where we affected either the adhesion force or the contractility of the neighbouring cells. To manipulate the adhesion force, we analysed cortex detachment upon moe^{RNAi}, as well as in $E\text{-}Cad^{k03401}$/+ heterozygous background (*E-Cad*1x). Moesin is the only ERM protein in flies and it plays an essential role in membrane cortex-attachment, since it can directly bind both F-actin and the membrane[16]. As predicted theoretically, upon moe^{RNAi} or in the *E-Cad*1x mutant condition, cortex detachment occurs earlier and at higher angles than in *wt* neighbours (b-d). Similarly, increasing the neighbouring cells contractility by generating $sds22^{RNAi}$ neighbours, which increases phospho-MyoII at the AJs[59], also results in precocious cortex detachment and detachment at higher angles (b-d). Altogether this data supports that a balance between the adhesion force, cortex contractility and local membrane curvature regulates cortex detachment, in response to the pulling forces generated in the dividing cell.

(b) E-Cad::GFP and MyoII::mChFP localization at cortex detachment in *wt*, *E-Cad*1x heterozygous mutant condition, moe^{RNAi} and $sds22^{RNAi}$ neighbouring cells (N). White dots: moe^{RNAi} and $sds22^{RNAi}$ cells in the corresponding panels. White asterisks: separation of the MyoII::mChFP and the E-Cad::GFP signals at the ingressing region.

(c) Graph of the angle of cortex detachment in *wt*, *E-Cad*1x, moe^{RNAi} and $sds22^{RNAi}$ neighbouring cells (mean±SEM). For all conditions, except *E-Cad*1x, the dividing cell is *wt.* Note that the rate of contractile constriction is similar for *wt* and *E-Cad*1x cells and no detectable defects were observed during cytokinesis. *n:* number of cells. Kruskal-Wallis test, *:$p<0.05$, ***: $p<0.001$, ****: $p<0.0001$.

(d) Graph of the angle of cortex detachment (plotted in c) versus the amount of ring constriction at detachment in *wt*, *E-Cad*1x, moe^{RNAi} and $sds22^{RNAi}$ neighbouring cells (mean±SEM). *n:* number of cells.

Scale bars: 5µm (b)

Extended Data Figure 3.

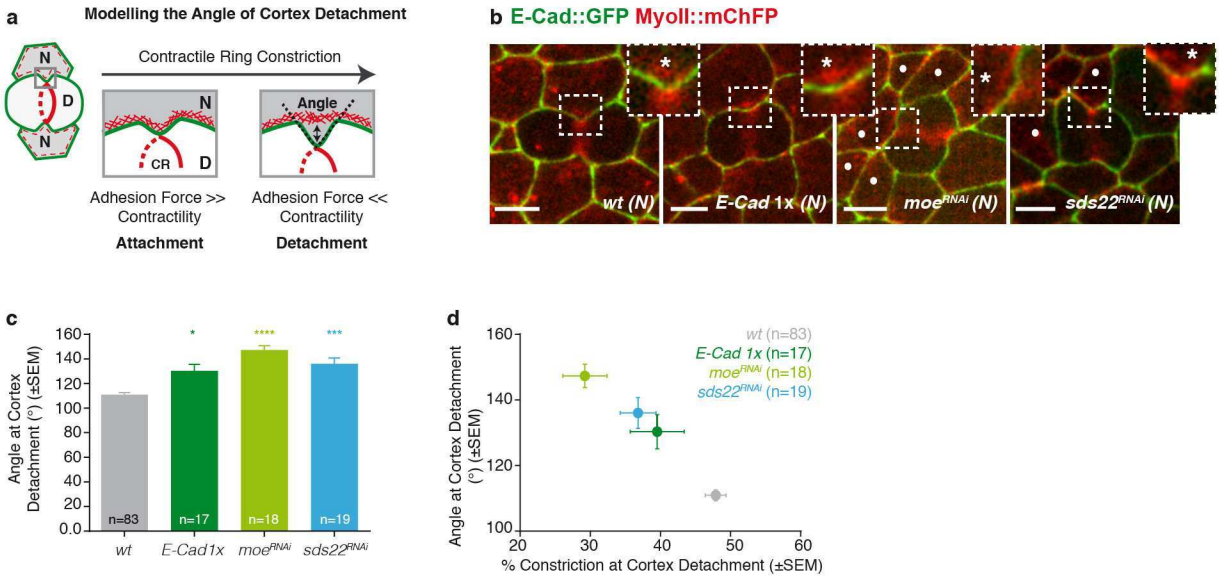

Extended Data Figure 4: Decrease of E-Cadherin concentration at the ingressing AJ is not impaired upon Dynamin, Rab11 or Sec5 loss-of-function.

(a) E-Cad::GFP//E-Cad::3XmTagRFP cell patches during cytokinesis of a E-Cad::GFP dividing cell (D) neighbouring an E-Cad::3XmTagRFP neighbouring cell (N). Yellow open arrowheads: concomitant decrease of E-Cad::GFP and E-Cad::3XmTagRFP at the ingressing AJ. *n*=17 cells.

(b) E-Cad::GFP localization in the dividing cell (D) and its neighbour expressing a dominant negative temperature-sensitive *dynamin* allele, $shi^{ts1.k}$ (N), at 29°C. White dots: $shi^{ts1.k}$ expressing cells. Yellow open arrowheads: E-Cad::GFP decrease at the ingressing AJ. *n*=21 cells.

(c) E-Cad::GFP localization in a $YFP::Rab11^{DN}$ dominant negative expressing dividing cell (D) and its neighbour (N). White dots: $YFP::Rab11^{DN}$ expressing cells. Yellow open arrowheads: E-Cad::GFP decrease at the ingressing AJ. *n*=22 cells.

(d) E-Cad::GFP localization in a *sec5* dividing cell (D) and its neighbouring cells (N). White dots: *sec5* cells, marked by the absence of nls::GFP. Yellow open arrowheads: E-Cad::GFP decrease at the ingressing AJ. *n*=9 cells.

(e-g) Graph of the integrated density (IntDen) of E-Cad::GFP at the ingressing AJ (mean±SEM) at the onset of AJ elongation ($t_{30\%\ constriction}$) and upon full contractile ring constriction (t_{final}) for *wt* dividing cells facing either *wt* or rok^{RNAi} neighbouring cells and $pnut^{RNAi}$ dividing cells. D: Dividing cell. N: Neighbouring cell. See the Methods section for the description of the quantification method used to quantify E-Cad::GFP IntDen along the ingressing AJ. *n:* number of cells. Paired Student t-test, **:$p<0.01$ and *:$p<0.05$.

Scale bars: 5µm (a,b,c,d)

Extended Data Figure 4.

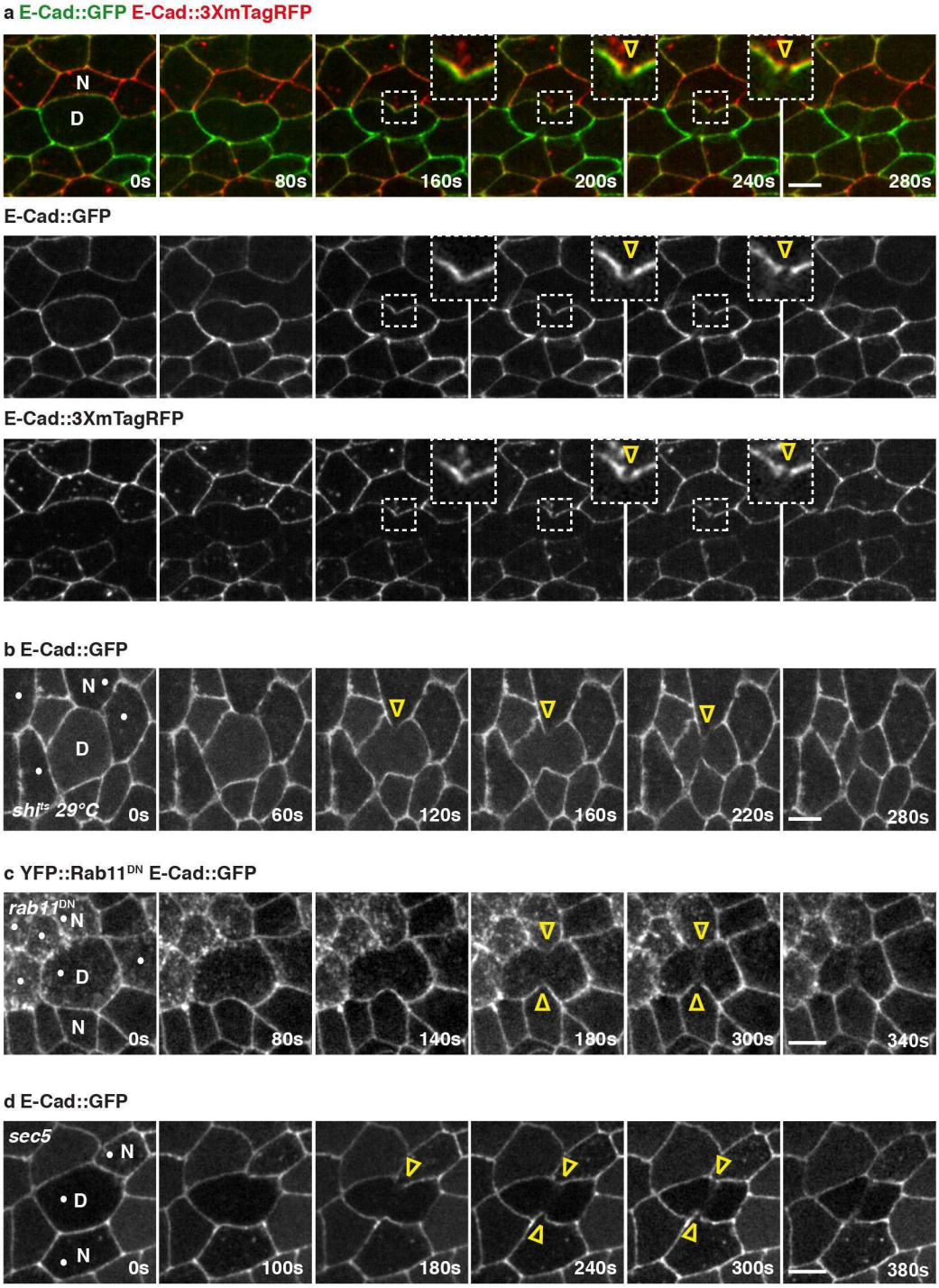

Extended Data Figure 5: Local AJ elongation is sufficient to trigger a decrease of E-Cad concentration at the ingressing AJ.

(a,b) Graph of the ingressing region width normalized by the total curvilinear AJ length (a) and of the height of the ingressing region (µm, b) in function of the amount of constriction for *wt* dividing cells facing *wt* or rok^{RNAi} neighbouring cells and cells neighbouring $pnut^{RNAi}$ dividing cells (mean±SEM). D: Dividing cell. N: Neighbouring cell. Insets: Representation of the ingressing region width and height (E-Cad::GFP, green; MyoII::mChFP, red, also shown in Fig. 2a). For *wt* dividing cells facing *wt* neighbours, the normalized width of the ingressing AJ is small (average 0.12) and decreases during contractile ring constriction, whereas the height increases, thereby indicating that AJ elongation is a rather local process. Similarly, in *wt* dividing cells facing rok^{RNAi} neighbours, the normalized width remains small during constriction (average 0.26) and the height increases, which again indicated that the elongation of the AJ is also mainly local. Contrary to the *wt* and rok^{RNAi} cases, in cells neighbouring $pnut^{RNAi}$ dividing cells, the normalized width of the pulled region is much wider (average 0.49) and the height is much smaller and remains constant during constriction. This argues for a more global elongation of the ingressing AJ. For further details on the quantification strategy, see the Methods Section. *n:* number of cells.

(c) Graph of the normalized local E-Cad::GFP intensity at the ingressing AJ versus the normalized total AJ elongation. Experimental *wt* data is shown in grey (mean±SEM) and the theoretical integration for 58% elongation is shown in green (line corresponds to the best-fit parameters measured by E-Cad::GFP FRAP, shaded regions correspond to a confidence interval within one standard deviation, see Supplementary Table 1 and Supplementary Theory Note). D: Dividing cell. To evaluate the goodness of the fit, the coefficient of determination and standard deviation of the residuals was determined and found to equal to $R^2 = 0.82$ and S = 0.11. *n:* number of cells.

(d) E-Cad::GFP and MyoII::mChFP localization in *wt* and rok^{RNAi} neighbouring cells (N) facing a *wt* dividing cell. White dots: rok^{RNAi} expressing cells. White arrowheads: MyoII::mChFP accumulation in the neighbouring cells. White open arrowheads: reduced MyoII::mChFP accumulation in the neighbouring cells. Note that the phenotype of rok^{RNAi} neighbouring cells is specific, as $pnut^{RNAi}$ and ani^{RNAi} neighbours facing a *wt* dividing cell still accumulate MyoII (see below, n).

(e) Graph of the normalized MyoII accumulation at 80% of the initial cell diameter (mean±SEM) for *wt* and rok^{RNAi} cells neighbouring (N) *wt* dividing cells. *n:* number of cells. Mann-Whitney test, ****:p<0.0001.

(f) Graph of the normalized total AJ elongation (mean±SEM) upon full contractile ring constriction of *wt* dividing cells (t_{final}) facing either *wt* (grey) or rok^{RNAi} neighbours (blue) and $pnut^{RNAi}$ dividing cells (pink). D: Dividing cell. N: Neighbouring cell. *n:* number of cells. Kruskal-Wallis test, ns: not significant, ****:p<0.0001.

(g) Graph of the normalized local E-Cad::GFP intensity at the ingressing AJ versus the normalized total AJ elongation. Experimental data for *wt* dividing cells facing rok^{RNAi} neighbours is shown in grey (mean±SEM) and the theoretical integration for 40% elongation is shown in blue (line corresponds to the best-fit parameters measured by E-Cad::GFP FRAP, shaded regions correspond to a confidence interval within one standard deviation, see Supplementary Table 1 and Supplementary Theory Note). To evaluate the goodness of the fit, the coefficient of determination and standard deviation of the residuals was determined and found to equal to $R^2 = 0.74$ and S = 0.13. N: Neighbouring cell. *n:* number of cells.

(h-j) E-Cad::GFP and MyoII::mChFP distribution in a *wt* dividing cell (D) facing on one side a rok^{RNAi} neighbour (rok^{RNAi} (N)) and on the other side a *wt* neighbour (*wt* (N)). Yellow dashed line: junction used for the kymograph in (i). Red dashed line: junction used for the kymograph in (j). White open arrowheads: reduced MyoII::mChFP accumulation in the neighbouring cells. Yellow arrowheads: absence of E-Cad::GFP signal decrease at the ingressing AJ. Yellow open arrowheads: decrease of E-Cad::GFP at the ingressing AJ. In 15% of the cases (n=20), we found that the contractile ring is positioned off-centre. In these cases, junction elongation on the *wt* side is small and no decrease of E-Cad is observed (see also kymograph in i). Furthermore, MyoII does not accumulate in this *wt* neighbour facing a *wt* dividing cell. As shown in the main text, in the *rok* side, the junction elongates and E-Cad decreases (j and Fig. 3e-g). This further argues that junction elongation is an important factor in the local E-Cad concentration decrease.

(k-l) E-Cad::GFP distribution in a $pnut^{RNAi}$ dividing cell (D) and its neighbouring cells (N). Yellow dashed line: junction used to generate the kymograph in (l). Yellow open arrowheads: transient reduction of E-Cad::GFP signal decrease at the ingressing AJ. Yellow arrowheads: absence of a marked E-Cad::GFP signal decrease at the ingressing AJ. In 14 of the 28 cells analysed, we found that cells neighbouring $pnut^{RNAi}$ dividing cells show a transient decrease of E-Cad::GFP levels at the ingressing AJ (yellow open arrowheads). In all cases, these reductions of E-Cad levels occur during earlier stages of contractile ring constriction and are transient.

(m) Graph of the normalized total E-Cad::GFP intensity at the ingressing AJ versus the normalized total AJ elongation. Experimental data for *pnut* dividing cells is shown in grey (mean±SEM) and the theoretical integration for 25% elongation is shown in pink (line corresponds to the best-fit parameters measured by E-Cad::GFP FRAP in $pnut^{RNAi}$ cells, shaded regions correspond to a confidence interval within one standard deviation, see Supplementary Table 1 and Supplementary Theory Note). D: Dividing cell. To evaluate the goodness of the fit, the coefficient of determination and standard deviation of the residuals was determined and found to equal to $R^2 = 0.73$ and $S = 0.03$. *n:* number of cells

(n) E-Cad::GFP and MyoII::mChFP localization in *wt* (*n*=32 cells), $pnut^{RNAi}$ (*n*=29 cells) and ani^{RNAi} (*n*=20 cells) neighbouring cells (N) facing *wt* dividing cells. White arrowheads: MyoII::mChFP accumulation in the neighbouring cells.

Scale bars: 5µm (d,h,k,n)

Extended Data Figure 5.

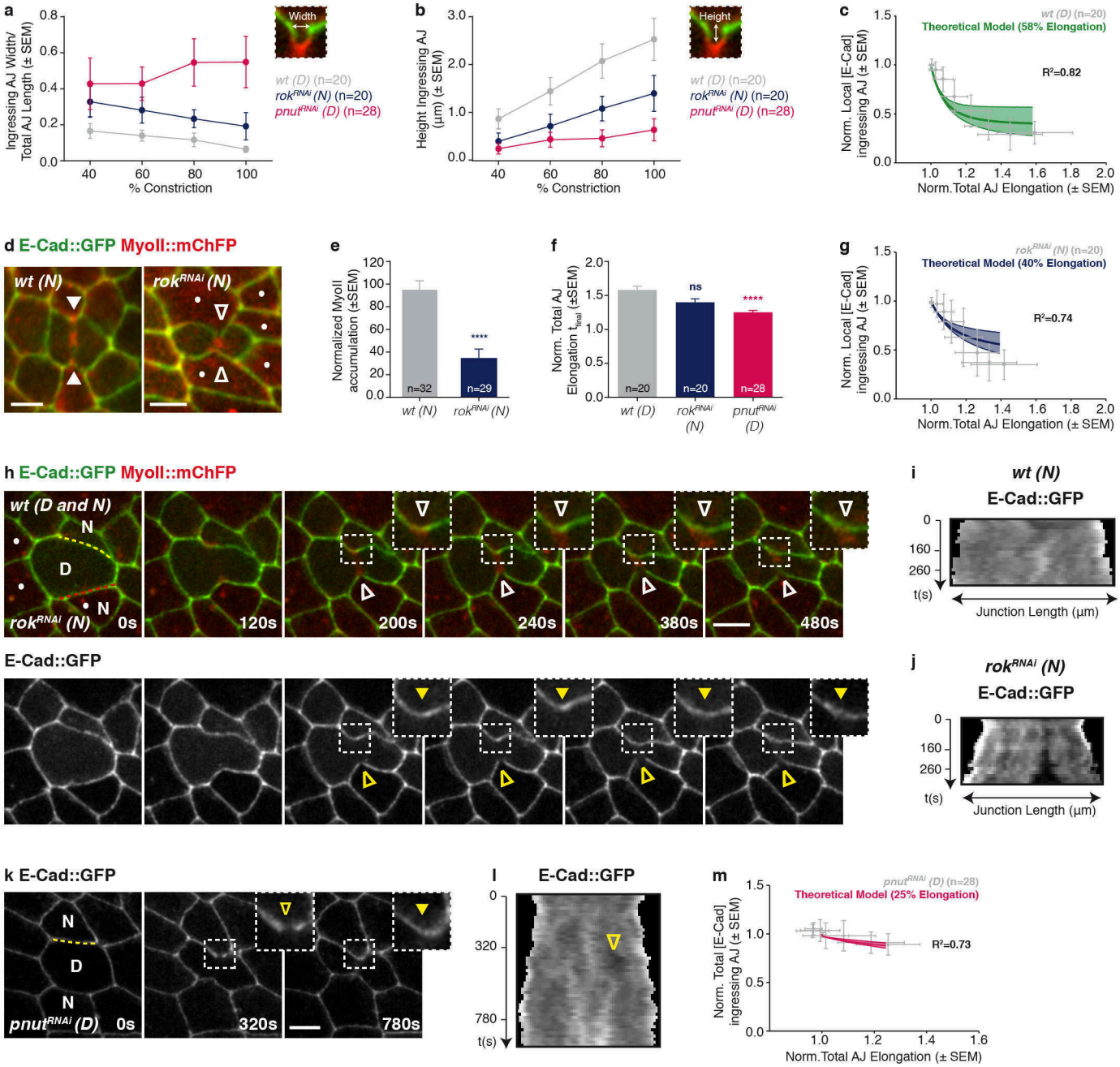

Extended Data Figure 6: Lowering E-Cad concentration in cells neighbouring a *pnut* dividing cell rescues MyoII accumulation.

(a) E-Cad::GFP and MyoII::3XmKate2 distribution in a *pnut* dividing cell (D), marked by 2 copies of E-Cad::GFP, and its *E-Cad* mutant neighbour (N, white dots), marked by the absence of E-Cad::GFP (top panel is also shown in Fig. 3m). White arrowheads: MyoII::3XmKate2 accumulation in the *E-Cad* neighbour. White open arrowheads: reduced MyoII::3XmKate2 accumulation in the *wt* neighbour. Yellow arrowheads: absence of E-Cad::GFP decrease at the ingressing AJ. Yellow brackets: reduced E-Cad::GFP at the ingressing AJ. Note that the E-Cad::GFP signal is present exclusively in the dividing cell, as its *E-Cad* neighbour is marked by the absence of E-Cad::GFP. Nevertheless, since the E-Cad signal decreases similarly in the dividing cell and its neighbours during cytokinesis (see Extended Data Fig. 4a), the additional decrease of E-Cad::GFP signal observed at the ingressing AJ formed between the *pnut* dividing cell and its *E-Cad* mutant neighbour indicates that E-Cad levels further decreased during constriction. *n*=19 cells.

(b) Graph of the percentage of cytokinesis failure of *pnut* dividing cells facing *wt* or *E-Cad* neighbours. D: Dividing cell. N: Neighbouring cell. In contrast to previous findings[3], our data shows that the percentage of cytokinesis failure of *pnut* dividing cells is not rescued by reducing E-Cad levels in the neighbouring cells, supporting that such defects are intrinsic to the dividing cell. n/n: number of cells that failed cytokinesis/corresponding number of dividing cells counted.

(c) Graph of the rate of contractile ring constriction (s^{-1}, mean±SEM) in *wt* and *pnut* dividing cells facing either *wt* or *E-Cad* neighbouring cells. D: Dividing cell. N: Neighbouring Cell. In agreement with (b), we find that the rate of contractile ring constriction is similar in *pnut* dividing cells facing either *wt* or *E-Cad* neighbouring cells. *n:* number of cells. ANOVA test, *:p<0.05 and ****:p<0.0001.

(d) Graph of the normalized AJ elongation at the onset of AJ elongation ($t_{30\%\ constriction}$), at 80% of the initial cell diameter ($t_{80\%,}$ timing where MyoII accumulation in the neighbouring cells was measured) and upon full contractile ring constriction (t_{final}) (mean±SEM) of *wt* and *pnut* dividing cells neighboured by *wt* or *E-Cad* mutant neighbouring cells. D: Dividing cell. N: Neighbouring cell. Total AJ elongation of *pnut* dividing cells neighbouring *wt* or *E-Cad* neighbouring cells is similar, supporting that the rescue of MyoII accumulation observed by reducing E-Cad levels in cells neighbouring *pnut* dividing cells is not due to a difference in AJ elongation.

(e) *E-Cad^{JH}* mutant (dashed outline), *wt* and *pnut* mutant (white dots) cells marked by 0, 1 and 2 copies of E-Cad::GFP, respectively. E-Cad levels inside the *E-Cad^{JH}* mutant cells were assessed by antibody staining. White arrows: E-Cad staining at the AJ. Dashed arrows: decreased E-Cad staining at the AJ. *n*=79 clones from 11 fixed tissues.

Scale bars: 5µm (a,e)

Extended Data Figure 6.

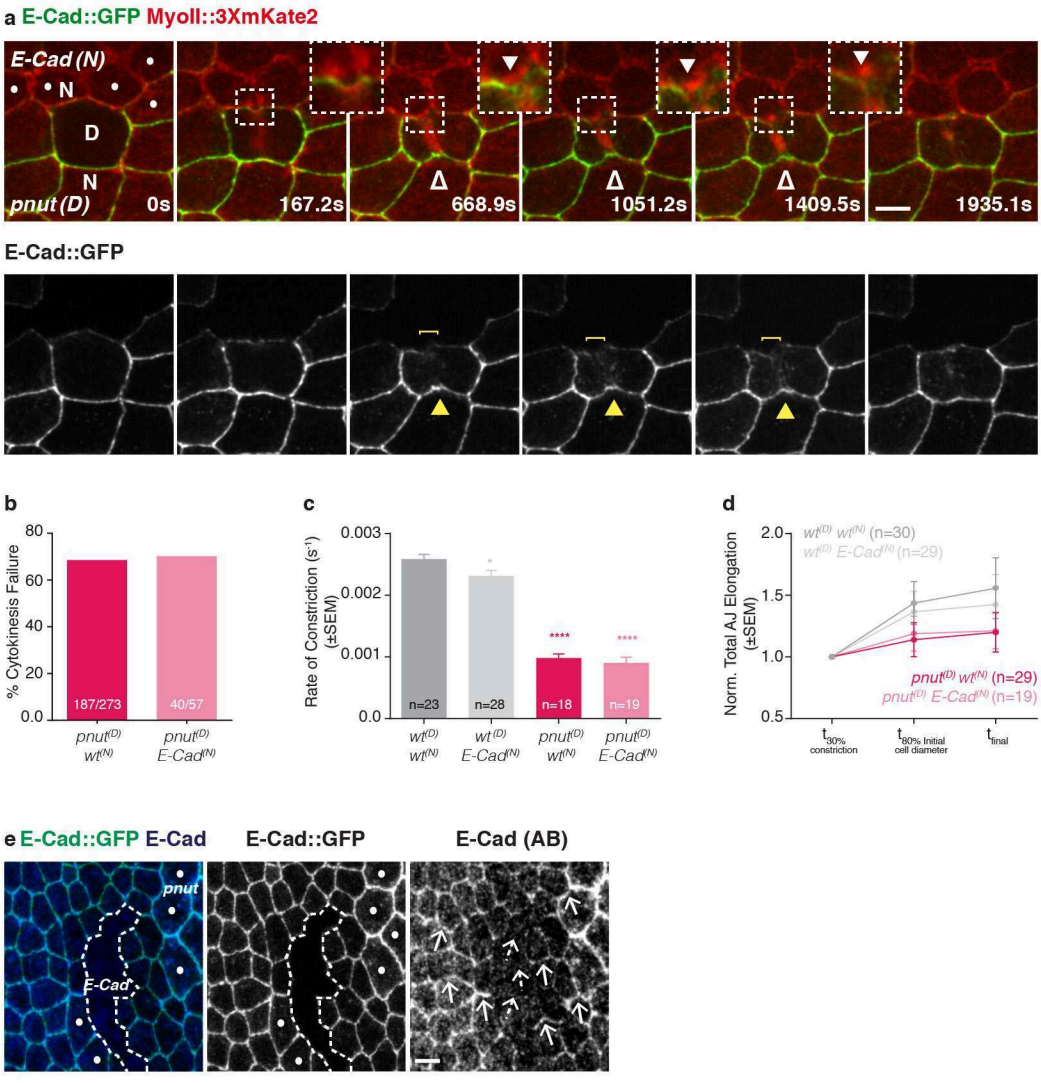

Extended Data Figure 7: Vinc, Rho, Dia and Arp2/3 functions are not essential for MyoII accumulation in the neighbours.

(a) Structure of the $vinc^{\Delta 3}$ and the GFP::Vinc alleles generated by CrispR/Cas9-mediated homologous recombination. For further details, see the Molecular biology section - Methods. M1 (Methionine 1), P2 (Proline 2) and Y961 (Tyrosine 961) correspond to the amino acid identity and position where the GFP tag was inserted relative to the Vinc coding sequence.

(b) E-Cad::GFP and MyoII::mChFP localization in *wt* and *vinc* dividing cells, as well as its neighbours (N). White arrowheads: MyoII::mChFP accumulation in the neighbouring cells.

(c) Graph of the rate of contractile ring constriction (s^{-1}, mean±SEM) in *wt* and *vinc* dividing cells. *n:* number of cells. Mann-Whitney test, ns: not significant.

(d) Graph of the normalized MyoII accumulation at 80% of the initial cell diameter (mean±SEM) for *wt* and *vinc* neighbouring cells (N). *n*: number of cells. Student *t*-test, ns: not significant.

(e) GFP::Vinc and MyoII::3XmKate2 localization in the dividing cell (D) and its neighbours (N) during cytokinesis. During contractile ring constriction, GFP::Vinc is reduced along the ingressing AJ and it does not accumulate with MyoII::3XmKate2 at the base of the ingressing membrane. Greyscale inset: GFP::Vinc localization upon full contractile ring constriction in the dividing cell. *n*=46 cells.

(f) Graph of the percentage of cytokinesis failure observed in rok^{RNAi}, *rho* and *dia* dividing cells. *n/n:* number of cells that failed cytokinesis/corresponding number of dividing cells counted.

(g) E-Cad::GFP and MyoII::mChFP localization in a *rho* mutant cell (N) neighbouring a *wt* dividing cell (D). White dots: indicates *rho* mutant cells, marked by the absence of nls::GFP. White open arrowheads: decreased MyoII::mChFP accumulation from mid-constriction until 80% of the initial cell diameter. White arrowheads: MyoII::mChFP accumulation in the neighbouring cells.

(h) Graph of the normalized MyoII accumulation at 80% of the initial cell diameter and 1 min after midbody (MB) formation (mean±SEM) in *wt* (*n*=53 cells), *rho* mutant (*n*=30 cells) and rok^{RNAi} (*n*=29 cells) neighbouring cells (N) facing *wt* dividing cells. Kruskal-Wallis test, ns: not significant, *:$p<0.05$, ****:$p<0.0001$.

(i) E-Cad::GFP and MyoII::mChFP localization in a *wt* dividing cell (D) facing either a *wt* neighbour or a *dia* neighbouring cell. N: neighbouring cell. White dots: *dia* mutant cells, marked by the absence of nls::GFP. White open arrowheads: reduced MyoII::mChFP accumulation in the *dia* neighbouring cell from mid-constriction until 80% of the initial cell diameter. White arrowheads: MyoII::mChFP accumulation.

(j) Graph of the normalized MyoII accumulation at 80% of the initial cell diameter and 1 min after midbody (MB) formation (mean±SEM) in *wt* (*n*=53 cells), *dia* mutant (*n*=30 cells) or rok^{RNAi} (*n*=29 cells) neighbouring cells (N) facing *wt* dividing cells. Kruskal-Wallis test, ns: not significant, *:$p<0.05$, ****:$p<0.0001$.

(k) Dia::eGFP expressing neighbours (N) facing a MyoII::3XmKate2 dividing cell (D). Dia::eGFP was expressed in clones to reveal its distribution exclusively in the neighbouring cells. Greyscale inset: Dia::eGFP localization upon full contractile ring constriction in the dividing cell. *n*=33 cells.

(l) E-Cad::GFP and MyoII::mChFP localization in *wt* and *arpc1* mutant neighbouring cells (N) facing a *wt* dividing cell. White dots: *arpc1* mutant cells, marked by the absence of nls::GFP. White arrowheads: MyoII::mChFP accumulation in the neighbouring cells.

(m) Graph of the normalized MyoII accumulation at 80% of the initial cell diameter (mean±SEM) for *wt* and *arpc1* neighbouring cells (N) facing *wt* dividing cells. *n*: number of cells. Student *t*-test, ns: not significant.
(n) Arp3::GFP expressed in clones to reveal its distribution in the neighbouring cells (N) in a MyoII::3XmKate2 expressing tissue. D: Dividing cell. Greyscale inset: Arp3::GFP localization upon full contractile ring constriction in the dividing cell. Both Dia::eGFP (k) and Arp3::GFP (n) are uniformly localized along the ingressing region throughout constriction in the dividing cell. *n*=30 cells.
Scale bars: 5µm (b,e,g,i,k,l,n)

Extended Data Figure 7.

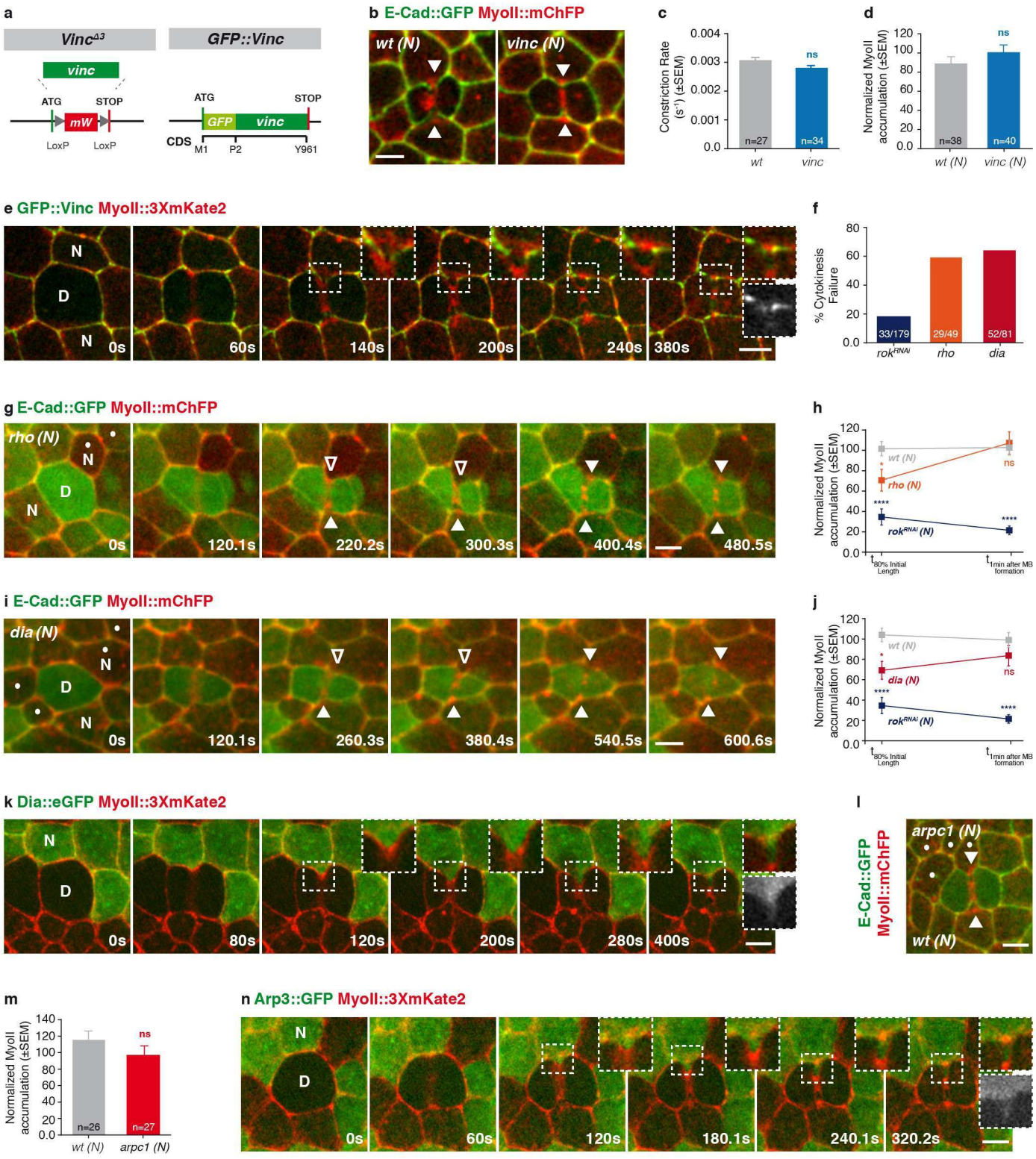

Extended Data Figure 8: Modelling the neighbouring cells response.

(a-e) One-dimensional numerical integration of the active gel equations, here the friction coefficient is shown in grey and MyoII final concentration is shown in blue. (a) For a decreased value of the friction coefficient at the centre of the integration box, MyoII shows two accumulations at the two interfaces between high and low frictions. (b,c) For a decreased value of the friction coefficient at the edge of the simulation box, Myosin final intensity shows two possible solutions: accumulation at the boundary between the low and high friction domains (b), or accumulation at the low friction edge of the simulation box (c). (d,e) Same one-dimensional numerical integration as in (b,c), but with either preferential polymerization in the high friction zone (d, see Supplementary Theory Note) or advancing low friction region (e, see Supplementary Theory Note), to mirror AJ ingression during contractile ring constriction. In both cases, MyoII robustly accumulates at the interface between the high and low friction domains.

(f) Geometry of the domain used for the numerical integration of the active gel equations, using a Finite Element method. The geometrical parameters are extracted from the experimental data (see Supplementary Theory Note). The assumption is that friction is low in the ingressing membrane (thick grey line) and high in the surrounding cortex (thick black line). All other parameters are constant in space and time. The initial mesh used for the numerical integration, is shown in thin grey lines. Also shown in Fig. 4a.

(g) Same numerical integration as in Fig. 4b with a three-dimensional representation of the steady-state concentration of MyoII, showing a MyoII depletion (green) in the ingressing region and a MyoII accumulation at the base of the ingressing membrane (deep blue). Scale: color-coded representation of MyoII concentration.

(h,i) Steady-state velocity of the actomyosin flows in the vertical or horizontal direction, respectively v_x - (h) and v_y- (i). Low velocities are color-coded in red and high velocities are color-coded in black. Scale: color-coded representation of the actomyosin flow velocity.

(j) Steady-state concentration of MyoII for increasing protrusion lengths, at constant contractility (same colour code as in g). Actomyosin flows can only occur above a critical length threshold, and the strength of the accumulation increases with the protrusion length.

(k) Steady-state concentration of MyoII for increasing contractility, at constant protrusion length (same colour code as in g). Actomyosin flows can only occur above a critical contractility threshold, and the strength of the accumulation increases with the increase of contractility.

(**l**) Steady-state concentration of MyoII for intermediate contractility and same protrusion length and friction parameters as in (g), with a zero-flux boundary condition. The results are qualitatively similar, with the peak of MyoII accumulation showing a slight shift downwards when compared to (g). Scale: color-coded representation of MyoII concentration.

(m) Steady-state concentration of MyoII with friction uniformly low everywhere (remaining parameters are kept similar to l). Under these conditions, MyoII accumulation can have multiple and random locations (right and left-side vertices in this simulation) instead of a robust accumulation at the base of the protrusion. Scale: color-coded representation of MyoII concentration.

Extended Data Figure 8.

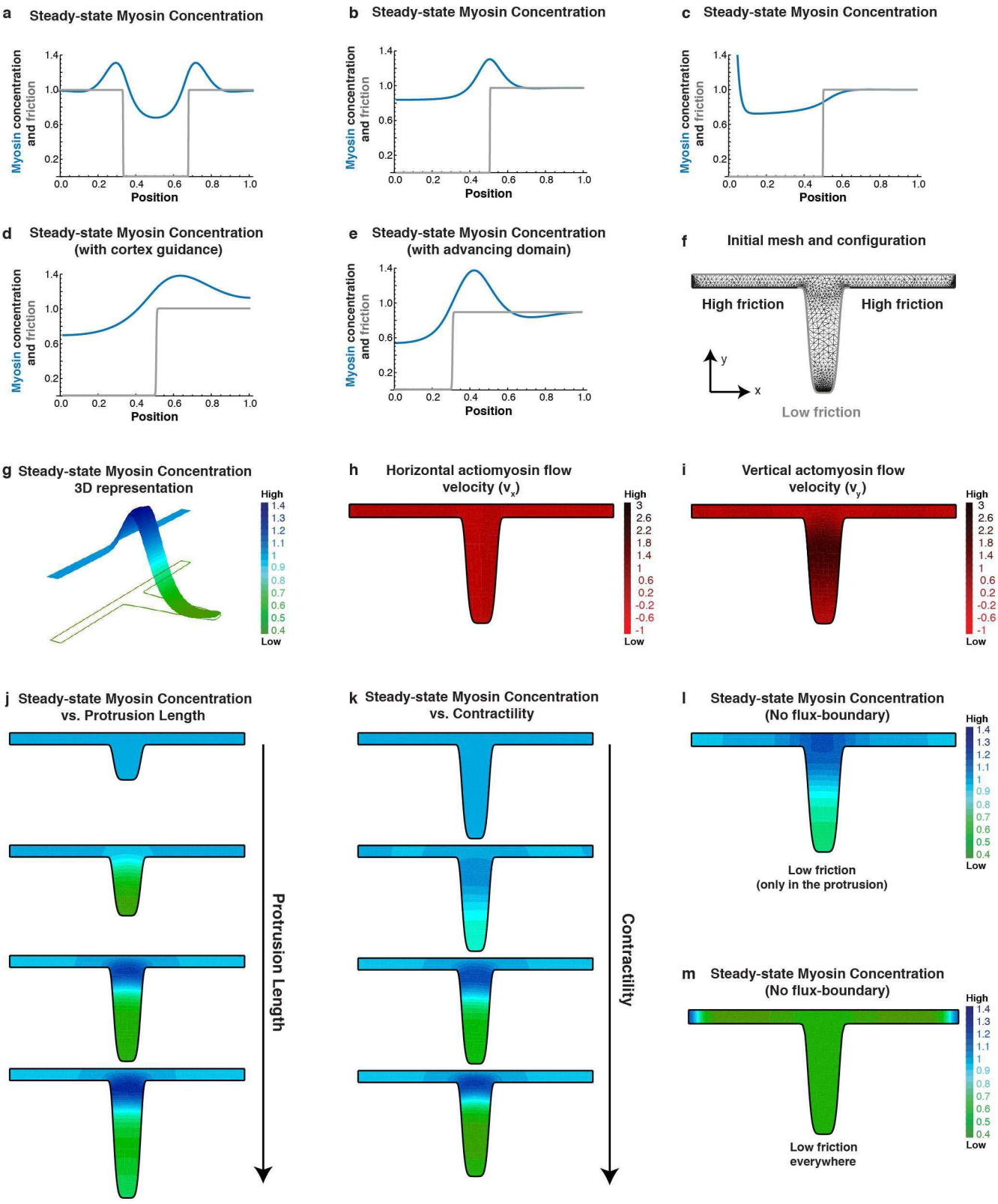

1. SUPPLEMENTARY TABLES

Supplementary Table 1: E-Cad::GFP turnover, accessed by FRAP, for *wt* and *pnut*^{RNAi} interphase cells, as well as for *wt* cells undergoing cytokinesis.

Genotype	*Mobile Fraction (±SEM)*	*Turnover Time (s) (±SEM)*	*Coefficient of Diffusion (±SEM)*
wt interphase cells	0,44 ± 0,08 (*n*=17)	64 ± 21 (*n*=17)	0,0006 ± 0,0004 (*n*=18)
wt cells during cytokinesis	0,41 ± 0,12 (*n*=22)	46 ± 14 (*n*=22)	Not determined
pnut^{RNAi} interphase cells	0,55 ± 0,13 (*n*=34)	69 ± 28 (*n*=34)	0,0008 ± 0,0007 (*n*=20)

Supplementary Table 2: Alleles and transgenes used in this study.

Drosophila stock	*Reference or Source*
ubi-E-Cad::GFP	Ref[60]
E-Cad::GFP	Ref[61]
E-Cad::3XmTagRFP	this study
E-Cad::3XmKate2	this study
α-Cat::GFP	Ref[62]
MyoII::mChFP	Ref[35]
MyoII::3XmKate2	this study, Methods, Molecular Biology
UAS-CAAX::mOrg	Ref[63]
UAS-arp3::GFP	Bloomington Stock Center
UAS-dia::eGFP	Bloomington Stock Center
Lifeact::GFP	Bloomington Stock Center
β_H-spectrin::GFP	Bloomington Stock Center
GFP::Vinc	this study
ubi-Rok::GFP	Ref[58]
Actin5C-FRT-y$^+$-FRTGal4	Bloomington Stock Center
Tub-FRT-GFP-FRT-Gal4	Bloomington Stock Center
FRTG13 ubi-GFP-nls	Bloomington Stock Center
FRT40A MyoII::GFP	Ref[1]
FRT40A MyoII::RFP	Ref[1]
FRT42D nls::GFP	Bloomington Stock Center
FRT40A nls::GFP	Bloomington Stock Center
FRT19A *rok*^{2}	Ref[64], Bloomington Stock Center
FRTG13 *pnut*^{xp}	Ref[65], gift from Manos Mavrakis
FRTG13 *shg*^{JH}	Ref[66]
FRT42D *rho*^{72M1}	Ref[67]
FRT40A *dia*^{SY2}	Ref[68]
FRT40A *arpc1*^{Q25SD}	Ref[69]
FRT40A *sec5*^{E10}	Ref[70]
hsFlp, tub-GAL80, FRT19A	Bloomington Stock Center
tub-Gal80 FRT40A	Bloomington Stock Center
Tubulin-Gal4	Bloomington Stock Center
Actin5C-Gal4	Bloomington Stock Center
vinc$^{\Delta 3}$	this study
shg^{k03401}	Ref[71]

UAS-*pnut*^{RNAds}	VDRC Stock Center
UAS-*rok*^{RNAds}	Bloomington Stock Center
UAS-*ani*^{RNAds}	VDRC Stock Center
UAS-*moe*^{RNAds}	Bloomington Stock Center
UAS-*sds22*^{RNAds}	VDRC Stock Center
UAS-*shi*$^{ts1.k}$	Bloomington Stock Center
UAS-YFP::*Rab11.S25N*	Bloomington Stock Center

2. SUPPLEMENTARY REFERENCES:

47. Bosveld, F., Markova, O., Guirao, B., Martin, C., *et al.* Epithelial tricellular junctions act as interphase cell shape sensors to orient mitosis. *Nature* **530,** 495-498 (2016).

48. Xu, T. & Rubin, G. M. Analysis of genetic mosaics in developing and adult Drosophila tissues. *Development* **117,** 1223-1237 (1993).

49. Lee, T. & Luo, L. Mosaic analysis with a repressible cell marker for studies of gene function in neuronal morphogenesis. *Neuron* **22,** 451-461 (1999).

50. Gratz, S. J., Ukken, F. P., Rubinstein, C. D., Thiede, G., *et al.* Highly specific and efficient CRISPR/Cas9-catalyzed homology-directed repair in Drosophila. *Genetics* **196,** 961-971 (2014).

51. Ren, X., Sun, J., Housden, B. E., Hu, Y., *et al.* Optimized gene editing technology for Drosophila melanogaster using germ line-specific Cas9. *Proc Natl Acad Sci U S A* **110,** 19012-19017 (2013).

52. Huang, J., Zhou, W., Watson, A. M., Jan, Y. N. & Hong, Y. Efficient ends-out gene targeting in Drosophila. *Genetics* **180,** 703-707 (2008).

53. Baena-Lopez, L. A., Alexandre, C., Mitchell, A., Pasakarnis, L. & Vincent, J. P. Accelerated homologous recombination and subsequent genome modification in Drosophila. *Development* **140,** 4818-4825 (2013).

54. Royou, A., Sullivan, W. & Karess, R. Cortical recruitment of nonmuscle myosin II in early syncytial Drosophila embryos: its role in nuclear axial expansion and its regulation by Cdc2 activity. *J Cell Biol* **158,** 127-137 (2002).

55. Ségalen, M., Johnston, C. A., Martin, C. A., Dumortier, J. G., *et al.* The Fz-Dsh planar cell polarity pathway induces oriented cell division via Mud/NuMA in Drosophila and zebrafish. *Dev Cell* **19,** 740-752 (2010).

56. Oda, H., Uemura, T., Harada, Y., Iwai, Y. & Takeichi, M. A Drosophila homolog of cadherin associated with armadillo and essential for embryonic cell-cell adhesion. *Dev Biol* **165,** 716-726 (1994).

57. Bosveld, F., Bonnet, I., Guirao, B., Tlili, S., *et al.* Mechanical Control of Morphogenesis by Fat/Dachsous/Four-Jointed Planar Cell Polarity Pathway. *Science* **336,** 724-727 (2012).

58. Bardet, P. L., Guirao, B., Paoletti, C., Serman, F., *et al.* PTEN Controls Junction Lengthening and Stability during Cell Rearrangement in Epithelial Tissue. *Dev Cell* **25,** 534-546 (2013).

59. Grusche, F. A., Hidalgo, C., Fletcher, G., Sung, H. H., *et al.* Sds22, a PP1 phosphatase regulatory subunit, regulates epithelial cell polarity and shape [Sds22 in epithelial morphology]. *BMC Dev Biol* **9,** 14 (2009).

60. Oda, H., Tsukita, S. & Takeichi, M. Dynamic behavior of the cadherin-based cell-cell adhesion system during Drosophila gastrulation. *Dev Biol* **203,** 435-450 (1998).

61. Huang, J., Zhou, W., Dong, W., Watson, A. M. & Hong, Y. Directed, efficient, and versatile modifications of the Drosophila genome by genomic engineering. *Proc Natl Acad Sci U S A* **106,** 8284-8289 (2009).

62. Lye, C. M., Naylor, H. W. & Sanson, B. Subcellular localisations of the CPTI collection of YFP-tagged proteins in Drosophila embryos. *Development* **141,** 4006-4017 (2014).

63. Kanca, O., Caussinus, E., Denes, A. S., Percival-Smith, A. & Affolter, M. Raeppli: a whole-tissue labeling tool for live imaging of Drosophila development. *Development* **141,** 472-480 (2014).

64. Winter, C. G., Wang, B., Ballew, A., Royou, A., *et al.* Drosophila Rho-associated kinase (Drok) links Frizzled-mediated planar cell polarity signaling to the actin cytoskeleton. *Cell* **105,** 81-91 (2001).

65. Neufeld, T. P. & Rubin, G. M. The Drosophila peanut gene is required for cytokinesis and encodes a protein similar to yeast putative bud neck filament proteins. *Cell* **77,** 371-379 (1994).

66. Bécam, I. E., Tanentzapf, G., Lepesant, J. A., Brown, N. H. & Huynh, J. R. Integrin-independent repression of cadherin transcription by talin during axis formation in Drosophila. *Nat Cell Biol* **7,** 510-516 (2005).

67. Strutt, D. I., Weber, U. & Mlodzik, M. The role of RhoA in tissue polarity and Frizzled signalling. *Nature* **387,** 292-295 (1997).

68. Yan, S., Lv, Z., Winterhoff, M., Wenzl, C., *et al.* The F-BAR protein Cip4/Toca-1 antagonizes the formin Diaphanous in membrane stabilization and compartmentalization. *J Cell Sci* **126,** 1796-1805 (2013).

69. Zallen, J. A., Cohen, Y., Hudson, A. M., Cooley, L., *et al.* SCAR is a primary regulator of Arp2/3-dependent morphological events in Drosophila. *J Cell Biol* **156,** 689-701 (2002).

70. Langevin, J., Morgan, M. J., Rosse, C., Racie, V., *et al.* Drosophila Exocyst Components Sec5, Sec6, and Sec15 Regulate DE-Cadherin Trafficking from Recycling Endosomes to the Plasma Membrane. *Dev Cell* **9,** 365-376 (2005).

71. Tepass, U., Gruszynski-DeFeo, E., Haag, T. A., Omatyar, L., *et al.* shotgun encodes Drosophila E-cadherin and is preferentially required during cell rearrangement in the neurectoderm and other morphogenetically active epithelia. *Genes Dev* **10,** 672-685 (1996).

In this Supplementary Note, we detail our data analyses and modelling approaches to understand the mechanisms of myosin (MyoII) accumulation in the neighbouring cells. As shown in (Fig. 2a-b), MyoII accumulation in the neighbouring cells is preceded by the detachment of the cortex and a marked decrease in E-Cadherin (E-Cad) signal along the ingressing *adherens* junction (AJ) pulled by the contractile ring. We first examine how the interplay between cortical attachment and contractility regulate the timing of cortex detachment. We then study E-Cad dynamics, in order to understand the mechanism of E-Cad depletion in the ingressing AJ during cytokinesis. Finally, we propose a model, based on the active gel theory, on how a local depletion of E-Cad can drive MyoII accumulation via self-triggered actomyosin flows.

1 Cortex detachment

In order to probe the potential role of cortex detachment for MyoII accumulation in neighbouring cells, we analyse from a theoretical point of view the mechanisms and mechanics associated with the detachment event.

The cortex is a contractile layer lining the AJ. If it becomes curved, either because of an external deformation (i.e. the contractile ring constriction in the dividing cell) or a pressure difference between two cells, this produces inward forces perpendicular to the membrane, that need to be balanced by adhesion to prevent cortex detachment [72]. The biophysical role of E-Cad in this membrane-cortex interaction has been studied *in vitro* in the past [72], but to a lesser extent *in vivo*, although much work has been dedicated to the role of E-Cad as integrators of stress in mechanotransduction [73, 74], and as part of the E-cad/α-catenin complex in adhesion [75].

1.1 Theoretical considerations

Following the classical active gel theory [76, 77, 78], we model the cortex as a thin viscous layer, of thickness h. We denote γ the local tension in the cortex, χ the contractility (in Pascals) due to MyoII motor power-stroke and η the cortical viscosity. Thus, along the direction x parallel to the membrane, the tension γ is the sum of active and viscous contributions $\gamma = h(\chi + \eta\partial_x v)$, with v the local velocity in the layer, under the lubrification regime [77]. We are interested in a cortex connected to an AJ, which can be curved with local curvature $\mathscr{C}(x,t)$. In the quasi-static regime of ingressing AJ elongation [72], the cortex will detach if the normal forces $\gamma\mathscr{C}$ is greater than the maximal adhesion force density f_c, which is proportional to the strength of the adhesion between the cortex and the membrane, as well as the local concentration $c(x)$ of linker protein, such as E-Cad/α-catenin or ERM proteins [72, 79]. This is analogous to the de Gennes criteria for the unbinding of adhesive vesicles [80]. It should be noted that this adhesion energy is active in nature, and can be reinforced actively through cytoskeletal remodelling [81]. Therefore, for constant tension and adhesion strength, one expects the cortex to detach once a well-defined curvature $\mathscr{C}_c$, imposed by the contractile ring, is reached, such that:

$$\mathscr{C}_c = \frac{f_c}{\gamma}$$

and the deformation is slow enough that the viscous stress can be neglected compared to the active stress, so that $\mathscr{C}_c = \frac{f_c}{\chi h}$. We then predict that the critical curvature of cortical detachment can be modulated *in vivo*: the maximal curvature at the time of detachment should increase with either an increase in membrane-cortex attachment, or a decrease in cortical tension (and vice-versa). This criteria bears similarities with the physics of blebbing [82], although in that case, the driving force causing AJ curvature and cortex detachment is the internal pressure

within the cell, instead of an external force, applied by the contractile ring of the dividing cell as in our case.

1.2 Experimental verification

We validated this model (Extended Data Fig. 3a-d) by manipulating experimentally either cortical tension or cortex attachment (Extended Data Fig. 3a-d). As curvature cannot be robustly defined in the region of the ingressing AJ, given the length scales examined, we alternatively measured the angle θ between the two sides of the ingressing AJ (as sketched on Extended Data Fig. 3a). With d_0 being the characteristic width of the ingressing region, this angle is related to curvature via $\mathscr{C} \propto (\pi - \theta)/d_0$.

We first sought to decrease cortex attachment, either by knocking down *moesin* (Extended Data Fig. 3b-d, Fig. 2g and Supplementary Video 6), a key membrane-cortex linker, via moe^{RNAi}, or by decreasing the amount of E-Cad at the junction, using an heterozygous E-Cad mutant (Extended Data Fig. 3b-d). In both cases (Extended Data Fig. 3b-d), the cortex detached for smaller AJ deformation, i.e. for larger critical angle/smaller local AJ curvature. To increase contractility we inactivated the function of *sds22*, a known inhibitor of MyoII contractility [83]. Interestingly, reducing *sds22* activity also resulted in cortex detachment at smaller AJ deformations (Extended Data Fig. 3b-d). This indicates that the curvature upon cortex detachment depends on the ratio of cortical active tension and cortical attachment strength, and thus can be manipulated in a predictable manner *in vivo*.

Crucially, as discussed in the main text, this theoretical analysis and its experimental validation allowed us to uncover the role of *moe* in this process and test whether the position of MyoII accumulation in the neighbouring cells depends on the initial position of the detached cortex. In moe^{RNAi} neighbouring cells, cortex detachment is precocious, thus the initial position of the detached cortex is displaced away from the base of the ingressing AJ. However, we found that MyoII still accumulates at the boundary between high and low E-Cad, and not at the position of the initially detached cortex. Together with the additional findings presented in the manuscript, these results exclude that MyoII accumulation arises only from the contraction of the detached cortex.

2 E-Cad dynamics

As we saw in the main text (Fig. 2a-b), MyoII accumulation is preceded by a marked decrease in E-Cad concentration along the ingressing AJ formed between the dividing cell and it's neighbour. The decrease in concentration is concomitant with the neighbouring junction elongation (Fig. 3a-c), and it is not impaired when we perturb regulators of endocytosis and E-Cad recycling pathway (Extended Data Fig. 4b-d). Therefore, a natural hypothesis is that E-Cad depletion could be a simple dilution effect. To test this idea quantitatively, we first model the dynamics of E-Cad on a homeostatic junction, i.e. a junction of constant length, and then on an elongating junction, mirroring cytokinesis.

2.1 E-Cad dynamics on a junction of constant length

2.1.1 Theoretical considerations

Following Ref. [84, 85, 86, 87], we write diffusion-reaction equations for both the mobile and immobile E-Cad concentrations (resp. $c_m(x,t)$ and $c_i(x,t)$) at a static junction that keeps a constant length l:

$$\partial_t c_i = D_i \partial_{xx} c_i \tag{1}$$

$$\partial_t c_m = D_m \partial_{xx} c_m - \frac{c_m - f_m c^0}{\tau} \tag{2}$$

where τ is the turnover time of the mobile fraction, c^0 the homeostatic total E-Cad concentration, f_m the mobile fraction of E-Cad, assumed constant (so that $f_m c^0$ is the homeostatic concentration of mobile E-Cad), and D_i (resp. D_m) the diffusion coefficient of the immobile (resp. mobile) E-Cad. Here, we used a linear model with the turnover and diffusion constants being independent of respective E-Cad concentrations, an hypothesis we verify later in the text.

In order to test the dilution model, we need to measure all the above parameters associated with E-Cad turnover. For that, we performed Fluorescence Recovery After Photobleaching (FRAP) experiments on E-Cad::GFP junctions of interphase cells. To extract each parameter independently in our system, we define $\delta c_m(x,t) = c_m - f_m c^0$ the difference between E-Cad concentration and its homeostatic value, as well as the i-moment of its distribution $M_i^m(t) = \int dx \delta c_m(x,t) x^i$. It can then be shown [88] that

$$M_0^m = M_0^m(0) e^{-t/\tau} \tag{3}$$

and

$$\frac{M_2^m}{M_0^m}(t) = 2D_m t + \frac{M_2^m}{M_0^m}(0) \tag{4}$$

A corresponding relationship can be found for the normalized second moment $M_2^i(t)$ of the immobile E-Cad concentration. Therefore, the evolution of the zeroth moment depends only on the turnover τ, whereas the value of the normalised second-moment depends only on the diffusion D_m, independently of the initial condition (i.e. on how the FRAP experiment was done). From a physical point of view, this means that turnover changes the total mass of E-Cad present at the interface, whereas diffusion only changes the width of the bleached region. Combining the equations of the mobile and immobile fraction predicts that the second moment $M_2(t)$ of the total E-Cad concentration evolves as $\frac{M_2}{M_0}(t) = \frac{M_2}{M_0}(0) + 2t\frac{D_i M_0^i + D_m M_0^m(t)}{M_0^i + M_0^m(t)}$, which after a characteristic time τ also increases linearly as $\frac{M_2}{M_0}(t) \to 2D_i t$. We will therefore see that the mobile fraction turns over sufficiently fast that its diffusion coefficient is irrelevant. Moreover, in the limit that $D_i \approx D_m$, the evolution of the normalized second moment becomes purely affine. We therefore drop the indices in the following sections, and refer to D_i as simply D.

2.1.2 Parameter extraction and fitting

These analytical expressions offer us a way to test *a posteriori* the assumptions of our linear model, by predicting that the two moments should recover as exponential and linear curves respectively. To fit the recovery curves of E-Cad::GFP upon photobleaching using the predictions above, we used a classical least-square fit approach. Firstly, each recovery curve was always well-fitted by a single-exponential, from which we could extract both the turnover time and the mobile fraction. We fitted only the first $100s$ of each FRAP recovery curve, as they were the least sensitive to noise and subsequent bleaching. We found a turnover time $\tau = 64s \pm 21s$ and a mobile fraction of $f_s = 0.44 \pm 0.08$ (Supplementary Table 1). To assess the goodness of the fits, we compared in each recovery curves the experimental recovery with the best fit prediction, and calculated the coefficient of determination R^2 of the fit (the closer this value is to 1, the more accurate is the fit). The average of all coefficients of determination was $\langle R^2 \rangle = 0.92$, while the lowest value we found was $R^2 = 0.79$, indicative of consistently good fits.

Secondly, we measured the variance of the size of the bleached region in time to extract the diffusion coefficient (from the first $200s$ of each movie). Individual variance extracted from

the recovery curves showed a consistent increase in time. As there was substantial noise associated with the measurement, we averaged $n = 18$ experiments, and show that the average curve is well-fitted (coefficient of determination $R^2 = 0.84$) by an affine function, as expected from the theory. By fitting the slope of the affine function, we could extract the E-cad diffusion coefficient $D = 6 \pm 4\ 10^{-4} \mu m^2 s^{-1}$ (Supplementary Table 1). In particular, we could not detect a correction to the linear increase in the normalized second moment, which could indicate that $D_m \approx D_i$. As noted earlier, the goodness of both fits validates *a posteriori* the model that we used, showing that linear diffusion and turnover is a good approximation for E-Cad::GFP dynamics in this system.

One should note that the value we extracted for the diffusion coefficient is of the same order of magnitude, albeit 4-fold smaller, than what was reported from MDCK cultured cells in Ref. [86]. In contrast to MDCK cells however, we show that a large fraction of the E-Cad pool in the *Drosophila* notum is immobile on the timescale of cytokinesis.

To give a better physical intuition on the relative magnitude of diffusion and mobile turnover for junction homeostasis, a useful quantity to define is the characteristic length of diffusion $l_D = \sqrt{D\tau}$. On length scales larger than l_D, turnover is the dominant mode of recovery, whereas for length scales smaller than l_D, diffusion is the dominant mode. With the values we measured, $l_D \approx 0.2 \mu m$, validating the idea that turnover is much more important than diffusion at the length scale of the whole junction ($l \approx 7 \mu m$ typically), and that we do not expect significant recoveries from diffusion at the scale of a few microns, as in the case of local AJ elongation.

We then turned to the E-Cad::GFP recovery dynamics on the junctions of cells undergoing cytokinesis. In this case, long-term data is not easily accessible because of the complex three-dimensional movements associated with cytokinesis, so measuring a diffusion coefficient was not technically possible. Nevertheless, we performed high-frequency imaging (one frame per second) in order to study the short-term FRAP recovery. For AJs of cells undergoing cytokinesis, we found that the E-Cad::GFP mobile fraction and the average turnover time are respectively $\tau = 46s \pm 14s$ and $f_s = 0.41 \pm 0.12$. Interestingly, the distribution of the mobile fraction did not show any statistically significant difference between the interphase and cytokinesis cases ($n = 22$ dividing cells and $n' = 17$ interphase cells, $P > 0.2$), although the turnover time displayed a significant, albeit slight, difference ($P < 0.05$). For the sake of consistency, we also performed FRAP on the junction of interphase cells at one frame per second, and saw no statistical differences with the results from movies at a rate of one frame per $5s$ ($n = 26$ interphase cells, $P > 0.1$ for the mobile fraction, $P > 0.05$ for the turnover time). When comparing the $1s$ interphase data to the $1s$ cytokinesis data directly, we also found no statistically significant difference ($P > 0.2$ for the mobile fraction, $P > 0.2$ for the turnover time).

Altogether, these results show that E-Cad turnover and mobile fraction are largely unaffected during cytokinesis.

2.2 E-Cad dynamics on an elongating junction

Having determined the parameters of E-Cad::GFP dynamics, we analysed how the local elongation of the junction can contribute to modulate E-Cad concentration.

2.2.1 Theoretical considerations

In order to get simple analytical insights into E-Cad dynamics on an elongating junction, we start by considering an AJ of variable length $l(t)$ being globally dilated, so that the concentrations of mobile and immobile E-Cad are independent of the position x, and only vary in time.

The equation for the mobile and immobile E-Cad concentrations then reads

$$\frac{dc_m}{dt} = -\frac{c_m - f_m c^0}{\tau} - \frac{c_m}{l}\frac{dl}{dt} \tag{5}$$

and

$$\frac{dc_i}{dt} = -\frac{c_i}{l}\frac{dl}{dt} \tag{6}$$

Physically, this means that when the AJ elongates exponentially at a rate $r = \frac{1}{l}\frac{dl}{dt}$, the immobile fraction gets passively diluted as the same rate, whereas the mobile fraction can respond by turnover, and maintain a steady state concentration c_m^∞, with:

$$c_m^\infty = \frac{c_m(r=0)}{1+r\tau} \tag{7}$$

As expected, as the rate of AJ elongation r becomes large compared to the turnover rate $1/\tau$, steady state E-Cad concentration drops to low values.

Guided by our experimental results (see below), we must also consider theoretically the alternative possibility for the AJ elongation to be local. In the following section, we therefore note and measure f, the fraction of the AJ being elongated. In this scenario, we cannot consider E-Cad concentration to be independent on position x, and must therefore adapt Eq. (1)-(2) to a locally elongation AJ. We first adimensionalise all lengths x by the length of the junction l, so that our equation is defined on the domain $x \in [0,1]$. The elongating region is defined initially as $x \in [x_i, x_f]$ with $x_i = (1-f)/2$ and $x_f = (1+f)/2$. We then assume that the deformation is affine, and define the stretched coordinates $y = f(x)$, such as

$$f(x) = \begin{cases} x & \text{for } x < x_i \\ x + \int_0^t r(t)dt(x - x_i) & \text{for } x \in [x_i, x_f] \\ x + \int_0^t r(t)dt(x_f - x_i) & \text{for } x > x_f \end{cases} \tag{8}$$

$r(t)$ being the local stretch ratio at a given time t, and the previous Eq. (1)-(2) can be re-written on the y coordinates, therefore taking into account the locality of the AJ elongation. In the following section, we analyzed whether the local or global model applies, and then performed numerical integration of the corresponding equations using a finite difference method.

2.2.2 Predictions and numerical integration of the model

wt dividing cells

We first start by simulating AJ elongation in the case of *wt* dividing cells facing *wt* neighbours. In order to estimate the fraction f of the AJ being elongated, we measured the width t of the ingressing region normalized by total AJ length, and estimated from the time average (Extended Data Fig. 5a-b) that $f = 12\%$ of the initial junction is pulled by the contractile ring in the wild type condition. We then set the parameters of E-Cad dynamics D, τ and f_s to the values extracted experimentally above ($D = 6.10^{-4}\mu m^2 s^{-1}$, $\tau = 46s$ and $f = 0.41$). Using the results from the measurements of the main text, we consider a junction growing linearly from $l = 7\mu$m to $l = 11\mu$m (i.e. a 58% junctional growth, see Fig.3a-c) in $T = 326$s (which corresponds to the average time of cytokinesis), after an initial phase of junctional retraction (see Methods section for additional details). Therefore, experimentally, $r\tau \ll 1$, and from the analytical expression (7) above, we can predict that the mobile fraction is largely unaffected by the AJ elongation, as cytokinesis is slow enough that the mobile fraction is recovered by turnover.

One can also estimate the characteristic time $\tau_{diff} = l_d^2/D$ that diffusion would take to fill a E-Cad depletion of characteristic size $l_d \approx 1\mu m$. With the coefficient of diffusion measured, $\tau_{diff} \approx 2.10^3$ s. This time is larger that the time T of cytokinesis, meaning that we do not expect diffusion to significantly homogenise the E-Cad::GFP depletion. Indeed, as shown in the kymograph of the full numerical simulation of *wt* cells (Fig. 3d), the simulations predict a persistent E-Cad depletion throughout the process, to levels around 40% of their homeostatic value (Fig. 3d). As the mobile fraction recovers fast, the bulk of the decrease corresponds to the dilution of the immobile fraction, which therefore plays a crucial role to explain E-Cad depletion upon junction elongation in this system.

To further compare the prediction of the model to the experimental data, we computed the E-Cad concentration in the centre of the depletion as a function of AJ elongation (Extended Data Fig. 5c). In order to estimate a confidence interval for our predictions, we ran the simulations again using the extremal values for the turnover τ, diffusion D and immobile fraction f reported above (i.e. $\pm$ their standard deviation). We then plotted the extremal values for our prediction of the evolution of E-Cad::GFP concentration vs total AJ elongation (Extended Data Fig. 5c), which takes into account the uncertainty on the E-Cad::GFP dynamics parameters. We observe that the dilution model can account for a large fraction of the E-Cad::GFP depletion, as well as displaying the correct temporal trend. To quantify the agreement between the experimental data and the model, we calculated the coefficient of determination of our prediction for E-Cad::GFP concentration vs AJ elongation, and found $R^2 = 0.82$, indicative of a good quantitative prediction. As we are dealing with non-linear curves, we also quantified the standard deviation of the residuals, and found $S = 0.11$.

rok neighbouring cells

In order to challenge the model, we first tested the role of *rok* in the E-Cad decrease at the ingressing AJ, as contractility was suggested to contribute to regulate E-Cad stability at the AJs [89]. For that, we first measured the normalized width t of the ingressing region to assess the locality of the elongation, and found a fraction $f \approx 26\%$ being pulled (Extended Data Fig. 5a,b), arguing for a local elongation, although on a larger scale than in the case of *wt* dividing cells facing *wt* neighbours. Moreover, we found that AJ elongation imposed by a *wt* dividing cell facing a *rok* neighbour is 40%, (Fig. 3e-g), and that the duration of cytokinesis is similar to the *wt* case, suggesting that the neighbour's contractility does not influence these parameters. When we performed our numerical integration under these conditions, simply changing the maximum elongation to 40%, we observed an intermediary phase of milder depletions, similar to the experimental observations (Fig. 3e-h and Extendend Data Fig. 5g). Since Rok is required for MyoII accumulation in the neighbouring cells, these results further show that MyoII accumulation in the neighbours is not required for the decrease of E-Cad concentration along the elongating junction. These findings are also in agreement with the fact that E-Cad decrease precedes MyoII accumulation in the neigbours. To quantify the goodness of our fits, we calculated again the coefficients of determination and standard deviation of the residuals, and found $R^2 = 0.74$ and $S = 0.13$.

pnut dividing cells

Finally, to further validate our model, we examined the effect of *pnut* loss of function on the E-Cad::GFP dynamics during cytokinesis. We find that cells neighbouring *pnut*^{RNAi} cells do not display a marked E-Cad depletion (Fig. 3i,k). We analysed whether the characteristics and kinetics of cytokinesis in *pnut* dividing cells could account for the lack of depletion. Compared to *wt*, as the total time for cytokinesis in *pnut*^{RNAi} is nearly four times longer ($T = 1111s$, Fig.

1g and Supplementary Video 2), and the elongation is markedly reduced (25%, Fig. 3i-k). Moreover, we measured again the width t of the ingressing region normalized by the length of the AJ to assess the locality of the elongation, and found that, upon *pnut*^{RNAi}, the bulk of the AJ is deformed (Extended Data Fig. 5a,b), thereby often resulting in a triangular-shaped AJ. This was in contrast with the characteristic finger-shaped AJ observed in *wt* cells. We thus implemented a global, rather than local, AJ elongation in the numerical integrations for *pnut*. Therefore, the prediction of our model would indeed be that E-Cad is less diluted and has more time to recover, largely suppressing the E-Cad decrease.

Before reaching this conclusion, we needed to exclude a specific function of *pnut* in regulating E-Cad levels or dynamics. Therefore, we measured the parameters of E-Cad dynamics in *pnut* cells by performing FRAP experiments on interphase *pnut*^{RNAi} cells, using the conditions and analysis pipeline previously described. We found an immobile fraction only slightly, although significantly, smaller than in *wt* cells ($f = 0.55 \pm 0.13$, $P < 0.01$, $n = 34$ cells, see Supplementary Table 1), and both the turnover time and diffusion coefficient were statistically indistinguishable to the wild type (respectively $\tau = 69s \pm 28$, $P > 0.2$, $n = 34$ cells and $D = 8 \pm 7\ 10^{-4} \mu m^2 s^{-1}$, $P > 0.2$, $n = 20$ cells, see Supplementary Table 1). Therefore, E-Cad kinetics upon *pnut*^{RNAi} are similar to *wt*, and cannot account for the lower E-Cad depletion.

We then ran our simulations for these updated parameter values. The smaller immobile fraction measured in *pnut*^{RNAi}, but more importantly the fact that AJ elongation is decreased and occurs on a more global scale, decreased drastically the E-Cad depletion. Altogether, this accounts quantitatively for the absence of E-Cad depletion observed in cells neighbouring *pnut*^{RNAi}, validating our hypothesis (Fig. 3l and Extended Data Fig. 5m). To quantify the goodness of our fits, we calculated again the coefficients of determination and standard deviation of the residuals, and found $R^2 = 0.73$ and $S = 0.03$.

One should note that for the sake of simplicity, we have assumed here that the elongation in *pnut*^{RNAi} was fully global, although some cells displayed slightly more local AJ elongation, in particular in the early stages of constriction. Interestingly, we noted that in 50% of cases, we could measure a small E-Cad depletion in *pnut*^{RNAi} at the early stages of constriction, but these depletions were always very short-lived (Extended Data Fig. 5k,l). This type of complex and transient behavior goes beyond the scope of our simple model, but could be explained in a natural manner by modifying dynamically the locality of the AJ elongation for a given condition.

Altogether our model and its validation using wt and mutant conditions indicates that a passive dilution mechanism can account for the bulk of E-Cad depletion at the ingressing AJ between dividing and neighbouring cells. One should note that this E-Cad decrease effect is expected to facilitate cortical the detachment studied in the first part of this Theory Notes, by locally lowering the concentration of E-Cad molecules.

3 Actomyosin accumulation in neighbouring cells

So far, we have shown that E-Cad depletion and cortex detachment are likely to be passive consequences of the pulling forces produced during contractile ring constriction in the dividing cell. As we have shown that pnut dividing cells, which produce lower pulling forces, can nevertheless induce cortex detachment in the neighbouring cell in 50% of the cases ($n = 20$ cells, Fig. 2e), and as we found that E-Cad decrease is sufficient to rescue MyoII accumulation under lower pulling forces (Fig. 3m,n), we sought to study theoretically how MyoII accumulation could result from an E-Cad depletion, again only using first principles. Theoretically, there could be two classes of origins for the MyoII accumulation:

- either it arises from a local recruitment of MyoII via a classical mechanotransduction

mechanism, for instance protein unfolding, as in the case of Vinc and α-cat, which leads to Actin binding and/or MyoII recruitment [74, 90, 84], or from a signalling role of the E-cad/catenin complex [91]

- either it arises from a convection mechanism, with actomyosin flowing from one region to the next.

As detailed in the main text, we have shown (Extended Data Fig. 7a-d) that MyoII accumulation in the neighbours is independent on the classical Vinculin mechano-transduction pathway, as Vinc was not necessary for the accumulation, and did not colocalise with MyoII near the base of the ingressing membrane (Extended Data Fig. 7e). Moreover, although E-Cad is known to generate intracellular signals for Rho GTPase signalling and cytoskeletal organization, we found that loss of function of Rho or Diaphanous (Dia) only had a minor influence on MyoII accumulation (Extended Data Fig. 7f-k). Furthermore, loss of function of Arp2/3 in the neighbouring cells did not significantly affect MyoII accumulation either (Extended Data Fig. 7l-n).

Therefore, we decided to explore the second hypothesis. In particular, given the robust relationship between E-Cad depletion and MyoII accumulation uncovered in the main text, we wished to examine whether local changes in the mechanical environment of the contractile actomyosin cortex (such as loss of linkage) could theoretically result in actomyosin flows and MyoII accumulation.

3.1 Description of the model

We thus start by writing a simple hydrodynamic theory for the actomyosin cortex, using the active gel theory, which has been shown to be adapted to describe actomyosin structures in many instances [88, 77, 78, 92, 93]. We aim to describe the condition for a stable uniform cortex, and the converse condition for actomyosin flows to occur. Indeed, in the past years, actomyosin flows have been reported in a variety of settings, and proposed to be linked to intrinsic properties of the actomyosin network, such as its contractility [88, 93, 95, 96]. Thus, we write down a one-dimensional theory for MyoII and Actin concentrations (resp. ρ and a) in the ingressing region. The conservation equation for the bound fraction of MyoII, considered as a solute in the Actin gel and of density ρ reads:

$$\partial_t \rho + \partial_x(\rho v) - D\partial_{xx}\rho = \frac{\rho_0 - \rho}{\tau_m} \tag{9}$$

where τ_m is the turnover time of MyoII and D an effective diffusion coefficient of MyoII relative to the Actin gel. Such a coefficient is needed to prevent infinite accumulation of actomyosin in an infinitely small region. The reference density of MyoII ρ_0 denotes the ratio of polymerisation over depolymerisation rates, assuming first order kinetics and v refers to the velocity of the Actin gel on which the MyoII motors attach. We thus model actomyosin as a viscous and contractile gel of length l. Force balance and constitutive equation at linear order of the actomyosin gel then read, respectively:

$$\partial_x \sigma = \xi v \tag{10}$$

$$\sigma = \chi \rho/\rho_0 + \eta \partial_x v \tag{11}$$

where σ is the stress in the gel, η its viscosity, χ the contractility arising from bound MyoII motors, ξ the friction coefficient between the actomyosin gel and its neighbours and/or the apical ECM. These equations must be complemented by two mechanical boundary conditions,

$v(0,t) = v(l,t) = 0$, since the actomyosin gel is clamped at both ends. We also specify two no-flux boundary conditions $\partial_x \rho(0,t) = \partial_x \rho(l,t) = 0$, i.e. no MyoII flux can enter into the system at the boundaries. The filamentous Actin concentration can be then directly deduced once the velocity v has been determined, through the conservation equation $\partial_t a + \partial_x(av) = R(a)$, R being a reactive term taking into account actin turnover. One should note that our two conservation laws for filamentous actin (resp. bound MyoII) assume implicitly that monomeric actin and unbound MyoII are in excess and diffuse rapidly in the cytoplasm on the timescale of turnover, a reasonable hypothesis as verified experimentally by FRAP in cultured cells [98, 99]. As detailed in the main text, we concentrate here on the distribution ρ of MyoII, since we are interested in particular in the MyoII accumulation.

In our model, we describe the coupling between the actin cytoskeleton and AJ, which is mediated by their interaction via the $\alpha-$catenin/E-Cad complex, as an effective friction coefficient [100, 101]. This friction coefficient ξ has been studied in various contexts, and theoretically is the sum of several different contributions, which can be hard to disentangle [102, 103]: coupling of the *adherens* junction to the apical extracellular matrix [104], protein friction linked to the engagement of homophilic adhesion molecules [100] or internal friction from cross-linkers in the gel itself [105, 106]. Importantly, we expect that lowering the linkage between the cortex and the membrane, in particular by decreasing E-Cad concentration, as described in Section 1, should lower this effective friction. Finally, these equations can be conveniently adimensionalised by rescaling all lengths by the hydrodynamical wavelength $L = \frac{\eta}{\xi}$, all times by $\eta/\xi D$ and all concentrations by ρ_0, as well as using the rescaled junction length $\alpha = l/L$, the rescaled contractility $\chi = \frac{\rho_0 \chi_0}{\xi D}$ and the rescaled turnover $\phi = \frac{\eta}{D\tau_m \xi}$.

3.2 Condition for a stable homogeneous cortex and parameter estimation

In the following paragraphs, we provide successively a qualitative argument and a quantitative criterion as a function of contractility and friction for the appearance of spontaneous MyoII accumulations. Because actomyosin is contractile, an homogeneous state can be spontaneously broken: a small accumulation of MyoII causes contractile flows, which constitute a self-reinforcing loop and can lead to the accumulation of actomyosin locally. Nevertheless, because of turnover, actomyosin is constantly added in the depleted region, and removed in the dense region, causing a steady state flow. It should be noted that this description is very similar to the one proposed for cell motility in Ref. [94, 97]. Starting from an initially uniform MyoII density and an infinitely large cortex, a linear stability analysis of the set of equations (9)-(11) predicts that a uniform cortex is only stable [88] if its contractility χ is smaller than a critical value χ_1^c defined as

$$\chi_1^c = \left(\sqrt{\frac{\eta}{\tau_m}} + \sqrt{D\xi} \right)^2 \tag{12}$$

Therefore, this threshold for the appearance of spontaneous actomyosin flows depends on the value of the friction coefficient ξ, i.e. on the attachment between the cortex and its surrounding through the plasma membrane. In the case of cell motility, authors have explored the idea [97] that a local upregulation of contractility χ allows the system to pass the threshold χ_1^c, therefore triggering ameboid motion. Here, we propose the converse idea that, at constant contractility, a change in the properties of the gel, such as friction ξ, is sufficient to trigger actomyosin flows. The advantage of such a model would be that it is self-triggered and self-maintained, without the need for an active signal triggering a contractility increase. In our model, the local elongation of the junction depletes E-Cad concentration at the ingressing AJ (Fig. 3a-d and Extended Data Fig. 5c), and this physical cue would be enough to trigger an actomyosin response, via flows, resulting from an intrinsic physical instability of the cor-

tex. This could be a complementary mode of mechano-sensing, relying on generic physical properties of the cytoskeleton rather than on a classical signalling cascade.

One model parameter that can be accessed experimentally in a straightforward manner is the turnover time of MyoII τ_m. Using photobleaching experiments of the MyoII accumulation in the neighbours, performed on MyoII::GFP clones facing MyoII::RFP dividing cells (Fig. 4d,e, Supplementary Video 8, see also Methods), we found $\tau_m = 22s \pm 2$ (average $\pm$ s.e.m, $n = 14$ cells), consistent with previous experimental values [82]. Moreover, using orders of magnitude from the literature [93, 107, 108, 109] ($\chi\rho_0 \approx 10^3 Pa, \eta \approx 10^4 Pa.s$ $\xi \approx 10^{16} Pa.m^2.s^{-1}$, $D \approx 10^{-13} m^2 s^{-1}$), we estimate that $\frac{\eta}{\tau} \approx 10^3 Pa$ and $D\xi \approx 10^3 Pa$, confirming quantitatively that friction plays an important role in setting the contractility threshold described above. Using these orders of magnitude yields for the non-dimensional ratios: $\chi \approx 1$, $\phi \approx 1$ and $\alpha \approx 10$, which are the values we keep in all the numerical integrations below. It is also worth noting that the actomyosin in the medial pool is known to be much more dynamic, displaying large scale flows, than the junctional actomyosin [96], which could be due to their differential attachment or to their differential turnover [110].

Therefore we propose that, at constant contractility and constant cortical properties, a decrease in friction, i.e. cortical attachment, due to E-Cad decrease in the ingressing AJ is sufficient to spontaneously generate actomyosin flows. From Eq. (12), friction has to decrease below a critical threshold $\xi_c = \frac{1}{D}\left(\sqrt{\chi - \frac{\eta}{\tau}}\right)^2$, in order for spontaneous flows to form. The characteristic speed in the friction-less ingressing AJ of length l is then $v_c \propto \frac{\chi\rho_0 l}{\eta}$ which, as expected, increases with contractility, as well as with the length of the ingressing AJ.

In the absence of friction, as studied by Turlier *et al.* [77] spontaneous flows occur if contractility is larger than a second, lower critical value χ_2^c defined as:

$$\chi > \chi_2^c = \frac{\eta}{\tau_m} \tag{13}$$

Interestingly, another parameter that can be extracted from experiments is the ratio of viscosity η over the active contractility χ, which dictates the characteristic time $\tau_r = \frac{\eta}{\chi}$ of junctional recovery upon laser ablation of a junction. Therefore, the criterion for flows to occurs from Eq. (13) can be rewritten as

$$\frac{\chi}{\chi_2^c} = \frac{\tau_m}{\tau_p} > 1 \tag{14}$$

Using laser ablation in pupae from 14 to 18 hAPF, we have previously shown that $\tau_p \approx 10s$ [111]. Therefore, we find a ratio $\tau_m/\tau_p \approx 2$, and the theory predicts that one should see actomyosin flows upon loss of friction, as we confirmed experimentally (Fig. 4d-g). The characteristic flow velocity can also be estimated as

$$v_c \propto \frac{l}{\tau_p} \approx 0.2 \mu m s^{-1}$$

which has the same order of magnitude as the experimentally measured (Fig. 4m) value of $v_{exp} = 0.1 \pm 0.04 \mu m s^{-1}$ (mean $\pm$ standard deviation).

Interestingly, as noted in the main text, although we observed sustained flows in the ingressing region, where E-Cad is low, the contribution of flows seems to be minimal in the lateral direction, i.e. coming from the remaining attached cortical actomyosin, in a region where E-Cad is high (Fig. 4d-g and Supplementary Videos 8,9). If the accumulation was mainly due to a local up-regulation of the contractility χ at the base of the ingressing region, we would predict equal flows from both regions, on the lengthscale of the hydrodynamic length $l_h = \sqrt{\frac{\eta}{\xi}}$.

The experimentally observed prevalence of flows along the ingressing region therefore reinforces the idea that E-Cad depletion is necessary to induce large-scale flows, and that friction along the AJ in the E-Cad high region is sufficiently large to strongly reduce flows along the lateral direction. Indeed, using the parameters described above yields a hydrodynamic length of $l_h \approx 1\mu m$, consistent with a large screening role for friction.

3.3 Localisation of the accumulation

Next, we explore how a local decrease in friction can dictate the position of an actomyosin accumulation, successively in one-dimensional and in two-dimensional models.

3.3.1 One-dimensional model

For an actomyosin gel of length l with spatially homogeneous properties, studied in the context of cell migration [94, 97], the accumulation arises with equal probability at both sides of the gel ($x = 0$ or $x = l$). To go further, and in particular explore the directionality of the flows in the case of non-uniform friction, we performed a full numerical integration of our one-dimensional model.

For the sake of simplicity, we start with the simplified case of an actomyosin gel of length l with uniformly high friction $\xi_h > \xi_c$ (for a normal cortex, we know that $\xi > \xi_c$ since we do not observe spontaneous flows), except in the centre of the gel, where friction is much lower than the threshold ($\xi_l \ll \xi_c$) on a length l_{hole}, on a domain $x \in [l/2 - l_{hole}, l/2 + l_{hole}]$. We used the same boundary conditions as described above. We performed a parameter sweep, varying the central lower friction ($\xi_l = \xi_h/2, \xi_h/5, \xi_h/10, 0$), as well as the contractility χ and the size of the low-friction domain. For each value of the parameter set, we performed 100 parallel numerical integrations, starting from different random initial conditions, and performed statistics on the resulting actomyosin profile. This is important, as previous work has shown that this system of equations has a large amount of metastable, long-lived states [88]. In all the conditions examined, provided that $l < \lambda_c = 2\pi(\eta D\tau/\xi_l)^{1/4}$, actomyosin accumulations formed at the boundaries between low and high friction (Extended Data Fig. 8a for $\xi_l = 0, \chi = 1.3\chi_c$). This analysis, in a simplified geometry, suggests that an actomyosin accumulation can be guided and localised by spatial modulation of friction, with the accumulation occurring at the interfaces between low and high frictions.

Next, we wished to examine the more complex, but more biologically realistic case, of the localisation of actomyosin due to the juxtaposition of a low friction region ($x \in [0, l/2]$) and high friction region ($x \in [l/2, l]$). Although this case might superficially look similar to the previous one, it actually bears crucial differences, as this configuration allows for an alternative actomyosin localisation at $x = 0$, i.e. at the boundary of the gel in the low friction region. To come back to the *in vivo* situation, this corresponds to the possibility of actomyosin accumulating at the tip of the ingressing region versus accumulating at the base of the ingressing region, at the high/low E-Cad boundary. Indeed, in that case, performing the same parameter sweep as before on ξ and χ, we find (Extended Data Fig. 8b,c for $\xi_l = 0, \chi = 1.3\chi_c$) that the accumulation can take place with nearly equal probability at the boundary between high and low friction ($x = l/2$), or at the boundary of the gel ($x = 0$). Nevertheless, as these two solutions have similar stabilities, even a very small imperfection or tilt would be enough to robustly localise actomyosin at the base of the ingressing region, as observed experimentally.

Therefore, in the next paragraphs, we explore three possibilities, based on our experimental observations, which can robustly guide the actomyosin accumulation at the base of the ingressing region: the role of the detached cortex, the role of the temporal increase in the length of the ingressing region, and the two-dimensional geometry of the ingressing region.

Firstly, the presence of a cortex at the base of the junction can theoretically serve as a guiding cue for actomyosin accumulation, although we have seen in the main text (Fig. 2e-g) that this cannot be the exclusive determinant. This can be seen qualitatively by considering the fact that actomyosin flows towards denser (i.e. more contractile) regions, so that a dense cortex can serve as a strong cue. To demonstrate this, we performed the same numerical integration as above (Extended Data Fig. 8d), assuming that the steady state value ρ_0 of MyoII (and Actin) from turnover is 10% larger in the cortex (high friction region) than in the ingressing domain (low friction region), and saw that this was enough to robustly localise the accumulation at the high/low friction boundary (100 $\%$ of the time in $n = 100$ numerical integrations, starting from different random initial conditions).

Secondly, taking into account the slow advancement of the ingressing region localises the actomyosin accumulation at the base of the ingressing AJ (at the high/low friction boundary). To take this into account in our system of equations, we now make the length of the domain $l(t)$ explicitly dependent on time. We take $l(t) = l_0(1 + r't)$ linearly increasing in time, as the data from the main text suggest, with

$$r' \approx 2.10^{-3} s^{-1}$$

We must modify the clamped boundary condition to take into account that we now have an expanding domain ($x \in [l_0 - l(t), l_0]$), with $v(l_0 - l(t)) = -l'(t)$ replacing $v(0) = 0$ (see Ref.[94] for details on moving boundary conditions in this system). Qualitatively, this depletes actomyosin at the front of expansion, biasing accumulation at the base of the ingressing region. If friction was low everywhere, the accumulation would travel to the trailing front, but the high friction zone blocks such flows, causing the accumulation to localise at the low/high friction interface. Quantitatively, we integrated our system of equations with these new boundary conditions, and again could see a robust localisation of actomyosin at the high/low friction interface in all cases considered ($\xi_l = 0.01\xi_h, \chi = 2\chi_c$, 100 $\%$ of the time in $n = 100$ numerical integrations, starting from different random initial conditions, see Extended Data Fig. 8e for the steady-state MyoII concentration profile).

3.3.2 Two-dimensional numerical integrations for the ingressing region

The simple one-dimensional model has helped us establish that a local decrease in friction can both trigger and guide actomyosin flows. Nevertheless, the geometry of the ingressing region *in vivo* is two dimensional in nature, and could also participate in guiding the accumulation.

Therefore, as a third possibility, we sought to perform a more realistic two dimensional integration of our set of active gel equations, taking into account the geometric parameters of the ingressing region, in order to make more refined predictions on the localisation of the actomyosin accumulation. In particular, we wished to examine whether simulations can robustly reproduce the presence of the accumulation at the base of the ingressing AJ. This would resonate with *in vitro* experiments, which have suggested that the geometrical architecture of the cortex can determine MyoII activity and resulting steady-state configuration [112].

Position of the problem

To simplify the analysis, we adopt a quasi-static approach, where the geometry of the ingressing region is fixed in time, and investigate the steady-state configuration for different amounts of ingression. As we saw earlier in the one-dimensional model, the AJ advancement helps to localise the accumulation at the base of the ingressing AJ. However, we wish here to examine whether this feature can arise from simpler geometrical considerations. We

parametrise the ingressing region by the height function $h(x) = w_0 + h_0 exp(-x^4/d_0^4)$, h_0 being the maximal length of the ingressing region, d_0 its characteristic width, and w_0 the typical thickness of the cortex.

In order to solve our system of equation, we use a classical finite element method (with the Freefem++ software). We consider a two-dimensional domain, defining as before l the rescaled initial junction length:

$$\Omega = \{(x,y) \in \mathbb{R}^2 : \{y \in [0,h(x)], x \in [l/2, l/2]\}\}$$

on which we solve the non-dimensional conservation equation and force balance

$$\left.\begin{aligned} \partial_t \rho &= -\alpha^{-1}\partial_x(\rho \mathbf{v}) + \alpha^{-2}\Delta\rho - \phi(\rho - 1) \\ 0 &= \chi\alpha^{-1}\nabla\rho + \alpha^{-2}(\Delta\mathbf{v} + \nabla(\nabla.\mathbf{v})) \end{aligned}\right\} \text{in } \Omega$$

as well as the clamped and no normal (along vector **n**) flux boundary conditions.

$$\left.\begin{aligned} \mathbf{v}.\mathbf{n} &= 0 \\ \partial\rho/\partial n &= 0 \end{aligned}\right\} \text{on } \partial\Omega$$

Additionally, friction now enters as a surface, rather than bulk force, therefore setting a boundary condition for the tangential stress:

$$(\sigma.\mathbf{n}).\mathbf{t} = \xi \mathbf{v}.\mathbf{t} \text{ on } \partial\Omega$$

with σ the stress tensor and **t** the vector tangential to Γ. To guaranty the stability of the numerical scheme, we use a very small time step compared to the turnover time $dt \ll 1$ (in practise, we used $dt = 10^{-3}$), and an adaptive meshing, to concentrate more accurately on the sharp variations of ρ (Fig. 4a and Extended Data Fig. 8f for typical initial mesh). Finally, we monitor the second moment of the density distribution ρ in time, to make sure the profiles we report are at steady state. One should note that we assume the bulk viscosity η_b and shear viscosity η_s to be equal.

Finally, we need to define an non-homogenous friction force at the boundary at the tissue. We defined three boundaries: Γ_m the interface with the medial pool ($y = 0$), $\Gamma_0 = \{(x,y) \in \mathbb{R}^2 : \{y = h(x), x \in [-2d_0, 2d_0]\}\}$ the interface with the dividing cell with low friction (lining the ingressing AJ) and Γ_d the rest of the interface with the dividing cell, together with the left and right borders. Therefore $\Gamma = \partial\Omega = \Gamma_m \cup \Gamma_0 \cup \Gamma_d$ and $\Gamma_m \cap \Gamma_0 \cap \Gamma_d = \emptyset$. We thus consider a very high friction $\xi \to \infty$ on Γ_d (i.e. no slip boundary condition at the E-Cad-rich AJ (Fig. 4a and Extended Data Fig. 8f), whereas the friction Γ_0 is low $\xi = \xi_{low}$ on Γ_d (ingressing region).

Moreover, as our aim is to model only the cortical region close to the membrane, we assume that the turnover kinetics of MyoII (and all other coefficients apart from friction) are uniform in space and time. Clearly, this is an approximation, as the presence of a detached cortex could imply enhanced polymerisation at the base of the ingressing region. As discussed in the one-dimensional model (subsection 3.3.1), this would further enhance the localisation of actomyosin at the base of the ingressing AJ. Nevertheless, in order to verify that actomyosin accumulation can form at the correct location without the need for such cues, we neglect it.

This two-dimensional approach leaves open the question of the exact nature and contribution of the medial pool: indeed, taking it into account would require adding parameters for its turnover, viscosity, diffusion etc, which would increase significantly the parameter space of the problem, without giving rise to qualitatively different physics. As this is largely out of the scope of this study, and we have experimentally shown that the medial pool did not contribute significantly to the MyoII accumulation (Fig. 4d-g and Supplementary Videos 8,9), we restrict the integration domain to a small domain of width w_0 below the AJ, in order to consider only

the vicinity of the cortical region. We consider that the cortex is in frictional contact with the medial pool, although we expect the friction to be lower than the one at the AJ. We then performed simulations for various values of both ξ_{low} on Γ_0 and ξ_0 on Γ_m, and saw that they only had a very weak effect on the results. In the data shown in Extended Data Fig. 8f-m, we use $\xi_{low} = \xi_0 = 0.1$.

Finally, in order to analyse whether our findings are general, we use two different boundary conditions at the interface with the medial pool ($y = 0$): either the no-flux (Neumann) boundary condition described above $\partial_y \rho(x,0,t) = 0$, or a Dirichlet boundary condition $\rho(x,0,t) = \rho_0$, which could arise from an intrinsic regulation of actomyosin density at the interface with the medial pool. We also use again the non-dimensional ratios $\phi = 1$ and $\alpha = 10$, and the non-dimensional geometric factors $d_0 = 2w_0 = 1$, and $h_0 \in [0, 2.5]$.

Simulation results

First, we verify, for the sake of consistency, that if contractility χ is lower than the threshold $\chi_2^c = \eta/\tau$, (i.e. the flow threshold in the regions of zero friction), an homogeneous distribution of actomyosin is observed. Similarly, as an important control of the consistency of our numerical simulation, we tested that if friction is uniformly high everywhere, no accumulation takes place even for $\chi > \chi_2^c$ (provided of course contractility is below the global instability threshold with friction χ_1^c).

Next, we performed two-dimensional numerical simulations where we considered a non-uniform friction on the domains Ω_p and Ω_m. Starting from random initial conditions, we found a consistent MyoII accumulation at the base of the ingressing region (Fig. 4b and Extended Data Fig. 8g), mirroring the experimental data. As expected from the analytical expression above, we found that above a contractility χ_2^c, actomyosin flows formed and after a transient phase, created a gradient of MyoII concentration from the top to the base of the ingressing region. We did find some transient phases of actomyosin accumulation at the tips for some initial conditions, but these were unstable, with the steady-state accumulation re-localizing at the base of the ingressing region. The vast majority of the MyoII feeding the accumulation came from the ingressing region, not from the neighbouring cortex, as shown by the fact that the horizontal velocity (Fig.4c and Extended Data Fig. 8h,i) v_x, in the direction of the cortex, was an order of magnitude smaller than the vertical velocity (Extended Data Fig. 8h,i) v_y, in the direction of the ingressing region. This is because of the high friction, which prevents flows along the attached cortex from being long-ranged. Extended Data Fig. 8g-k shows results for the boundary condition $\rho(x,0,t) = \rho_0$, while Extended Data Fig. 8l-m shows results for the boundary condition $\partial_y \rho(x,0,t) = 0$.

Moreover, the concentration in the accumulation, as well as the magnitude of the flows, increased with the length of the ingressing region, at constant contractility (we show in Extended Data Fig. 8j respectively $h_0 = 0.75$, $h_0 = 1.25$, $h_0 = 2$ and $h_0 = 2.5$). In particular, the accumulation does not occur until a minimum length of the protrusion, dependent on the value of contractility, is reached.

Similarly, the concentration in the accumulation, as well as the magnitude of the flows, increased with contractility (we show in Extended Data Fig. 8k respectively $\chi = 0.9\chi^c$, $\chi = 1.1\chi^c$, $\chi = 1.7\chi^c$ and $\chi = 2.6\chi^c$), thereby confirming our previous conclusions from the one-dimensional simple criteria derived above. Fig. 4a-c and Extended Data Fig. 8f-i,k-m shows results of simulations taking a length of ingressing region of $h_0 = 2$ and $\chi = 2\chi_c$. We confirmed experimentally this prediction by showing that loss of *rok* in the neighbouring cells (Fig. 4h-i, l,m and Extended Data Fig.5d,e) drastically reduced Actin flow velocity in the ingressing membrane and MyoII accumulation at the base. On the other hand, based on our theory, we would not expect a major contribution of Actin polymerisation to the MyoII accumulation (as stated

above, Actin serves as a substrate transporting MyoII, although it could have a secondary feedback effect on the value of contractility). As mentioned in the subsection above, we found that loss of Arp2/3 activity (Extended Data Fig. 7l-n) did not affect Myo accumulation, while loss of Dia activity only delays MyoII accumulation, and correlatively it only slightly decreases flow velocity (Fig. 4j-m and Extended Data Fig. 7i,j).

For the Neumann boundary conditions, the results are qualitatively unchanged, although the peak of the accumulation forms at the boundary $y = 0$ (Extended Data Fig. 8l for $\chi = 1.2\chi^c$, $h_0 = 2$). On the other hand, if we assume that friction is low everywhere, for the same values of contractility and ingressing region height, MyoII can still accumulate via the formation of spontaneous flows, but the localisation of the accumulation becomes non-stereotypic, with several solutions coexisting for a given parameter set (example plotted on Extended Data Fig. 8m for $\chi = 1.2\chi^c$, $h_0 = 2$ with Neumann boundary conditions).

Therefore, our modelling of the actomyosin cortex as an active contractile gel is consistent with the idea that a local modification in its physical properties can, in the absence of any specific cue in contractility, create spontaneous actomyosin flows. In this Supplementary Note, we have explored the possibility that a local decrease in friction, due to the decrease in concentration of linker proteins such as E-Cad, both triggers and guides self-maintained actomyosin flows. We show quantitatively that, in the absence of friction, the condition for flows to arise is fulfilled *in vivo*, and predict the correct order of magnitude for the velocity of such actomyosin flows. These actomyosin flows transmit the proliferative forces from the dividing cell to its neighbours, and could serve as a previously unreported mode of mechano-sensing during cytokinesis.

References

[72] Tabdanov, E., Borghi, N., Brochard-Wyart, F., Dufour, S., and Thiery, J. P. (2009). Role of E-Cad in membrane-cortex interaction probed by nanotube extrusion. Biophys. J, 96(6), 2457-2465.

[73] Borghi, N., Sorokina, M., Shcherbakova, O. G., Weis, W. I., Pruitt, B. L., Nelson, W. J., and Dunn, A. R. (2012). E-Cad is under constitutive actomyosin-generated tension that is increased at cell-cell contacts upon externally applied stretch. Proc. Nat. Acad. Sci, 109(31), 12568-12573.

[74] Hoffman, B.D. and Yap, A.S. (2015). Towards a Dynamic Understanding of E-Cad-Based Mechanobiology. Trends Cell Biol, 25(12), 803-814.

[75] Martin, A. C., Gelbart, M., Fernandez-Gonzalez, R., Kaschube, M., and Wieschaus, E. F. (2010). Integration of contractile forces during tissue invagination. J. Cell Biol, 188(5), 735-749.

[76] Kruse, K., Joanny, J. F., Julicher, F., Prost, J., and Sekimoto, K. (2005). Generic theory of active polar gels: a paradigm for cytoskeletal dynamics. Euro Phys J E, 16(1), 5-16.

[77] Turlier, H., Audoly, B., Prost, J., and Joanny, J. F. (2014). Furrow constriction in animal cell cytokinesis. Biophys. J, 106(1), 114-123.

[78] Prost, J., Julicher, F., and Joanny, J. F. (2015). Active gel physics. Nat. Phys., 11(2), 111-117.

[79] Mangeat, P., Roy, C., and Martin, M. (1999). ERM proteins in cell adhesion and membrane dynamics. Trends Cell Biol, 9(5), 187-192.

[80] Brochard-Wyart F., De Gennes P.G (2003) Unbinding of adhesive vesicles. C.R. Phys. 4: 281-287.

[81] Chu, Y. S., Thomas, W. A., Eder, O., Pincet, F., Perez, E., Thiery, J. P., and Dufour, S. (2004). Force measurements in E-Cad mediated cell doublets reveal rapid adhesion strengthened by Actin cytoskeleton remodeling through Rac and Cdc42. J. Cell Biol, 167(6), 1183-1194.

[82] Salbreux, G., Charras, G., and Paluch, E. (2012). Actin cortex mechanics and cellular morphogenesis. Trends Cell Biol, 22(10), 536-545.

[83] Grusche, F. A., Hidalgo, C., Fletcher, G., Sung, H. H., Sahai, E., and Thompson, B. J. (2009). Sds22, a PP1 phosphatase regulatory subunit, regulates epithelial cell polarity and shape. BMC Dev Biol, 9(1), 1.

[84] Yamada, S., Pokutta, S., Drees, F., Weis, W. I., and Nelson, W. J. (2005). Deconstructing the E-Cad-catenin-Actin complex. Cell, 123(5), 889-901.

[85] Cavey, M., Rauzi, M., Lenne, P. F., and Lecuit, T. (2008). A two-tiered mechanism for stabilization and immobilization of E-Cad. Nature, 453(7196), 751-756.

[86] de Beco, S., *et al.* (2009). Endocytosis is required for E-Cad redistribution at mature *adherens* junctions." Proc. Nat. Acad. Sci. 106.17 (2009): 7010-7015.

[87] de Beco, S., Perney, J. B., Coscoy, S., and Amblard, F. (2015). Mechanosensitive adaptation of E-Cad turnover across *adherens* junctions. PloS one, 10(6), e0128281.

[88] Hannezo, E., Dong, B., Recho, P., Joanny, J. F., and Hayashi, S. (2015). Cortical instability drives periodic supracellular Actin pattern formation in epithelial tubes. Proc. Nat. Acad. Sci., 112(28), 8620-8625.

[89] Engl, W., Arasi, B., Yap, L. L., Thiery, J. P., and Viasnoff, V. (2014). Actin dynamics modulate mechanosensitive immobilization of E-Cad at *adherens* junctions. Nat Cell Biol, 16(6), 584-591.

[90] Yao, M., Qiu, W., Liu, R., Efremov, A. K., Cong, P., Seddiki, R., ... and Yan, J. (2014). Force-dependent conformational switch of α-catenin controls vinculin binding. Nat Comm, 5.

[91] Drees, F., Pokutta, S., Yamada, S., Nelson, W. J., and Weis, W. I. (2005). α-catenin is a molecular switch that binds E-cadherin-α-catenin and regulates actin-filament assembly. Cell, 123(5), 903-915.

[92] Thoresen, T., Lenz, M., and Gardel, M. L. (2013). Thick filament length and isoform composition determine self-organized contractile units in actoMyoII bundles. Biophys. J., 104(3), 655-665.

[93] Mayer, M., Depken, M., Bois, J. S., Julicher, F., and Grill, S. W. (2010). Anisotropies in cortical tension reveal the physical basis of polarizing cortical flows. Nature, 467(7315), 617-621.

[94] Recho, P., Putelat, T., and Truskinovsky, L. (2013). Contraction-driven cell motility. Phys. Rev. Lett., 111(10), 108102.

[95] Wedlich-Soldner, R., Altschuler, S., Wu, L., and Li, R. (2003). Spontaneous cell polarization through actoMyoII-based delivery of the Cdc42 GTPase. Science, 299(5610), 1231-1235.

[96] Munjal, A., Philippe, J. M., Munro, E., and Lecuit, T. (2015). A self-organized biomechanical network drives shape changes during tissue morphogenesis. Nature, 524(7565), 351-355.

[97] Ruprecht, V. *et al.* (2015). Cortical contractility triggers a stochastic switch to fast amoeboid cell motility. Cell, 160(4), 673-685.

[98] Fritzsche, M., Lewalle, A., Duke, T., Kruse, K., and Charras, G. (2013). Analysis of turnover dynamics of the submembranous actin cortex. Mol Biol Cell, 24(6), 757-767.

[99] Uehara, R., Goshima, G., Mabuchi, I., Vale, R. D., Spudich, J. A., and Griffis, E. R. (2010). Determinants of myosin II cortical localization during cytokinesis. Curr. Biol, 20(12), 1080-1085.

[100] Tawada, K., and Sekimoto, K. (1991). Protein friction exerted by motor enzymes through a weak-binding interaction. J Theor. Biol., 150(2), 193-200.

[101] Bormuth, V., Varga, V., Howard, J., and Schffer, E. (2009). Protein friction limits diffusive and directed movements of kinesin motors on microtubules. Science, 325(5942), 870-873.

[102] Bergert, M., Erzberger, A., Desai, R. A., Aspalter, I. M., Oates, A. C., Charras, G., ... and Paluch, E. K. (2015). Force transmission during adhesion-independent migration. Nat Cell Biol.

[103] Dierkes, K., Sumi, A., Solon, J., and Salbreux, G. (2014). Spontaneous oscillations of elastic contractile materials with turnover. Phys Rev Lett, 113(14), 148102.

[104] Bokel, C., Prokop, A., and Brown, N. H. (2005). Papillote and Piopio: Drosophila ZP-domain proteins required for cell adhesion to the apical extracellular matrix and microtubule organization. J. Cell Sci., 118(3), 633-642.

[105] Shapiro, L., Fannon, A. M., Kwong, P. D., Thompson, A., Lehmann, M. S., Grubel, G., ... and Hendrickson, W. A. (1995). Structural basis of cell-cell adhesion by cadherins. Nature, 374(6520), 327-337.

[106] Salbreux, Guillaume. "Modélisation des instabilités du cortex d'Actine." PhD diss., Université Pierre et Marie Curie-Paris VI, 2008.

[107] Hawkins, R. J., Poincloux, R., Bénichou, O., Piel, M., Chavrier, P., and Voituriez, R. (2011). Spontaneous contractility-mediated cortical flow generates cell migration in three-dimensional environments. Biophys. J., 101(5), 1041-1045.

[108] Marcy, Y., Prost, J., Carlier, M. F., and Sykes, C. (2004). Forces generated during Actin-based propulsion: a direct measurement by micromanipulation. Proc. Nat. Acad. Sci., 101(16), 5992-5997.

[109] Pierobon, P., Achouri, S., Courty, S., Dunn, A.R., Spudich, J.A., Dahan, M. and Cappello, G., (2009). Velocity, processivity, and individual steps of single MyoII V molecules in live cells. Biophys. J., 96(10), 4268-4275.

[110] Jodoin, J.N., Coravos, J.S., Chanet, S., Vasquez, C.G., Tworoger, M., Kingston, E.R., Perkins, L.A., Perrimon, N. and Martin, A.C., (2015). Stable Force Balance between Epithelial Cells Arises from F-Actin Turnover. Dev Cell, 35(6), 685-697.

[111] Bonnet, I., Marcq, P., Bosveld, F., Fetler, L., Bellaiche, Y., and Graner, F. (2012). Mechanical state, material properties and continuous description of an epithelial tissue. J. R. Soc. Interface, 9(75), 2614-2623.

[112] Reymann, A.C., Boujemaa-Paterski, R., Martiel, J.L., Guérin, C., Cao, W., Chin, H.F., Enrique, M., Théry, M. and Blanchoin, L., (2012). Actin network architecture can determine MyoII motor activity. Science, 336(6086), 1310-1314.

Studying cytokinesis in *Drosophila* epithelial tissues

D. Pinheiro[*,§,¶], **Y. Bellaïche**[*,§,1]

[*]*Institut Curie, PSL Research University, Paris, France*

[§]*Sorbonne Universités, Paris, France*

[¶]*Abel Salazar Biomedical Sciences Institute, University of Porto, Porto, Portugal*

[1]*Corresponding author: E-mail: yohanns.bellaiche@curie.fr*

CHAPTER OUTLINE

Abstract

Epithelial tissue cohesiveness is ensured through cell–cell junctions that maintain both adhesion and mechanical coupling between neighboring cells. During development, epithelial tissues undergo intensive cell proliferation. Cell division, and particularly cytokinesis, is coupled to the formation of new adhesive contacts, thereby preserving tissue integrity and propagating cell polarity. Remarkably, the geometry of the new interfaces is determined by the combined action of the dividing cell and its neighbors. To

Methods in Cell Biology, Volume 137, ISSN 0091-679X, http://dx.doi.org/10.1016/bs.mcb.2016.04.013

further understand the interplay between the dividing cell and its neighbors, as well as the role of cell division for tissue morphogenesis, it is important to analyze cytokinesis in vivo. Here we present methods to perform live imaging of cell division in *Drosophila* epithelial tissues and discuss some aspects of image processing and analysis.

INTRODUCTION

Epithelial tissues have as main function to physically separate body compartments, thereby allowing the coexistence of distinct biochemical and mechanical microenvironments. Epithelial architecture is dictated by the assembly of specialized junctions along the apical−basal axis of cells, namely the tight junctions (TJ) and the *adherens* junctions (AJ). In flies, however, the septate junctions are the functional equivalent to the TJs and are localized basally regarding the AJs. Such adhesive complexes are connected to the underlying actin−myosin cytoskeleton, to ensure not only tissue cohesiveness, but also mechanical coupling between neighboring cells (Brieher & Yap, 2013). During development, epithelial tissues, both in vertebrates and invertebrates, undergo intensive cell proliferation, cell−cell rearrangements, cell shape changes, cell delamination events and, even, large tissue-scale elongation, invagination and folding (for review see Heisenberg & Bellaïche, 2013; Munjal & Lecuit, 2014). Thus, it is critical to understand how epithelia can act as a barrier, yet exhibit such plasticity.

In this chapter, we will focus on how to study cytokinesis in vivo by combining fly genetics and advanced microscopy techniques. Cell division involves profound cell shape changes, particularly during cytokinesis, the process whereby the dividing cell cytoplasm is partitioned into the future daughter cells. Cytokinesis involves the formation and constriction of an actin−myosin ring at the cell equator. As constriction proceeds, the connection between the future daughters is progressively closed, until abscission individualizes the two cells (for review see Green, Paluch, & Oegema, 2012). Recent work, in both vertebrates and invertebrates, showed how epithelial cytokinesis is coupled to the formation of new adhesive contacts (Firmino, Rocancourt, Saadaoui, Moreau, & Gros, 2016; Founounou, Loyer, & Le Borgne, 2013; Guillot & Lecuit, 2013; Herszterg, Leibfried, Bosveld, Martin, & Bellaïche, 2013; Morais-de-Sá & Sunkel, 2013). Such mechanism should allow the maintenance of polarity and adhesion during tissue proliferation, an essential aspect of epithelia integrity. In the *Drosophila* pupal notum and pupal wing, it was shown that the cells neighboring the dividing cell participate in setting the length of the newly formed contact, supporting that, in a tissue, division is a multicellular process. Altogether studying cell division in vivo is likely to be a rather critical step towards a better understanding of the mechanisms regulating epithelial dynamics, as well as tissue cohesiveness.

1. METHODS AND EXPERIMENTAL SETUP

In this section, we will provide a detailed protocol to image cytokinesis during morphogenesis of *Drosophila* pupal epithelial tissues, namely the dorsal thorax (notum) and

the pupal wing, which have been extensively used to decipher the mechanisms of epithelial polarity and dynamics (Bardet et al., 2013; Bosveld et al., 2012; Etournay et al., 2015; Georgiou, Marinari, Burden, & Baum, 2008; Guirao et al., 2015; Herszterg et al., 2013; Langevin et al., 2005; Leibfried, Fricke, Morgan, Bogdan, & Bellaiche, 2008; Levayer, Dupont, Levayer, Dupont, & Moreno, 2016; Marinari et al., 2012). For that, we show as an example a time-lapse movie of a pupa expressing E-Cadherin tagged with GFP (E-Cad::GFP (Huang, Zhou, Dong, Watson, & Hong, 2009)), which labels the AJs and MyoII fused with mChFP (MyoII::mChFP (Martin, Kaschube, & Wieschaus, 2009)), which labels the contractile ring (Fig. 1B).

1.1 MOUNTING THE *DROSOPHILA* PUPAE FOR TIME-LAPSE IMAGING OF EPITHELIAL TISSUES

To optimize the imaging session, pupae can be timed; the pupal notum displays two peaks of cell proliferation at 15−18 hours after puparium formation (hAPF) and at 21−24hAPF, while the pupal wing displays a single peak of cell divisions around 18hAPF (Etournay et al., 2015; Guirao et al., 2015). Therefore, white pupae should be collected at puparium formation and kept in petri dishes, lined with moist paper, until mounting. Alternatively, pupae can be collected later and the timing can then be set by head eversion.

The material required for the mounting is detailed below:

1. 25 × 75 × 1.0 mm slides;
2. 18 × 18 mm cover slips;
3. 24 × 40 mm cover slips;
4. double-sided tape—Scotch 3M;
5. glass pasteur pipettes 150 mm;
6. Voltalef oil 10S (VWR Prolabo);
7. quick-dry nail polish;
8. Kleenex paper towel; and
9. a set of forceps (Dumont #5—fine forceps).

In Fig. 1A,A' we provide a schematic representation of the mounting chamber (top and side views).

1. Carefully dry the pupae in a paper towel with a brush, to ensure that it will adhere to the double-sided tape.
2. Glue the ventral side of the pupae to the slide. To avoid hurting the pupae, you can easily hold it by the spiracles.
3. Using the forceps carefully pull the spiracles to detach the operculum.
4. Insert the forceps (alternatively you can use fine scissors) through the opercula opening, parallel to the pupae and tear the pupal case from head to abdomen.
5. Gently pull the pupal case at each side of the incision and glue it on the slide.
6. Glue a stripe of wet paper on the slide to maintain humidity in the mounting chamber.

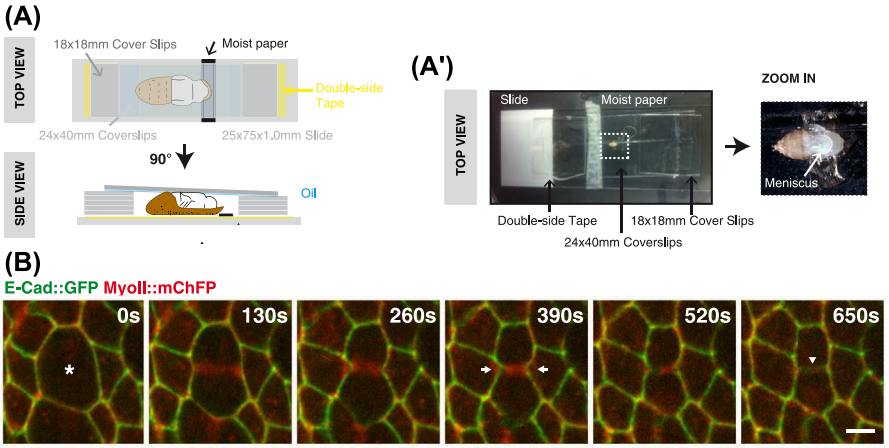

FIGURE 1 A simple method to perform live imaging of the *Drosophila* pupal notum.

(A,A') Schematic representation of the mounting chamber (side and top views) and an example of a pupal notum prepared for live imaging (top view). (B) Apical view of a dividing cell (*asterisk*) and its neighbors expressing E-Cad::GFP and MyoII::mChFP. *Arrows*: MyoII accumulation in the neighboring cells at the edges of the furrow. *Arrowhead*: new *adherens* junction formation between the daughter cells. Scale bar: 5 μm (B).

7. Carefully place a coverslip previously coated with a thin layer of oil on top of the pillars at each side of the pupae. Stabilize the coverslip with nail polish and make sure a meniscus is formed between the pupal notum and the coverslip. Avoid pressing too hard with the coverslip.

The protocol to image the *Drosophila* pupal wing is very similar with a key difference regarding the positioning of the pupae on the slide—which should be placed laterally, rather than ventrally, so that the pupal wing will be facing the coverslip.

1.2 IMAGE ACQUISITION

Samples can be imaged with a confocal spinning disk microscope (CSU-X1, Yokogawa spinning disc head mounted on an inverted microscope and piloted by Metamorph, Roper Scientific) using either a 60× or an 100× objective. To image at 100×, a confocal spinning disk wide is a great alternative, as the field of imaging is 4× larger than the classical confocal spinning disk microscopes, allowing you to record more events of cell division in a single time-lapse. A laser-scanning confocal microscope can also be used; however, in our experience, photobleaching is higher. The microscope should be enclosed in a temperature box, which can be stably tuned at 25°C or 29°C, depending on the experiment's requirements; in this example, we set the microscope at 25°C (Fig. 1B).

High sensitivity cameras are crucial for live imaging experiments, in order to increase the signal-to-noise ratio and allow long-term imaging with reduced

photobleaching. In the lab, we use either a CoolSNAP HQ2 (Photometrics) or a CMOS (Hamamtsu) camera. Alternatively, an EMCCD camera can be used to further increase sensitivity; however, the pixel size is bigger when compared to the CMOS camera (0.13 × 0.13 μm vs 0.065 × 0.065 μm, at 100×, Binning 1 × 1). The time of exposure and the laser power should be optimized to avoid saturation, this is especially important when you wish to perform intensity quantifications; in this case, we used 20% laser power, for both 491 and 561 nm lasers (confocal spinning disk microscope—raw laser power at 491 nm is 50 mW and 100 mW at 561 nm), and 200 ms of exposure (Fig. 1B).

Since the pupae epithelium can move, it is preferable to acquire a z-stack (with a step size of 0.2−0.5 μm) along the apical−basal axis of the tissue at each time point. Depending on the size of the stack acquired, the time resolution can increase up to 1 frame/5 s. For example, to image contractile ring constriction, which takes on average 320 s in the pupal notum, we set a 20-s interval sampling frequency to acquire a 7−8 μm z-stack (0.5 μm step). To image cell division at the tissue scale, time resolution drops to 1−5 min/stack, depending on how many positions are acquired. To generate such movies we use the autofocus option of the Metamorph software, to avoid drift along the z-axis.

1.3 LASER ABLATION AND PHOTOBLEACHING

To probe the contractile ring pulling forces, for example, it is possible to couple live imaging with laser ablation experiments. For that, we use a laser-scanning confocal microscope (LSM710 NLO, Carl Zeiss) equipped with the Ti:Sapphire laser (Mai Tai DeepSee, Spectra Physics) at 800 nm with <100 fs pulses with a 80 MHz repetition rate, typically set at 20−25% power. Following laser ablation, confocal images or a confocal stack can be acquired (see Herszterg et al., 2013 for an example). Upon laser ablation of the contractile ring, the measured recoil velocity is indicative of both the ring tension and the pulling forces generated by the contractile ring (Mayer et al., 2010). It can be useful to perform such experiments in different mutant conditions to understand how a certain gene affects force production within the contractile ring (assuming similar friction in *wild-type* and mutant conditions).

To analyze the dynamics of a protein of interest, for example, MyoII within the contractile ring, we can perform FRAP experiments (fluorescence recovery after photobleaching). For that, we use a confocal spinning disk equipped with a FRAP module (iLas^2 system). The number of iterations and the laser power used to photobleach a region of a given size has to be optimized; for the example mentioned above, we used the 491 nm laser, 100% laser power, with 40−50 iterations. Importantly, the size of the bleached region should be carefully considered and kept constant for all experiments (for further details see Fritzsche & Charras, 2015). Following photobleaching, a time-lapse movie can be acquired. Photoconversion and photoactivation experiments are also possible in the described setup and can be very instructive and complementary to the photobleaching experiments described above.

2. DATA PROCESSING AND ANALYSIS

In this section, we provide an overview of methods suitable to project and analyze time-lapse movies in Fiji (http://fiji.sc/), focused in the context of cytokinesis. To open the time-lapses, we use the Bio-Formats importer (File > Import > Bio-Formats), which is suitable for many life sciences file formats. Furthermore, it extracts basic metadata (such as spatial calibration), if they are available in the file.

2.1 PROJECTING CONFOCAL Z-STACKS

As mentioned above, the pupae epithelium can move along the z-axis during the acquisition of the time-lapse, therefore the first challenge when analyzing this type of data is the z-stack projection. Rather than projecting the entire stack, which greatly increases out-of-focus fluorescence, the projection should be restricted to the relevant stack positions, which will probably change over time; in this example, we restricted the projection to the level of the AJs (top view) (Fig. 1B). For that, we generated a set of custom-made macros for Fiji (available upon request). After running the macro, you should manually select, by a single click, the z position of interest at each frame; in this case, it corresponds to the maximum E-Cad::GFP intensity (Fig. 1B). The macro automatically registers the coordinates in a results table, which is then used as an input for the extraction of the z positions throughout the time-lapse. As a single z may not be sufficient to fully visualize the structure of interest—AJs span 1.5–2 μms, which corresponds to 3–4 z positions (0.5 μm step)—you can extract z positions above and below the one you have selected, at each frame, thereby generating a new stack centered at the levels of the AJs. This stack can then be easily projected using the Z Project option in Fiji (Image > Stacks > Z Project) (Fig. 1B).

To use the time-lapses for intensity measurements, it is preferable to generate a sum projection and to apply a bleach correction before the quantification (Image -> Adjust > Bleach Correction > Histogram Matching). Such method can be useful, for example, to quantify the recovery of a protein of interest upon photobleaching experiments. For that, the mean intensity at the bleached region, and corresponding background, can be measured manually in Fiji, at each frame. After subtracting the background, you can plot the mean intensity at the bleached region over time. Using the best-fit to the experimental data, you can extract several parameters describing the dynamics of your protein of interest, namely the turnover time, as well as the mobile and immobile fraction.

2.2 GENERATING KYMOGRAPHS

A very useful way to visualize the dynamics of the AJ or of MyoII after projection is to generate kymographs. Several methods exist for this purpose; a simple option is to use the Re-slice tool in Fiji (Image > Stacks > Re-slice; before using the Re-slice, you need to change the image properties (Image > Properties—exchange the time

for z). To improve the reslicing, you can adjust the thickness of the line and/or apply a Stack Reg on your time-lapse, to align the stack images (Plugin > Stacks > Stack Reg; you may have to download this plugin online). Although, this Re-slice option can be very useful, when working with in vivo data it often happens that the alignment even after applying the Stack Reg is not ideal, thus we developed a Macro in Fiji that allows you define, at each frame, the landmarks for your kymograph (available upon request). After running the macro, you can manually select, by click, the two positions defining the extraction box at each frame. The length and width of the extraction box are adjustable. Upon extraction of the box, it is automatically rotated to align the extracted regions over time, thus generating a kymograph. For examples, see Herszterg et al. (2013).

2.3 MEASURING THE RATE OF CONTRACTILE RING CONSTRICTION

To monitor the constriction rate, we developed a Macro for Fiji that allows the user to quickly extract the contractile ring length over time (available upon request). Then, the rate of constriction is determined as the slope of the linear fit of the contractile ring length, normalized to the length at the onset of cytokinesis, as a function of time (see Herszterg et al., 2013). For dividing cells that constrict very slowly, only the linear part of the curves can be fitted to determine the constriction rate.

2.4 MEASURING THE RECOIL VELOCITY UPON CONTRACTILE RING LASER ABLATION

To measure the recoil velocity upon contractile ring laser ablation, you can generate a kymograph along the contractile ring encompassing both the dividing cell and its neighbors. Using the kymograph, the dividing cell diameter over time is measured using a custom-made MATLAB code (available upon request). For this specific example, the recoil velocity is then measured between t_0—time of laser ablation, and t_{20}—20 s after laser ablation (averaging the two time points closest to t_{20}). The amount of constriction prior to contractile ring laser ablation can be measured as the ratio of the difference in cell diameter prior to contractile ring ablation and upon full cell relaxation. A similar strategy can be employed to measure the recoil velocity in other contexts, for example, upon AJ laser ablation.

2.5 ANALYZING THE CONTRIBUTION OF CELL PROCESSES TO TISSUE-SCALE MORPHOGENESIS

More automated tools for image analysis adapted to epithelial tissues allow selective z-stack projection of the time-lapse, followed by a pipeline to segment and track cells at the tissue scale, over time. Cell features, such as area, topology, divisions, delaminations or cell−cell rearrangements, are extracted in a semiautomated fashion. In the lab, we developed a custom-made pipeline optimized to segment and track the cell contours throughout morphogenesis of the *Drosophila* pupal notum (Guirao et al.,

2015). Such pipeline can also be applied to other epithelial tissues with minimal adjustments. Alternatively, you can perform a similar analysis using the Fiji plugins for segmentation (Plugins > Segmentation). Recently, a software package—EpiTools (Heller et al., 2016)—was developed for biologists with little computer expertise and, it is thus accompanied by a detailed website, which includes tutorials.

Finally, to understand how cell shape changes, cell divisions, rearrangements and delaminations actually contribute for tissue-scale morphogenesis, an approach unifying the quantitative characterization of all those processes is required to be able to relate them and bridge the gap between the cell and the tissue scale. In the lab, such formalism was recently developed and tested on computer simulations, in the *Drosophila* pupal notum and in the pupal wing (Guirao et al., 2015). The authors collected and averaged several animals to build an archetypal *wild-type* tissue and determine the biological variability, thereby allowing a robust and meaningful comparison with mutant conditions. Using this approach, it became clear that the interplay between cell processes is much more complex than originally anticipated; for example, cell division can contribute either positively or negatively to tissue deformation depending on the region of the notum and on the developmental time point. Furthermore, the cell processes are not strictly independent of each other; for example, blocking cell division in the pupal notum, in addition to suppressing the contribution of division, also affects the amount and the anisotropy of cell shape changes and cell rearrangements, as well as their contribution for tissue deformation (Guirao et al., 2015). Alternatively, a different framework was developed and applied to the *Drosophila* pupal wing (Etournay et al., 2015).

3. MARKERS AND GENETIC TOOLS TO STUDY EPITHELIAL CYTOKINESIS IN VIVO

To perform live imaging, it is critical to use GFP/mChFP reporter lines, thus we compiled in Table 1 a list of useful fly stocks to study cytokinesis in vivo. As previously discussed, in an epithelial tissue, the cells neighboring the dividing cell also participate in the formation of the new adhesive contact (Firmino et al., 2016; Founounou et al., 2013; Herszterg et al., 2013). These findings highlighted the importance of studying how cell division, and in particular cytokinesis, impacts the surrounding tissue. Thus, the ability to generate adjacent patches of genetically distinct cells is essential to correctly address this question. In flies, two techniques have been widely used to generate clones, namely mitotic recombination, mediated by FRT sites and the flp-out clone technique (for review see del Valle Rodríguez, Didiano, & Desplan, 2011). Combining these alleles with reporters and/or mutant lines allows you to discriminate the localization and function of a particular gene exclusively in the dividing cell or its neighbors. Using FRT-mediated recombination, we generated adjacent patches of cells expressing MyoII::GFP or MyoII::RFP, allowing us to determine that MyoII accumulation upon contractile ring constriction takes place in the neighboring cells, rather than in the dividing cell itself (Herszterg

Table 1 Alleles and Transgenes Useful to Study Cytokinesis In Vivo

Drosophila Stock	Reference or Source
ubi-*H2B:RFP*	Bosveld et al. (2012)
ubi-E-Cad::GFP	Oda, Tsukita, and Takeichi (1998)
E-Cad::GFP	Huang et al. (2009)
E-Cad::3XGFP	Unpublished line generated by the Bellaiche Lab
E-Cad::3XmTagRFP	Unpublished line generated by the Bellaiche Lab
E-Cad::3XmKate2	Unpublished line generated by the Bellaiche Lab
MyoII::mChFP	Martin et al. (2009)
MyoII::3XmKate2	Unpublished line generated by the Bellaiche Lab
MyoII::3XGFP	Unpublished line generated by the Bellaiche Lab
UAS-CAAX::mOrg	Kanca, Caussinus, Denes, Percival-Smith, and Affolter (2014)
ubi-PLCγPH:GFP	Herszterg et al. (2013)
UAS-PH::ChFP	Herszterg et al. (2013)
Utr(ABD)::GFP	Rauzi, Lenne, and Lecuit (2010)
Lifeact::GFP	Bloomington Stock Center
Ubla-Ani(RBD)::GFP	Munjal, Philippe, Munro, and Lecuit (2015)
ubi-Rok::GFP	Bloomington Stock Center
ubi-*α-Tub::GFP*	Grieder, de Cuevas, and Spradling (2000)
ubi-*RFP:α-Tub*	Basto et al. (2008)
Act > y^+ > Gal4	Bloomington Stock Center
Tub > GFP > Gal4	Bloomington Stock Center
FRT40A, MyoII::GFP	Herszterg et al. (2013)
FRT40A, MyoII::RFP	Herszterg et al. (2013)

et al., 2013). A similar approach was used to demonstrate that, upon contractile ring constriction in the dividing cell, the neighboring cells become interposed in between the dividing cell membranes until midbody formation (Founounou et al., 2013; Herszterg et al., 2013).

CONCLUSIONS AND FUTURE PERSPECTIVES

Here we presented a simple protocol to image and analyze cytokinesis in vivo in two *Drosophila* epithelial tissues—the pupal notum and pupal wing. Combining this experimental setup with advanced microscopy techniques and the power of *Drosophila* genetics allows researchers to study cell division in a tissue context.

A very important aspect for future work would be to regulate actin–myosin dynamics at the subcellular scale. With this in mind, an optogenetic tool to locally inhibit cell contractility was recently developed and tested in the *Drosophila*

ectoderm (Guglielmi, Barry, Huber, & De Renzis, 2015). The authors adapted the CRY2-CIBN protein dimerization system to recruit, upon light exposure, the catalytic domain of the inositol polyphosphate 5-phosphatase OCRL to the plasma membrane, where it modulates the levels of both phosphoinositides and actin. As a proof-of-principle, the authors showed that activation of CRY2-OCRL in the whole embryo, or even in patches of ventral cells, is able to arrest ventral furrow formation or even revert it, if invagination had already started at the time of CRY2 activation.

A critical difficulty of studying cell division in vivo is the intrinsically complex 3D geometry of an epithelial tissue, with two sets of junctions assembled apically and basolaterally, as well as the contacts established between epithelial cells and the underlying extracellular matrix. To understand cell division in 3D, correlative electron microscopy would be a useful complementary approach to the live imaging described above. Alternatively, super resolution microscopy can also be employed to increase the spatial resolution. Such methods may allow researchers to further understand, for example, the organization of the actin−myosin cytoskeleton at the subcellular scale.

ACKNOWLEDGMENTS

We thank Boris Guirao for comments on the manuscript. Diana Pinheiro acknowledges fellowships from FCT (SFRH/BD/51700/2011) and FRM (FDT20150531972) for funding. Work in the Bellaïche lab is supported by ANR-MaxForce, ANR-MorphoDro, ERC Advanced (TiMoprh, 340784), ARC (SL220130607097), ANR Labex DEEP 11-LBX-0044, ANR-10-IDEX-0001-02 PSL grants.

REFERENCES

Bardet, P. L., Guirao, B., Paoletti, C., Serman, F., Léopold, V., Bosveld, F., … Bellaïche, Y. (2013). PTEN controls junction lengthening and stability during cell rearrangement in epithelial tissue. *Developmental Cell, 25*(5), 534−546. http://dx.doi.org/10.1016/j.devcel.2013.04.020.

Basto, R., Brunk, K., Vinadogrova, T., Peel, N., Franz, A., Khodjakov, A., & Raff, J. W. (2008). Centrosome amplification can initiate tumorigenesis in flies. *Cell, 133*(6), 1032−1042. http://dx.doi.org/10.1016/j.cell.2008.05.039.

Bosveld, F., Bonnet, I., Guirao, B., Tlili, S., Zhimin, W., Petitalot, A., … Bellaïche, Y. (2012). Mechanical control of morphogenesis by fat/dachsous/four-jointed planar cell polarity pathway. *Science (New York, NY), 336*, 724−727. http://dx.doi.org/10.1126/science.1221071.

Brieher, W. M., & Yap, A. S. (2013). Cadherin junctions and their cytoskeleton(s). *Current Opinion in Cell Biology, 25*(1), 1−8. http://dx.doi.org/10.1016/j.ceb.2012.10.010.

Etournay, R., Popović, M., Merkel, M., Nandi, A., Blasse, C., Aigouy, B., … Eaton, S. (2015). Interplay of cell dynamics and epithelial tension during morphogenesis of the *Drosophila* pupal wing. *eLife, 4*, e07090. http://dx.doi.org/10.7554/eLife.07090.

Firmino, J., Rocancourt, D., Saadaoui, M., Moreau, C., & Gros, J. (2016). Cell division drives epithelial cell rearrangements during gastrulation in chick. *Developmental Cell, 36*(3), 249−261. http://dx.doi.org/10.1016/j.devcel.2016.01.007.

Founounou, N., Loyer, N., & Le Borgne, R. (2013). Septins regulate the contractility of the actomyosin ring to enable adherens junction remodeling during cytokinesis of epithelial cells. *Developmental Cell, 24*(3), 242−255. http://dx.doi.org/10.1016/j.devcel.2013.01.008.

Fritzsche, M., & Charras, G. (2015). Dissecting protein reaction dynamics in living cells by fluorescence recovery after photobleaching. *Nature Protocols, 10*(5), 660−680. http://dx.doi.org/10.1038/nprot.2015.042.

Georgiou, M., Marinari, E., Burden, J., & Baum, B. (2008). Cdc42, Par6, and aPKC regulate Arp2/3-mediated endocytosis to control local adherens junction stability. *Current Biology, 18*(21), 1631−1638. http://dx.doi.org/10.1016/j.cub.2008.09.029.

Green, R. A., Paluch, E. K., & Oegema, K. (2012). Cytokinesis in animal cells. *Annual Review of Cell and Developmental Biology, 31*, 169−213. http://dx.doi.org/10.1146/annurev-cellbio-101011-155718.

Grieder, N. C., de Cuevas, M., & Spradling, A. C. (2000). The fusome organizes the microtubule network during oocyte differentiation in *Drosophila*. *Development (Cambridge, England), 127*(19), 4253−4264.

Guglielmi, G., Barry, J. D., Huber, W., & De Renzis, S. (2015). An optogenetic method to modulate cell contractility during tissue morphogenesis. *Developmental Cell, 35*(35), 1−15. http://dx.doi.org/10.1016/j.devcel.2015.10.020.

Guillot, C., & Lecuit, T. (2013). Adhesion disengagement uncouples intrinsic and extrinsic forces to drive cytokinesis in epithelial tissues. *Developmental Cell, 24*(3), 227−241. http://dx.doi.org/10.1016/j.devcel.2013.01.010.

Guirao, B., Rigaud, S. U., Bosveld, F., Bailles, A., Lopez-Gay, J., Ishihara, S., … Bellaïche, Y. (2015). Unified quantitative characterization of epithelial tissue development. *eLife, 4*, e08519. http://dx.doi.org/10.7554/eLife.08519.

Heisenberg, C.-P., & Bellaïche, Y. (2013). Forces in tissue morphogenesis and patterning. *Cell, 153*(5), 948−962. http://dx.doi.org/10.1016/j.cell.2013.05.008.

Heller, D., Hoppe, A., Restrepo, S., Gatti, L., Tournier, A. L., Tapon, N., … Mao, Y. (2016). EpiTools: an open-source image analysis toolkit for quantifying epithelial growth dynamics. *Developmental Cell, 36*(1), 103−116. http://dx.doi.org/10.1016/j.devcel.2015.12.012.

Herszterg, S., Leibfried, A., Bosveld, F., Martin, C., & Bellaïche, Y. (2013). Interplay between the dividing cell and its neighbors regulates adherens junction formation during cytokinesis in epithelial tissue. *Developmental Cell, 24*(3), 256−270. http://dx.doi.org/10.1016/j.devcel.2012.11.019.

Huang, J., Zhou, W., Dong, W., Watson, A. M., & Hong, Y. (2009). Directed, efficient, and versatile modifications of the *Drosophila* genome by genomic engineering. *Proceedings of the National Academy of Sciences of the United States of America, 106*(20), 8284−8289. http://dx.doi.org/10.1073/pnas.0900641106.

Kanca, O., Caussinus, E., Denes, A. S., Percival-Smith, A., & Affolter, M. (2014). Raeppli: a whole-tissue labeling tool for live imaging of *Drosophila* development. *Development (Cambridge, England), 141*(2), 472−480. http://dx.doi.org/10.1242/dev.102913.

Langevin, J., Morgan, M. J., Rossé, C., Racine, V., Sibarita, J. B., Aresta, S., … Bellaïche, Y. (2005). *Drosophila* exocyst components sec5, sec6, and Sec15 regulate DE-Cadherin trafficking from recycling endosomes to the plasma membrane. *Developmental Cell, 9*(3), 365−376. http://dx.doi.org/10.1016/j.devcel.2005.07.013.

Leibfried, A., Fricke, R., Morgan, M. J., Bogdan, S., & Bellaiche, Y. (2008). *Drosophila* Cip4 and WASp define a branch of the Cdc42-Par6-aPKC pathway regulating e-cadherin endocytosis. *Current Biology, 18*(21), 1639–1648. http://dx.doi.org/10.1016/j.cub.2008.09.063.

Levayer, R., Dupont, C., Levayer, R., Dupont, C., & Moreno, E. (2016). Tissue crowding induces caspase-dependent competition for space. *Current Biology, 26*(5), 1–8. http://dx.doi.org/10.1016/j.cub.2015.12.072.

Marinari, E., Mehonic, A., Curran, S., Gale, J., Duke, T., & Baum, B. (2012). Live-cell delamination counterbalances epithelial growth to limit tissue overcrowding. *Nature, 484*(7395), 542–545. http://dx.doi.org/10.1038/nature10984.

Martin, A. C., Kaschube, M., & Wieschaus, E. F. (2009). Pulsed contractions of an actin-myosin network drive apical constriction. *Nature, 457*(7228), 495–499. http://dx.doi.org/10.1038/nature07522.

Mayer, M., Depken, M., Bois, J. S., Jülicher, F., Grill, S. W., Mayer, M., … Grill, S. W. (2010). Anisotropies in cortical tension reveal the physical basis of polarizing cortical flows. *Nature, 467*(7315), 617–621. http://dx.doi.org/10.1038/nature09376.

Morais-de-Sá, E., & Sunkel, C. (2013). Adherens junctions determine the apical position of the midbody during follicular epithelial cell division. *EMBO Reports, 14*(8), 696–703. http://dx.doi.org/10.1038/embor.2013.85.

Munjal, A., & Lecuit, T. (2014). Actomyosin networks and tissue morphogenesis. *Development (Cambridge, England), 141*(9), 1789–1793. http://dx.doi.org/10.1242/dev.091645.

Munjal, A., Philippe, J.-M., Munro, E., & Lecuit, T. (2015). A self-organized biomechanical network drives shape changes during tissue morphogenesis. *Nature, 524*(7565), 351–355. http://dx.doi.org/10.1038/nature14603.

Oda, H., Tsukita, S., & Takeichi, M. (1998). Dynamic behavior of the cadherin-based cell-cell adhesion system during *Drosophila* gastrulation. *Developmental Biology, 203*(2), 435–450. http://dx.doi.org/10.1006/dbio.1998.9047.

Rauzi, M., Lenne, P.-F., & Lecuit, T. (2010). Planar polarized actomyosin contractile flows control epithelial junction remodelling. *Nature, 468*(7327), 1110–1114. http://dx.doi.org/10.1038/nature09566.

del Valle Rodríguez, A., Didiano, D., & Desplan, C. (2011). Power tools for gene expression and clonal analysis in *Drosophila*. *Nature Methods, 9*(1), 47–55. http://dx.doi.org/10.1038/nmeth.1800.

Review

CellPress

A multicellular view of cytokinesis in epithelial tissue

Sophie Herszterg, Diana Pinheiro, and Yohanns Bellaïche

Institut Curie, UMR3215, U934, Team Polarity Division and Morphogenesis, 26 rue d'Ulm 75248 Paris cedex 05, France

The study of cytokinesis in single-cell systems provided a wealth of knowledge on the molecular and biophysical mechanisms controlling daughter cell separation. In this review, we outline recent advances in the understanding of cytokinesis in epithelial tissues. These findings provide evidence for how the cytokinetic machinery adapts to a multicellular context and how the cytokinetic machinery is itself exploited by the tissue for the preservation of tissue function and architecture during proliferation. We propose that cytokinesis in epithelia should be viewed as a multicellular process, whereby the biochemical and mechanical interactions between the dividing cell and its neighbors are essential for successful daughter cell separation while defining epithelial tissue organization and preserving tissue integrity.

On the challenges of separating daughter cells in an epithelial tissue

Cytokinesis is the final step of cell division and ensures the physical separation of the two daughter cells after chromosome segregation. In animal cells, the partition of the dividing cell relies on the constriction of an actomyosin contractile ring, which assembles at the division plane and drives the invagination of the cell membrane. Contractile ring assembly is mainly controlled by spindle microtubules, which signal to the cell cortex at early anaphase to create a narrow zone of RhoA activation at the division plane. Once activated, RhoA directs the assembly of the contractile ring by stimulating unbranched actin polymerization via formins and by activating non-muscle Myosin II (MyoII) via Rho-kinase and Citron-kinase, which phosphorylate MyoII and allow the assembly of bipolar MyoII minifilaments. The contractile ring also contains Septin filaments, which are crosslinked together with F-actin and MyoII by the scaffolding protein Anillin [1]. Ring constriction drives the ingression of the cleavage furrow until a narrow intercellular bridge remains, containing the midbody, which is formed by the reorganization of the central spindle microtubules and maturation of the contractile ring. The midbody serves as a platform for the recruitment of the abscission machinery, which eventually separates the two daughter cells via ESCRT-III-mediated membrane fission [2,3].

Although an extensive molecular and biophysical characterization of cytokinesis exists for single-cell systems such as budding and fission yeast, one-celled embryos, and cultured cells, and the basic mechanisms of cytokinesis are conserved in tissues, it has remained largely unknown whether the tissue context imposes specific requirements to the cytokinetic machinery. This is probably due to the fact that single-cell systems are advantageous for the dissection of the molecular pathways involved in cytokinesis – as illustrated by the important screens that identified pivotal regulators of cytokinesis [4–9] – as well as for the study of the mechanical aspects of cytokinesis [10,11]. These studies provided a wealth of knowledge on the mechanisms governing cytokinesis and can now serve as a valuable basis for studying how these mechanisms operate in tissues, which possess particular architectural features and perform specialized functions that need to be preserved during cell division.

Four recent works performed in *Drosophila* tackled the question of how cytokinesis occurs in epithelial tissues and provided novel contributions to the understanding of several aspects of epithelial cytokinesis *in vivo* [12–15]. Epithelial tissues act as physical and chemical barriers between different body compartments and are essential during development for the shaping of organs and tissues. These functions rely on a precise tissue architecture in which the cells are polarized along the apical–basal axis and strongly adhere to each other through different types of intercellular junctions [16]. In particular, adherens junctions (AJs) are one of the main mediators of intercellular adhesion and assemble in a characteristic apical adhesion belt, the zonula adherens (ZA), which is tightly connected to the actomyosin cytoskeleton and ensures mechanical coupling among the cells in the tissue. The core molecular components present at epithelial AJs are the E-Cadherin adhesion receptors and their conserved cytoplasmic partners p120-catenin, β-catenin, and α-catenin [17]. Given the complex nature of epithelial architecture, cytokinesis is a challenging event. First, because it entails important cell shape changes that have to be accommodated in the tissue and second because a new AJ has to be assembled *de novo* and correctly positioned at the new daughter cell interface, so that tissue polarity, cohesiveness, and architecture are preserved.

In this review, we focus on the recent advances in the understanding of cytokinesis in epithelial tissues. We do not review the mechanisms of cytokinesis as these were

Corresponding author: Bellaïche, Y. (yohanns.bellaiche@curie.fr).
Keywords: epithelial polarity; adherens junction; E-Cadherin; actin; Myosin II.

0962-8924/$ – see front matter
 http://dx.doi.org/10.1016/j.tcb.2013.11.009

recently compiled in three excellent reviews [1–3]. Here, we put forward the notion that cytokinesis in epithelial tissues should be viewed from a multicellular perspective, whereby the physical and biochemical interactions between the dividing cell and its neighbors play essential roles.

Dividing with and against neighbors

A major aspect to be considered when studying cytokinesis in epithelia is the presence of neighbors. Several works have shown that epithelial cells remain polarized during division and maintain their apical adhesion belt [12–15,18,19]. The persistence of cell–cell adhesion implies that the dividing cell remains mechanically coupled to its neighbors during cytokinesis and is consequently subjected to the tension exerted by them. Therefore, the cytokinetic apparatus needs not only to exert the contractile force necessary to constrict the dividing cell, as in single-cell systems, but also to overcome the opposing forces exerted by the neighbors.

Recently it was shown that Septins are specifically required for the completion of cytokinesis in cell divisions that occur in the plane of the epithelium, when the dividing cell has to pull on surrounding AJs [12]. In cells where Septin function is lost, cytokinesis failure occurs at late steps, after the contractile ring has reached its maximal constriction and the midbody ring is formed [12]. This is in agreement with the fact that Septins are required to anchor the midbody ring to the plasma membrane of the intercellular bridge in cultured *Drosophila* S2 cells [20]. Taken together, these data suggest that contractile rings devoid of Septins can still support furrow ingression in the face of AJs, but that the intercellular bridge cannot be stabilized when the tension due to neighboring cells is too high. Accordingly, eliminating the tension exerted by neighboring cells via laser ablation is sufficient to rescue the cytokinetic defects upon Septin loss of function [12], showing that epithelial tissues do impose specific requirements on the cytokinetic machinery for successful daughter cell separation.

It has also been proposed that Septins are required to drive local disengagement of AJs between the dividing cell and its neighbors at the level of the furrow [12,13] (Figure 1). *In vivo* time-lapse imaging of AJs during cytokinesis revealed that furrow ingression is accompanied by a twofold decrease in E-Cadherin concentration at the furrow membrane [12–15]. This decrease depends on Septins and Anillin [12,13]. It was proposed that the E-Cadherin decrease reflects a local disengagement of the AJs and therefore an uncoupling between the dividing cell and its neighbors at the furrow zone, thereby allowing the formation of a new adhesive interface between the daughter cells [12,13] (Figure 1). Because Anillin- and Septin-mutant contractile rings constrict slower than wild type, it was suggested that AJ disengagement is driven by the tension exerted by the contractile ring, which needs to be high enough to overcome the adhesive strength between the dividing cell and its neighbors [12,13] (Figure 1). In a study performed on the *Drosophila* embryonic ectoderm, this hypothesis is supported by the observation that a prominent gap can be seen between the dividing cell and its neighbors at the furrow zone by electron microscopy [13] (Figure 1).

However, in other epithelial tissues, cell cohesiveness seems to be maintained during cytokinesis. In the *Drosophila* dorsal thorax, although a twofold decrease in E-Cadherin concentration is also observed at the furrow membrane, no gap seems to appear between the dividing cell and its neighbors [12,14] (Figure 1), as shown by two-color membrane labeling [14]. Furthermore, in the mouse intestine, electron microscopy showed that the neighboring cells remain closely apposed to the dividing cell at all times, even following midbody formation [18]. Hence, tissue cohesiveness does not seem to be perturbed during cytokinesis in several epithelial tissues, suggesting tissue-specific mechanisms of AJ remodeling during cytokinesis (Figure 1).

Cytokinesis and mechanotransduction

An essential property of cells is their ability to respond to mechanical inputs through mechanotransduction pathways. Mechanotransduction is mediated by receptors that sense forces and are able to translate them into biochemical pathways that elicit cellular responses [21]. Mechanotransduction is involved in the control of various processes, ranging from cell fate specification and proliferation to tissue morphogenesis (for a review, see [22]). In epithelial tissues, mechanotransduction has been implicated in different contexts of morphogenesis, including cell intercalation in the *Drosophila* germ band [23], *Drosophila* mesoderm invagination [24], and the formation of the *Drosophila* wing hexagonal packing [25,26].

Strikingly, mechanotransduction might also play a role during epithelial cytokinesis. During furrow ingression in the *Drosophila* pupal notum, neighboring cells are pulled by the contractile ring and accumulate and activate MyoII at the edges of the furrow, in a Rho-kinase-dependent manner [14]. This process allows neighboring cells to exert tension on the dividing cell and bring the two daughter cells close together. This tension sets the geometry of the future interface and, by facilitating cell–cell contact, promotes the formation of a long AJ between the daughter cells [14] (Figure 2). This observation indicates that neighboring cells are able to sense cell division and respond by accumulating MyoII. A likely possibility is that MyoII accumulation in the neighboring cells is a mechanotransduction response to the tension exerted by the contractile ring (Figure 2). This is consistent with findings that laser ablation of the contractile ring before constriction prevents MyoII accumulation in the neighboring cells [14]. In line with this idea, previous work has shown that the application of a local pulling force through pipette aspiration in *Dictyostelium* and in the *Drosophila* embryonic epithelium is sufficient to induce MyoII accumulation in the region submitted to force [23,27].

Notably, AJs are sites of force transmission and they not only resist disruptive forces, but also actively respond to forces by modulating the actomyosin cytoskeleton, making them important sites of mechanotransduction [22,28]. At AJs, force sensing and transduction is attributed to the Cadherin complex, because both E-Cadherin and α-catenin become stretched in a tension-dependent manner [29,30].

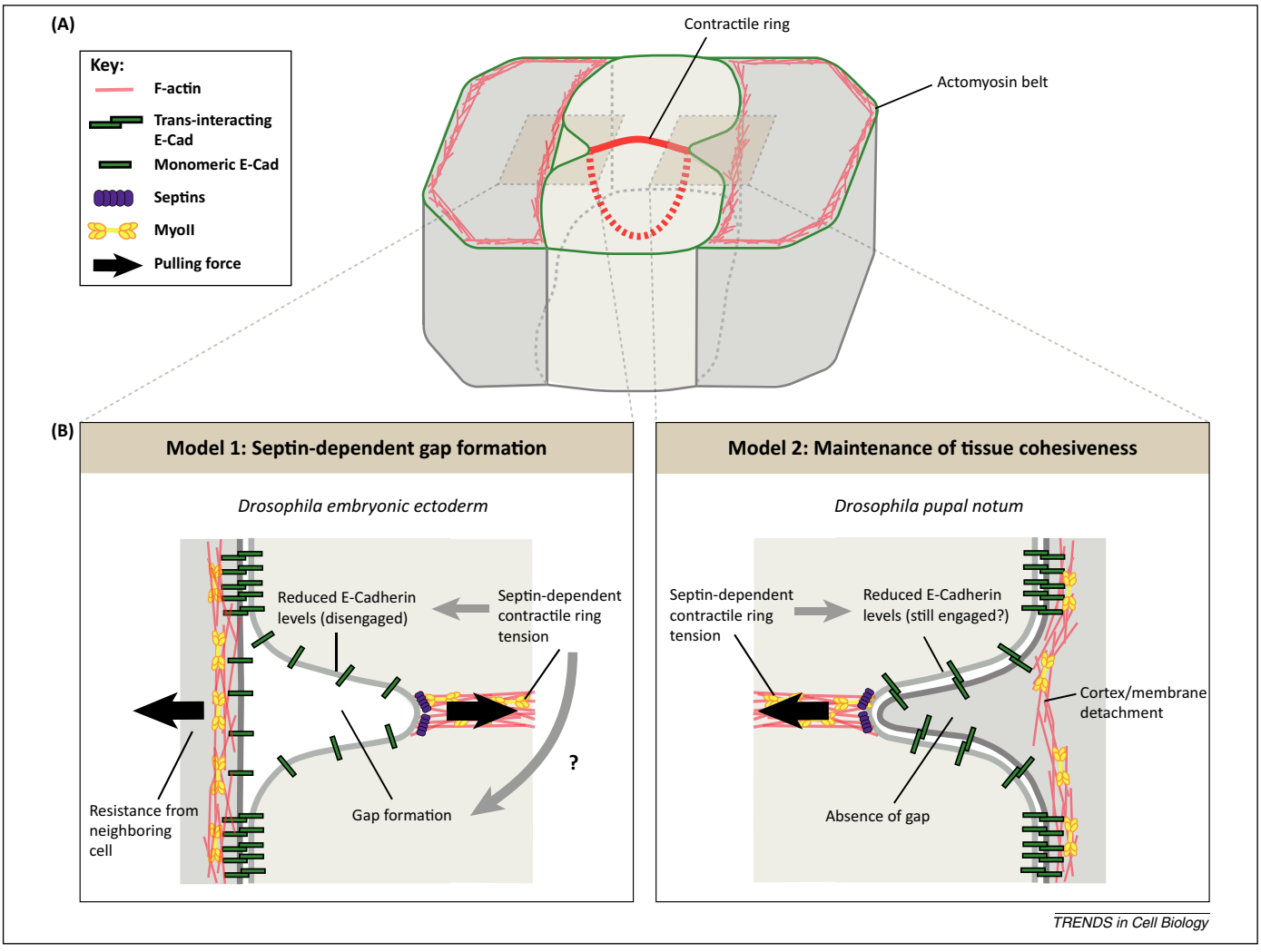

Figure 1. Two models for the organization of the membranes of the dividing cell and its neighbors during cytokinesis. **(A,B)** Schematic representation of a dividing cell and its neighbors during early furrow ingression. The zones highlighted in (A) are enlarged in (B). (B) In both models, Septins are required to induce downregulation of E-Cadherin levels at the furrow zone. In a first model, proposed in the *Drosophila* embryonic ectoderm [13], the application of opposing forces at the cell–cell interface – one exerted by the contractile ring and the other by the neighboring cells (black arrows) – overcomes the adhesive strength of the E-Cadherin complexes and leads to E-Cadherin disengagement and to the formation of a gap between the dividing cell and its neighbors (left). In a second model, proposed in the *Drosophila* pupal notum [12,14] and mouse intestine [18] (right), the dividing cell remains connected to its neighbors and no gap is formed. A possible way of relieving the tension exerted by neighboring cells in this case is through cortex–membrane detachment, which has been observed in the *Drosophila* notum [12,14]. E-Cad, E-Cadherin; MyoII, non-muscle Myosin II.

Once stretched, α-catenin exposes a cryptic site that interacts with the actin-binding protein Vinculin and that might also interact with other actin regulators, such as α-actinin and Afadin and the actin nucleator Formin 1 [28]. Importantly, application of force to Cadherin molecules leads to an increase in actomyosin tension accompanied by junction stiffening [31,32]. This AJ response to force has been shown to require the recruitment of Vinculin to α-catenin in a tension-dependent manner [30,32,33]. Therefore, it will be interesting to address whether E-Cadherin-mediated mechanotransduction is involved in the neighboring cell response.

Together, these findings suggest that epithelial cytokinesis could be a novel system in which to study mechanotransduction *in vivo*. Therefore, future studies of epithelial cytokinesis could provide insights into general force-dependent mechanisms used to maintain tissue homeostasis.

Asymmetric furrowing in epithelial cells: does it matter?

A commonly observed feature of epithelial cytokinesis is that furrowing occurs asymmetrically. Asymmetric furrowing is characterized by unilateral ingression of the cleavage furrow, from the basal to the apical domain of epithelial cells, resulting in apical midbody formation. This has been observed in several epithelial tissues, such as the mouse intestine [18,34], polarized monolayers of MDCK cells [19], cultured mouse hepatocytes [35], and, more recently, the *Drosophila* pupal notum [12,14], embryonic ectoderm [13], and follicular epithelium [15], suggesting it could be a conserved feature of epithelial cell division. The recent studies performed in *Drosophila* epithelial tissues not only provided insights into the mechanisms controlling asymmetric furrowing, but also highlighted that other modes of cytokinesis also occur in epithelia [12–15]. Strikingly, regardless of the mode of furrowing, the midbody is systematically formed at the apical part of the daughter cell interface, suggesting that midbody positioning, rather than asymmetric furrowing, is the conserved aspect of epithelial cytokinesis. So far, four modes of cytokinesis leading to apical midbody positioning have been identified in epithelia (Figure 3): (i) asymmetric furrowing controlled

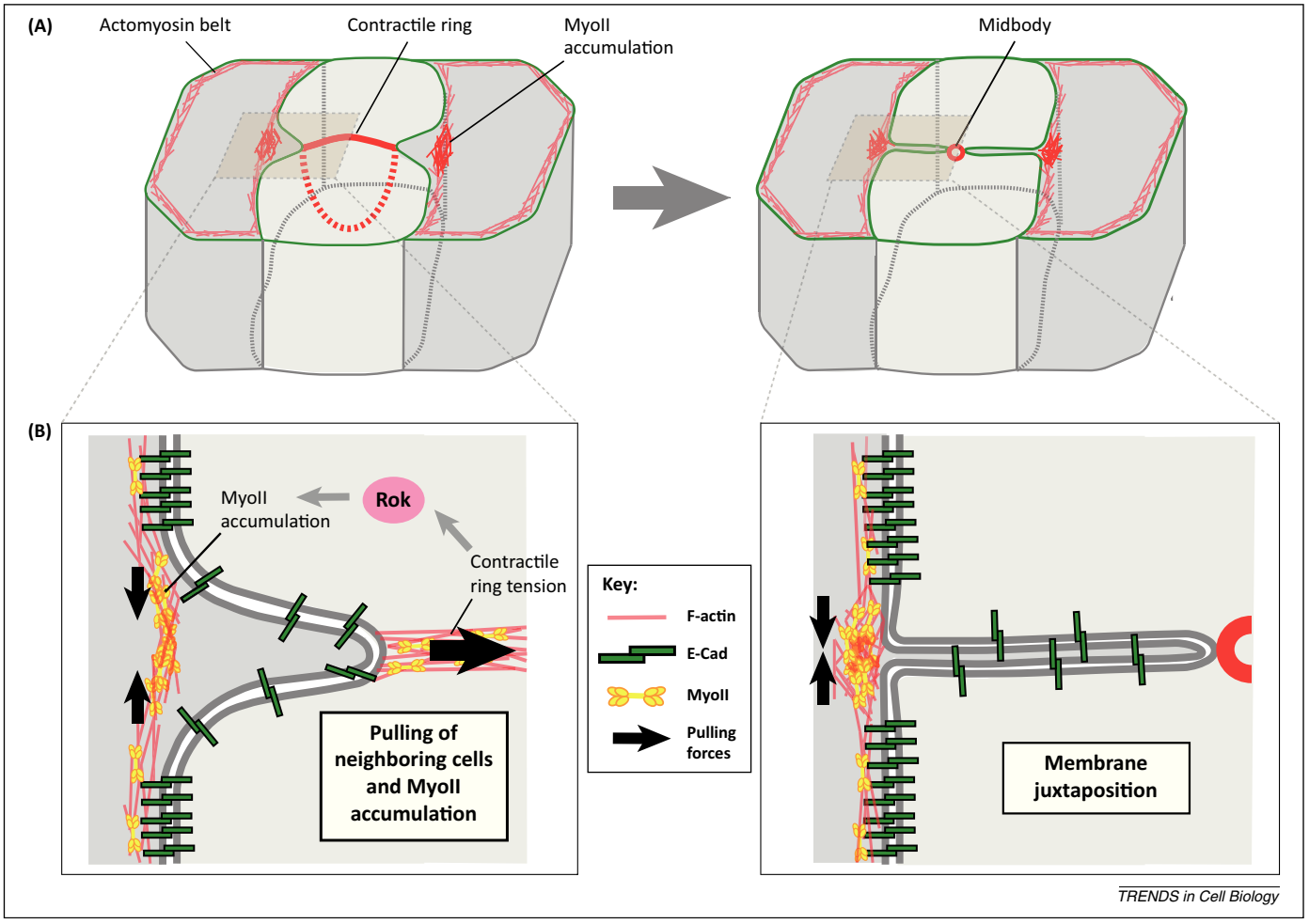

Figure 2. Cytokinesis and mechanotransduction. **(A,B)** Schematic representation of a dividing cell and its neighbors during cytokinesis. The zones highlighted in (A) are enlarged in (B). Left: During early furrow ingression, the pulling of the neighboring cells by the contractile ring leads to Rho-kinase activation and non-muscle Myosin II (MyoII) accumulation in the neighboring cells, at the edges of the furrow. This MyoII accumulation allows neighbors to exert tension on the furrow (black arrows), which comprises the connected membranes of the dividing cell and the neighboring cell. Right: As the furrow ingresses and the midbody forms, the tension exerted by MyoII accumulation (black arrows) induces the juxtaposition of the furrow, bringing the two daughter cells into close proximity. Note that the neighboring membrane is still inserted between the daughter cell membranes at the moment of membrane juxtaposition. E-Cad, E-Cadherin; Rok, Rho-kinase.

by a symmetric contractile ring harboring a homogeneous distribution of MyoII that is anchored to the AJs [13,15]; (ii) asymmetric furrowing controlled by an asymmetric contractile ring harboring a polarized distribution of MyoII [12,14]; (iii) symmetric furrowing coupled to apical cell extrusion [14,15]; and (iv) symmetric furrowing followed by upward lifting of the midbody [15].

Apical midbody positioning through asymmetric furrowing

Asymmetric furrowing has been observed not only in epithelial tissues, but also in the vertebrate neuroepithelium, where it also occurs in a basal-to-apical direction [36–39], and in early embryos, where the direction of furrowing is random [40,41]. In the *Caenorhabditis elegans* zygote, asymmetric furrowing is driven by an asymmetric contractile ring, where the distributions of MyoII and Septins are polarized, being enriched at the pole that constricts the most [40]. In this system, stochastic symmetry-breaking events, dependent on Anillin and Septins, are proposed to be sufficient to polarize MyoII distribution and thereby lead to asymmetric furrow ingression [40]. However, in the epithelial tissues studied so far, neither Anillin nor Septins are required for asymmetric furrowing [12,13,15], suggesting that asymmetric furrowing in epithelial tissues does not rely on an asymmetric distribution of Septins and Anillin.

In the *Drosophila* embryonic ectoderm and follicular epithelium, the distributions of Septins and MyoII in the contractile ring are fairly uniform. Despite this, asymmetric furrowing is still observed [13,15]. Notably, in both epithelia, the apical side of the contractile ring remains in close contact with the AJs. Loss of β-catenin function [15] or depletion of E-Cadherin or α-catenin [13] abolishes asymmetric furrow ingression, supporting the view that AJ integrity is essential for polarizing furrow ingression in these systems. Furthermore, polarization of the E-Cadherin intracellular domain in cultured *Drosophila* S2 cells by the use of an Echinoid–E-Cadherin fusion protein [42] is sufficient to recruit the midbody to sites of E-Cadherin enrichment [15]. Taken together, these observations support a model in which the anchoring of a symmetric contractile ring to the AJs should lead to its upward lifting, thereby polarizing furrow ingression and ultimately positioning the midbody apically (Figure 3).

In contrast to the aforementioned *Drosophila* tissues, in the *Drosophila* pupal notum the contractile ring is

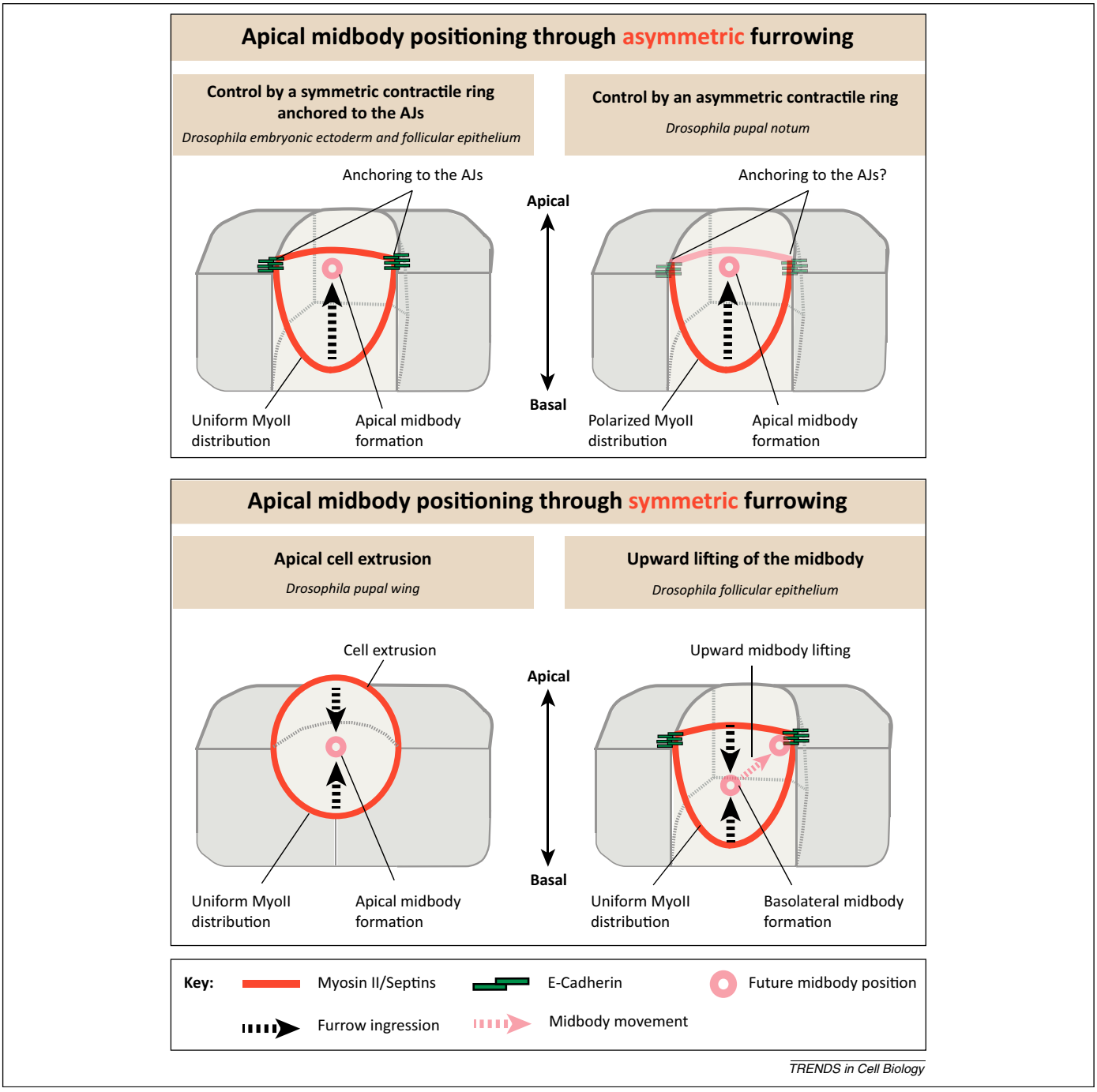

Figure 3. Different ways to achieve apical midbody positioning. Schematic representation of the different modes of cytokinesis described in epithelial tissues. Top: Apical midbody positioning can be achieved through basal–apical asymmetric furrowing. Asymmetric furrowing can be driven either by a symmetric contractile ring, with Myosin II (MyoII) being uniformly distributed, that is anchored to the adherens junctions (AJs) (left) [12,14], or by an asymmetric contractile ring, with MyoII being enriched at the basolateral part of the ring (right), which could be anchored to the AJs [12,14]. Bottom: Apical midbody positioning can also be achieved through symmetric furrow ingression, in combination with partial apical cell extrusion (left) [12,14], or by the posterior upward lifting of the midbody in an AJ-dependent manner (right) [12,14].

asymmetric. Both Septins and MyoII are enriched at the basal part of the ring [12,14], where the rate of ring constriction is higher [14]. Because asymmetric furrowing can be achieved through the polarization of MyoII distribution in the contractile ring [40], it will be important to address in this tissue whether asymmetric furrowing is controlled by AJs or by the asymmetric distribution of Myosin II in the ring.

In summary, asymmetric furrowing in epithelial tissues can be driven either by a symmetric contractile ring that is anchored to the AJs or by an asymmetric contractile ring, where the role of AJs remains to be explored (Figure 3).

Apical midbody positioning through symmetric furrowing

Although asymmetric furrowing was thought to be a general feature of epithelial cytokinesis, recent data established that other modes of cytokinesis exist in epithelia, also leading to apical midbody positioning. In the *Drosophila* pupal wing, apical midbody positioning is achieved

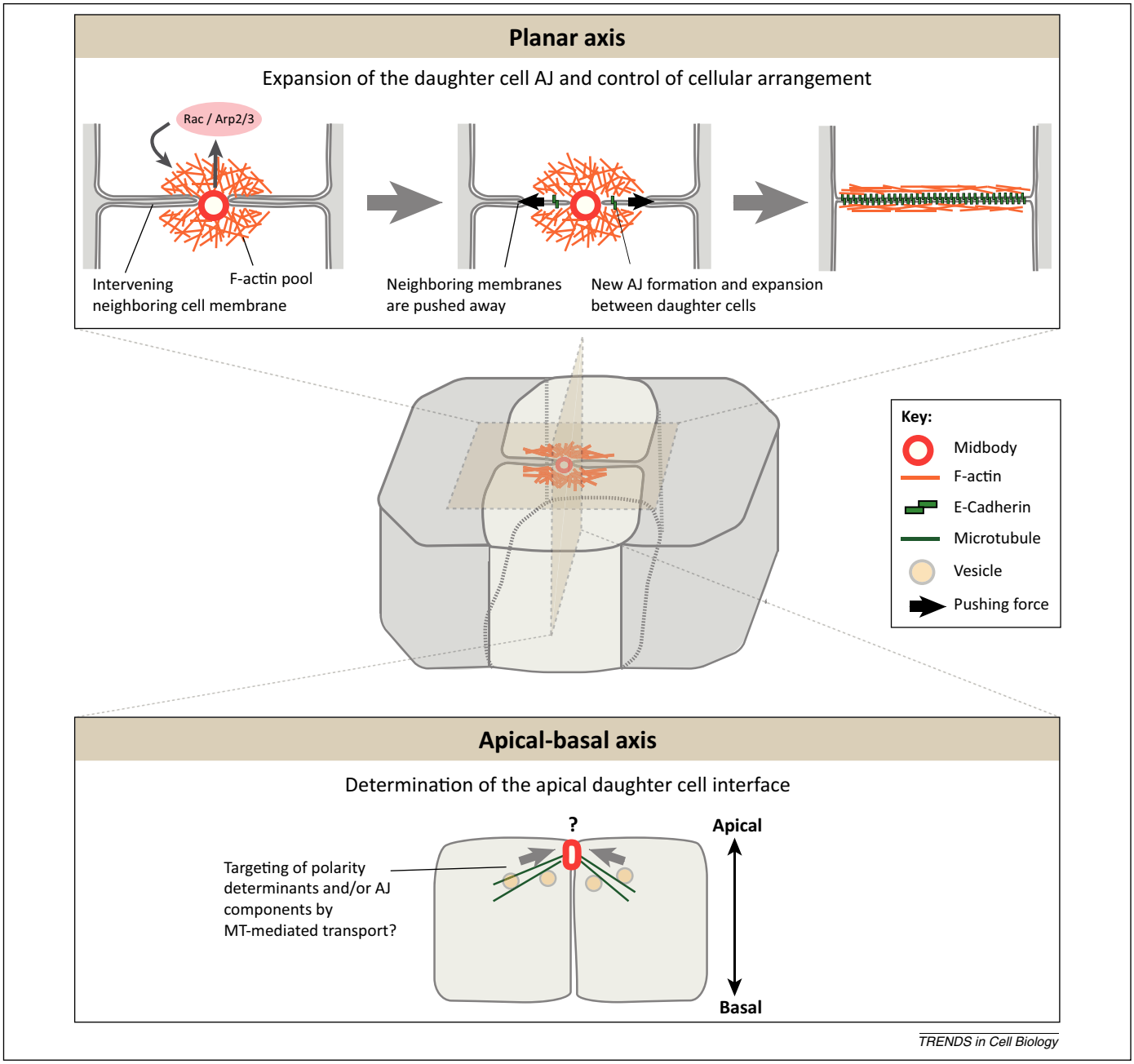

Figure 4. Novel roles of the midbody during epithelial cytokinesis. Schematic representation of a dividing cell at the time of midbody formation, depicting the pool of F-actin that accumulates around the midbody (orange). The regions highlighted in the center are enlarged in the upper and lower panels. Top: Rac- and Arp2/3-dependent actin polymerization around the midbody (left) allows the dividing cell to push away the intervening neighboring membranes from the new interface (center, black arrows), ultimately leading to the formation and expansion of a new adherens junction (AJ) between the daughter cells (right). This mechanism allows the midbody to control the planar arrangement of the cells upon cytokinesis. Bottom: The midbody has also been proposed to provide a spatial cue for the positioning of the apical daughter cell interface. This function could rely on the targeting of apical determinants and AJ components toward the midbody through microtubule-mediated vesicular trafficking. MT, microtubule.

by the coupling of symmetric furrow ingression to apical cell extrusion [14]. In this tissue, the dividing cell becomes partially extruded from the epithelium, resulting in the repositioning of its geometrical center toward the apical domain of the tissue. Therefore, although furrowing is symmetric and relies on a uniform distribution of MyoII, the midbody forms apically at the end of cytokinesis [14] (Figure 3). Interestingly, in the *Drosophila* follicular epithelium, where partial apical extrusion also occurs, it was recently reported that a correlation exists between the degree of extrusion and the asymmetry of furrowing [15]. The more the cell extrudes from the epithelial layer, the more symmetric the furrowing. These studies suggest the existence of a self-regulatory mechanism, whereby the balance between apical extrusion and furrow asymmetry ensures apical midbody positioning.

In addition, epithelial cells appear to have implemented a backup mechanism for apical midbody formation. In the *Drosophila* follicular epithelium, it was shown that even if the midbody forms in a more central position along the apical–basal axis due to symmetric furrowing, it can still be subsequently lifted upward in an AJ-dependent manner

[15], hence revealing another mode of apical midbody positioning that is independent of asymmetric furrowing (Figure 3).

In summary, asymmetric furrowing is achieved by at least two distinct mechanisms that are dependent on the distribution of MyoII in the contractile ring. Furthermore, it is not the sole mode of cytokinesis in epithelia. Remarkably, regardless of the type of furrowing used in each system, it ultimately leads to apical midbody positioning (Figure 3). Taken together, these findings suggest that apical midbody positioning, and not asymmetric furrowing *per se*, is the conserved and functionally relevant feature of epithelial cytokinesis.

Role of apical midbody positioning in planar tissue architecture and apical–basal polarity propagation

The recent studies performed in *Drosophila* epithelial tissues highlighted that the apically positioned midbody acts not only as a platform for cytokinetic abscission, but also as a cue to control planar tissue architecture and the propagation of apical–basal polarity upon cytokinesis. [14,15] (Figure 4).

Role of the midbody in the planar organization of epithelial tissues on cytokinesis

Studies in the *Drosophila* pupal notum, wing, and follicular epithelium provided evidence that midbody formation is accompanied by the appearance of an F-actin pool near the daughter cell interface [14,15]. This pool has been shown to be Rac and Arp2/3 dependent [14] (Figure 4). Furthermore, displacing the midbody to a more basal position along the apical–basal axis basally displaces the F-actin pool to the vicinity of the midbody, supporting the direct involvement of the midbody in the generation of a transient Rac- and Arp2/3-dependent wave of actin polymerization [14,15]. Notably, this observation explains how a *de novo* AJ can be formed between the daughter cells while tissue cohesiveness is maintained during cytokinesis, as detailed below (Figure 4).

As mentioned above, on furrow ingression in the *Drosophila* pupal notum, the neighboring cells are pulled by division and become interposed between the future daughter cells (Figure 4). This allows the maintenance of tissue cohesiveness but poses a topological obstacle for the formation of new AJs between the daughter cells. Live imaging revealed that, as the midbody forms and the wave of actin polymerization occurs, the neighboring membranes are pushed away, as the novel AJ between the daughter cells expands [14]. Importantly, dividing cells mutant for *rac* or *arp3* fail to expand and stabilize the new daughter cell AJ, which becomes significantly shorter than the wild type [14]. Also, in a percentage of cases, *rac*- and *arp3*-mutant dividing cells are unable to form a new AJ between their daughters and the new AJ forms between the two neighbors, resulting in a distinct cellular arrangement [14]. These results show that Rac and Arp2/3 activities are required in the dividing cell to push away the neighbors and allow the expansion of the daughter cell interface, thereby defining the planar arrangement of the daughter cells within the tissue (Figure 4). Together, these findings reveal a novel role for the midbody, along with Rac and Arp2/3 activities, in regulating daughter cell arrangement and therefore tissue architecture.

Experimental and theoretical evidence indicate that the formation of an interface between the daughter cells on division and, particularly, the geometry of that interface are essential in many contexts, including the control of planar tissue architecture, planar cell polarity, clone compactness, and cell fate specification involving daughter cell–cell signaling [25,43–47]. Therefore, Rac and Arp2/3 activities in the dividing cell might provide a means to control the arrangement of the daughter cells on cytokinesis and thus regulate planar tissue architecture and daughter cell–cell signaling.

Role of the midbody in the propagation of apical–basal polarity on cytokinesis

The midbody has also been proposed to be a positional cue for the formation of the apical daughter cell interface. In the *Drosophila* follicular epithelium, displacement of the midbody to more basal positions results in the formation of abnormal epithelial invaginations. Strikingly, the new apical interface between the daughter cells also forms more basally, just above the midbody [15]. This finding strongly supports a role for the midbody in providing a spatial cue for the formation of the apical daughter cell interface and therefore in preserving the apical–basal tissue architecture during proliferation.

One way through which the midbody could determine the apical daughter cell interface is by directing the targeting of polarity determinants and AJ components to the new daughter cell interface. Indeed, the midbody constitutes an important scaffold for stable microtubules, which serve as tracks for the targeting of various intracellular vesicles toward the midbody [48]. In MDCK cells cultured in 3D, the polarity protein Crumbs is targeted to the daughter cell interface during cytokinesis via the spindle microtubules to direct lumen formation [49]. Also, during the first cleavages of the zebrafish embryo, the localization of Cadherin and β-catenin to the interface between the daughter cells occurs during furrow ingression and depends on microtubules that are directed toward the furrow zone [50]. In addition, vesicles that are targeted to the midbody, such as Rab11- and Rab35-positive vesicles, are important for the trafficking and localization of Cadherin at AJs in interphasic cells [51–55]. Therefore, the targeting of AJ components and polarity proteins to the midbody needs to be further investigated to better understand the mechanisms of *de novo* AJ formation and polarity establishment on cytokinesis.

Concluding remarks

In conclusion, the recent works performed in *Drosophila* [12–15] provide novel insights into epithelial cytokinesis. Remarkably, they highlight that, in epithelial tissues, the cytokinetic machinery serves not only to ensure daughter cell separation, but also to control a series of events that are required for the maintenance of epithelial integrity during proliferation. For instance, the tension generated by the contractile ring favors the formation of a new daughter cell adhesive interface, both by inducing the remodeling of the AJs between the dividing cell and its

neighbors at the furrow zone and by triggering a non-autonomous MyoII response in the neighboring cells. Furthermore, apical midbody formation serves as a cue for the control of epithelial architecture, by controlling both the planar organization of the daughter cells upon division and the positioning of the apical daughter cell interface along the apical–basal axis. This reveals the existence of an important coordination in space and time between the cytokinetic and epithelial adhesion and polarity machineries. In addition, the characterization of the biochemical and physical interplay between the dividing cell and its neighbors in epithelia frames cytokinesis as a multicellular process, where cell–cell adhesion and contractility need to be taken into account for a comprehensive understanding of epithelial cytokinesis.

Acknowledgments

We apologize to all authors whose primary papers could not be cited because of space constraints. Work in Y.B. lab is supported by the ANR-MorphoDro, ARC, ERC-CePoDro grants as well as funds by the CNRS, the INSERM and the Curie Institute.

References

1 Green, R.A. *et al.* (2012) Cytokinesis in animal cells. *Annu. Rev. Cell Dev. Biol.* 28, 29–58
2 Agromayor, M. and Martin-Serrano, J. (2013) Knowing when to cut and run: mechanisms that control cytokinetic abscission. *Trends Cell Biol.* 23, 433–441
3 Fededa, J.P. and Gerlich, D.W. (2012) Molecular control of animal cell cytokinesis. *Nat. Cell Biol.* 14, 440–447
4 Echard, A. *et al.* (2004) Terminal cytokinesis events uncovered after an RNAi screen. *Curr. Biol.* 14, 1685–1693
5 Eggert, U.S. *et al.* (2004) Parallel chemical genetic and genome-wide RNAi screens identify cytokinesis inhibitors and targets. *PLoS Biol.* 2, e379
6 Gonczy, P. *et al.* (2000) Functional genomic analysis of cell division in *C. elegans* using RNAi of genes on chromosome III. *Nature* 408, 331–336
7 Kittler, R. *et al.* (2004) An endoribonuclease-prepared siRNA screen in human cells identifies genes essential for cell division. *Nature* 432, 1036–1040
8 Skop, A.R. *et al.* (2004) Dissection of the mammalian midbody proteome reveals conserved cytokinesis mechanisms. *Science* 305, 61–66
9 Somma, M.P. *et al.* (2002) Molecular dissection of cytokinesis by RNA interference in *Drosophila* cultured cells. *Mol. Biol. Cell* 13, 2448–2460
10 Salbreux, G. *et al.* (2012) Actin cortex mechanics and cellular morphogenesis. *Trends Cell Biol.* 22, 536–545
11 West-Foyle, H. and Robinson, D.N. (2012) Cytokinesis mechanics and mechanosensing. *Cytoskeleton (Hoboken)* 69, 700–709
12 Founounou, N. *et al.* (2013) Septins regulate the contractility of the actomyosin ring to enable adherens junction remodeling during cytokinesis of epithelial cells. *Dev. Cell* 24, 242–255
13 Guillot, C. and Lecuit, T. (2013) Adhesion disengagement uncouples intrinsic and extrinsic forces to drive cytokinesis in epithelial tissues. *Dev. Cell* 24, 227–241
14 Herszterg, S. *et al.* (2013) Interplay between the dividing cell and its neighbors regulates adherens junction formation during cytokinesis in epithelial tissue. *Dev. Cell* 24, 256–270
15 Morais-de-Sa, E. and Sunkel, C. (2013) Adherens junctions determine the apical position of the midbody during follicular epithelial cell division. *EMBO Rep.* 14, 696–703
16 St Johnston, D. and Ahringer, J. (2010) Cell polarity in eggs and epithelia: parallels and diversity. *Cell* 141, 757–774
17 Harris, T.J. and Tepass, U. (2010) Adherens junctions: from molecules to morphogenesis. *Nat. Rev. Mol. Cell Biol.* 11, 502–514
18 Jinguji, Y. and Ishikawa, H. (1992) Electron microscopic observations on the maintenance of the tight junction during cell division in the epithelium of the mouse small intestine. *Cell Struct. Funct.* 17, 27–37
19 Reinsch, S. and Karsenti, E. (1994) Orientation of spindle axis and distribution of plasma membrane proteins during cell division in polarized MDCKII cells. *J. Cell Biol.* 126, 1509–1526
20 Kechad, A. *et al.* (2012) Anillin acts as a bifunctional linker coordinating midbody ring biogenesis during cytokinesis. *Curr. Biol.* 22, 197–203
21 Gomez, G.A. *et al.* (2011) Productive tension: force-sensing and homeostasis of cell–cell junctions. *Trends Cell Biol.* 21, 499–505
22 Heisenberg, C.P. and Bellaiche, Y. (2013) Forces in tissue morphogenesis and patterning. *Cell* 153, 948–962
23 Fernandez-Gonzalez, R. *et al.* (2009) Myosin II dynamics are regulated by tension in intercalating cells. *Dev. Cell* 17, 736–743
24 Pouille, F. *et al.* (2009) Input normalization by global feedforward inhibition expands cortical dynamic range. *Nat. Neurosci.* 12, 1577–1585
25 Aigouy, B. *et al.* (2010) Cell flow reorients the axis of planar polarity in the wing epithelium of *Drosophila*. *Cell* 142, 773–786
26 Sugimura, K. and Ishihara, S. (2013) The mechanical anisotropy in a tissue promotes ordering in hexagonal cell packing. *Development* 140, 4091–4101
27 Bastos, R.N. *et al.* (2012) CYK4 inhibits Rac1-dependent PAK1 and ARHGEF7 effector pathways during cytokinesis. *J. Cell Biol.* 198, 865–880
28 Twiss, F. and de Rooij, J. (2013) Cadherin mechanotransduction in tissue remodeling. *Cell. Mol. Life Sci.* 70, 4101–4116
29 Borghi, N. *et al.* (2012) E-cadherin is under constitutive actomyosin-generated tension that is increased at cell–cell contacts upon externally applied stretch. *Proc. Natl. Acad. Sci. U.S.A.* 109, 12568–12573
30 Yonemura, S. *et al.* (2010) alpha-Catenin as a tension transducer that induces adherens junction development. *Nat. Cell Biol.* 12, 533–542
31 Kris, A.S. *et al.* (2008) VASP involvement in force-mediated adherens junction strengthening. *Biochem. Biophys. Res. Commun.* 375, 134–138
32 le Duc, Q. *et al.* (2010) Vinculin potentiates E-cadherin mechanosensing and is recruited to actin-anchored sites within adherens junctions in a myosin II-dependent manner. *J. Cell Biol.* 189, 1107–1115
33 Twiss, F. *et al.* (2012) Vinculin-dependent cadherin mechanosensing regulates efficient epithelial barrier formation. *Biol. Open* 1, 1128–1140
34 Fleming, E.S. *et al.* (2007) Planar spindle orientation and asymmetric cytokinesis in the mouse small intestine. *J. Histochem. Cytochem.* 55, 1173–1180
35 Kojima, T. *et al.* (2001) Occludin and claudin-1 concentrate in the midbody of immortalized mouse hepatocytes during cell division. *J. Histochem. Cytochem.* 49, 333–340
36 Das, T. *et al.* (2003) *In vivo* time-lapse imaging of cell divisions during neurogenesis in the developing zebrafish retina. *Neuron* 37, 597–609
37 Dubreuil, V. *et al.* (2007) Midbody and primary cilium of neural progenitors release extracellular membrane particles enriched in the stem cell marker prominin-1. *J. Cell Biol.* 176, 483–495
38 Kosodo, Y. *et al.* (2004) Asymmetric distribution of the apical plasma membrane during neurogenic divisions of mammalian neuroepithelial cells. *EMBO J.* 23, 2314–2324
39 Kosodo, Y. *et al.* (2008) Cytokinesis of neuroepithelial cells can divide their basal process before anaphase. *EMBO J.* 27, 3151–3163
40 Maddox, A.S. *et al.* (2007) Anillin and the septins promote asymmetric ingression of the cytokinetic furrow. *Dev. Cell* 12, 827–835
41 Rappaport, R. (1996) *Cytokinesis in Animal Cells*, Cambridge University Press
42 Johnston, C.A. *et al.* (2009) Identification of an Aurora-A/PinsLINKER/Dlg spindle orientation pathway using induced cell polarity in S2 cells. *Cell* 138, 1150–1163
43 Classen, A.K. *et al.* (2005) Hexagonal packing of *Drosophila* wing epithelial cells by the planar cell polarity pathway. *Dev. Cell* 9, 805–817
44 Farhadifar, R. *et al.* (2007) The influence of cell mechanics, cell–cell interactions, and proliferation on epithelial packing. *Curr. Biol.* 17, 2095–2104
45 Gibson, M.C. *et al.* (2006) The emergence of geometric order in proliferating metazoan epithelia. *Nature* 442, 1038–1041

46 Knoblich, J.A. (2010) Asymmetric cell division: recent developments and their implications for tumour biology. *Nat. Rev. Mol. Cell Biol.* 11, 849–860
47 Knox, A.L. and Brown, N.H. (2002) Rap1 GTPase regulation of adherens junction positioning and cell adhesion. *Science* 295, 1285–1288
48 Echard, A. (2008) Membrane traffic and polarization of lipid domains during cytokinesis. *Biochem. Soc. Trans.* 36, 395–399
49 Schluter, M.A. *et al.* (2009) Trafficking of Crumbs3 during cytokinesis is crucial for lumen formation. *Mol. Biol. Cell* 20, 4652–4663
50 Jesuthasan, S. (1998) Furrow-associated microtubule arrays are required for the cohesion of zebrafish blastomeres following cytokinesis. *J. Cell Sci.* 111, 3695–3703
51 Allaire, P.D. *et al.* (2013) Interplay between Rab35 and Arf6 controls cargo recycling to coordinate cell adhesion and migration. *J. Cell Sci.* 126, 722–731
52 Charrasse, S. *et al.* (2013) Rab35 regulates cadherin-mediated adherens junction formation and myoblast fusion. *Mol. Biol. Cell* 24, 234–245
53 Langevin, J. *et al.* (2005) *Drosophila* exocyst components Sec5, Sec6, and Sec15 regulate DE-cadherin trafficking from recycling endosomes to the plasma membrane. *Dev. Cell* 9, 365–376
54 Lock, J.G. and Stow, J.L. (2005) Rab11 in recycling endosomes regulates the sorting and basolateral transport of E-cadherin. *Mol. Biol. Cell* 16, 1744–1755
55 Roeth, J.F. *et al.* (2009) Rab11 helps maintain apical crumbs and adherens junctions in the *Drosophila* embryonic ectoderm. *PLoS ONE* 4, e7634

DISCUSSION:

As highlighted in the Introduction and Results Chapters, cell division in an epithelial tissue involves several challenges, as it: (i) requires the remodelling of the cell-cell contacts established between the dividing cell and its neighbours; (ii) involves the polarization of a new set of junctions between the future daughter cells, namely the AJ and the TJ (SJ in flies); and; (iii) requires that tissue cohesion is maintained throughout cell division, in order to conserve the tissue's barrier function. A series of recent publications showed that both in invertebrate and vertebrate epithelia cell division requires a tight collaboration between the dividing cell and its neighbours. Notwithstanding some differences (that will be extensively discussed later on), in all epithelial tissues studied so far, the dividing cell and the neighbouring cell membranes remain apposed throughout division, resulting in junction remodelling at the edges of the contractile ring[1–6]. In the Drosophila pupal tissues and the chick embryo, concomitant to junction remodelling, MyoII accumulates in the neighbouring cells[1,2,5]. Non-autonomous MyoII accumulation promotes membrane juxtaposition of the dividing cell membranes, thereby contributing for the establishment of a new membrane interface between the daughter cells and regulating their arrangement in the tissue (Fig. 23 and 24)[1,5]. These findings highlight a remarkably active role for the neighbouring cells during epithelial cell division[5]. Therefore, the aim of my PhD project was to understand how the dividing cell signals to its neighbours, thereby clarifying how the behaviour of epithelial cells is coordinated to preserve epithelial integrity and set the geometry of the new junction. In this Discussion, I will outline the main findings of this work, as well as discuss them in light of the current knowledge regarding epithelial cell division, junction remodelling and actomyosin flows in the context of force sensing and transmission.

A. Transmission of cytokinesis forces via E-Cadherin dilution and actomyosin flows

The main finding of this work is that the coordination between the dividing cell and its neighbours is based on a mechanotransduction event, whereby the mechanical forces produced during cytokinesis are sensed and transmitted to the neighbouring cells. Using a combination of contractile ring laser ablation experiments and genetic manipulations, we showed that: (i) contractile ring constriction is required for MyoII accumulation in the neighbours; and, (ii) lowering the mechanical forces produced by contractile ring constriction diminishes MyoII accumulation in cells neighbouring cells. Thus, our results support that MyoII accumulation in the

neighbours depends on the pulling forces produced during contractile ring constriction in the dividing cell.

To dissect the mechanism underlying force sensing and transmission during epithelial cell division, we characterized the events preceding MyoII accumulation in the neighbours. We found that contractile ring constriction imposes local local junction elongation at the interface shared by the dividing cell and its neighbours, thereby decreasing E-Cadherin (E-Cad) concentration at the ingressing junction. Concomitantly, cortical MyoII (along with other cortical markers, such as β_H-Spectrin) locally detaches from the ingressing AJs. Since mechanotransduction has been associated with tight reinforcement of the attachment between the Cad-Catenins complexes and the underlying actomyosin cortex[7,27], these findings suggest that mechanotransduction during epithelial cell division may rely on a previously uncharacterized mechanism. Using a complementary set of experiments, we demonstrated that MyoII accumulation in the neighbours does not arises from a simple contraction of the detached cortex, leading us to focus on the local decrease of E-Cad concentration at the ingressing AJ.

Combining live imaging, genetic manipulations and simulations, we demonstrated that the local reduction of E-Cad concentration results from extensive junction elongation at the edges of the contractile ring, imposed by constriction. Moreover, we found that lowering E-Cad concentration along with the contractility of the neighbouring cells is sufficient to promote self-organized actomyosin flows, ultimately leading to MyoII accumulation at the base of the ingressing AJ. Altogether our findings support that an alternative mechano-sensing mechanism coordinates actomyosin dynamics between epithelial cells and sustains AJ remodelling in response to mechanical forces (Fig. 25).

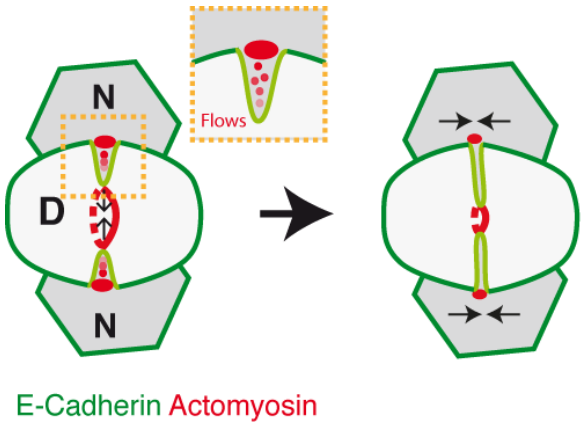

Figure 25: Schematic model of the interplay between epithelial cells during cytokinesis.
The pulling forces (represented by the black arrows) generated during contractile ring constriction in the dividing cell (D) deform the neighbouring cell membranes (N), promoting local membrane elongation and E-

Cadherin dilution (represented by light green). The local loss of actomyosin network anchorage at the ingressing AJ, along with the neighbouring cell's contractility, promotes self-organized and self-triggered actomyosin flows, eventually leading to their accumulation in the neighbours (red dots; shaded dots represent the previous position of MyoII during the emergence of the flows). Actomyosin activity in the neighbouring cells provides the cortical tension required for membrane juxtaposition in the dividing cell, contributing to set the final length of the new AJ formed between the future daughter cells (previous work from the team[1]).

B. Epithelial cell division:

In the last five years, epithelial cell division was described in a variety of model systems, namely in Drosophila, Xenopus, and chicken for a total of six epithelia analysed. Together these studies allow us to extract some general trends in epithelial cell division, as well as discriminate specific behaviours of the different epithelial tissues. Thus, in this section, I will compare and contrast the different systems with the Drosophila pupal notum, as well as discuss how our own findings could, or not, apply to other systems.

(i) Cytokinesis: an endogenous force generator

In the Drosophila pupal notum, two concurrent studies reported that, during contractile ring constriction, the cells neighbouring the dividing cell co-ingress with it to preserve membrane apposition and presumably tissue integrity[1,2]. To demonstrate that tight membrane apposition persists throughout cell division, Sophie Herszterg in the lab used a classical genetic trick in an uncommon way to generate adjacent mitotic clones expressing the same membrane marker, but labelled with different fluorescent proteins. This technique allowed to discriminate the dividing and neighbouring cell membranes, despite their tight arrangement in the tissue. Time-lapse imaging of cell division at the clone boundary demonstrated that the neighbouring cell membranes indeed become interposed in between the dividing cell membranes until midbody formation[1]. Since the neighbouring cells become increasingly deformed during cytokinesis, we tested whether the mechanical forces generated by the contractile ring are sufficient to deform both the dividing cell and its neighbours and whether the forces produced within the ring increase during constriction. We found that, upon contractile ring laser ablation, both the dividing cell and its neighbours rapidly relaxed, indicative of strong applied forces (Fig. 1c,d). Moreover, lowering the pulling forces produced by the contractile ring, by performing pnut (Septin7 in vertebrates), ani (Anillin in vertebrates) and rok (ROCK in vertebrates) RNAi, affects both the rate and extent of neighbouring cells deformation (Fig. 1e-i). Strikingly, we also found that the mechanical forces produced by the

contractile ring increase during constriction, a feature that to the best of our knowledge had not been reported yet (Extended Data Fig. 1a-h). Importantly, a theoretical model by Biron and colleagues had predicted a similar correlation between the amount of ring constriction and the magnitude of the mechanical forces produced by the ring. In their model, this correlation arises due to the densification of the actomyosin network within the ring during constriction[265]. Thus, it would be interesting to test whether this is indeed the case in vivo and whether this behaviour is, or not, a general trend.

Altogether, we concluded that, in an epithelial tissue, the mechanical forces produced during contractile ring constriction are transmitted to the neighbouring cells and coordinate both cells behaviours. In agreement with a general role for mechanical forces in coordinating the dividing cell and its neighbours during division, in the Drosophila embryonic[3] and follicular epithelia[4] and in both Xenopus[6] and chick embryos[5] the dividing cell and its neighbours also co-ingress during contractile ring constriction. Although the finding that contractile ring constriction generates strong pulling forces on the surrounding cells is in itself quite intuitive, establishing cytokinesis as a system to understand force sensing and transmission is essential, as it allows us to dissect how epithelial cells sense endogenous forces in vivo.

(ii) Cortex Detachment in the Neighbouring Cells

We found that, during cell division, cortical MyoII and β_H-Spectrin detach from the ingressing AJs (Fig. 2a-c), indicative of local cortex detachment in the neighbouring cells. Interestingly, in the Drosophila follicular epithelia, a similar detachment of cortical MyoII is observed at the most deformed AJ[4]. Thus, it would be important to find whether other cortical markers exhibit a similar behaviour. To study the role of cortex detachment during cell division, we analysed theoretically and experimentally the mechanisms regulating cortex attachment in vivo. For that, we developed a theoretical model describing a locally curved actomyosin cortex as a one-dimensional contractile fibre. In a curved geometry, the model predicts a tug-of-war between the adhesion forces mediating membrane-cortex attachment and the normal forces arising from MyoII contractility, which tend to detach the cortex. Under these conditions, detachment is expected to occur when the normal forces resulting from MyoII contractility at the cortex overcome the adhesion force maintaining its attachment. Thus, modulating cortex contractility and membrane-cortex attachment is expected to alter the critical curvature at which the cortex detaches (Supplementary Theory Notes).

To test this model experimentally, we manipulated the two parameters in vivo and analysed the critical curvature of cortex detachment during cell division. As curvature is difficult to determine experimentally, we analysed the angle formed by the ingressing AJ, a proxy for the local

membrane curvature (Extended Data Fig. 3a and Supplementary Theory Note). In agreement with the theoretical model, increasing MyoII activity by generating sds22 neighbours, which increases phospho-MyoII at the AJs[561], promotes cortex detachment at higher angles, resulting in a precocious detachment (Extended Data Fig. 3b-d). To manipulate the adhesion force, we analysed cortex detachment in moesin neighbours, as well as in an E-Cad^{k03401} heterozygous background (E-Cad1x). Moesin is the only ERM protein in flies and it plays an essential role in membrane cortex-attachment, since it can directly bind both F-Actin and the plasma membrane[562]. As predicted theoretically, lowering membrane-cortex adhesion also results in premature detachment and at higher angles than in wt neighbours (Extended Data Fig. 3b-d). Overall, our analysis supports that a balance between the adhesion force, cortex contractility and local membrane curvature regulates membrane-cortex attachment in vivo. During cell division, the pulling forces produced in the dividing cell, locally curve the neighbouring cell membranes and a balance between membrane-cortex adhesion and cell contractility sets the critical detachment curvature.

Having determined how a local pulling force modulates membrane-cortex attachment, we tested whether the detachment event is sufficient for MyoII accumulation in the neighbours. An intuitive model would be that MyoII accumulation arises from the contraction of the detached cortex. Using a complementary set of experiments, we were able to exclude this model, as we found that: (i) in cells neighbouring pnut dividing cells, cortex detachment was still observed in 50% of the cases, yet MyoII accumulation in the neighbours is strongly reduced (Fig. 2e); (ii) upon laser ablation of the detached cortex, MyoII is able to re-accumulate at the base of the ingressing membranes in the neighbouring cells (Fig. 2f); and, (iii) inducing a precocious cortex detachment by reducing Moesin function (Fig. 2g), resulted in the displacement of the initially detached MyoII away from the ingressing AJ. Under these conditions, although a transient MyoII accumulation could be observed around the position of the detached cortex, MyoII became strongly enriched away from it, at the base of the ingressing AJ, nearby the boundary between low and high E-Cad signal (Fig. 2g).

Collectively, these findings imply that a local contraction of the detached cortex is not sufficient to generate sustained MyoII accumulation in the neighbours and it rather suggests that the position of MyoII accumulation is determined by the asymmetry in E-Cad levels. Importantly, our subsequent analysis supports that the detached cortex may nevertheless cooperate with the E-Cadherin asymmetry to localize actomyosin accumulation in the neighbours (discussed in detail in sub-section iv).

(iii) Junction Remodelling during Cell Division

The tight apposition between the dividing cell and its neighbours throughout cytokinesis is indicative of strong adhesion between epithelial cells. Accordingly, in the Xenopus embryo, E-Cadherin complexes at the edges of the contractile ring are stabilized possibly by Vinculin recuitment[6]. Somehow paradoxically, in the other systems discussed so far, E-Cadherin levels at the ingressing AJ decrease significantly during contractile ring constriction[1–5]. These findings raise several interesting paradoxes, such as: (i) how adhesion is maintained between the dividing cell and its neighbours; (ii) how mechanotransduction is compatible with junction remodelling; and, (iii) possible differences between epithelial cell division in the Xenopus embryo and the other reported systems.

- Possible mechanism underlying adhesion during cell division:

Regarding the first point, one possibility is that the TJs/SJs are sufficient to sustain adhesion during cell division. Accordingly, we found that, in E-Cad or α-Cat RNAi clones, although the AJ integrity is lost, the actomyosin belt is collapsed in the centre of the cell and the membranes are highly distorted apically, at the level of the SJs (1.5-2 μm below the AJ), cells remain tightly adhered to their neighbours and tissue integrity is seemingly preserved. Tissue integrity is nevertheless affected when morphogenesis starts, as even more basally, cells detach from one another (not shown). These findings suggest that, in a static epithelium, the SJs are likely to be sufficient to withstand adhesion. In line with this, we found that during constriction, Dlg::GFP, a marker of the SJs, is still present at the plasma membrane (not shown), suggesting that indeed adhesion between the dividing cell and its neighbours is likely to be sustained by the SJs. Thus, now it is important to test whether the integrity of the SJs is indeed required for tight membrane apposition during epithelial cell division, as suggested by these findings.

- Adhesion Disengagement:

As discussed in Chapter IV, work from the Le Borgne and Lecuit labs suggested that local E-Cad down-regulation at the edges of the contractile ring is required to weaken the tensile forces exerted by the neighbours and allow the contractile ring to drive constriction[2,3]. Our findings now challenge this model in the Drosophila pupal notum, as we found that: (i) wt dividing cells facing E-Cad mutant neighbours still constrict at normal speed and with a similar profile of membrane deformation as cells facing wt neighbours (Extended Data Fig. 6c,d); (ii) similarly, in the presence of rok RNAi neighbours, which are not contractile and cannot generate strong resisting forces, the

constriction rate in the dividing cell is not altered and E-Cad still decreases at the ingressing AJ (Fig. 3e,f); and finally, (iii) E-Cad mutant neighbours are unable to rescue cytokinesis failure of pnut RNAi dividing cells, suggesting that lowering the adhesion between the dividing cell and its immediate neighbours is not sufficient to rescue the intrinsic defects of pnut dividing cells (Fig. 3m,n and Extended Data Fig. 6a-c). Altogether these findings rather support that, at least in the notum, the dividing cell sets the rate and dynamics of contractile ring constriction and that the resisting forces exerted by the neighbours are minor compared with the forces produced during constriction, as well as the resisting forces intrinsic to the dividing cell itself.

To understand how junction remodelling occurs during cell division, we dissected the mechanism underlying E-Cad decrease at the ingressing AJ. Since it was recently shown that in MDCK monolayers that mechanical forces increase E-Cad turnover[428], we analysed whether endocytosis and the trafficking machinery regulate E-Cad levels during epithelial cell division. To our surprise, E-Cad concentration still decreases at the ingressing AJ even in cells expressing dominant-negative Dynamin (Shibire in flies, or Shi), Rab11, as well as Sec5 mutant cells (component of the Exocyst complex, for details see Chapter I; Extended Data Fig. 4a-c). Thus, we envisioned an alternative model whereby mechanical forces locally pull the neighbouring cell membranes, thereby diluting E-Cad concentration at the ingressing junctions. In short, we found that, at least, theoretically this minimal model is sufficient to reproduce the dynamics and extent of E-Cad decrease in wt dividing cells (note that all the model parameters were determined experimentally, making this a parameter-free test).

To further challenge the model, we analysed E-Cad levels at the ingressing AJ in rok neighbouring cells, as actomyosin contractility is a well-known regulator of junction organization[127,130,194,563,564]. We found that a minimal adjust in the extent of junction elongation to the one observed in wt dividing cells facing rok neighbours is sufficient to account for E-Cad decrease at the ingressing AJ also in this condition (Fig. 3e-h and Extended Data Fig. 5a,b,f,g). Finally, we tested how lowering the contractile ring pulling forces affects E-Cad concentration at the ingressing AJ, as observed in pnut dividing cells. We found that, under this condition, junction elongation is significantly lower and less local and this is sufficient to account for the lack of E-Cad decrease at the ingressing AJ observed in this condition (Fig. 3i-l and Extended Data Fig. 5a,b,f,m). Since our model takes exclusively into account the average time of cytokinesis, the extent and locality of neighbouring junction elongation and the E-Cad turnover time, mobile/immobile fractions, one would assume such model can reproduce E-Cad dynamics in any other system as long as we input these experimentally determined parameters. Accordingly, it had been shown that during cytokinesis in the Drosophila follicular epithelium, where AJ deformation is consistently asymmetric and in the embryonic ectoderm, where unequal AJ deformation can also occur, that the dynamics of E-Cad decrease is also uneven. Accordingly, more deformed junctions

show earlier decrease of E-Cad[3,4]. Although the mechanism regulating E-Cad decrease was not explored in these two studies, their findings are fully consistent with our model and imply that the dilution mechanism may be indeed of general importance during cell division.

- Junction Remodelling: different strategies to preserve tissue integrity?

The striking decrease of E-Cad concentration observed during cell division is not observed in the Xenopus embryonic epithelium. The authors showed that the mobile fraction of E-Cad and β-Cat are significantly reduced at the ingressing AJ, suggesting that the E-Cad-Cat complexes are stabilized at the edges of the contractile ring. Accordingly, expression of a dominant-negative fragment of Vinculin, specifically destabilized the ingressing AJ that now showed a strong reduction of E-Cad concentration (although the authors did not determine the relative mobile/immobile fractions of E-Cad, which could be an important test to their model)[6]. These findings are consistent with Vinculin-mediated AJ reinforcement under tension. In contrast with this, in the pupal notum, Vinculin null dividing cells have similar constriction rate as wt cells, the neighbouring cell membranes still deform normally and, consequently, E-Cad concentration decreases at the ingressing AJ (Extended Data Fig. 7a-d). These findings argue that, in the notum, Vinculin is dispensable for E-Cad dynamics during cell division. In line with this, Vinculin does not accumulate at the ingressing AJ (Extended Data Fig. 7a,e). Finally, we also performed FRAP experiments at the ingressing AJ to test whether E-Cad dynamics at this region is somehow altered. We found that E-Cad mobile/immobile fraction and turnover in dividing cells is similar to non-dividing cells (Supplementary Table 1). Since in all the other reported systems E-Cadherin concentration at the ingressing AJ decreases during cytokinesis[1–5], one could envision that the Xenopus embryonic epithelium may have specific properties that prompt it for a different behaviour.

A first obvious difference between flies and Xenopus embryos is the duration of cytokinesis. On average, in the pupal notum, contractile ring constriction takes 5-6 min (similar duration of cytokinesis is reported in all Drosophila epithelial tissues), while in the Xenopus embryonic epithelium contractile ring constriction lasts on average up to 12 min, with some cells taking up to 20 min to complete contractile ring constriction (Fig. 4F in the publication[6]). In the dilution model we proposed, the duration of cytokinesis is an essential parameter, as longer division provides additional time for E-Cad molecules to be recruited to the ingressing AJ and compensate the junction elongation. Interestingly, pnut dividing cells exhibit similar duration of division (~18 min) as wt cells in the Xenopus embryos and, in this case, E-Cad levels at the ingressing AJ also remain high throughout cytokinesis. Moreover, when comparing pnut dividing cells in the pupal notum and wt cells in the Xenopus embryo, there is a striking resemblance in the

ingression profile of the AJ in both systems, as well as a similar geometry of the neighbouring cells membranes (Fig. 3a-c and i-k; compare with Fig. 4d,e in the publication[6]). Since, in the notum, pnut dividing cells elongate less and less locally than wt cells, it would be interesting to measure neighbouring cells elongation in the Xenopus embryo. The combined effect of longer cytokinesis timing and lower membrane elongation is likely to contribute for the different behaviour of E-Cad in the Xenopus embryonic epithelium.

An intriguing possibility that could account for these differences would be that the tension generated within the contractile ring is different in flies and in Xenopus cells. Although this may seem like a far-fetched possibility, in the pupal notum, we found a striking correlation between the rate of contractile ring constriction and the magnitude of the pulling forces produced by the contractile ring, with wt cells pulling stronger and faster than pnut, rok and ani dividing cells (Fig. 1e,g). Assuming this intuitive correlation is generally valid, one would predict that epithelial cells in the Xenopus embryo produce lower pulling forces on the neighbouring AJs than observed in the other systems. Accordingly, in MTC assays (Box 3D), Vinculin-recruitment by α-Catenin unfolding is reversible above a ~30 pN of applied force[380], supporting that above this critical force Vinculin recruitment to the AJs is no longer sustained. Whether the pulling forces produced by the contractile ring exceed this critical force remains to be tested, but it would be interesting to analyse whether the forces driving ring constriction are variable in different organisms. Estimating the absolute force produced during constriction is quite difficult, however it would be important to, at least, perform similar contractile ring laser ablation experiments in the Xenopus embryo (assuming similar cortical viscosities, one can compare the recoil velocities in the two systems). Another interesting test to this idea would be to determine whether in conditions where the pulling forces are lower in the notum, such as observed in pnut dividing cells, the classical Vinculin now pathway participates in sustaining E-Cad levels at the ingressing AJ. For that, we can generate pnut dividing cells in Vinculin null tissues and analyse E-Cad dynamics during cell division.

(iv) MyoII Accumulation in the Neighbouring Cells

Non-autonomous MyoII accumulation in the neighbours during cytokinesis was already reported in both vertebrate and invertebrate epithelia[1,2,4,5]. Our findings support that, at least in the pupal notum, a local reduction of E-Cad concentration at the ingressing AJ, along with the neighbouring cells' contractility, promotes local actomyosin accumulation during cytokinesis. As discussed in Chapter II, actomyosin flows produce mechanical forces to organize cell polarity, e.g. antero-posterior axis polarization in the C. elegans zygote[166], cell shape, e.g. cytokinesis[270], cell movement, e.g. at the lamella during cell migration[268] and amoeboid migration[211,269], junction

remodelling, e.g. germ-band extension in Drosophila[271] and during wound closure in Xenopus[273], as well as power tissue morphogenesis, e.g. the enveloping layer spreading in the Zebrafish embryo[272]. It has become increasingly clear that the ability of MyoII to slide and move Actin filaments is essential not only to sustain actomyosin flows, but also to polarize them via contractility gradients. Although the upstream cues regulating contractility differ, when MyoII contractility exceeds a threshold, a uniform cortex destabilizes into a local accumulation. In turn, a small accumulation of MyoII is sufficient to produce a contractility imbalance and, in combination with Actin turnover, trigger contractile flows[269,283,565,566]. This was recently shown to be the case for amoeboid cell migration, where an up-regulation of contractility is sufficient to polarize cells for locomotion[269]. Since we found that the concentration of the E-Cad-Catenins complexes decreases at the ingressing AJ, we explored the role of friction in setting the contractility threshold. As discussed in the Supplementary Theory Notes, the friction coefficient can result from several contributions, namely the coupling of the actomyosin cytoskeleton to the AJs, as mediated by α-Catenin, friction resulting from homophilic engagement of adhesion receptors, such as E-Cad and/or internal friction from the crosslinkers in the actomyosin meshwork. Therefore, we expect that lowering the concentration of the E-Cad-Cat complexes decreases the attachment between the cortex and the junction, thereby reducing the effective friction. Thus, we propose that, at constant contractility, lowering the network attachment, i.e. lower effective friction is sufficient to trigger actomyosin flows. Such model does not necessarily require a local increase in contractility and, as E-Cad-Cat reduction at the ingressing AJ is a consequence of a dilution phenomenon, actomyosin flows are, not only self-sustained, but also self-triggered.

In order to test this model, we generated cells expressing Lifeact::GFP in a tissue expressing MyoII::mKate2(x3) and found prominent Actin speckles moving along the neighbouring cell membranes (Fig. 4f,g). Importantly, we found similar results for MyoII::GFP expressed exclusively in the neighbouring cells (Fig. 4d,e). Moreover, as predicted theoretically, we observed that the majority of the MyoII and Actin feeding the neighbouring cells accumulation flows from the ingressing AJ, with the adjacent cortical regions exhibiting very little or no detectable mobilization of MyoII and Actin (Fig. 4a-g). Since E-Cad levels are low exclusively at the ingressing AJs (Fig. 2a), this argues that high friction, i.e. strong attachment of the actomyosin network to the AJ prevents actomyosin flows. Therefore, our findings strongly suggest that, even a very local modulation of the actomyosin attachment to the AJs is sufficient to trigger localized flows. To further test our current model, we are planning to artificially increase actomyosin attachment to the AJs and test whether that is indeed sufficient to modulate the actomyosin flows observed in the neighbouring cells during cell division. For that, we are building new fly lines expressing the α-Catenin or the Utrophin Actin-binding domain fused to a CAAX motif, which is sufficient for membrane association[567]. Under these conditions, even though E-Cadherin levels at

the ingressing AJ will decrease, we would expect friction to remain high due to the localization of the Actin-binding domains of α-Catenin or the Utrophin at the plasma membrane.

Importantly, actomyosin flows during cell division not only require a local friction reduction, but also the intrinsic contractility of the neighbouring cells (Extended Data Fig. 8k). Accordingly, we found that rok mutant neighbours exhibit a dramatic reduction of the velocity of Actin flows and, subsequent MyoII accumulation in the neighbours (Fig. 4h,i,l,m and Extended Data Fig. 5d,e). To further test this model, we examined the role of the main Actin nucleators during cell division. In contrast to the Arp2/3 complex, we found that Dia has a minor role in the neighbouring cells response. Dia loss of function induced a weak decrease in speckle velocity and a delay in MyoII accumulation (Fig. 4j-m and Extended Data Fig. 7i,j). These findings are in full agreement with our theoretical model, as it assumes that both monomeric and unbound Actin are in excess and diffuse rapidly in the cytoplasm. Thus, its impact on the flow velocity is rather secondary, via its effect on contractility. Consistent with this model, we performed an RNAi screen for the remaining five Formins and found that in all cases MyoII still accumulated in the neighbours. These findings highlight that basal levels of Actin polymerization are likely to be sufficient to sustain actomyosin flows in the neighbours, as predicted theoretically. To further strengthen this point, we will proceed with a more careful characterization of the dynamics of MyoII accumulation during cell division in each formin mutant.

As extensively discussed above, a local reduction in the effective friction is sufficient to trigger local actomyosin flows in the neighbours. Thus, we explored whether the friction asymmetry is also sufficient to reliably position the actomyosin accumulation, as observed in vivo (Fig. 2a). For this, we initially applied our minimal set of equations successively in one-dimensional (1D) and in two-dimensional (2D) models. We found that, in 1D models, the accumulation arises with equal probability at both sides of the gel, which corresponds in vivo to a 50% probability of actomyosin accumulation at the base of the ingressing AJ or at the tip of the ingressing AJ (Extended Data Fig. 8a and Supplementary Theory Notes). Nevertheless, as both scenarios have similar stabilities, any additional cue can robustly shift the equilibrium towards one of the solutions. Therefore, the presence of a detached cortex at the base of the ingressing AJ or the dynamic increase in AJ length are sufficient to reliably localize MyoII accumulation at the base of the ingressing region, as observed experimentally (Extended Data Fig. 8d,e and Supplementary Theory Notes). Strikingly, if now we consider the geometry of the ingressing region in vivo, which is intrinsically 2D, we found that the actomyosin accumulation is stably localized at the base of the deformed cortex in 100% of the cases (Fig. 4a,b and Supplementary Theory Notes). Moreover, the model predicts that, at constant contractility, the magnitude of actomyosin accumulation increases with the length of the ingressing AJ (Extended Data Fig. 8j). Theoretically, MyoII accumulation is not expected until a minimal length is reached. In line with this, our experimental observations

show that MyoII accumulation is only observed after 50% of contractile ring constriction (Fig. 2a).

Altogether, our experimental data and theoretical analysis support that a local decrease of E-Cad concentration at the ingressing AJ, resulting from the pulling forces produced by contractile ring constriction, along with the neighbouring cells' contractility plays a major role in driving actomyosin flows in the neighbouring cells. An interesting set of experiments to further challenge our model would be to manipulate the degree of Actin crosslinking and turnover. More cross-linked networks would be expected to only display actomyosin flows at a higher contractility threshold, regardless of the friction decrease, while increasing F-Actin turnover should reduce actomyosin accumulation in the neighbours.

C. Mechanotransduction at the AJ: is adhesion reinforcement the only way?

Over the last decade, it became increasingly clear that the Adherens Junctions sense and respond to mechanical forces. At the molecular level, force modulates the adhesive strength of E-Cadherin dimers, as well as α-Catenin interaction with F-Actin and the E-Cad-Cat complex. Additionally, other ABPs, such as Vinculin are recruited to the cell-cell contacts to further reinforce the connection between the adhesion machinery and the underlying cytoskeleton[7,27]. At the tissue level, many morphogenetic processes are driven by mechanical forces, suggesting that active generation, transmission and sensing of mechanical forces plays pivotal roles in modulating Cadherin-mediated adhesion.

The mechanotransduction field is polarized by the concept that "mechanotransmission is dictated by the ability of protein-protein interactions to resist mechanical loading. In the extreme case, breaking any link in a mechanotransmission pathway will terminate the mechanical signals and cause any mechanosensitive proteins to revert to their unloaded state"[7,27]. Even though this is quite an intuitive view observations during development, where extensive junction remodelling occurs under tension, suggest a more complex model. Accordingly, during germ-band extension in Drosophila for instance, the adhesion machinery and the actomyosin network adopt a planar polarized localization, with RhoGEF2, MyoII, Rok, Shroom and F-Actin accumulating at anterior-posterior junctions and E-Cad, β-Cat and Baz enriched at the dorsal-ventral junctions[106,161,326,329–331]. This complementary pattern drives junctional contraction along the anterior-posterior junctions and subsequent junction elongation in the orthogonal direction[326,332]. Similar observations were reported during cell-cell contact extension[357], dorsal closure and multicellular wound healing[568,569]. Importantly, E-Cad overexpression or blocking E-Cad endocytosis impairs the formation of the actomyosin cable and, consequently, prevents wound healing[570]. These studies support that, at least

during development, AJ remodelling often occurs under tension.

Our findings during epithelial cell division are fully consistent with this view and further suggest that mechanical forces can be transmitted via a decrease in E-Cadherin concentration and actomyosin flows. Our work highlights the importance of actomyosin anchoring to the adhesion machinery in an unexpected way, thereby extending the well-known role of the E-Cadherin-Catenins complexes in the stabilization of the cell-cell contacts[357]. Interesting parallels can be drawn with the studies mentioned above, where E-Cadherin distribution is also asymmetric and often non-overlapping with the actomyosin cytoskeleton. Therefore, it is tempting to speculate that this strategy of segregating adhesion complexes and the actomyosin cytoskeleton is a very general strategy to undergo junction remodelling under tension and a particularly useful one during tissue morphogenesis.

One important question that arises is under which conditions epithelial cells adopt the Vinculin-dependent AJ reinforcement pathway or undergo junctional remodelling. One interesting model would be that the magnitude of the applied force determines the response of the AJs. Similarly to Vinculin[380], above a critical threshold of mechanical load, E-Cadherin (~30 pN) and α-Catenin (~10 pN) bonds act as slip bonds, favouring the dissociation of the adhesive complexes and their interactions with the underlying actomyosin cytoskeleton[70,371], suggesting that adhesion strengthening is maximal at low forces and weak at large forces. Since a single Myosin motor can exert a force of ~3-4 pN[571], as little as 10 motors would be theoretically sufficient to reach the high force regime and weaken adhesion. This is likely to be an underestimation of the ability of the Cadherin complexes to withstand forces in vivo; yet, it argues that, at high forces, adhesion is intrinsically weak. Therefore, at high forces (corresponding to high MyoII concentrations, as observed during tissue morphogenesis), junction remodelling may be required to sustain force transmission and tissue integrity. Thus, it would be very important to determine the order of magnitude of the forces acting in developing tissues and relate them with the behaviours of the AJs and the actomyosin network.

D. Regulating Membrane-Cortex Attachment in vivo

During our analysis, we found that local events of cortex detachment are not restricted to cell division and are also observed rather frequently at the Tricellular Junctions (TCJs). Interestingly, the critical angle for cortex detachment determined during cell division (110.9º ± 1.71º) is also observed transiently at the TCJs. We observed that following a detachment event, MyoII transiently accumulates at the detached cortex. Transient MyoII accumulation appears to result from local cortex contraction, although additional experiments will be required to further

strengthen this point. Importantly, the detachment events observed at the TCJs are not necessarily associated with fluctuations of E-Cadherin (not shown). Based on this data, we speculate that transient MyoII accumulation following cortex detachment may contribute to locally reduce curvature and favour membrane-cortex re-attachment. Indeed, we observe that transient MyoII accumulation tends to re-approximate the cortex to the TCJs and re-attachment quickly ensues (not shown). To test this model in vivo, it would be important to locally modulate cortex contractility and test whether re-attachment still occurs. This kind of experiments requires optogenetic tools, as constitutively inactivating MyoII impairs cortex integrity (Extended Data Fig. 5d). Such tools were recently developed and tested in the Drosophila ectoderm. Guglielmi and colleagues adapted the CRY2-CIBN protein dimerization system to recruit, upon light exposure, the catalytic domain of the inositol polyphosphate 5-phosphatase OCRL to the plasma membrane, where it modulates the levels of both phospho-inositides and Actin. As a proof-of-principle, the authors showed that activation of CRY2-OCRL in the whole embryo, or even in patches of ventral cells, is able to arrest ventral furrow formation or even revert it, if invagination had already started at the time of CRY2 activation[572]. We recently received these flies and will test whether we can also achieve local inactivation of MyoII contractility. This approach will nicely complement our set of experiments to study the role of cortex detachment during cell division, as well as allow us to explore further the detachment events observed at the TCJs and their functional significance. Moreover, it would also be important to re-visit our data and characterize whether, as expected, modulating cell contractility and the adhesion forces also affects cortex detachment at the TCJs. Overall, our findings during cell division, could represent a general framework describing the dynamics of membrane-cortex attachment, as well as highlight the extremely dynamic character of cortex attachment to the plasma membrane. Since the hexagonal packing typically observed in epithelia would give rise to an angle of 120º at the TCJs (above the critical angle for detachment determined during cell division)[559,573], this preferred tissue packing is likely to stabilize membrane-cortex attachment in mature epithelia.

Finally, an interesting parallel with our studies is the process of blebbing. Blebs are highly dynamic plasma membrane protrusions with a rounded morphology that undergo quick cycles of expansion and retraction (~1 min)[522]. Blebbing is initiated by a local disruption of membrane-cortex interaction, as a result of an increase in internal hydrostatic pressure[535] or by a local increase in cortical contractility[574]. Although the mechanism for bleb retraction is quite different from the neighbouring cells' response during cell division[575], bleb formation also involves loss of membrane-cortex attachment. Thus, it would be interesting to test whether a similar model as described above may determine where a new bleb will form. Accordingly, it would be interesting to find whether bleb formation is preceded by a local down-regulation of the adhesion machinery, such as Moesin or by a local up-regulation of contractility, as either event is likely to facilitate local

membrane-cortex detachment.

E. E-Cadherin-Catenins Complexes: going back to the basics

E-Cadherins are essential adhesion receptors and along with their obligatory binding partners, the Catenins, it possesses three main functions: (i) to mediate cell-cell adhesion, by engaging in trans and cis interactions with other E-Cadherin molecules; (ii) to signal to the actomyosin cytoskeleton and regulate its organization at cell-cell contacts; and, (iii) to resist the actomyosin pulling forces and integrate them among neighbouring cells. Conversely, the organization of the actomyosin network itself impacts on E-Cadherin cluster organization, thereby modulating the adhesive force acting at cell-cell contacts. Thus, the dynamics of the AJs and the actomyosin cytoskeleton are intrinsically connected. Our findings are among a number of studies where this crosstalk is highlighted. Importantly, we found that, during cell division, this interplay is essentially mechanical, as mutant neighbours for Vinculin, Rho, Rac, Dia and the Arp2/3 complex exhibited at most a delay in MyoII accumulation in the neighbours (Extended Data Fig. 7a-m and [1]). Our findings rather emphasise the role of the E-Cadherin-Catenins complex as an essential anchor for the cytoskeleton, rather than as a signalling complex.

Since this is actually the core function of E-Cadherin-Catenins complexes, we envision our findings to be valid in other tissues and beyond cell division. Indeed, using fast time-lapse imaging of E-Cad::GFP and MyoII::chFP in non-dividing cells, we found that, in wt steady-state AJs, local, and often strong, fluctuations of E-Cad concentration occur rather frequently (not shown). The role of such fluctuations is for now unclear, but it could impact actomyosin anchorage and concentration at the AJs. Accordingly, junctional MyoII reduces concomitantly to E-Cad, in agreement with previous findings reporting that E-Cad depletion reduces Rho and Rho-GTP levels at the AJs, due to decreased Ect2 junctional localization[564]. If these local fluctuations impact Rho signalling and actomyosin anchorage at the AJs, one could envision that a subsequent mechanism must act to recover E-Cad/MyoII levels to homeostasis. Strikingly, our preliminary findings show that following E-Cad/MyoII fluctuations, additional MyoII is recruited to these sites, thereby contracting the AJ and rescuing E-Cad and MyoII local concentration (not shown). The source of these fluctuations is still unclear, but it is unlikely to result exclusively from E-Cad endocytosis or trafficking, as cells expressing dominant-negative Dynamin or Rab11 cells still exhibit such local fluctuations (not shown). One interesting possibility would be that these fluctuations result from local membrane protrusions powered by Actin polymerization, consistent with the known role of E-Cadherin in preventing Actin nucleation at the cell-cell contacts. To test this idea, we expressed Lifeact::GFP in clones and found indeed occasional filopodia-like protrusions at the level of the

AJs, however, only in a fraction of cases these protrusions coincided with local decreases in E-Cad concentration. Thus, in the future, we will further characterize these local fluctuations of E-Cad and its binding partner α-Catenin, as well as their role in junction homeostasis.

Another interesting aspect of the dilution model we propose is that it is, in principle, applicable to any other molecule present at the ingressing AJ. Accordingly, during cytokinesis, Bazooka (Par-3 in vertebrates), Canoe (AF6/Afadin in vertebrates) and Echinoid (Ed; Nectins in vertebrates) concentration at the ingressing AJ also decreases (not shown). Importantly, in Baz mutant cells, the localization of E-Cad, Crb, Arm (β-Cat in vertebrates), Ed is unaffected with the exception of aPKC, which is slightly diminished at the cortex (Table 5). Thus, in contrast to Par6 and aPKC, in the pupal notum Baz is not required for the maintenance of epithelial cell polarity[140,141]. Moreover, we found that in E-Cad mutant cells, both Canoe and Echinoid still localize at the AJs, in agreement with our conclusion that E-Cadherin decrease is the key for promoting actomyosin flows in the neighbours (although simultaneous decrease of these complexes is likely to amplify the effect of the E-Cad-Cat decrease at the ingressing AJs; not shown). Nevertheless, these findings support that a local pulling force is sufficient to dilute any adhesion receptor (or attached protein) sitting at the plasma membrane (the extent of depletion is expected to vary according to the turnover, mobile and immobile fraction of the protein considered). Thus, it is tempting to speculate that in, other contexts, local reduction of the concentration of Echinoid-Canoe complexes may also play a role in regulating actomyosin distribution and dynamics, as these complexes also mediate actomyosin cortex attachment to the cell-cell contacts. Accordingly, in the Drosophila wing disc epithelium, actomyosin cables form at the interfaces between Echinoid mutant cells and wt cells, similarly to those observed between E-Cadherin mutant cells and wt cells[82]. Similar observations were reported in the Drosophila follicular epithelium and embryo, where specific epithelial domains lack Ed expression, thereby creating an endogenous interface between Echinoid+ and - cells[85]. Whether in these systems the role of Echinoid is to modulate actomyosin network attachment is unclear, but it is tempting to speculate that a friction model analogous to the one we proposed during cell division could account for this sorting behaviour. Finally, another interesting paradigm for this model would be cell migration, as the strength of adhesion to the substrate was shown to regulate the velocity of the actomyosin flows. Thus, low substrate adhesion accelerates the velocity of the Actin flows[209,210]. Since the velocity of the flows is intrinsically connected to the persistence and speed of migrating cells[283–285], lowering the adhesion to the substrate is generally expected to promote faster and more persistent migration.

Although the exact contribution of friction for all the aforementioned processes is likely to be modulated by context-specific signalling modules, the role of differential actomyosin anchorage to the adhesion machinery in generating complex network behaviours such as flows, is likely to be of very general importance.

F. The role of Actomyosin Flows in Force Transmission

For the last decade, actomyosin flows were reported in a variety of model systems and shown to contribute to a wide range of cellular processes, from cell division to cell migration. Flows rely on fluid-like properties of the actomyosin network, as they require remodelling and/or sliding of Actin filaments by MyoII motors. The ability of actomyosin flows to generate mechanical forces is well illustrated by Actin treadmilling at the leading edge of migrating cells, which contributes to power lamellipodia protrusion[278,279]. Importantly, actomyosin flows not only transport Actin filaments and Myo motors, but also re-align Actin filaments and re-distribute actomyosin regulators. Actomyosin flow initiation requires a symmetry-breaking event, which can be a chemoattractant, as observed during cell migration or an upstream cue to locally increase contractility, as observed during cytokinesis or amoeboid migration[187,283]. Our work now highlights that asymmetric anchorage of the actomyosin network can also trigger a symmetry-breaking event and lower the contractility threshold for actomyosin flows to arise.

Our observations during cell division are reminiscent of previous findings in germ-band extension in flies. In the germ-band, E-Cad, β-Cat and Baz (Bazooka in flies) localization is planar polarized, with a depletion of the adhesion complexes from the anterior-posterior junctions (or vertical junctions) where RhoGEF2, Rok, Shroom, MyoII and F-Actin is enriched[106,161,326,329–331]. In this system, medial Myosin II flows are oriented by the planar polarized distribution of E-Cadherin complexes, with MyoII flowing towards vertical junctions[271]. The symmetry-breaking event in this system was proposed to be the near-instantaneous imbalances in E-Cad concentration between vertical junctions resulting from endocytosis[333]. Since the medial pool is not directly connected to the adhesion machinery, it is unclear how the medial of MyoII senses anchoring to the AJs. Our findings with junctional actomyosin during cell division could link these observations in a coherent framework. One would expect that even small friction imbalances of junctional actomyosin could easily propagate to the medial pool, which is highly contractile in germ-band cells. Thus, endocytosis-dependent E-Cadherin asymmetries generate imbalances in actomyosin anchoring at the AJs, allowing it to detach and flow away from the junction, which could, in turn, polarize the medial pool, promoting prominent flows towards the converse AJ. Such ping-pong cycle is then repeated upon E-Cad removal from the junction, re-directing the flows towards the other AJ and so on. Further studies are now required to test these ideas and to understand how germ-band cells are sensitized to respond to such small changes in E-Cadherin anchoring.

An unforeseen aspect of our model is that it allows the transmission of a mechanical signal at a distance, a feature that is more commonly associated with the Focal Adhesions. During cell migration, actomyosin pulling forces act on the focal adhesions to simultaneously contract the rear

and sustain an anterograde flow of Actin monomers essential to feed Actin polymerization at the leading edge[187,226,274]. Thus, contractile forces act mostly at the rear, but also contribute to the organization of Actin filaments at the leading edge[279]. Similarly, during cell division, mechanical forces are applied at the tip of the ingressing AJ, resulting in subsequent E-Cad dilution and actomyosin flows throughout the ingressed region, which, in turn, accumulate at the base of the ingressed junction, where E-Cad concentration remains high (Fig. 2a). Therefore, the mechanical signal produced by the dividing cell travels from the cell membrane to the base of the ingressed AJ.

Overall, our work uncovers a novel mechanism to sense and transmit mechanical forces during cell division and highlights an unexpected role for E-Cadherin and actomyosin flows in coordinating the behaviour of epithelial cells during cell division.

In summary, our findings support the view that actomyosin attachment is highly dynamic and its local modulation is sufficient to redistribute actomyosin in the cell, which, in turn, impacts the organization of the AJs themselves. We therefore foresee that our observations during cell division may have wide implications in a number of cell processes, e.g. cell division, blebbing and cell migration and morphogenetic models, e.g. cell sorting, oriented cell intercalations and multicellular wound healing.

CONCLUSIONS:

In conclusion, our findings highlight an unexpected mechanism to sense and transmit mechanical forces during epithelial cell division. The mechanical crosstalk between the dividing cell and its neighbours relies on the intrinsic properties of the adhesion machinery and on the contractility of the actomyosin network. Our findings support a model whereby locally modulating the actomyosin anchorage to the AJs, by a local downregulation of the E-Cadherin-Catenins complexes at the ingressing AJ along with the neighbouring cells' contractility, promotes self-organized actomyosin flows. Altogether our work establishes epithelial cell cytokinesis as an endogenous source of mechanical stress and uncovers a force sensing and transmission mechanism that is compatible with AJ remodelling, thereby extending the current understanding of mechanotransduction[6,7]. Finally, these findings also emphasize a novel role for actomyosin flows in force sensing and transmission, which may be of importance during other flow-driven processes, such as cell division or cell polarization.

Nevertheless, many exciting challenges still lie ahead. One critical aspect for the future will be to extend these studies by describing epithelial cell division in 3D, considering also the Septate Junctions, as well as the contacts established with the underlying extracellular matrix. For this, correlative electron microscopy would be a useful complementary approach to the live imaging described above. Another interesting avenue of research that we are starting to address is how the new AJ is assembled by the daughter cells. Our preliminary data suggests that two mechanisms cooperate for de novo junction assembly by recruiting E-Cadherin and actomyosin to the cell-cell contact. Finally, it will be interesting to find how cell division occurs in more complex epithelia, which contain several cell types and are multi-layered in nature, such as the skin. Overall, studying epithelial cell cytokinesis in vivo is likely to be a very important step stone to advance our understanding of epithelial biology.

ANNEXES:

Table 1: Main classes of Actin-binding proteins and their molecular mechanism of action.

Class of Actin-Binding Proteins:	Examples:	Molecular Mechanism:
G-Actin Binding Proteins Bind G-Actin monomers, thereby inhibiting their association with the barbed ends.	**Profilin**	Profilin associates with G-Actin monomers with high affinity, thereby inhibiting spontaneous filament assembly. Profilin-loaded monomers are competent for filament polymerization, but generally not for nucleation[183,185]. However, high concentration of Profilin may have negative impact on Formin-dependent Actin polymerization, due to free Profilin binding to their FH1 domain[217]. Finally, Profilin was recently implicated in regulating the homeostasis between different Actin networks, due to its ability to favour Formin-dependent polymerization[576–578].
	Thymosin-β4	Actin monomer-sequestering protein that forms a ternary complex with Profilin and Actin[579], thereby preventing spontaneous filament polymerization. Both Profilin and Thymosin-β4 regulate the local availability of G-Actin[580], however, Tβ4-bound monomers cannot be used for filament nucleation, nor elongation (although, Actin monomers can be readily transferred to Profilin)[183] . It was recently shown that Thymosin-β4 prompts Formin-based F-Actin assembly and/or filament elongation in lamellipodia[280].
F-Actin Nucleators Promote de novo Actin filament formation. So far, three classes of Actin nucleators have been characterized, namely: (i) the Formins, which nucleate linear Actin networks; (ii) the Arp2/3 complex, which nucleates branched networks; and, (iii) the tandem-monomer binding class, which was more recently	**Formins**	The Formin FH1 and FH2 domains cooperate during F-Actin assembly - the FH1 domain binds to Profilin-bound Actin and the FH2 domain associates processively with the barbed end. Formins can cooperate with other F-Actin nucleators, namely the Arp2/3 complex, Spire and the APC[185].
	Arp2/3 complex	Initiates nucleation of filament branches on the sides of existing mother Actin filaments at a characteristic angle of 70°, by anchoring the pointed end of the daughter filament to the mother filament while the free barbed end of the daughter filament grows away from the complex. Nucleation-promoting factors (such as: SCAR/WAVE or WASP), Actin filaments and monomers cooperate to induce polymerization by the intrinsically inactive Arp2/3 complex[217].
	Spire	Contains G-Actin-binding motifs in tandem that bring together Actin monomers to assemble a polymerization seed. In flies, Spire directly interacts with the Formin Cappuccino to organize Actin networks in vivo; while human Spire1/2 were shown to interact with FMN1/2[218]. Finally, Spire has also been reported to sever Actin filaments and modulate barbed end polymerization[219].

discovered and includes: Spire, Cordon Bleu, JMY, APC and Leiomodin. The tandem-monomer nucleators tend to polymerize F-Actin in cooperation with other F-Actin nucleators.	**Cordon Bleu**	Cordon Bleu stabilizes trimeric Actin seeds, due to its G-Actin binding domains and linker region. It polymerizes non-bundled and unbranched Actin filaments from the barbed-end with high efficiency and it is present in all vertebrates. In vivo, Cordon bleu promotes neurite growth in hippocampal neurons[581] and it is required for motile cilia development in Zebrafish[582].
	JMY	Contains several G-Actin binding domains able to capture Actin monomers and assemble a filament nucleus. Similarly to Cordon Bleu, JMY appears to be present exclusively in vertebrates[583]. In vitro assays showed that JMY activates the Arp2/3 complex to nucleate branched Actin filaments; however, alone JMY rather polymerizes unbranched networks[583]. JMY localizes to the nucleus in many cell types and conflicting reports proposed an additional function for JMY at the leading edge of migrating cells[218,584]. However, it remains unclear whether JMY's main function is to nucleate Actin filaments, act as an Arp2/3 activator and/or a transcriptional regulator[218,584].
	APC Adenomatous Polyposis Coli	Contains several G-Actin binding domains, namely the ANS1/2 (Actin-nucleating sequences) domains. APC dimers nucleate unbranched F-Actin, but do not remain associated with the barbed-end during the subsequent elongation phase. Also, the APC was shown to synergize with Formins to promote Actin nucleation, both in mammals (mDia1) and in flies (Diaphanous)[177,219,585–588].
	Leimodin	Contains several G-Actin binding domains, namely WH2, Tmh/Ah (tropomyosin and Actin-binding helices) and LRR (leucine-rich repeat) domains, thereby mediating the assembly of a filament nucleus[589,590]. Leiomodin is expressed in skeletal, cardiac and smooth muscle and it was described to be important for sarcomere organization and cell morphology[589].
Capping Proteins Bind to the barbed ends of growing Actin filaments and have a dual impact on polymerization: (i) a negative impact, as it prevents filament elongation; and (ii) a positive role, as it increases the concentration of G-Actin monomers, thereby favouring the polymerization of uncapped filaments. Capping proteins compete for barbed-end binding with F-Actin elongation factors.	**Capping Proteins**	CPs are able to compete for barbed-end binding in its hetero-dimeric form, which is composed of α- and β-subunits. It competes for barbed-end binding with elongation factors, such as Formins and Ena/VASP and it is required for Arp2/3-mediated assembly of dendritic Actin filament networks, thus it promotes the formation of protrusions at the leading edge of a migrating cell. CPs also contribute to the assembly of cortical Actin[591,592].
	Gelsolin	Requires Ca^{2+} to act as a capping protein. Ena/VASP, an elongation factor described in detail below, is able to antagonize the capping activity of Gelsolin in vitro[591]. Gelsonin can nucleate F-Actin by binding to two Actin monomers, thereby stabilizing the Actin nuclei and preventing its severing-activity[593].
	Tensin	Large modular protein that caps Actin filaments at the FAs[274]. Tensin contributes for adhesion strengthening at the FAs[274,594–596]. It also associates with phosphorylated-Tyr residues, a trait more common in signalling molecules and this binding was proposed to contribute for Tensin's function, although conflicting data has been reported[274,596–598].
	Twinfilin	Binds to monomeric Actin and also has capping activity, with a preference for ADP-Actin. It interacts with the CPs and Actin simultaneously, and this association is important for Twinfilin's function in vivo[591]. It shows sequence homology with ADF/Cofilin domains, although it possesses no severing activity (except for yeast Twinfilin)[593].
	CapG	CapG binds reversibly to the barbed-end of Actin filaments, in a Ca^{2+}-dependent manner. It is a member of the Gelsolin family protein, however sequence divergence impaired the CapG's severing activity[599]. It is involved

		in cell motility/chemotaxis[274].
	Hip1R	Hip1R forms a complex with Cortactin and blocks Actin filament barbed-end elongation during endocytosis. In line with this, it also associates with Clathrin light chains, bridging the endocytic vesicles and the Actin cytoskeleton[274].
	Eps8	It is an auto-inhibited capping protein that is activated upon Abi1 binding. Eps8 was also shown to have crosslinking activity, especially when bound to IRSp53. It localizes along the leading edge of lamellipodia and supports filopodia formation and efficient motility of Listeria in host cells[274]. More recently, Eps8 was implicated in bleb-based motility downstream of ERK signalling[600].
Crosslinking Proteins Interact with Actin filaments and crosslink them, thereby tuning the mechanical properties of the Actin network. A key property of the crosslinker is the distance by which it can bridge two Actin filaments. This property, in turn, determines its impact on the overall network organization, thus simply: (i) short-distance crosslinkers, such as Fascin or Fimbrin, promote tight Actin bundle formation; and (ii) long-range crosslinkers, namely α-Actinin and Filamin, organize branched networks.	**α-Actinin**	An Actin-binding protein that loosely crosslinks Actin filaments in parallel or anti-parallel orientation and localizes to stress fibres, FAs and filopodia[601,602]. α-Actinin cooperates with MyoII in several processes, such as: cytokinesis, cell motility and muscle contraction[601,602] and with other Actin crosslinkers to modulate the mechanical properties of the Actin network, namely Fascin[603] and Filamin[604]. Intramolecular associations prevent α-Actinin from interacting with Actin filaments and Integrins; this inhibition in relieved upon PIP2 binding and when the molecule is under tension[601,602].
	Fimbrin	Fimbrin contains two structurally related Actin-binding sites, allowing it to crosslink Actin filaments into tight bundles *in vivo*. It was initially discovered at microvilli and stress fibres[605–607].
	Filamin	Forms Y-shaped dimers, which organize filaments into parallel or orthogonal networks, depending on the Filamin/F-Actin ratio. Filamin binds several RhoGTPases, namely Ral, Rac1, Cdc42 and RhoA and it localizes mainly to stress fibres. Filamin is also necessary for lamellipodia formation[608]. Filamin cooperates with other crosslinkers, namely α-Actinin to increase the Actin network stiffness[604]. Recently, Filamin was shown to react to shear stress[412,609].
	Fascin	Fascin contains two Actin-binding sites[610] and organizes tightly packed filament bundles usually found in filopodia, dendrites and invadopodia[611]. Fascin also promotes side-branching of Actin filaments and it can crosslink filaments without forming bundles[612]. Fascin can cooperate with α-Actinin to modulate the mechanical response of the Actin network (increased stiffness)[603].
	Villin	Crosslinker protein able to bind F-Actin in a Ca^{2+}-dependent manner. Villin is homologous to Gelsonin and it was also reported to have nucleating, capping and severing activities. The Actin modifying activities of Villin are also regulated by phosphoinositides (enhances bundling and inhibits filament capping) and by phosphorylation (inhibits filament nucleation and bundling, while enhancing filament severing). It was reported to localize to lamellipodia, filopodia and microspikes[613].
Elongation Factors Associate with the barbed ends and favour G-Actin incorporation	**Ena/VASP**	Profilin-binding, Actin assembly proteins that bind to the barbed ends of growing filaments, thus blocking capping protein binding and enhancing barbed-end growth[423,578,614]. It was suggested that Ena/VASP inhibits Arp2/3-dependent branching, thereby favouring bundled filament elongation[423,424]. This inhibition is unlikely to be direct, as adding Ena/VASP to in vitro polymerization assays in the presence of the Arp2/3 complex

directly/indirectly, by competing with capping proteins.		didn't affect F-Actin polymerization per se, rather suggesting an indirect inhibition via competition for Actin monomers[424,578]. Nevertheless, recent work showed that, in flies, Ena actually cooperates with WAVE to activate the Arp2/3 complex[425]. Thus, further work is now required to understand what is the exact contribution of Ena/VASP for Arp2/3-dependent polymerization. More recently, Ena was reported to also inhibit Formin-dependent polymerization, independently of Profilin[427]. Finally, in vitro assays showed that VASP protects growing filaments from the severing action of Gelsolin[615]. Since Ena can gather and simultaneously promote the elongation of multiple barbed-ends, it can favour the assembly/elongation of Actin bundles (in the presence of crosslinking proteins)[616], thereby rendering filaments less accessible to the action of severing proteins[593].
	Formins	Most Formins bind processively to the barbed ends of growing filaments, thereby promoting rapid elongation (especially in the presence of Profilin-bound Actin). The ability of Formins to simultaneously incorporate Actin monomers and remain associated with the barbed-end stems from the interaction between its FH1 and FH2 domains, which promotes/stabilizes the FH2 open conformation[185]. Tension on the growing filaments was recently proposed to synergize with the FH1 domain and further stabilize the open conformation required for filament elongation[398,400].
Severing Proteins Bind the lateral side of Actin filaments and cut them. Severing proteins are essential for the rapid turnover of Actin filaments, due to: (i) recycling of Actin monomers for a new round of polymerization, and (ii) severing of pre-existing filaments and subsequent exposure of new ends, where Actin monomers can be rapidly added.	**ADF/Cofilin**	Ca^{2+}-independent severing activity, resulting in an increase in the number of free ends[593]. ADF/Cofilin binds Actin filaments (preferentially ADP-bound Actin) in a cooperative manner, thus generating local stress accumulation at the boundaries of bare and ADF/Cofilin-decorated filament segments[185]. ADF/Cofilin also has depolymerizing activity, since it accelerates the dissociation of Actin subunits from the pointed ends[593]. Finally, Cofilin also acts as a de-branching enzyme due to its ability to compete with the Arp2/3 complex for filament binding[282].
	Gelsonin	In the presence of Ca^{2+} (or under low pH conditions), Gelsonin binds the side of Actin filaments (preferentially at ADP-bound Actin) and severs them. Gelsonin also caps the barbed ends[593].
	MyoII	Although it is not a classical severing protein, at high concentrations MyoII induces network disassembly[263]. The current model is that fragmentation results from filament buckling, due to MyoII-dependent contraction[185].

Table 2: Regulation of MyoII phosphorylation and dephosphorylation cycles.

MyoII Subunit:	Regulator:	Molecular Mechanism:
Regulatory Light Chain (RLC) RLC phosphorylation allows F-Actin binding, ATPase activity and minifilament assembly, thereby activating MyoII.	**ROCK** (Rho Associated Protein Kinase; known as Rok in flies)	ROCK phosphorylates MyoII in 1:1 ratio, primarily at the Ser19 and secondly at the Thr18 (in vertebrates)[617]. ROCK is an auto-inhibited kinase that is activated upon Rho, Shroom and arachinoid acid binding[617–621]. However, recent in vitro data disputed this view and showed that ROCK is rather a constitutive dimer, whose activity is not determined by membrane binding, RhoA or phosphorylation. These authors rather propose that ROCK activity is determined by the length of its coiled-coil domains[622]. ROCK phosphorylates and inhibits the Myosin-Binding Subunit (MBS) of MLCP, thereby further promoting MyoII activation[618]. ROCK also phosphorylates the LIM kinase, Adducin and the ERM proteins[618]. Importantly, aPKC and ZO1/2 are reported to inhibit ROCK junctional localization and activity, respectively[25].
	Citron Kinase	Serine/Threonine kinase that phosphorylates the RLC at both Ser19 and the Thr18 (in vertebrates), increasing the amount of di-phosphorylated MyoII. It is activated upon Rho binding[623,624]. Citron kinase activates MyoII during cytokinesis[623,625].
	MRCK (Myotonic Dystrophy-Related Cdc42 Binding Kinase)	Serine/Threonine kinase homologous to ROCK that phosphorylates MyoII RLC at Ser19 and the Thr18 (in vertebrates) and is activated upon Cdc42 binding[621]. MRCK also binds Rac1, however the functional significant of this interaction is not yet clear[626].
	MLCK (Myosin light chain kinase)	MLCK is activated by Ca^{2+}/Calmodulin and is also regulated by phosphorylation[187].
	MLCP (MLC phosphatase)	MLCP dephosphorylates the RLC, thereby negatively regulating actomyosin contractility. It is composed by three subunits, namely: the Myosin-Binding Subunit (MBS, also known as MYPT), the catalytic subunit PP1 (Protein Phosphatase Type 1) and a small non-catalytic subunit of unknown function[621]. As mentioned above, MLCP is inhibited by ROCK-dependent phosphorylation[618].
Heavy Chain (MHC) MHC phosphorylation prevents minifilament assembly, as well as its de novo assembly.	**PKC** (Protein Kinase C)	PKC phosphorylates sites at the C-terminal end of the heavy chain, in the coiled-coil and tailpiece regions of all MyoII isoforms, thereby blocking its activity[188]. It also phosphorylates RLC, rendering it a poorer substrate for MLCK, thereby decreasing MyoII activity[10].
	CSII (Casein Kinase II)	CSII is typically found in tetrameric complexes consisting of two catalytic α or α‘ subunits and two additional regulatory β subunits, which possess Serine/Threonine kinase activity[627]. CSII phosphorylates sites at the C-terminal end of the heavy chain, in the coiled-coil and tailpiece regions of all MyoII isoforms, thereby inhibiting MyoII[188].

Table 3: Summary of the main Nucleation Promoting Factor (NPFs) involved in Arp2/3 complex activation.

NPF Class:	NPF:	Molecular Mechanism:	Cellular Function:
Class I Contain a WCA domain that mediates Arp2/3 binding and WH2 motifs, required for Actin monomer binding.	**WASP** (Wiskott-Aldrich Syndrome Protein)	Composed of an N-terminal WASP Homology 1 domain (WH1), a Cdc42 and Rac interactive binding (CRIB), auto-inhibitory motifs – GTPase-binding domain (GBD) and a Pro-rich domain (PRD) adjacent to its WCA domain. WASP is intrinsically inactive due to intramolecular interactions with the GBD and binding of WH1-interActing proteins, such as WASP-interacting protein (WIP). WASP is activated by the cooperative actions of Rho family GTPases (Rac and Cdc42) and PIP2, thereby promoting its interaction with the Arp2/3 complex[217,218].	Clathrin-dependent endocytosis[140,141,628], Filopodia formation, phagocytosis and T-cell signalling[218], AJs integrity[629]
	Scar/WAVE (WASP-Family Verprolin Homologue)	Scar/WAVE complex are constitutively active, as they lack the GBD region (see above). Nevertheless, it is kept inactive by association with the WAVE Regulatory Complex (WRC). GTP-Rac1 and PIP2 favour Scar/WAVE activation, by releasing it from WRC binding[217,218].	Cell migration[218,425,630], Endocytosis[628,631], AJs integrity[563,632]
	WASH (WASP and SCAR Homologue)	WASH has the classical modular domain organization of type I NPFs (see above). Similarly to the WAVE complex, WASH is maintained in an inhibited state by a pentameric complex composed of Fam21, Strumpellin, SWIP and Ccdc53. WASH also interacts with microtubules and the Actin nucleator Spire[584,629].	Endosome trafficking and sorting[584]
	WHAMM (WASP Homologue Associated with Actin, Membranes and Microtubules)	Contains WCA domains, containing two WH2 motifs, adjacent poly-proline motifs and a central region predicted to form coiled coils and it seems to be present exclusively in vertebrates. WHAMM is a less potent Arp2/3 activator than WASP, but it seems to be a constitutively active NPF[218,584].	Anterograde transport ER-Golgi[218,584], Autophagy[633]
	JMY (Junction-Mediating Regulatory Protein)	JMY is present exclusively in vertebrates and it is composed of WCA domains, adjacent poly-proline motifs and a predicted coiled-coil domain. However, it contains three WH2 domains, one of which can also nucleate filaments without Arp2/3 binding[218,584].	Cell motility, Transcriptional regulation (e.g. E-Cad)[218,584]
Class II Contain acidic peptides at their N-terminus mediating Arp2/3-binding, but lack	**Cortactin**	Cortactin enhances WASP-mediated activation of the Arp2/3 complex. Cortactin also inhibits spontaneous dissociation of Arp2/3-bound filament branch junctions in vitro, thereby stabilizing Y-branches[217,218].	Endocytosis, trans-Golgi export, phagocytosis, AJs integrity[634,635], cell migration[217,218,629,636]

WH2 domains required for G-Actin binding. Instead, they harbour repetitive sequences that interact with F-Actin. Class II NPFs are less potent Arp2/3 activators.	**Coronin**	Only direct inhibitor of the Arp2/3 complex. Coronin also binds F-actin and prevents de novo Actin assembly. It also possesses debranching activity, by directly displacing the Arp2/3 from Y-branches[218].	Cell migration[218]

Table 4: Main classes of Formins and a summary of their regulation and biological functions.

Classes of Formins: *Based on FH2 sequence divergence.	**Molecular Mechanism:**	**Functions:**
DRFs (Diaphanous-Related Formins)	As described in the main text, DRFs exist in an autoinhibited state mediated by intramolecular interactions between the DID and DAD domains. RhoA contributes for DRFs activation.	Cytokinesis, cell migration, AJs and FAs integrity
FRLs (Formin-Related Proteins in Leucocytes)	FRLs also exist in an autoinhibited conformation due to intramolecular interaction (except for FRL3 that is constitutively active). In an analogous manner to RhoA, Cdc42 can partially activate FRLs. Interestingly, the FH1–FH2 and DAD domains of FRL1 also possesses severing activity[218,637].	Phagocytosis
DAAMs (Dishevelled-Associated Activators of Morphogenesis)	DAAMs also exist in an inhibited conformation. RhoA, RhoB, RhoC or Dishevelled binding can activate DAAMs[218,637].	Non-canonical Wnt signalling (PCP)
FHODs (Formin Homology Domain Proteins)	Less is known about FHODs regulation, but, at least, FHOD1 is autoinhibited by interactions between its C-terminal DAD and the divergent N terminus[218]. FHOD1 function in vivo depends on RhoA, ROCK1 and possibly Rac1. Importantly, ROCK phosphorylates and activates FHOD1, thereby promoting stress fibre assembly[638,639].	Stress fibre assembly
FMNs (Formins)	FMN1 and FMN2 seem to play different functions in vivo; FMN1 mutant mice show defective FAs and cell migration, while FMN2 was implicated in meiotic spindle positioning[640,641]. FMN1 and 2 interact with Spire, a tandem-monomer Actin nucleator[637].	Cell migration, FAs integrity
INFs (Inverted Formins)	INFs do not exhibit significant sequence similarity with other Formins outside of their FH1-FH2 module, which is inverted. It is still unclear whether IFNs retain or not Actin nucleation activity. INF1 is involved in stress fibre formation, while INF2 exhibits both Actin nucleation and severing activities[218].	Stress fibre assembly

Table 5: The Polarity complexes position the intercellular junctions and organize the plasma membrane into distinct domains.

Polarity Domain:	Polarity Domain Composition:	Molecular Mechanism:
Supra-apical Localizes at the apical most part of the cell, above the AJs.	**Crumbs Complex** Crumbs (Crb in flies, CRB1-3 in mammals), Stardust (Sdt in flies, PALS1/MPP5 in mammals), PatJ (Pals1-associated tight junction protein) and Lin7	The Crb complex is the critical determinant of apical identity, both in Drosophila and in vertebrates, at least partly by recruiting Moesin and β_H-Spectrin, which are important organizers of the apical actomyosin cytoskeleton. In vertebrates, this complex is a crucial determinant of TJs formation by interacting with and recruiting several TJ-associated proteins. Additionally, the Crb complex also contributes to AJs positioning (described below)[19]. aPKC, a member of the Par complex, phosphorylates Crb and this was proposed to contribute to set apical identity, although a subsequent study did not confirm these findings[642,643].
Apical	**Par (Partition Defective) Complex** Bazooka (Baz in flies and Par-3 in mammals), Par-6, aPKC (Atypical Protein Kinase C) and Cdc42	The Par complex association is context-dependent, as it is determined by the maturation status ot the epithelial tissue. In mature epithelia, Par-6 and aPKC associate with the Crb complex, and are found at the apical domain and the apical most part of the lateral domain, just above the AJs[644]. In contrast, Baz is found at the level of the AJs, where it determines it's assembly and positioning by: (i) associating with AJ components, such as Echinoid and Armadillo in Drosophila and Nectin-1/-3 in mammals[13]; and, by (ii) regulating the actomyosin cytoskeleton organization via: the small GTPase Rac[124], Moesin recruitment[154] and by regulating phosphoinositide levels[149,150] at the apical domain.
Basal-lateral	**Lgl Complex** Lgl (Lethal giant larvae), Dlg (Discs large), Scribble (Scrib) and Par-1 (MARKs in mammals)	These proteins are critical to define the basal-lateral domain of epithelial cells and to restrict the size of the apical and junctional domains[9]. Par-1 directly phosphorylates Baz, thereby inhibiting its membrane association and preventing the expansion of the apical junction towards the lateral domain[645]. Conversely, Lgl and Par-1 are phosphorylated by aPKC, thereby preventing their accumulation at the apical domain. Yrt acts as an upstream negative regulator of Crb activity upon apical membrane formation[9].
	Yrt/Cora Yurt (Yrt), Coracle (Cora), Na^+, K^+-ATPase and Neurexin IV (Nrx-IV)	

*The polarity proteins antagonize each other, thereby restricting their respective membrane domains[644]. To provide an example, I will briefly describe the mechanism underlying Baz junctional localization. At the apical domain, the exclusion of Baz requires both aPKC and Crb. aPKC phosphorylates Baz and this phosphorylation significantly weakens its interaction with Sdt and aPKC itself, allowing it to dissociate from the apical domain[646–649]. The complete dissociation of Baz from the apical domain also relies on the presence of Crb, which out-competes Baz for the binding to Par-6, thus excluding it from the apical domain[648].

REFERENCES:

1. Herszterg, S., Leibfried, A., Bosveld, F., Martin, C. & Bellaïche, Y. Interplay between the Dividing Cell and Its Neighbors Regulates Adherens Junction Formation during Cytokinesis in Epithelial Tissue. Dev. Cell **24,** 256–270 (2013).

2. Founounou, N., Loyer, N. & Le Borgne, R. Septins Regulate the Contractility of the Actomyosin Ring to Enable Adherens Junction Remodeling during Cytokinesis of Epithelial Cells. Dev. Cell **24,** 242–255 (2013).

3. Guillot, C. & Lecuit, T. Adhesion Disengagement Uncouples Intrinsic and Extrinsic Forces to Drive Cytokinesis in Epithelial Tissues. Dev. Cell **24,** 227–241 (2013).

4. Morais-de-Sá, E. & Sunkel, C. Adherens junctions determine the apical position of the midbody during follicular epithelial cell division. EMBO Rep. **14,** 696–703 (2013).

5. Firmino, J., Rocancourt, D., Saadaoui, M., Moreau, C. & Gros, J. Cell Division Drives Epithelial Cell Rearrangements during Gastrulation in Chick. Dev. Cell **36,** 249–261 (2016).

6. Higashi, T., Arnold, T. R., Stephenson, R. E., Dinshaw, K. M. & Miller, A. L. Maintenance of the Epithelial Barrier and Remodeling of Cell-Cell Junctions during Cytokinesis. Curr. Biol. **16,** 185–192 (2016).

7. Hoffman, B. D. & Yap, A. S. Towards a Dynamic Understanding of Cadherin- Based Mechanobiology. Trends Cell Biol. **25,** 803 – 814 (2015).

8. McCaffrey, L. M. & Macara, I. G. Epithelial organization, cell polarity and tumorigenesis. Trends Cell Biol. **21,** 727–735 (2011).

9. Tepass, U. The apical polarity protein network in Drosophila epithelial cells: regulation of polarity, junctions, morphogenesis, cell growth, and survival. Annu. Rev. Cell Dev. Biol. **28,** 655–85 (2012).

10. Vicente-Manzanares, M., Ma, X., Adelstein, R. S. & Horwitz, A. R. Non-muscle myosin II takes centre stage in cell adhesion and migration. Nat. Rev. Mol. Cell Biol. **10,** 778–790 (2009).

11. Heisenberg, C.-P. & Bellaïche, Y. Forces in tissue morphogenesis and patterning. Cell **153,** 948–62 (2013).

12. Munjal, A. & Lecuit, T. Actomyosin networks and tissue morphogenesis. Development **141,** 1789–93 (2014).

13. St Johnston, D. & Sanson, B. Epithelial polarity and morphogenesis. Curr. Opin. Cell Biol. **23,** 540–546 (2011).

14. Müsch, A. Microtubule organization and function in epithelial cells. Traffic **5,** 1–9 (2004).

15. Meng, W. & Takeichi, M. Adherens Junction: Molecular Architecture and Regulation. Cold Spring Harb. Perspect. BilogyPerspectives **120,** 1–14 (2014).

16. Farquhar, M. G. & Palade, G. E. Junctional Complexes in various Epithelia. J. Cell Biol. **17,** 375–412 (1963).

17. Balda, M. S. & Matter, K. Tight junctions as regulators of tissue remodelling. Curr. Opin. Cell Biol. **42,** 94–101 (2016).

18. Niessen, C. M. Tight junctions/adherens junctions: basic structure and function. Jounal Investig. Dermatology **127,** 2525–2532 (2007).

19. St Johnston, D. & Ahringer, J. Cell polarity in eggs and epithelia: Parallels and diversity. Cell **141,** 757–774 (2010).

20. Niessen, C. M., Leckband, D. E. & Yap, A. S. Tissue organization by cadherin adhesion molecules: dynamic molecular and cellular mechanisms of morphogenetic regulation. Physiol. Rev. **91,** 691–731 (2011).

21. Broussard, J. A. Desmosome regulation and signaling in disease. Cell Tissue Res. **360,** 37–54 (2015).

22. Tepass, U. & Tanentzapf, G. Epithelial Cell Polarity and Cell Junctions in drosophila. Annu. Rev. Genet. **35,** 747–784 (2001).

23. Yonemura, S. Cadherin-actin interactions at adherens junctions. Curr. Opin. Cell Biol. **23,** 515–522 (2011).

24. Twiss, F. & De Rooij, J. Cadherin mechanotransduction in tissue remodeling. Cell. Mol. Life Sci. **70,** 4101–4116 (2013).

25. Takeichi, M. Dynamic contacts: rearranging adherens junctions to drive epithelial remodelling. Nat. Rev. Mol. Cell Biol. **15,** 397–410 (2014).

26. Coopman, P. & Djiane, A. Adherens Junction and E-Cadherin complex regulation by epithelial polarity. Cell. Mol. Life Sci. 1–19 (2016). doi:10.1007/s00018-016-2260-8

27. Leckband, D. E. & de Rooij, J. Cadherin adhesion and mechanotransduction. Annu. Rev. Cell Dev. Biol. **30,** 291–315 (2014).

28. Harrison, O. J. et al. Two-step adhesive binding by classical cadherins. Nat. Struct. Mol. Biol. **17,** 348–57 (2010).

29. Hong, S., Troyanovsky, R. B. & Troyanovsky, S. M. Cadherin exits the junction by switching its adhesive bond. J. Cell Biol. **192,** 1073–1083 (2011).

30. Leckband, D. & Sivasankar, S. Cadherin recognition and adhesion. Curr. Opin. Cell Biol. **24,** 620–627 (2012).

31. Ciatto, C. et al. T-cadherin structures reveal a novel adhesive binding mechanism. Nat. Struct. Mol. Biol. **17,** 339–347 (2010).

32. Harrison, O. J. et al. The extracellular architecture of adherens junctions revealed by crystal structures of type i cadherins. Structure **19,** 244–256 (2011).

33. Wu, Y., Vendome, J., Shapiro, L., Ben-Shaul, A. & Honig, B. Transforming binding affinities from three dimensions to two with application to cadherin clustering. Nature **475,** 510–3 (2011).

34. Chen, Y. T., Stewart, D. B. & Nelson, W. J. Coupling assembly of the E-cadherin/α-catenin complex to efficient endoplasmic reticulum exit and basal-lateral membrane targeting of E-cadherin in polarized MDCK cells. J. Cell Biol. **144,** 687–699 (1999).

35. Bajpai, S. et al. α-Catenin mediates initial E-cadherin-dependent cell-cell recognition and subsequent bond strengthening. Proc. Natl. Acad. Sci. U. S. A. **105,** 18331–18336 (2008).

36. Pacquelet, A. & Rørth, P. Regulatory mechanisms required for DE-cadherin function in cell migration and other types of adhesion. J. Cell Biol. **170,** 803–812 (2005).

37. Sarpal, R. et al. Mutational analysis supports a core role for Drosophila alpha-Catenin in adherens junction function. J. Cell Sci. **125,** 233–245 (2012).

38. Desai, R. et al. Monomeric α-catenin links cadherin to the actin cytoskeleton. Nat. Cell Biol. **15,** 261–73 (2013).

39. Bianchini, J. M. et al. Reevaluating αE-catenin monomer and homodimer functions by characterizing

E-cadherin/αE-catenin chimeras. J. Cell Biol. **210,** 1065–1074 (2015).

40. Gorfinkiel, N. & Arias, A. M. Requirements for adherens junction components in the interaction between epithelial tissues during dorsal closure in Drosophila. J. Cell Sci. **120,** 3289–98 (2007).

41. Peng, X., Cuff, L. E., Lawton, C. D. & DeMali, K. A. Vinculin regulates cell-surface E-cadherin expression by binding to beta-catenin. J. Cell Sci. **123,** 567–577 (2010).

42. Rhee, J., Buchan, T., Zukerberg, L., Lilien, J. & Balsamo, J. Cables links Robo-bound Abl kinase to N-cadherin-bound beta-catenin to mediate Slit-induced modulation of adhesion and transcription. Nat. Cell Biol. **9,** 883–892 (2007).

43. Langevin, J. et al. Drosophila exocyst components sec5, sec6, and Sec15 regulate DE-Cadherin trafficking from recycling endosomes to the plasma membrane. Dev. Cell **9,** 365–376 (2005).

44. Ligon, L. A., Karki, S., Tokito, M. & Holzbaur, E. L. F. Dynein binds to beta-catenin and may tether microtubules at adherens junctions. Nat. Cell Biol. **3,** 913–917 (2001).

45. Ligon, L. A. & Holzbaur, E. L. F. Microtubules tethered at eepithelial cell junctions by dynein facilitate efficient junction assembly. Traffic **8,** 808–819 (2007).

46. Shibamoto, S. et al. Association of p120, a tyrosine kinase substrate, with E- cadherin/catenin complexes. J. Cell Biol. **128,** 949–957 (1995).

47. Ireton, R. C. et al. A novel role for p120 catenin in E-cadherin function. J. Cell Biol. **159,** 465–476 (2002).

48. Davis, M. A., Ireton, R. C. & Reynolds, A. B. A core function for p120-catenin in cadherin turnover. J. Cell Biol. **163,** 525–534 (2003).

49. Xiao, K. et al. Cellular levels of p120 catenin function as a set point for cadherin expression levels in microvascular endothelial cells. J. Cell Biol. **163,** 535–545 (2003).

50. Xiao, K. et al. p120-Catenin Regulates Clathrin-dependent Endocytosis of VE-Cadherin. Mol. Biol. Cell **16,** 5141–5151 (2005).

51. Miyashita, Y. & Ozawa, M. A dileucine motif in its cytoplasmic domain directs beta-catenin-uncoupled E-cadherin to the lysosome. J. Cell Sci. **120,** 4395–4406 (2007).

52. Ishiyama, N. et al. Dynamic and Static Interactions between p120 Catenin and E-Cadherin Regulate the Stability of Cell-Cell Adhesion. Cell **141,** 117–128 (2010).

53. Nanes, B. A. et al. P120-Catenin Binding Masks an Endocytic Signal Conserved in Classical Cadherins. J. Cell Biol. **199,** 365–380 (2012).

54. Troyanovsky, R. B., Klingelhofer, J. & Troyanovsky, S. M. Ahpa-Catenin contributes to the strength of E-cadherin-p120 interactions. Mol. Biol. Cell **22,** 4247–4255 (2011).

55. Chen, X., Kojima, S. I., Borisy, G. G. & Green, K. J. P120 Catenin Associates With Kinesin and Facilitates the Transport of Cadherin-Catenin Complexes To Intercellular Junctions. J. Cell Biol. **163,** 547–557 (2003).

56. Meng, W., Mushika, Y., Ichii, T. & Takeichi, M. Anchorage of Microtubule Minus Ends to Adherens Junctions Regulates Epithelial Cell-Cell Contacts. Cell **135,** 948–959 (2008).

57. Shahbazi, M. N. et al. CLASP2 interacts with p120-catenin and governs microtubule dynamics at adherens junctions. J. Cell Biol. **203,** 1043–1061 (2013).

58. Magie, C. R., Pinto-Santini, D. & Parkhurst, S. M. Adherens junction components in Drosophila. Development **129,** 3771–3782 (2002).

59. Fox, D. T. et al. Rho1 regulates Drosophila adherens junctions independently of p120ctn.

Development **132,** 4819–4831 (2005).

60. Reynolds, A. B. p120-catenin: Past and present. Biochim. Biophys. Acta - Mol. Cell Res. **1773,** 2–7 (2007).

61. Yu, H. H., Dohn, M. R., Markham, N. O., Coffey, R. J. & Reynolds, A. B. p120-catenin controls contractility along the vertical axis of epithelial lateral membranes. J. Cell Sci. **129,** 80–94 (2015).

62. Wildenberg, G. A. et al. p120-Catenin and p190RhoGAP Regulate Cell-Cell Adhesion by Coordinating Antagonism between Rac and Rho. Cell **127,** 1027–1039 (2006).

63. Tian, Y. et al. Interaction of p190RhoGAP with C-terminal domain of p120-catenin modulates endothelial cytoskeleton and permeability. J. Biol. Chem. **288,** 18290–18299 (2013).

64. Myster, S. H., Cavallo, R., Anderson, C. T., Fox, D. T. & Peifer, M. Drosophila p120 catenin plays a supporting role in cell adhesion but is not an essential adherens junction component. J. Cell Biol. **160,** 433–449 (2003).

65. Pacquelet, A., Lin, L. & Rørth, P. Binding site for p120/δ-catenin is not required for Drosophila E-cadherin function in vivo. J. Cell Biol. **160,** 313–319 (2003).

66. Pettitt, J., Cox, E. A., Broadbent, I. D., Flett, A. & Hardin, J. The Caenorhabditis elegans p120 catenin homologue, JAC-1, modulates cadherin-catenin function during epidermal morphogenesis. J. Cell Biol. **162,** 15–22 (2003).

67. Bulgakova, N. A. & Brown, N. H. Drosophila p120catenin is critical for endocytosis of the dynamic E-cadherin-Bazooka complex. J. Cell Sci. **129,** 477–482 (2016).

68. Drees, F., Pokutta, S., Yamada, S., Nelson, W. J. & Weis, W. I. α-catenin is a molecular switch that binds E-cadherin-α-catenin and regulates actin-filament assembly. Cell **123,** 903–915 (2005).

69. Yamada, S., Pokutta, S., Drees, F., Weis, W. I. & Nelson, W. J. Deconstructing the cadherin-catenin-actin complex. Cell **123,** 889–901 (2005).

70. Buckley, C. D. et al. The minimal cadherin-catenin complex binds to actin filaments under force. Science (80-.). **346,** 1254211–8 (2014).

71. Imamura, Y., Itoh, M., Maeno, Y., Tsukita, S. & Nagafuchi, A. Functional domains of α-catenin required for the strong state of cadherin-based adhesion. J. Cell Biol. **144,** 1311–1322 (1999).

72. Tang, V. W. & Brieher, W. M. α-Actinin-4/FSGS1 is required for Arp2/3-dependent actin assembly at the adherens junction. J. Cell Biol. **196,** 115–130 (2012).

73. Abe, K. & Takeichi, M. EPLIN mediates linkage of the cadherin catenin complex to F-actin and stabilizes the circumferential actin belt. Proc. Natl. Acad. Sci. U. S. A. **105,** 13–19 (2008).

74. Taguchi, K., Ishiuchi, T. & Takeichi, M. Mechanosensitive EPLIN-dependent remodeling of adherens junctions regulates epithelial reshaping. J. Cell Biol. **194,** 643–656 (2011).

75. Takai, Y., Miyoshi, J., Ikeda, W. & Ogita, H. Nectins and nectin-like molecules: roles in contact inhibition of cell movement and proliferation. Nat. Rev. Mol. Cell Biol. **9,** 603–15 (2008).

76. Mandai, K., Rikitake, Y., Shimono, Y. & Takai, Y. Afadin/AF-6 and canoe: Roles in cell adhesion and beyond. Progress in Molecular Biology and Translational Science **116,** (Elsevier Inc., 2013).

77. Tachibana, K. et al. Two cell adhesion molecules, nectin and cadherin, interact through their cytoplasmic domain-associated proteins. J. Cell Biol. **150,** 1161–1175 (2000).

78. Honda, T. et al. Antagonistic and agonistic effects of an extracellular fragment of nectin on formation of E-cadherin-based cell-cell adhesion. Genes to Cells **8,** 51–63 (2003).

79. Kurita, S., Ogita, H. & Takai, Y. Cooperative role of nectin-nectin and nectin-afadin interactions in

formation of nectin-based cell-cell adhesion. J. Biol. Chem. **286,** 36297–36303 (2011).

80. Zhadanov, A. B. et al. Absence of the tight junctional protein AF-6 disrupts epithelial cell-cell junctions and cell polarity during mouse development. Curr. Biol. **9,** 880–888 (1999).

81. Ikeda, W. et al. Afadin: A key molecule essential for structural organization of cell- cell junctions of polarized epithelia during embryogenesis. J. Cell Biol. **146,** 1117–1131 (1999).

82. Wei, S. Y. et al. Echinoid is a component of adherens junctions that cooperates with DE-cadherin to mediate cell adhesion. Dev. Cell **8,** 493–504 (2005).

83. Islam, R., Wei, S.-Y., Chiu, W.-H., Hortsch, M. & Hsu, J.-C. Neuroglian activates Echinoid to antagonize the Drosophila EGF receptor signaling pathway. Development **130,** 2051–2059 (2003).

84. Sawyer, J. K., Harris, N. J., Slep, K. C., Gaul, U. & Peifer, M. The Drosophila afadin homologue Canoe regulates linkage of the actin cytoskeleton to adherens junctions during apical constriction. J. Cell Biol. **186,** 57–73 (2009).

85. Laplante, C. & Nilson, L. A. Differential expression of the adhesion molecule Echinoid drives epithelial morphogenesis in Drosophila. Development **133,** 3255–64 (2006).

86. Sawyer, J. K. et al. A contractile actomyosin network linked to adherens junctions by Canoe/afadin helps drive convergent extension. Mol. Biol. Cell **22,** 2491–508 (2011).

87. Takahashi, K., Matsuo, T., Katsube, T., Ueda, R. & Yamamoto, D. Direct binding between two PDZ domain proteins canoe and ZO-1 and their roles in regulation of the Jun N-terminal kinase pathway in Drosophila morphogenesis. Mech. Dev. **78,** 97–111 (1998).

88. Boettner, B. et al. The AF-6 homolog canoe acts as a Rap1 effector during dorsal closure of the Drosophila embryo. Genetics **165,** 159–169 (2003).

89. Kurita, S., Yamada, T., Rikitsu, E., Ikeda, W. & Takai, Y. Binding between the junctional proteins afadin and PLEKHA7 and implication in the formation of adherens junction in epithelial cells. J. Biol. Chem. **288,** 29356–29368 (2013).

90. Sopko, R. & McNeill, H. The skinny on Fat: an enormous cadherin that regulates cell adhesion, tissue growth, and planar cell polarity. Curr. Opin. Cell Biol. **21,** 717–723 (2009).

91. Chen, X. & Gumbiner, B. M. Crosstalk between different adhesion molecules. Curr. Opin. Cell Biol. **18,** 572–578 (2006).

92. Morishita, H. & Yagi, T. Protocadherin family: diversity, structure, and function. Curr. Opin. Cell Biol. **19,** 584–592 (2007).

93. Chen, X. & Gumbiner, B. M. Paraxial protocadherin mediates cell sorting and tissue morphogenesis by regulating C-cadherin adhesion activity. J. Cell Biol. **174,** 301–313 (2006).

94. Yasuda, S. et al. Activity-Induced Protocadherin Arcadlin Regulates Dendritic Spine Number by Triggering N-Cadherin Endocytosis via TAO2β and p38 MAP Kinases. Neuron **56,** 456–471 (2007).

95. Emond, M. R., Biswas, S., Blevins, C. J. & Jontes, J. D. A complex of protocadherin-19 and n-cadherin mediates a novel mechanism of cell adhesion. J. Cell Biol. **195,** 1115–1121 (2011).

96. Vasioukhin, V., Bauer, C., Yin, M. & Fuchs, E. Directed actin polymerization is the driving force for epithelial cell-cell adhesion. Cell **100,** 209–219 (2000).

97. Hong, S., Troyanovsky, R. B. & Troyanovsky, S. M. Spontaneous assembly and active disassembly balance adherens junction homeostasis. Proc. Natl. Acad. Sci. U. S. A. **107,** 3528–3533 (2010).

98. Wu, Y., Kanchanawong, P. & Zaidel-bar, R. Actin-delimited adhesion-independent clustering of E-Cadherin Forms the Nanoscale Building Blocks of Adherens Junctions. Dev. Cell **32,** 1–16 (2015).

99. Truong Quang, B. A., Mani, M., Markova, O., Lecuit, T. & Lenne, P.-F. Principles of E-cadherin supramolecular organization in vivo. Curr. Biol. **23,** 2197–2207 (2013).

100. Strale, P. O. et al. The formation of ordered nanoclusters controls cadherin anchoring to actin and cell-cell contact fluidity. J. Cell Biol. **210,** 333–346 (2015).

101. Zhang, Y., Sivasankar, S., Nelson, W. J. & Chu, S. Resolving cadherin interactions and binding cooperativity at the single-molecule level. Proc. Natl. Acad. Sci. U. S. A. **106,** 109–114 (2009).

102. Hong, S., Troyanovsky, R. B. & Troyanovsky, S. M. Binding to F-actin guides cadherin cluster assembly, stability, and movement. J. Cell Biol. **201,** 131–143 (2013).

103. Cavey, M., Rauzi, M., Lenne, P.-F. & Lecuit, T. A two-tiered mechanism for stabilization and immobilization of E-cadherin. Nature **453,** 751–756 (2008).

104. Yap, A. S., Gomez, G. A. & Parton, R. G. Adherens Junctions Revisualized: Organizing Cadherins as Nanoassemblies. Dev. Cell **35,** 12–20 (2015).

105. Wu, S. K. et al. Cortical F-actin stabilization generates apical-lateral patterns of junctional contractility that integrate cells into epithelia. Nat. Cell Biol. **16,** 167–78 (2014).

106. Levayer, R., Pelissier-Monier, A. & Lecuit, T. Spatial regulation of Dia and Myosin-II by RhoGEF2 controls initiation of E-cadherin endocytosis during epithelial morphogenesis. Nat. Cell Biol. **13,** 529–40 (2011).

107. Indra, I., Troyanovsky, R. & Troyanovsky, S. M. Afadin controls cadherin cluster stability using clathrin-independent mechanism. Tissue barriers **2,** e28687 (2014).

108. Tybulewicz, V. L. J. & Henderson, R. B. Rho family GTPases and their regulators in lymphocytes. Nat. Rev. Immunol. **9,** 630–644 (2009).

109. Sit, S.-T. & Manser, E. Rho GTPases and their role in organizing the actin cytoskeleton. J. Cell Sci. **124,** 679–683 (2011).

110. Yamada, S. & Nelson, W. J. Localized zones of Rho and Rac activities drive initiation and expansion of epithelial cell-cell adhesion. J. Cell Biol. **178,** 517–527 (2007).

111. Ratheesh, A. et al. Centralspindlin and α-catenin regulate Rho signalling at the epithelial zonula adherens. Nat. Cell Biol. **14,** 818–828 (2012).

112. Terry, S. J. et al. Spatially restricted activation of RhoA signalling at epithelial junctions by p114RhoGEF drives junction formation and morphogenesis. Nat. Cell Biol. **13,** 159–66 (2011).

113. Knox, A. L. & Brown, N. H. Rap1 GTPase Regulation of Adherens Junction Positioning and Cell Adhesion. Science (80-.). **295,** 1285–1288 (2002).

114. Collinet, C. & Lecuit, T. Stability and dynamics of cell-cell junctions. Progress in Molecular Biology and Translational Science **116,** (Elsevier Inc., 2013).

115. Braga, V. M., Betson, M., Li, X. & Lamarche-Vane, N. Activation of the small GTPase Rac is sufficient to disrupt cadherin-dependent cell-cell adhesion in normal human keratinocytes. Mol. Biol. Cell **11,** 3703–21 (2000).

116. Zandy, N. L., Playford, M. & Pendergast, A. M. Abl tyrosine kinases regulate cell-cell adhesion through Rho GTPases. Proc. Natl. Acad. Sci. U. S. A. **104,** 17686–91 (2007).

117. Yamazaki, D., Oikawa, T. & Takenawa, T. Rac-WAVE-mediated actin reorganization is required for organization and maintenance of cell-cell adhesion. J. Cell Sci. **120,** 86–100 (2007).

118. Lampugnani, M. G. et al. VE-Cadherin Regulates Endothelial Actin Activating Rac and Increasing Membrane Association of Tiam. Mol. Biol. Cell **13,** 1175–1189 (2002).

119. Malliri, A., Van Es, S., Huveneers, S. & Collard, J. G. The Rac exchange factor Tiam1 is required for the establishment and maintenance of cadherin-based adhesions. J. Biol. Chem. **279,** 30092–30098 (2004).

120. Kraemer, A., Goodwin, M., Verma, S., Yap, A. S. & Ali, R. G. Rac is a dominant regulator of cadherin-directed actin assembly that is activated by adhesive ligation independently of Tiam1. Am. J. Physiol. Cell Physiol. **292,** C1061–9 (2007).

121. Kitt, K. N. & Nelson, W. J. Rapid suppression of activated rac1 by cadherins and nectins during De Novo cell-cell adhesion. PLoS One **6,** e17841 (2011).

122. Marie, H. et al. The LIM protein ajuba is recruited to cadherin-dependent cell junctions through an association with α-catenin. J. Biol. Chem. **278,** 1220–1228 (2003).

123. Nola, S. et al. Ajuba is required for Rac activation and maintenance of E-cadherin adhesion. J. Cell Biol. **195,** 855–871 (2011).

124. Chen, X. & Macara, I. G. Par-3 controls tight junction assembly through the Rac exchange factor Tiam1. Nat. Cell Biol. **7,** 262–269 (2005).

125. Bustos, R. I., Forget, M. A., Settleman, J. E. & Hansen, S. H. Coordination of Rho and Rac GTPase Function via p190B RhoGAP. Curr. Biol. **18,** 1606–1611 (2008).

126. Delanoe-Ayari, H., Kurdi, R. Al, Vallade, M., Gulino-Debrac, D. & Riveline, D. Membrane and acto-myosin tension promote clustering of adhesion proteins. PNAS **101,** 2229–2234 (2004).

127. Shewan, A. M. et al. Myosin 2 Is a Key Rho Kinase Target Necessary for the Local Concentration of E-Cadherin at Cell–Cell Contacts. Mol. Biol. Cell **14,** 4531–4542 (2005).

128. Miyake, Y. et al. Actomyosin tension is required for correct recruitment of adherens junction components and zonula occludens formation. Exp. Cell Res. **312,** 1637–1650 (2006).

129. le Duc, Q. et al. Vinculin potentiates E-cadherin mechanosensing and is recruited to actin-anchored sites within adherens junctions in a myosin II-dependent manner. J. Cell Biol. **189,** 1107–1115 (2010).

130. Smutny, M. et al. Myosin II isoforms identify distinct functional modules that support integrity of the epithelial zonula adherens. Nat. Cell Biol. **12,** 696–702 (2010).

131. Yonemura, S., Wada, Y., Watanabe, T., Nagafuchi, A. & Shibata, M. α-Catenin as a tension transducer that induces adherens junction development. Nat. Cell Biol. **12,** 533–42 (2010).

132. Twiss, F. et al. Vinculin-dependent Cadherin mechanosensing regulates efficient epithelial barrier formation. Biol. Open **1,** 1128–1140 (2012).

133. Sen, A., Nagy-Zsver-Vadas, Z. & Krahn, M. P. Drosophila PATJ supports adherens junction stability by modulating Myosin light chain activity. J. Cell Biol. **199,** 685–698 (2012).

134. Choi, W. et al. Remodeling the zonula adherens in response to tension and the role of afadin in this response. J. Cell Biol. **213,** 243–260 (2016).

135. Kim, S. H., Li, Z. & Sacks, D. B. E-cadherin-mediated cell-cell attachment activates Cdc42. J. Biol. Chem. **275,** 36999–37005 (2000).

136. Wang, B., Wylie, F. G., Teasdale, R. D. & Stow, J. L. Polarized trafficking of E-cadherin is regulated by Rac1 and Cdc42 in Madin-Darby canine kidney cells. Am. J. Physiol. Cell Physiol. **288,** C1411–9 (2005).

137. Izumi, G. et al. Endocytosis of E-cadherin regulated by Rac and Cdc42 small G proteins through IQGAP1 and actin filaments. J. Cell Biol. **166,** 237–248 (2004).

138. Nakagawa, M., Fukata, M., Yamaga, M., Itoh, N. & Kaibuchi, K. Recruitment and activation of Rac1 by the formation of E-cadherin-mediated cell-cell adhesion sites. J. Cell Sci. **114,** 1829–38 (2001).

139. Frasa, M. a M. et al. Armus is a Rac1 effector that inactivates Rab7 and regulates E-cadherin degradation. Curr. Biol. **20,** 198–208 (2010).

140. Georgiou, M., Marinari, E., Burden, J. & Baum, B. Cdc42, Par6, and aPKC Regulate Arp2/3-Mediated Endocytosis to Control Local Adherens Junction Stability. Curr. Biol. **18,** 1631–1638 (2008).

141. Leibfried, A., Fricke, R., Morgan, M. J., Bogdan, S. & Bellaïche, Y. Drosophila Cip4 and WASp Define a Branch of the Cdc42-Par6-aPKC Pathway Regulating E-Cadherin Endocytosis. Curr. Biol. **18,** 1639–1648 (2008).

142. Harris, K. P. & Tepass, U. Cdc42 and Par proteins stabilize dynamic adherens junctions in the Drosophila neuroectoderm through regulation of apical endocytosis. J. Cell Biol. **183,** 1129–1143 (2008).

143. Hogan, C. et al. Rap1 Regulates the Formation of E-Cadherin-Based Cell-Cell Contacts. Mol. Cell. Biol. **24,** 6690–6700 (2004).

144. Dubé, N. et al. The RapGEF PDZ-GEF2 is required for maturation of cell-cell junctions. Cell. Signal. **20,** 1608–1615 (2008).

145. Price, L. S. et al. Rap1 regulates E-cadherin-mediated cell-cell adhesion. J. Biol. Chem. **279,** 35127–35132 (2004).

146. Hoshino, T. et al. Regulation of E-cadherin endocytosis by nectin through afadin, Rap1, and p120ctn. J. Biol. Chem. **280,** 24095–24103 (2005).

147. Balzac, F. et al. E-cadherin endocytosis regulates the activity of Rap1: a traffic light GTPase at the crossroads between cadherin and integrin function. J. Cell Sci. **118,** 4765–4783 (2005).

148. Ooshio, T. et al. Cooperative roles of Par-3 and afadin in the formation of adherens and tight junctions. J. Cell Sci. **120,** 2352–2365 (2007).

149. von Stein, W., Ramrath, A., Grimm, A., Müller-Borg, M. & Wodarz, A. Direct association of Bazooka/PAR-3 with the lipid phosphatase PTEN reveals a link between the PAR/aPKC complex and phosphoinositide signaling. Development **132,** 1675–1686 (2005).

150. Krahn, M. P., Klopfenstein, D. R., Fischer, N. & Wodarz, A. Membrane Targeting of Bazooka/PAR-3 Is Mediated by Direct Binding to Phosphoinositide Lipids. Curr. Biol. **20,** 636–642 (2010).

151. McGill, M. A., McKinley, R. F. A. & Harris, T. J. C. Independent cadherin-catenin and Bazooka clusters interact to assemble adherens junctions. J. Cell Biol. **185,** 787–796 (2009).

152. Harris, T. J. C. & Peifer, M. The positioning and segregation of apical cues during epithelial polarity establishment in Drosophila. J. Cell Biol. **170,** 813–823 (2005).

153. Harris, T. J. C. & Peifer, M. aPKC controls microtubule organization to balance adherens junction symmetry and planar polarity during development. Dev. Cell **12,** 727–738 (2007).

154. Pilot, F., Philippe, J.-M., Lemmers, C. & Lecuit, T. Spatial control of actin organization at adherens junctions by a synaptotagmin-like protein Btsz. Nature **442,** 580–584 (2006).

155. Imai, F. et al. Inactivation of aPKClambda results in the loss of adherens junctions in neuroepithelial cells without affecting neurogenesis in mouse neocortex. Development **133,** 1735–1744 (2006).

156. Suzuki, A. et al. aPKC kinase activity is required for the asymmetric differentiation of the premature junctional complex during epithelial cell polarization. J. Cell Sci. **115,** 3565–3573 (2002).

157. Kishikawa, M., Suzuki, A. & Ohno, S. aPKC enables development of zonula adherens by antagonizing centripetal contraction of the circumferential actomyosin cables. J. Cell Sci. **121,** 2481–92 (2008).

158. Ishiuchi, T. & Takeichi, M. Willin and Par3 cooperatively regulate epithelial apical constriction through aPKC-mediated ROCK phosphorylation. Nat. Cell Biol. **13,** 860–6 (2011).

159. Even-Faitelson, L. & Ravid, D. PAK1 and aPKCζ Regulate Myosin II-B Phosphorylation: A Novel Signaling Pathway Regulating Filament Assembly. Mol. Biol. Cell **17,** 2869–2881 (2006).

160. Nakayama, M. et al. Rho-Kinase Phosphorylates PAR-3 and Disrupts PAR Complex Formation. Dev. Cell **14,** 205–215 (2008).

161. Simões, S. de M. et al. Rho-kinase directs bazooka/Par-3 planar polarity during drosophila axis elongation. Dev. Cell **19,** 377–388 (2010).

162. Zhang, H. & Macara, I. G. The PAR-6 Polarity Protein Regulates Dendritic Spine Morphogenesis through p190 RhoGAP and the Rho GTPase. Dev. Cell **14,** 216–226 (2008).

163. David, D. J. V., Tishkina, A. & Harris, T. J. C. The PAR complex regulates pulsed actomyosin contractions during amnioserosa apical constriction in Drosophila. Development **137,** 1645–1655 (2010).

164. Röper, K. Anisotropy of Crumbs and aPKC Drives Myosin Cable Assembly during Tube Formation. Dev. Cell **23,** 939–953 (2012).

165. Wang, Y. & Riechmann, V. The Role of the Actomyosin Cytoskeleton in Coordination of Tissue Growth during Drosophila Oogenesis. Curr. Biol. **17,** 1349–1355 (2007).

166. Munro, E., Nance, J. & Priess, J. R. Cortical flows powered by asymmetrical contraction transport PAR proteins to establish and maintain anterior-posterior polarity in the early C. elegans embryo. Dev. Cell **7,** 413–424 (2004).

167. J., H., Van Nijen, G. & Bradander, M. De. Interaction of oncodazole (R 17934), a new anti-tumoral drug, with rat brain Tubulin. Biochem. Biophys. Res. Commun. **69,** 319–324 (1976).

168. Waterman-Storer, C. et al. Microtubules remodel actomyosin networks in Xenopus egg extracts via two mechanisms of F-actin transport. J. Cell Biol. **150,** 361–376 (2000).

169. Stehbens, S. J. et al. Dynamic microtubules regulate the local concentration of E-cadherin at cell-cell contacts. J. Cell Sci. **119,** 1801–1811 (2006).

170. Ivanov, A. I. et al. Microtubules regulate disassembly of epithelial apical junctions. BMC Cell Biol. **7,** 1–19 (2006).

171. Bellett, G. et al. Microtubule plus-end and minus-end capture at adherens junctions is involved in the assembly of apico-basal arrays in polarised epithelial cells. Cell Motil. Cytoskeleton **66,** 893–908 (2009).

172. Karki, S., Ligon, L. A., DeSantis, J., Tokito, M. & Holzbaur, E. L. F. PLAC-24 Is a Cytoplasmic Dynein-Binding Protein That Is Recruited to Sites of Cell-Cell Contact Sher. Mol. Biol. Cell **13,** 1722–1734 (2002).

173. Harris, T. J. & Tepass, U. Adherens junctions: from molecules to morphogenesis. Nat. Rev. Mol. Cell Biol. **11,** 502–514 (2010).

174. Murthy, K. & Wadsworth, P. Dual role for microtubules in regulating cortical contractility during cytokinesis. J. Cell Sci. **121,** 2350–9 (2008).

175. Bulgakova, N. A., Grigoriev, I., Yap, A. S., Akhmanova, A. & Brown, N. H. Dynamic microtubules produce an asymmetric E-cadherin-Bazooka complex to maintain segment boundaries. J. Cell Biol.

201, 887–901 (2013).

176. Slattum, G., McGee, K. M. & Rosenblatt, J. P115 RhoGEF and microtubules decide the direction apoptotic cells extrude from an epithelium. J. Cell Biol. **186,** 693–702 (2009).

177. Wen, Y. et al. EB1 and APC bind to mDia to stabilize microtubules downstream of Rho and promote cell migration. Nat. Cell Biol. **6,** 820–830 (2004).

178. Fujita, Y. et al. Hakai, a c-Cbl-like protein, ubiquitinates and induces endocytosis of the E-cadherin complex. Nat. Cell Biol. **4,** 222–231 (2002).

179. Kaido, M., Wada, H., Shindo, M. & Hayashi, S. Essential requirement for RING finger E3 ubiquitin ligase Hakai in early embryonic development of Drosophila. Genes to Cells **14,** 1067–1077 (2009).

180. Desclozeaux, M. et al. Active Rab11 and functional recycling endosome are required for E-cadherin trafficking and lumen formation during epithelial morphogenesis. Am. J. Physiol. Cell Physiol. **295,** C545–C556 (2008).

181. Woichansky, I., Beretta, C. A., Berns, N. & Riechmann, V. Three mechanisms control E-cadherin localization to the zonula adherens. Nat. Commun. **7,** 10834 (2016).

182. Kametani, Y. & Takeichi, M. Basal-to-apical cadherin flow at cell junctions. Nat. Cell Biol. **9,** 92–8 (2007).

183. Pollard, T. D. & Cooper, J. A. Actin, a central player in cell shape and movement. Science (80-.). **326,** 1208–12 (2009).

184. Gunning, P. W., Ghoshdastider, U., Whitaker, S., Popp, D. & Robinson, R. C. The evolution of compositionally and functionally distinct actin filaments. J. Cell Sci. **128,** 2009–2019 (2015).

185. Blanchoin, L., Boujemaa-Paterski, R., Sykes, C. & Plastino, J. Actin dynamics, architecture, and mechanics in cell motility. Physiol. Rev. **94,** 235–63 (2014).

186. Hartman, M. A. & Spudich, J. A. The myosin superfamily at a glance. J. Cell Sci. **125,** 1627–1632 (2012).

187. Levayer, R. & Lecuit, T. Biomechanical regulation of contractility: Spatial control and dynamics. Trends Cell Biol. **22,** 61–81 (2012).

188. Dulyaninova, N. G. & Bresnick, A. R. The heavy chain has its day: regulation of myosin-II assembly. Bioarchitecture **3,** 77–85 (2013).

189. Kovács, M., Wang, F., Hu, A., Zhang, Y. & Sellers, J. R. Functional divergence of human cytoplasmic myosin II: Kinetic characterization of the non-muscle IIA isoform. J. Biol. Chem. **278,** 38132–38140 (2003).

190. Wang, F. et al. Kinetic mechanism of non-muscle myosin IIB: Functional adaptations for tension generation and maintenance. J. Biol. Chem. **278,** 27439–27448 (2003).

191. Rosenfeld, S. S., Xing, J., Chen, L. Q. & Sweeney, H. L. Myosin IIB is unconventionally conventional. J. Biol. Chem. **278,** 27449–27455 (2003).

192. Kim, K. Y., Kovács, M., Kawamoto, S., Sellers, J. R. & Adelstein, R. S. Disease-associated mutations and alternative splicing alter the enzymatic and motile activity of nonmuscle myosins II-B and II-C. J. Biol. Chem. **280,** 22769–22775 (2005).

193. Ivanov, A. I. et al. A unique role for nonmuscle myosin heavy chain IIA in regulation of epithelial apical junctions. PLoS One **2,** e658 (2007).

194. Gomez, G. A. et al. An RPTPα/Src Family Kinase /Rap1 signaling module recruits Myosin IIB to support contractile tension at apical E-cadherin junctions. Mol. Biol. Cell **26,** 1249–1262 (2015).

195. Wen, Q. & Janmey, P. A. Polymer physics of the cytoskeleton. Curr. Opin. solid state Mater. Sci. **15,** 177–182 (2011).

196. Salbreux, G., Charras, G. & Paluch, E. Actin cortex mechanics and cellular morphogenesis. Trends Cell Biol. **22,** 536–545 (2012).

197. Berro, J., Michelot, A., Blanchoin, L., Kovar, D. R. & Martiel, J.-L. Attachment conditions control actin filament buckling and the production of forces. Biophys. J. **92,** 2546–2558 (2007).

198. Arai, Y. et al. Tying a molecular knot with optical tweezers. Nature **399,** 446–448 (1999).

199. Murrell, M., Oakes, P. W., Lenz, M. & Gardel, M. L. Forcing cells into shape: the mechanics of actomyosin contractility. Nat. Rev. Mol. Cell Biol. **16,** 486–498 (2015).

200. Janmey, P. A. et al. The Mechanical Properties of Actin gels: Elastic Modulus and Filament Motions. J. Biol. Chem. **269,** 32503–32513 (1994).

201. MacKintosh, F. C., Kas, J. & Janmey, P. A. Elasticity of biopolymer networks. Phys. Rev. Lett. **75,** 4425–4429 (1995).

202. Storm, C., Pastore, J. J., MacKintosh, F. C., Lubensky, T. C. & Jamney, P. A. Nonlinear elasticity in biological gels. Nature **435,** 191–194 (2005).

203. Fritzsche, M., Erlenkämper, C., Moeendarbary, E., Charras, G. & Kruse, K. Actin kinetics shapes cortical network structure and mechanics. Sci. Adv. **2,** 1–13 (2016).

204. Xu, J., Tseng, Y. & Wirtz, D. Strain hardening of actin filament networks: Regulation by the dynamic cross-linking protein α-actinin. J. Biol. Chem. **275,** 35886–35892 (2000).

205. Koenderink, G. H. et al. An active biopolymer network controlled by molecular motors. Proc. Natl. Acad. Sci. U. S. A. **106,** 15192–15197 (2009).

206. Laevsky, G. & Knecht, D. a. Cross-linking of actin filaments by myosin II is a major contributor to cortical integrity and cell motility in restrictive environments. J. Cell Sci. **116,** 3761–3770 (2003).

207. Humphrey, D., Duggan, C., Saha, D., Smith, D. & Käs, J. Active fluidization of polymer networks through molecular motors. Nature **416,** 413–416 (2002).

208. Murrell, M. P. & Gardel, M. L. F-actin buckling coordinates contractility and severing in a biomimetic actomyosin cortex. Proc. Natl. Acad. Sci. **109,** 20820–20825 (2012).

209. Alexandrova, A. Y. et al. Comparative dynamics of retrograde actin flow and focal adhesions: Formation of nascent adhesions triggers transition from fast to slow flow. PLoS One **3,** e3234 (2008).

210. Aratyn-Schaus, Y., Oakes, P. W. & Gardel, M. L. Dynamic and structural signatures of lamellar actomyosin force generation. Mol. Biol. Cell **22,** 1330–9 (2011).

211. Berre, L., Liu, Y. & Piel, M. Confinement and Low Adhesion Induce Fast Amoeboid Migration of Slow Mesenchymal Cells. Cell **160,** 659–672 (2015).

212. Hoffman, B. D. & Crocker, J. C. Cell mechanics: dissecting the physical responses of cells to force. Annu. Rev. Biomed. Eng. **11,** 259–288 (2009).

213. Salameh, A. & Dhein, S. Effects of mechanical forces and stretch on intercellular gap junction coupling. Biochim. Biophys. Acta - Biomembr. **1828,** 147–156 (2013).

214. Maître, J. L. & Heisenberg, C.-P. Three functions of cadherins in cell adhesion. Curr. Biol. **23,** R626–33 (2013).

215. Bernheim-Groswasser, A., Wiesner, S., Golsteyn, R. M., Carlier, M.-F. & Sykes, C. The dynamics of actin-based motility depend on surface parameters. Nature **417,** 308–311 (2002).

216. Boukellal, H., Campás, O., Joanny, J. F., Prost, J. & Sykes, C. Soft Listeria: Actin-based propulsion of liquid drops. Phys. Rev. E - Stat. Nonlinear, Soft Matter Phys. **69,** 1–5 (2004).

217. Pollard, T. D. Regulation of actin filament assembly by Arp2/3 complex and formins. Annu. Rev. Biophys. Biomol. Struct. **36,** 451–477 (2007).

218. Campellone, K. G. & Welch, M. D. A nucleator arms race: cellular control of actin assembly. Nat. Rev. Mol. Cell Biol. **11,** 237–51 (2010).

219. Firat-karalar, E. N. & Welch, M. D. New mechanisms and functions of actin nucleation. Curr. Opin. Cell Biol. **23,** 4–13 (2012).

220. Abella, J. V. G. et al. Isoform diversity in the Arp2/3 complex determines actin filament dynamics. Nat. Cell Biol. **18,** 76–86 (2015).

221. Pantaloni, D., Boujemaa, R., Didry, D., Gounon, P. & Carlier, M.-F. The Arp2/3 complex branches filament barbed ends: functional antagonism with capping proteins. Nat. Cell Biol. **2,** 385–391 (2000).

222. Haviv, L. et al. Reconstitution of the transition from lamellipodium to filopodium in a membrane-free system. Proc. Natl. Acad. Sci. U. S. A. **103,** 4906–4911 (2006).

223. Akin, O. & Mullins, R. D. Capping Protein Increases the Rate of Actin-Based Motility by Promoting Filament Nucleation by the Arp2/3 Complex. Cell **133,** 841–851 (2008).

224. Achard, V. et al. A 'Primer'-Based Mechanism Underlies Branched Actin Filament Network Formation and Motility. Curr. Biol. **20,** 423–428 (2010).

225. Wu, Y. I. et al. A genetically encoded photoactivatable Rac controls the motility of living cells. Nature **461,** 104–108 (2009).

226. Ridley, A. J. Life at the leading edge. Cell **145,** 1012–1022 (2011).

227. Lai, F. P. L. et al. Arp2/3 complex interactions and actin network turnover in lamellipodia. EMBO J. **27,** 982–92 (2008).

228. Svitkina, T. M., Verkhovsky, A. B., McQuade, K. M. & Borisy, G. G. Analysis of the actin-myosin II system in fish epidermal keratocytes: Mechanism of cell body translocation. J. Cell Biol. **139,** 397–415 (1997).

229. Weichsel, J., Urban, E., Small, J. V. & Schwarz, U. S. Reconstructing the orientation distribution of actin filaments in the lamellipodium of migrating keratocytes from electron microscopy tomography data. Cytom. Part A **81 A,** 496–507 (2012).

230. Raucher, D. & Sheetz, M. P. Cell spreading and lamellipodial extension rate is regulated by membrane tension. J. Cell Biol. **148,** 127–136 (2000).

231. Batchelder, E. L. et al. Membrane tension regulates motility by controlling lamellipodium organization. Proc. Natl. Acad. Sci. U. S. A. **108,** 11429–11434 (2011).

232. Houk, A. R. et al. Membrane tension maintains cell polarity by confining signals to the leading edge during neutrophil migration. Cell **148,** 175–188 (2012).

233. Keren, K. et al. Mechanism of shape determination in motile cells. Nature **453,** 475–480 (2008).

234. Dahlgaard, K., Raposo, A. A. S. F., Niccoli, T. & St Johnston, D. Capu and Spire Assemble a Cytoplasmic Actin Mesh that Maintains Microtubule Organization in the Drosophila Oocyte. Dev. Cell **13,** 539–553 (2007).

235. Falzone, T. T., Lenz, M., Kovar, D. R. & Gardel, M. L. Assembly kinetics determine the architecture of α-actinin crosslinked F-actin networks. Nat. Commun. **3,** 861 (2012).

236. Liu, A. P. et al. Membrane-induced bundling of actin filaments. Nat. Phys. **31,** 789–793 (2008).

237. Yang, C. & Svitkina, T. Filopodia initiation: focus on the Arp2/3 complex and formins. Cell Adh. Migr. **5,** 402–408 (2011).

238. Daniels, D. R. Effect of capping protein on a growing filopodium. Biophys. J. **98,** 1139–1148 (2010).

239. Sinnar, S. A., Antoku, S., Saffin, J.-M., Cooper, J. A. & Halpain, S. Capping protein is essential for cell migration in vivo and for filopodial morphology and dynamics. Mol. Biol. Cell **25,** 2152–60 (2014).

240. Suraneni, P. et al. The Arp2/3 complex is required for lamellipodia extension and directional fibroblast cell migration. J. Cell Biol. **197,** 239–251 (2012).

241. Wu, C. et al. Arp2/3 is critical for lamellipodia and response to extracellular matrix cues but is dispensable for chemotaxis. Cell **148,** 973–987 (2012).

242. Chhabra, E. S. & Higgs, H. N. The many faces of actin: matching assembly factors with cellular structures. Nat. Cell Biol. **9,** 1110–1121 (2007).

243. Footer, M. J., Kerssemakers, J. W. J., Theriot, J. A. & Dogterom, M. Direct measurement of force generation by actin filament polymerization using an optical trap. Proc. Natl. Acad. Sci. **104,** 2181–2186 (2007).

244. Reymann, A.-C. et al. Actin Network Architecture Can Determine Myosin Motor Activity. Science (80-.). **336,** 1310–1314 (2012).

245. Thoresen, T., Lenz, M. & Gardel, M. L. Thick filament length and isoform composition determine self-organized contractile units in actomyosin bundles. Biophys. J. **104,** 655–665 (2013).

246. Lenz, M., Thoresen, T., Gardel, M. L. & Dinner, A. R. Contractile units in disordered actomyosin bundles arise from f-actin buckling. Phys. Rev. Lett. **108,** 1–5 (2012).

247. Köhler, S., Schaller, V. & Bausch, A. R. Structure formation in active networks. Nat. Mater. **10,** 462–468 (2011).

248. Ennomani, H. et al. Architecture and Connectivity Govern Actin Network Contractility. Curr. Biol. **26,** 616–626 (2016).

249. Alvarado, J., Sheinman, M., Sharma, A., MacKintosh, F. C. & Koenderink, G. H. Molecular motors robustly drive active gels to a critically connected state. Nat. Phys. **9,** 591–597 (2013).

250. Sun, S. X., Walcott, S. & Wolgemuth, C. Cytoskeletal Cross-linking and Bundling in Motor-indepedent Contraction. Curr. Biol. **20,** R649–R654 (2010).

251. Neujahr, R., Heizer, C. & Gerisch, G. Myosin II-independent processes in mitotic cells of Dictyostelium discoideum: redistribution of the nuclei, re-arrangement of the actin system and formation of the cleavage furrow. J. Cell Sci. **110,** 123–37 (1997).

252. Ma, X. et al. Nonmuscle myosin II exerts tension but does not translocate actin in vertebrate cytokinesis. Proc. Natl. Acad. Sci. **109,** 4509–4514 (2012).

253. Green, R. A., Paluch, E. K. & Oegema, K. Cytokinesis in animal cells. Annu. Rev. Cell Dev. Biol. **28,** 29–58 (2012).

254. Wagner, E. & Glotzer, M. Local RhoA activation induces cytokinetic furrows independent of spindle position and cell cycle stage. J. Cell Biol. **213,** 641–649 (2016).

255. Sanger, J. M. & Sanger, J. W. Banding and polarity of actin filaments in interphase and cleaving cells. J. Cell Biol. **86,** 568–575 (1980).

256. Maupin, P. & Pollard, T. D. Arrangement of actin filaments and myosin-like filaments in the

contractile ring and of actin-like filaments in the mitotic spindle of dividing HeLa cells. J. Ultrastruct. Res. Mol. Struct. Res. **94,** 92–103 (1986).

257. Mabuchi, I., Tsukita, S. & Sawai, T. Cleavage furrow isolated from newt eggs: contraction, organization of the actin filaments, and protein components of the furrow. Proc. Natl. Acad. Sci. U. S. A. **85,** 5966–5970 (1988).

258. Kamasaki, T., Osumi, M. & Mabuchi, I. Three-dimensional arrangement of F-actin in the contractile ring of fission yeast. J. Cell Biol. **178,** 765–771 (2007).

259. Schwayer, C., Sikora, M., Slova, J., Kardos, R. & Heisenberg, C. Actin Rings of Power. Dev. Cell **37,** 493–506 (2016).

260. Mendes Pinto, I., Rubinstein, B., Kucharavy, A., Unruh, J. R. & Li, R. Actin Depolymerization Drives Actomyosin Ring Contraction during Budding Yeast Cytokinesis. Dev. Cell **22,** 1247–1260 (2012).

261. Guha, M., Zhou, M. & Wang, Y. L. Cortical actin turnover during cytokinesis requires myosin II. Curr. Biol. **15,** 732–736 (2005).

262. Murthy, K. & Wadsworth, P. Myosin-II-dependent localization and dynamics of F-actin during cytokinesis. Curr. Biol. **15,** 724–731 (2005).

263. Haviv, L., Gillo, D., Backouche, F. & Bernheim-Groswasser, A. A Cytoskeletal Demolition Worker: Myosin II Acts as an Actin Depolymerization Agent. J. Mol. Biol. **375,** 325–330 (2008).

264. Carvalho, A., Desai, A. & Oegema, K. Structural Memory in the Contractile Ring Makes the Duration of Cytokinesis Independent of Cell Size. Cell **137,** 926–937 (2009).

265. Biron, D., Alvarez-Lacalle, E., Tlusty, T. & Moses, E. Molecular model of the contractile ring. Phys. Rev. Lett. **95,** 1–4 (2005).

266. Carlsson, A. E. Contractile stress generation by actomyosin gels. Phys. Rev. E - Stat. Nonlinear, Soft Matter Phys. **74,** 1–6 (2006).

267. Mavrakis, M. et al. Septins promote F-actin ring formation by crosslinking actin filaments into curved bundles. Nat. Cell Biol. **16,** 322–34 (2014).

268. Pollard, T. D. & Borisy, G. G. Cellular motility driven by assembly and disassembly of actin filaments. Cell **112,** 453–465 (2003).

269. Ruprecht, V. et al. Cortical Contractility Triggers a Stochastic Switch to Fast Amoeboid Cell Motility. Cell **160,** 673–685 (2015).

270. Cao, L. G. & Wang, Y. L. Mechanism of the formation of contractile ring in dividing cultured animal cells. I. Recruitment of preexisting actin filaments into the cleavage furrow. J. Cell Biol. **110,** 1089–1095 (1990).

271. Rauzi, M., Lenne, P.-F. & Lecuit, T. Planar polarized actomyosin contractile flows control epithelial junction remodelling. Nature **468,** 1110–1114 (2010).

272. Behrndt, M., Roensch, J., Grill, S. W. & Heisenberg, C.-P. Forces Driving Epithelial Spreading in Zebrafish Gastrulation. Science (80-.). **338,** 257–260 (2012).

273. Mandato, C. A. & Bement, W. M. Contraction and polymerization cooperate to assemble and close actomyosin rings around Xenopus oocyte wounds. J. Cell Biol. **154,** 785–797 (2001).

274. Le Clainche, C. & Carlier, M.-F. Regulation of actin assembly associated with protrusion and adhesion in cell migration. Physiol. Rev. **88,** 489–513 (2008).

275. Nishita, M. et al. Spatial and temporal regulation of cofilin activity by LIM kinase and Slingshot is

critical for directional cell migration. J. Cell Biol. **171,** 349–359 (2005).

276. Gandhi, M. et al. GMF Is a Cofilin Homolog that Binds Arp2/3 Complex to Stimulate Filament Debranching and Inhibit Actin Nucleation. Curr. Biol. **20,** 861–867 (2010).

277. Poukkula, M. et al. GMF promotes leading-edge dynamics and collective cell migration in vivo. Curr. Biol. **24,** 2533–2540 (2014).

278. Wilson, C. A. et al. Myosin II contributes to cell-scale actin network treadmilling through network disassembly. Nature **465,** 373–7 (2010).

279. Burnette, D. T. et al. A role for actin arcs in the leading-edge advance of migrating cells. Nat. Cell Biol. **13,** 371–81 (2011).

280. Vitriol, E. A. et al. Two Functionally Distinct Sources of Actin Monomers Supply the Leading Edge of Lamellipodia. Cell Rep. **11,** 433–445 (2015).

281. Hsiao, J. Y., Goins, L. M., Petek, N. A. & Mullins, R. D. Arp2/3 Complex and Cofilin Modulate Binding of Tropomyosin to Branched Actin Networks. Curr. Biol. **25,** 1573–1582 (2015).

282. Chan, C., Beltzner, C. C. & Pollard, T. D. Cofilin Dissociates Arp2/3 Complex and Branches from Actin Filaments. Curr. Biol. **19,** 537–545 (2009).

283. Callan-Jones, A. C. & Voituriez, R. Actin flows in cell migration: from locomotion and polarity to trajectories. Curr. Opin. Cell Biol. **38,** 12–17 (2016).

284. Maiuri, P. et al. Actin Flows Mediate a Universal Coupling between Cell Speed and Cell Persistence Theory. Cell **161,** 1–13 (2015).

285. Maiuri, P. et al. The first World Cell Race. Curr. Biol. **22,** R673–R675 (2012).

286. Kovács, M., Tóth, J., Hetényi, C., Málnási-Csizmadia, A. & Seller, J. R. Mechanism of blebbistatin inhibition of myosin II. J. Biol. Chem. **279,** 35557–35563 (2004).

287. Lomakin, A. J. et al. Competition for actin between two distinct F-actin networks defines a bistable switch for cell polarization. Nat. Cell Biol. (2015). doi:10.1038/ncb3246

288. Yumura, S., Ueda, M., Sako, Y., Kitanishi-Yumura, T. & Yanagida, T. Multiple mechanisms for accumulation of myosin II filaments at the equator during cytokinesis. Traffic **9,** 2089–2099 (2008).

289. Zhou, M. & Wang, Y.-L. Distinct Pathways for the Early Recruitment of Myosin II and Actin to the Cytokinetic Furrow. Mol. Biol. Cell **19,** 318–326 (2008).

290. Uehara, R. et al. Determinants of myosin II cortical localization during cytokinesis. Curr. Biol. **20,** 1080–1085 (2010).

291. Bringmann, H. & Hyman, A. a. A cytokinesis furrow is positioned by two consecutive signals. Nature **436,** 731–734 (2005).

292. Dean, S. O., Rogers, S. L., Stuurman, N., Vale, R. D. & Spudich, J. A. Distinct pathways control recruitment and maintenance of myosin II at the cleavage furrow during cytokinesis. Proc. Natl. Acad. Sci. U. S. A. **102,** 13473–13478 (2005).

293. Werner, M., Munro, E. & Glotzer, M. Astral Signals Spatially Bias Cortical Myosin Recruitment to Break Symmetry and Promote Cytokinesis. Curr. Biol. **17,** 1286–1297 (2007).

294. Sedzinski, J. et al. Polar actomyosin contractility destabilizes the position of the cytokinetic furrow. Nature **476,** 462–6 (2011).

295. Yüce, Ö., Piekny, A. & Glotzer, M. An ECT2-centralspindlin complex regulates the localization and function of RhoA. J. Cell Biol. **170,** 571–582 (2005).

296. Zhao, W. & Fang, G. MgcRacGAP controls the assembly of the contractile ring and the initiation of cytokinesis. Proc. Natl. Acad. Sci. U. S. A. **102,** 13158–13163 (2005).

297. Nishimura, Y. & Yonemura, S. Centralspindlin regulates ECT2 and RhoA accumulation at the equatorial cortex during cytokinesis. J. Cell Sci. **119,** 104–114 (2006).

298. Salbreux, G., Prost, J. & Joanny, J. F. Hydrodynamics of cellular cortical flows and the formation of contractile rings. Phys. Rev. Lett. **103,** 1–4 (2009).

299. Mayer, M., Depken, M., Bois, J. S., Jülicher, F. & Grill, S. W. Anisotropies in cortical tension reveal the physical basis of polarizing cortical flows. Nature **467,** 617–21 (2010).

300. Turlier, H., Audoly, B., Prost, J. & Joanny, J. F. Furrow constriction in animal cell cytokinesis. Biophys. J. **106,** 114–123 (2014).

301. Keller, R. Physical Biology Returns to Morphogenesis. Science (80-.). **338,** 10–13 (2012).

302. Paluch, E. K. et al. Mechanotransduction: use the force(s). BMC Biol. **13,** 47 (2015).

303. Etournay, R. et al. Interplay of cell dynamics and epithelial tension during morphogenesis of the Drosophila pupal wing. Elife **4,** (2015).

304. Guirao, B. et al. Unified quantitative characterization of epithelial tissue development. Elife **4,** (2015).

305. Martin, A. C., Kaschube, M. & Wieschaus, E. F. Pulsed contractions of an actin-myosin network drive apical constriction. Nature **457,** 495–9 (2009).

306. Skoglund, P., Rolo, A., Chen, X., Gumbiner, B. M. & Keller, R. Convergence and extension at gastrulation require a myosin IIB-dependent cortical actin network. Development **135,** 2435–2444 (2008).

307. Kim, H. Y. & Davidson, L. A. Punctuated actin contractions during convergent extension and their permissive regulation by the non-canonical Wnt-signaling pathway. J. Cell Sci. **124,** 635–46 (2011).

308. Christodoulou, N. & Skourides, P. A. Cell-Autonomous Ca2+ Flashes Elicit Pulsed Contractions of an Apical Actin Network to Drive Apical Constriction during Neural Tube Closure. Cell Rep. **13,** 2189–2202 (2015).

309. Manning, A. J., Peters, K. A., Peifer, M. & Rogers, S. L. Regulation of epithelial morphogenesis by the G protein-coupled receptor mist and its ligand fog. Sci. Signal. **6,** ra98 (2013).

310. Kerridge, S. et al. Modular activation of Rho1 by GPCR signalling imparts polarized myosin II activation during morphogenesis. Nat. Cell Biol. **18,** 261–270 (2016).

311. Kölsch, V., Seher, T., Fernandez-ballester, G. J., Serrano, L. & Leptin, M. Control of Drosophila Gastrulation by Apical Localization of Adherens Junctions and RhoGEF2. Science (80-.). **315,** 384–387 (2007).

312. Dawes-Hoang, R. E. et al. Folded Gastrulation, Cell Shape Change and the Control of Myosin Localization. Development **132,** 4165–78 (2005).

313. Martin, A. C. & Goldstein, B. Apical constriction: themes and variations on a cellular mechanism driving morphogenesis. Development **141,** 1987–1998 (2014).

314. Nikolaidou, K. K. & Barrett, K. A Rho GTPase Signaling Pathway Is Used Reiteratively in Epithelial Folding and Potentially Selects the Outcome of Rho Activation. Curr. Biol. **14,** 1822–1826 (2004).

315. Martin, A. C., Gelbart, M., Fernandez-Gonzalez, R., Kaschube, M. & Wieschaus, E. F. Integration of contractile forces during tissue invagination. J. Cell Biol. **188,** 735–749 (2010).

316. Roh-Johnson, M. et al. Triggering a cell shape change by exploiting preexisting actomyosin

contractions. Science (80-.). **335,** 1232–5 (2012).

317. Vasquez, C. G., Tworoger, M. & Martin, A. C. Dynamic myosin phosphorylation regulates contractile pulses and tissue integrity during epithelial morphogenesis. J. Cell Biol. **206,** 435–50 (2014).

318. Munjal, A., Philippe, J.-M., Munro, E. & Lecuit, T. A self-organized biomechanical network drives shape changes during tissue morphogenesis. Nature **524,** 351–355 (2015).

319. Xie, S. & Martin, A. C. Intracellular signalling and intercellular coupling coordinate heterogeneous contractile events to facilitate tissue folding. Nat. Commun. **6,** 7161 (2015).

320. Mason, F. M., Tworoger, M. & Martin, A. C. Apical domain polarization localizes actin-myosin activity to drive ratchet-like apical constriction. Nat. Cell Biol. **15,** 926–36 (2013).

321. Jodoin, J. N. et al. Stable Force Balance between Epithelial Cells Arises from F-Actin Turnover Article. Dev. Cell **35,** 1–13 (2015).

322. Shindo, A. & Wallingford, J. B. PCP and septins compartmentalize collective cell movement. Science (80-.). **343,** 649–652 (2014).

323. Bosveld, F. et al. Mechanical Control of Morphogenesis by Fat/Dachsous/Four-Jointed Planar Cell Polarity Pathway. **336,** 724–727 (2012).

324. Irvine, K. D. & Wieschaus, E. F. Cell intercalation during Drosophila germband extension and its regulation by pair-rule segmentation genes. Development **120,** 827–841 (1994).

325. Paré, A. C. et al. A positional Toll receptor code directs convergent extension in Drosophila. Nature **515,** 523–527 (2014).

326. Bertet, C., Sulak, L. & Lecuit, T. Myosin-dependent junction remodelling controls planar cell intercalation. Nature **429,** 667–671 (2004).

327. Butler, L. C. et al. Cell shape changes indicate a role for extrinsic tensile forces in Drosophila germband extension. Nat. Cell Biol. **11,** 859–64 (2009).

328. da Silva, S. M. & Vincent, J.-P. Oriented cell divisions in the extending germband of Drosophila. Development **134,** 3049–3054 (2007).

329. Zallen, J. A. & Wieschaus, E. F. Patterned gene expression directs bipolar planar polarity in Drosophila. Dev. Cell **6,** 343–355 (2004).

330. Blankenship, J. T., Backovic, S. T., Sanny, J. S. P., Weitz, O. & Zallen, J. A. Multicellular Rosette Formation Links Planar Cell Polarity to Tissue Morphogenesis. Dev. Cell **11,** 459–470 (2006).

331. Simões, S. de M., Mainieri, A. & Zallen, J. A. Rho GTPase and Shroom direct planar polarized actomyosin contractility during convergent extension. J. Cell Biol. **204,** 575–589 (2014).

332. Rauzi, M., Verant, P., Lecuit, T. & Lenne, P.-F. Nature and anisotropy of cortical forces orienting Drosophila tissue morphogenesis. Nat. Cell Biol. **10,** 1401–1410 (2008).

333. Levayer, R. & Lecuit, T. Oscillation and Polarity of E-Cadherin Asymmetries Control Actomyosin Flow Patterns during Morphogenesis. Dev. Cell **26,** 162–175 (2013).

334. Fernandez-Gonzalez, R., Simões, S. de M., Röper, J. C., Eaton, S. & Zallen, J. A. Myosin II Dynamics Are Regulated by Tension in Intercalating Cells. Dev. Cell **17,** 736–743 (2009).

335. Collinet, C., Rauzi, M., Lenne, P. & Lecuit, T. Local and tissue-scale forces drive oriented junction growth during tissue extension. Nat. Cell Biol. **17,** 1247–1258 (2015).

336. Bardet, P. L. et al. PTEN Controls Junction Lengthening and Stability during Cell Rearrangement in Epithelial Tissue. Dev. Cell **25,** 534–546 (2013).

337. Rosenblatt, J., Raff, M. C. & Cramer, L. P. An epithelial cell destined for apoptosis signals its neighbors to extrude it by an actin- and myosin-dependent mechanism. Curr. Biol. **11,** 1847–1857 (2001).

338. Marinari, E. et al. Live-cell delamination counterbalances epithelial growth to limit tissue overcrowding. Nature **484,** 542–545 (2012).

339. Eisenhoffer, G. T. et al. Crowding induces live cell extrusion to maintain homeostatic cell numbers in epithelia. Nature **484,** 546–549 (2012).

340. Levayer, R., Dupont, C., Levayer, R., Dupont, C. & Moreno, E. Tissue Crowding Induces Caspase-Dependent Competition for Space. Curr. Biol. **26,** 1–8 (2016).

341. Monier, B. et al. Apico-basal forces exerted by apoptotic cells drive epithelium folding. Nature **12,** 245–8 (2015).

342. Monier, B. & Suzanne, M. The Morphogenetic Role of Apoptosis. Current Topics in Developmental Biology **114,** (Elsevier Inc., 2015).

343. Steinhusen, U. et al. Cleavage and Shedding of E-cadherin after Induction of Apoptosis. J. Biol. Chem. **276,** 4972–4980 (2001).

344. Kuipers, D. et al. Epithelial repair is a two-stage process driven first by dying cells and then by their neighbours. J. Cell Sci. **127,** 1229–41 (2014).

345. Gu, Y., Forostyan, T., Sabbadini, R. & Rosenblatt, J. Epithelial cell extrusion requires the sphingosine-1-phosphate receptor 2 pathway. J. Cell Biol. **193,** 667–676 (2011).

346. Tamada, M., Perez, T. D., Nelson, W. J. & Sheetz, M. P. Two distinct modes of myosin assembly and dynamics during epithelial wound closure. J. Cell Biol. **176,** 27–33 (2007).

347. Lubkov, V. & Bar-Sagi, D. E-Cadherin-Mediated Cell Coupling Is Required for Apoptotic Cell Extrusion. Curr. Biol. **24,** 868–74 (2014).

348. Bonnet, I. et al. Mechanical state, material properties and continuous description of an epithelial tissue. J. R. Soc. Interface **9,** 2614–2623 (2012).

349. Borghi, N. et al. E-cadherin is under constitutive actomyosin-generated tension that is increased at cell-cell contacts upon externally applied stretch. Proc. Natl. Acad. Sci. **109,** 19034–19034 (2012).

350. Cai, D. et al. Mechanical feedback through E-cadherin promotes direction sensing during collective cell migration. Cell **157,** 1146–1159 (2014).

351. Tabdili, H. et al. Cadherin-dependent mechanotransduction depends on ligand identity but not affinity. J. Cell Sci. **125,** 4362–4371 (2012).

352. Ladoux, B. et al. Strength dependence of cadherin-mediated adhesions. Biophys. J. **98,** 534–542 (2010).

353. Conway, D. E. et al. Fluid shear stress on endothelial cells modulates mechanical tension across VE-cadherin and PECAM-1. Curr. Biol. **23,** 1024–1030 (2013).

354. Barry, A. K. et al. α-Catenin Cytomechanics-Role in Cadherin-Dependent Adhesion and Mechanotransduction. J. Cell Sci. **127,** 1779–91 (2014).

355. Barry, A. K., Wang, N. & Leckband, D. E. Local VE-cadherin mechanotransduction triggers long-ranged remodeling of endothelial monolayers. J. Cell Sci. **128,** 1341–51 (2015).

356. Guo, Q., Park, S. & Ma, H. Microfluidic micropipette aspiration for measuring the deformability of single cells. Lab Chip **12,** 2687–95 (2012).

357. Maître, J. L. et al. Adhesion Functions in Cell Sorting by Mechanically Coupling the Cortices of

Adhering Cells. Science (80-.). **338,** 253–256 (2012).

358. Grashoff, C. et al. Measuring mechanical tension across vinculin reveals regulation of focal adhesion dynamics. Nature **466,** 263–266 (2010).

359. Leckband, D. E., le Duc, Q., Wang, N. & de Rooij, J. Mechanotransduction at cadherin-mediated adhesions. Curr. Opin. Cell Biol. **23,** 523–530 (2011).

360. Trier, S. M. & Davidson, L. A. Quantitative microscopy and imaging tools for the mechanical analysis of morphogenesis. Curr. Opin. Genet. Dev. **21,** 664–670 (2011).

361. Gupta, M. et al. Micropillar substrates: A tool for studying cell mechanobiology. Methods in Cell Biology **125,** (Elsevier Ltd, 2015).

362. Thomas, W. Catch bonds in adhesion. Annu. Rev. Biomed. Eng. **10,** 39–57 (2008).

363. Guo, B. & Guilford, W. H. Mechanics of actomyosin bonds in different nucleotide states are tuned to muscle contraction. Proc. Natl. Acad. Sci. U. S. A. **103,** 9844–9849 (2006).

364. Alon, R., Chen, S., Fuhlbrigge, R., Puri, K. D. & Springer, T. A. The kinetics and shear threshold of transient and rolling interactions of L-selectin with its ligand on leukocytes. Proc. Natl. Acad. Sci. U. S. A. **95,** 11631–11636 (1998).

365. Yago, T. et al. Catch bonds govern adhesion through L-selectin at threshold shear. J. Cell Biol. **166,** 913–923 (2004).

366. Sarangapani, K. K. et al. Low Force Decelerates L-selectin Dissociation from P-selectin Glycoprotein Ligand-1 and Endoglycan. J. Biol. Chem. **279,** 2291–2298 (2004).

367. Le Trong, I. et al. Structural Basis for Mechanical Force Regulation of the Adhesin FimH via Finger Trap-like Beta Sheet Twisting. Cell **141,** 645–655 (2010).

368. Kong, F., García, A. J., Mould, A. P., Humphries, M. J. & Zhu, C. Demonstration of catch bonds between an integrin and its ligand. J. Cell Biol. **185,** 1275–1284 (2009).

369. Chen, W., Lou, J. & Zhu, C. Forcing switch from short- to intermediate- and long-lived states of the αA domain generates LFA-1/ICAM-1 catch bonds. J. Biol. Chem. **285,** 35967–35978 (2010).

370. Perret, E., Leung, A., Feracci, H. & Evans, E. Trans-bonded pairs of E-cadherin exhibit a remarkable hierarchy of mechanical strengths. Proc. Natl. Acad. Sci. U. S. A. **101,** 16472–16477 (2004).

371. Rakshit, S., Zhang, Y., Manibog, K., Shafraz, O. & Sivasankar, S. Ideal, catch, and slip bonds in cadherin adhesion. Proc. Natl. Acad. Sci. **109,** 18815–18820 (2012).

372. Shi, Q., Chien, Y. H. & Leckband, D. Biophysical properties of cadherin bonds do not predict cell sorting. J. Biol. Chem. **283,** 28454–28463 (2008).

373. Chien, Y. H. et al. Two stage cadherin kinetics require multiple extracellular domains but not the cytoplasmic region. J. Biol. Chem. **283,** 1848–1856 (2008).

374. Shi, Q., Maruthamuthu, V., Li, F. & Leckband, D. Allosteric cross talk between cadherin extracellular domains. Biophys. J. **99,** 95–104 (2010).

375. Baumgartner, W. et al. Cadherin interaction probed by atomic force microscopy. Proc. Natl. Acad. Sci. U. S. A. **97,** 4005–4010 (2000).

376. Thomas, W. A. et al. α-Catenin and vinculin cooperate to promote high E-cadherin-based adhesion strength. J. Biol. Chem. **288,** 4957–4969 (2013).

377. Choi, H.-J. et al. αE-catenin is an autoinhibited molecule that coactivates vinculin. Proc. Natl. Acad. Sci. **109,** 8576–8581 (2012).

378. Ishiyama, N. et al. An autoinhibited structure of α-catenin and its implications for vinculin recruitment to adherens junctions. J. Biol. Chem. **288,** 15913–15925 (2013).

379. Kim, T. et al. Dynamic Visualization of α-Catenin Reveals Rapid , Reversible Conformation Switching between Tension States. Curr. Biol. **25,** 218–224 (2015).

380. Yao, M. et al. Force-dependent conformational switch of α-catenin controls vinculin binding. Nat. Commun. **5,** (2014).

381. Borgon, R. A., Vonrhein, C., Bricogne, G., Bois, P. R. J. & Izard, T. Crystal structure of human vinculin. Structure **12,** 1189–1197 (2004).

382. Bakolitsa, C. et al. Structural basis for vinculin activation at sites of cell adhesion. Nature **430,** 583–6 (2004).

383. Peng, X., Maiers, J. L., Choudhury, D., Craig, S. W. & DeMali, K. A. Alpha-Catenin uses a novel mechanism to activate vinculin. J. Biol. Chem. **287,** 7728–7737 (2012).

384. Rangarajan, E. S. & Izard, T. The cytoskeletal protein α-catenin unfurls upon binding to vinculin. J. Biol. Chem. **287,** 18492–18499 (2012).

385. Bays, J. L. et al. Vinculin phosphorylation differentially regulates mechanotransduction at cell-cell and cell-matrix adhesions. J. Cell Biol. **205,** 251–263 (2014).

386. Watabe-Uchida, M. et al. α-Catenin-vinculin interaction functions to organize the apical junctional complex in epithelial cells. J. Cell Biol. **142,** 847–857 (1998).

387. Sheikh, F. et al. αE-catenin inactivation disrupts the cardiomyocyte adherens junction, resulting in cardiomyopathy and susceptibility to wall rupture. Circulation **114,** 1046–1055 (2006).

388. Maddugoda, M. P., Crampton, M. S., Shewan, A. M. & Yap, A. S. Myosin VI and vinculin cooperate during the morphogenesis of cadherin cell-cell contacts in mammalian epithelial cells. J. Cell Biol. **178,** 529–540 (2007).

389. Liu, Z. et al. Mechanical tugging force regulates the size of cell-cell junctions. Proc. Natl. Acad. Sci. **107,** 9944–9949 (2010).

390. Huveneers, S. et al. Vinculin associates with endothelial VE-cadherin junctions to control force-dependent remodeling. J. Cell Biol. **196,** 641–652 (2012).

391. DeMali, K. A. Vinculin-a dynamic regulator of cell adhesion. Trends Biochem. Sci. **29,** 565–7 (2004).

392. Leerberg, J. M. et al. Tension-sensitive actin assembly supports contractility at the epithelial zonula adherens. Curr. Biol. **24,** 1689–1699 (2014).

393. Padmanabhan, A., Rao, M. V., Wu, Y. & Zaidel-Bar, R. Jack of all trades: Functional modularity in the adherens junction. Curr. Opin. Cell Biol. **36,** 32–40 (2015).

394. Wen, K. K., Rubenstein, P. A. & DeMali, K. A. Vinculin nucleates actin polymerization and modifies actin filament structure. J. Biol. Chem. **284,** 30463–30473 (2009).

395. Uehata, M. et al. Calcium sensitization of smooth muscle mediated by a Rho-associated protein kinase in hypertension. Nature **389,** 990–4 (1997).

396. Ishizaki, T. et al. Pharmacological properties of Y-27632, a specific inhibitor of rho-associated kinases. Mol. Pharmacol. **57,** 976–983 (2000).

397. Alatortsev, V. E., Kramerova, I. A., Frolov, M. V., Lavrov, S. A. & Westphal, E. D. Vinculin gene is non-essential in Drosophila melanogaster. FEBS Lett. **413,** 197–201 (1997).

398. Courtemanche, N., Lee, J. Y., Pollard, T. D. & Greene, E. C. Tension modulates actin filament

polymerization mediated by formin and profilin. Proc. Natl. Acad. Sci. **110,** 9752–9757 (2013).

399. Higashida, C. et al. F- and G-actin homeostasis regulates mechanosensitive actin nucleation by formins. Nat. Cell Biol. **15,** 395–405 (2013).

400. Jégou, A., Carlier, M.-F. & Romet-Lemonne, G. Formin mDia1 senses and generates mechanical forces on actin filaments. Nat. Commun. **4,** 1883 (2013).

401. Kris, A. S., Kamm, R. D. & Sieminski, A. L. VASP involvement in force-mediated adherens junction strengthening. Biochem. Biophys. Res. Commun. **375,** 134–138 (2008).

402. Posy, S., Shapiro, L. & Honig, B. Sequence and Structural Determinants of Strand Swapping in Cadherin Domains: Do All Cadherins Bind Through the Same Adhesive Interface? J. Mol. Biol. **378,** 952–966 (2008).

403. Kannan, N. & Tang, V. W. Synaptopodin couples epithelial contractility to α-actinin-4-dependent junction maturation. J. Cell Biol. **211,** 407–34 (2015).

404. Han, M. K. L. & de Rooij, J. Converging and Unique Mechanisms of Mechanotransduction at Adhesion Sites. Trends Cell Biol. **29,** 1–12 (2016).

405. Tornavaca, O. et al. ZO-1 controls endothelial adherens junctions, cell-cell tension, angiogenesis, and barrier formation. J. Cell Biol. **208,** 821–838 (2015).

406. Veigel, C., Molloy, J. E., Schmitz, S. & Kendrick-Jones, J. Load-dependent kinetics of force production by smooth muscle myosin measured with optical tweezers. Nat. Cell Biol. **5,** 980–986 (2003).

407. Altman, D., Sweeney, H. L. & Spudich, J. A. The mechanism of myosin VI translocation and its load-induced anchoring. Cell **116,** 737–749 (2004).

408. Purcell, T. J., Sweeney, H. L. & Spudich, J. A. A force-dependent state controls the coordination of processive myosin V. Proc. Natl. Acad. Sci. U. S. A. **102,** 13873–13878 (2005).

409. Kovács, M., Thirumurugan, K., Knight, P. J. & Sellers, J. R. Load-dependent mechanism of nonmuscle myosin 2. Proc. Natl. Acad. Sci. U. S. A. **104,** 9994–9 (2007).

410. Effler, J. C. et al. Mitosis-Specific Mechanosensing and Contractile-Protein Redistribution Control Cell Shape. Curr. Biol. **16,** 1962–1967 (2006).

411. Pouille, P.-A., Ahmadi, P., Brunet, A.-C. & Farge, E. Mechanical signals trigger Myosin II redistribution and mesoderm invagination in Drosophila embryos. Sci. Signal. **2,** 1–9 (2009).

412. Schiffhauer, E. S. et al. Mechanoaccumulative Elements of the Mammalian Actin Cytoskeleton. Curr. Biol. 1–7 (2016). doi:10.1016/j.cub.2016.04.007

413. Engl, W., Arasi, B., Yap, L. L., Thiery, J. P. & Viasnoff, V. Actin dynamics modulate mechanosensitive immobilization of E-cadherin at adherens junctions. Nat. Cell Biol. **16,** 587–94 (2014).

414. Sumida, G. M., Tomita, T. M., Shih, W. & Yamada, S. Myosin II activity dependent and independent vinculin recruitment to the sites of E-cadherin-mediated cell-cell adhesion. BMC Cell Biol. **12,** 48 (2011).

415. Maul, R. S. et al. EPLIN regulates actin dynamics by cross-linking and stabilizing filaments. J. Cell Biol. **160,** 399–407 (2003).

416. Scott, J. A. et al. Ena/VASP Proteins Can Regulate Distinct Modes of Actin Organization at Cadherin-adhesive Contacts. Mol. Biol. Cell **17,** 1085–1095 (2006).

417. Furman, C. et al. Ena/VASP is required for endothelial barrier function in vivo. J. Cell Biol. Cell Biol

179, 761–775 (2007).

418. Hansen, M. D. H. & Beckerle, M. C. Opposing roles of Zyxin/LPP ACTA repeats and the LIM domain region in cell-cell adhesion. J. Biol. Chem. **281,** 16178–16188 (2006).

419. Moody, J. D. et al. A zyxin head-tail interaction regulates zyxin-VASP complex formation. Biochem. Biophys. Res. Commun. **378,** 625–628 (2009).

420. Call, G. S. et al. Zyxin phosphorylation at serine 142 modulates the zyxin head-tail interaction to alter cell-cell adhesion. Biochem. Biophys. Res. Commun. **404,** 780–784 (2011).

421. Hirata, H., Tatsumi, H. & Sokabe, M. Mechanical forces facilitate actin polymerization at focal adhesions in a zyxin-dependent manner. J. Cell Sci. **121,** 2795–804 (2008).

422. Smith, M. A., Hoffman, L. M. & Beckerle, M. C. LIM proteins in actin cytoskeleton mechanoresponse. Trends Cell Biol. **24,** 575–583 (2014).

423. Bear, J. E. et al. Antagonism between Ena/VASP Proteins and Actin Filament Capping Regulates Fibroblast Motility. Cell **109,** 509–521 (2002).

424. Skoble, J., Auerbuch, V., Goley, E. D., Welch, M. D. & Portnoy, D. A. Pivotal role of VASP in Arp2/3 complex-mediated actin nucleation, actin branch-formation, and Listeria monocytogenes motility. J. Cell Biol. **155,** 89–100 (2001).

425. Chen, X. J. et al. Ena/VASP proteins cooperate with the WAVE complex to regulate the actin cytoskeleton. Dev. Cell **30,** 569–584 (2014).

426. Homem, C. C. F. & Peifer, M. Exploring the Roles of Diaphanous and Enabled Activity in Shaping the Balance between Filopodia and Lamellipodia. Mol. Biol. Cell **20,** 5138–5155 (2009).

427. Bilancia, C. G. et al. Enabled negatively regulates diaphanous-driven actin dynamics in vitro and in vivo. Dev. Cell **28,** 394–408 (2014).

428. de Beco, S., Perney, J.-B., Coscoy, S. & Amblard, F. Mechanosensitive Adaptation of E-Cadherin Turnover across adherens Junctions. PLoS One **10,** e0128281 (2015).

429. Yu, F. X. & Guan, K. L. The Hippo pathway: Regulators and regulations. Genes Dev. **27,** 355–371 (2013).

430. Yang, C.-C. et al. Differential regulation of the Hippo pathway by adherens junctions and apical-basal cell polarity modules. Proc. Natl. Acad. Sci. **112,** 1785–1790 (2015).

431. Rauskolb, C., Sun, S., Sun, G., Pan, Y. & Irvine, K. D. Cytoskeletal tension inhibits Hippo signaling through an Ajuba-Warts complex. Cell **158,** 143–156 (2014).

432. Rauskolb, C., Pan, G., Reddy, B. V. V. G., Oh, H. & Irvine, K. D. Zyxin links fat signaling to the hippo pathway. PLoS Biol. **9,** (2011).

433. Gaspar, P., Holder, M. V., Aerne, B. L., Janody, F. & Tapon, N. Zyxin antagonizes the FERM protein expanded to couple f-actin and yorkie-dependent organ growth. Curr. Biol. **25,** 679–689 (2015).

434. Badouel, C. et al. The FERM-Domain Protein Expanded Regulates Hippo Pathway Activity via Direct Interactions with the Transcriptional Activator Yorkie. Dev. Cell **16,** 411–420 (2009).

435. Oh, H., Reddy, B. V. V. G. & Irvine, K. D. Phosphorylation-independent repression of Yorkie in Fat-Hippo signaling. Dev. Biol. **335,** 188–197 (2009).

436. Fernández, B. G. et al. Actin-Capping Protein and the Hippo pathway regulate F-actin and tissue growth in Drosophila. Development **138,** 2337–2346 (2011).

437. Farge, E. Mechanical Induction of Twist in the Drosophila Foregut/Stomodeal Primordium. Curr.

Biol. **13,** 1365–1377 (2003).

438. Rotherham, M. & Haj, A. J. El. Remote activation of the Wnt/β-catenin signalling pathway using functionalised magnetic particles. PLoS One **10,** 1–18 (2015).

439. Kong, F. et al. Cyclic mechanical reinforcement of integrin-ligand interactions. Mol. Cell **49,** 1060–1068 (2013).

440. Papagrigoriou, E. et al. Activation of a vinculin-binding site in the talin rod involves rearrangement of a five-helix bundle. EMBO J. **23,** 2942–2951 (2004).

441. Del Rio, A. et al. Stretching Single Talin Rod Molecules Activates Vinculin Binding. Science (80-.). **323,** 638–642 (2009).

442. Kumar, A. et al. Talin tension sensor reveals novel features of focal adhesion force transmission and mechanosensitivity. J. Cell Biol. **213,** 371–383 (2016).

443. Klapholz, B. et al. Alternative Mechanisms for Talin to Mediate Integrin Function. Curr. Biol. **25,** 847–857 (2015).

444. Yao, M. et al. Mechanical activation of vinculin binding to talin locks talin in an unfolded conformation. Sci. Rep. **4,** 4610 (2014).

445. Chen, H., Choudhury, D. M. & Craig, S. W. Coincidence of actin filaments and talin is required to activate vinculin. J. Biol. Chem. **281,** 40389–40398 (2006).

446. Bois, P. R. J., O'Hara, B. P., Nietlispach, D., Kirkpatrick, J. & Izard, T. The vinculin binding sites of talin and α-actinin are sufficient to activate vinculin. J. Biol. Chem. **281,** 7228–7236 (2006).

447. Gilmore, A. P. & Burridge, K. Regulation of vinculin binding to talin and actin by phosphatidyl-inositol-4-5-biphosphate. Nature **381,** 531–535 (1996).

448. DeMali, K. A., Barlow, C. A. & Burridge, K. Recruitment of the Arp2/3 complex to vinculin: Coupling membrane protrusion to matrix adhesion. J. Cell Biol. **159,** 881–891 (2002).

449. Schliwa, M. Action of cytochalasin D on cytoskeletal networks. J. Cell Biol. **92,** 79–91 (1982).

450. Carlier, M.-F., Criquet, P., Pantaloni, D. & Korn, E. D. Interaction of Cytochalasin-D with Actin-Filaments in the Presence of Adp and Atp. J. Biol. Chem. **261,** 2041–2050 (1986).

451. Carisey, A. et al. Vinculin regulates the recruitment and release of core focal adhesion proteins in a force-dependent manner. Curr. Biol. **23,** 271–281 (2013).

452. Roca-Cusachs, P. P., Iskratsch, T. T. & Sheetz, M. P. M. P. Finding the weakest link: exploring integrin-mediated mechanical molecular pathways. J. Cell Sci. **125,** 3025–3038 (2012).

453. Xu, W., Baribault, H. & Adamson, E. D. Vinculin knockout results in heart and brain defects during embryonic development. Development **125,** 327–37 (1998).

454. Meng, F. & Sachs, F. Visualizing dynamic cytoplasmic forces with a compliance-matched FRET sensor. J. Cell Sci. **124,** 261–269 (2011).

455. Ye, N. et al. Direct observation of α-actinin tension and recruitment at focal adhesions during contact growth. Exp. Cell Res. **327,** 57–67 (2014).

456. Razinia, Z., Mäkelä, T., Ylänne, J. & Calderwood, D. A. Filamins in Mechanosensing and Signaling. Annu. Rev. Biophys. **41,** 227–246 (2012).

457. Hirata, H., Tatsumi, H. & Sokabe, M. Zyxin emerges as a key player in the mechanotransduction at cell adhesive structures. Commun. Integr. Biol. **1,** 192–5 (2008).

458. Smith, M. A. et al. A Zyxin-mediated mechanism for actin stress fiber maintenance and repair. Dev.

Cell **19,** 365–376 (2010).

459. Tojkander, S., Gateva, G., Husain, A., Krishnan, R. & Lappalainen, P. Generation of contractile actomyosin bundles depends on mechanosensitive actin filament assembly and disassembly. Elife 4:e06126 (2015). doi:10.7554/eLife.06126

460. Zhao, B. et al. Inactivation of YAP oncoprotein by the Hippo pathway is involved in cell contact inhibition and tissue growth control. Genes Dev. **21,** 2747–2761 (2007).

461. Wada, K.-I., Itoga, K., Okano, T., Yonemura, S. & Sasaki, H. Hippo pathway regulation by cell morphology and stress fibers. Development **138,** 3907–3914 (2011).

462. Dupont, S. et al. Role of YAP/TAZ in mechanotransduction. Nature **474,** 179–183 (2011).

463. Das, T. et al. A molecular mechanotransduction pathway regulates collective migration of epithelial cells. Nat. Cell Biol. **17,** (2015).

464. Cattaruzza, M., Lattrich, C. & Hecker, M. Focal Adhesion Protein Zyxin is a Mechanosensitive Modulator of Gene Expression in Vascular Smooth Muscle Cells. Hypertension **43,** 726–730 (2004).

465. Suresh Babu, S. et al. Mechanism of stretch-induced activation of the mechanotransducer zyxin in vascular cells. Sci. Signal. **5,** ra91 (2012).

466. Aragona, M. et al. A mechanical checkpoint controls multicellular growth through YAP/TAZ regulation by actin-processing factors. Cell **154,** 1047–1059 (2013).

467. Barbolina, M. V. et al. Matrix rigidity activates wnt signaling through down-regulation of dickkopf-1 protein. J. Biol. Chem. **288,** 141–151 (2013).

468. Du, J. et al. Extracellular matrix stiffness dictates Wnt expression through integrin pathway. Sci. Rep. **6,** 20395 (2016).

469. Diz-Muñoz, A., Fletcher, D. A. & Weiner, O. D. Use the force: Membrane tension as an organizer of cell shape and motility. Trends Cell Biol. **23,** 47–53 (2013).

470. Clark, A. G., Wartlick, O., Salbreux, G. & Paluch, E. K. Stresses at the cell surface during animal cell morphogenesis. Curr. Biol. **24,** R484–94 (2014).

471. Sens, P. & Plastino, J. Membrane tension and cytoskeleton organization in cell motility. J. Phys. Condens. matter **27,** 1–13 (2015).

472. Gauthier, N. C., Rossier, O. M., Mathur, A., Hone, J. C. & Sheetz, M. P. Plasma Membrane Area Increases with Spread Area by Exocytosis. Mol. Biol. Cell **20,** 3261–3272 (2009).

473. Gauthier, N. C., Fardin, M. A., Roca-Cusachs, P. & Sheetz, M. P. Temporary increase in plasma membrane tension coordinates the activation of exocytosis and contraction during cell spreading. Proc. Natl. Acad. Sci. U. S. A. **108,** 14467–72 (2011).

474. Gervasio, O. L., Phillips, W. D., Cole, L. & Allen, D. G. Caveolae respond to cell stretch and contribute to stretch-induced signaling. J. Cell Sci. **124,** 3581–3590 (2011).

475. Kosmalska, A. J. et al. Physical principles of membrane remodelling during cell mechanoadaptation. Nat. Commun. **6,** 1–8 (2015).

476. Staykova, M., Holmes, D. P., Read, C. & Stone, H. A. Mechanics of surface area regulation in cells examined with confined lipid membranes. Proc. Natl. Acad. Sci. U. S. A. **108,** 9084–9088 (2011).

477. Lieber, A. D., Yehudai-Resheff, S., Barnhart, E. L., Theriot, J. A. & Keren, K. Membrane tension in rapidly moving cells is determined by cytoskeletal forces. Curr. Biol. **23,** 1409–1417 (2013).

478. Martinac, B. The ion channels to cytoskeleton connection as potential mechanism of mechanosensitivity. Biochim. Biophys. Acta - Biomembr. **1838,** 682–691 (2014).

479. Saarikangas, J. et al. MIM-Induced Membrane Bending Promotes Dendritic Spine Initiation. Dev. Cell 644–659 (2015). doi:10.1016/j.devcel.2015.04.014

480. Elliot, H. et al. Myosin II Controls Cellular Branching Morphogenesis and Migration in 3D by Minimizing Plasma Membrane Curvature. Nat. Cell Biol. **17,** 137–147 (2015).

481. Bridges, A. A., Jentzsch, M. S., Oakes, P. W., Occhipinti, P. & Gladfelter, A. S. Micron-scale plasma membrane curvature is recognized by the septin cytoskeleton. J. Cell Biol. jcb.201512029 (2016). doi:10.1083/jcb.201512029

482. Simunovic, M. & Voth, G. a. Membrane tension controls the assembly of curvature-generating proteins. Nat. Commun. **6,** 1–8 (2015).

483. Mierzwa, B. & Gerlich, D. W. Cytokinetic Abscission: Molecular Mechanisms and Temporal Control. Dev. Cell **31,** 525–538 (2014).

484. Rappaport, R. Repeated furrow formation from a single mitotic apparatus in cylindrical sand dollar eggs. J. Exp. Zool. **234,** 167–171 (1985).

485. Cabernard, C., Prehoda, K. E. & Doe, C. Q. A spindle-independent cleavage furrow positioning pathway. Nature **467,** 91–4 (2010).

486. Bieling, P., Telley, I. A. & Surrey, T. A minimal midzone protein module controls formation and length of antiparallel microtubule overlaps. Cell **142,** 420–432 (2010).

487. Hu, C. K., Coughlin, M., Field, C. M. & Mitchison, T. J. KIF4 regulates midzone length during cytokinesis. Curr. Biol. **21,** 815–824 (2011).

488. Guse, A., Mishima, M. & Glotzer, M. Phosphorylation of ZEN-4/MKLP1 by aurora B regulates completion of cytokinesis. Curr. Biol. **15,** 778–786 (2005).

489. Touré, A. et al. Phosphoregulation of MgcRacGAP in mitosis involves Aurora B and Cdk1 protein kinases and the PP2A phosphatase. FEBS Lett. **582,** 1182–1188 (2008).

490. Hutterer, A., Glotzer, M. & Mishima, M. Clustering of Centralspindlin Is Essential for Its Accumulation to the Central Spindle and the Midbody. Curr. Biol. **19,** 2043–2049 (2009).

491. Douglas, M. E., Davies, T., Joseph, N. & Mishima, M. Aurora B and 14-3-3 Coordinately Regulate Clustering of Centralspindlin during Cytokinesis. Curr. Biol. **20,** 927–933 (2010).

492. Basant, A. et al. Aurora B Kinase Promotes Cytokinesis by Inducing Centralspindl in Oligomers thatAssociate with the Plasma Membrane . Dev. Cell **33,** 204–215 (2015).

493. Ban, R., Irino, Y., Fukami, K. & Tanaka, H. Human Mitotic Spindle-associated Protein PRC1 Inhibits MgcRacGAP Activity toward Cdc42 during the Metaphase. J. Biol. Chem. **279,** 16394–16402 (2004).

494. Lee, K.-Y., Esmaeili, B., Zealley, B. & Mishima, M. Direct interaction between centralspindlin and PRC1 reinforces mechanical resilience of the central spindle. Nat. Commun. **6,** 7290 (2015).

495. Lewellyn, L., Dumont, J., Desai, A. & Oegema, K. Analyzing the Effects of Delaying Aster Separation on Furrow Formation during Cytokinesis in the Caenorhabditis elegans Embryo. Mol. Biol. Cell **21,** 50–62 (2010).

496. Zhao, W. M. & Fang, G. Anillin is a substrate of anaphase-promoting complex/cyclosome (APC/C) that controls spatial contractility of myosin during late cytokinesis. J. Biol. Chem. **280,** 33516–33524 (2005).

497. Somers, W. G. & Saint, R. A RhoGEF and Rho family GTPase-activating protein complex links the contractile ring to cortical microtubules at the onset of cytokinesis. Dev. Cell **4,** 29–39 (2003).

498. Wolfe, B. A., Takaki, T., Petronczki, M. & Glotzer, M. Polo-like kinase 1 directs assembly of the HsCyk-4 RhoGAP/Ect2 RhoGEF complex to initiate cleavage furrow formation. PLoS Biol. **7,** (2009).

499. Burkard, M. E. et al. Plk1 self-organization and priming phosphorylation of HsCYK-4 at the spindle midzone regulate the onset of division in human cells. PLoS Biol. **7,** (2009).

500. Kim, H., Guo, F., Brahma, S., Xing, Y. & Burkard, M. E. Centralspindlin assembly and 2 phosphorylations on MgcRacGAP by Polo-like kinase 1 initiate Ect2 binding in early cytokinesis. Cell Cycle **13,** 2952–2961 (2014).

501. Jantsch-Plunger, V. et al. CYK-4: A rho family gtpase activating protein (gap) required for central spindle formation and cytokinesis. J. Cell Biol. **149,** 1391–1404 (2000).

502. Kitamura, T. et al. Role of MgcRacGAP/Cyk4 as a regulator of the small GTPase Rho family in cytokinesis and cell differentiation. Cell Struct. Funct. **26,** 645–51 (2001).

503. Miller, A. L. & Bement, W. M. Regulation of cytokinesis by Rho GTPase flux. Nat. Cell Biol. **11,** 71–7 (2009).

504. Loria, A., Longhini, K. M. & Glotzer, M. The RhoGAP domain of CYK-4 has an essential role in RhoA activation. Curr. Biol. **22,** 213–219 (2012).

505. Canman, J. C. et al. Inhibition of Rac by the GAP Activity of Centralspindlin Is Essential for Cytokinesis. Science (80-.). **322,** 1543–1546 (2008).

506. Murata-Hori, M. et al. Myosin II regulatory light chain as a novel substrate for AIM-1, an aurora/Ipl1p-related kinase from rat. J. Biochem. **128,** 903–7 (2000).

507. Chen, W., Foss, M., Tseng, K. F. & Zhang, D. Redundant mechanisms recruit actin into the contractile ring in silkworm spermatocytes. PLoS Biol. **6,** 1927–1941 (2008).

508. Bement, W. M., Benink, H. A. & Von Dassow, G. A microtubule-dependent zone of active RhoA during cleavage plane specification. J. Cell Biol. **170,** 91–101 (2005).

509. Foe, V. E. & Von Dassow, G. Stable and dynamic microtubules coordinately shape the myosin activation zone during cytokinetic furrow formation. J. Cell Biol. **183,** 457–470 (2008).

510. Von Dassow, G., Verbrugghe, K. J. C., Miller, A. L., Sider, J. R. & Bement, W. M. Action at a distance during cytokinesis. J. Cell Biol. **187,** 831–845 (2009).

511. Dechant, R. & Glotzer, M. Centrosome separation and central spindle assembly act in redundant pathways that regulate microtubule density and trigger cleavage furrow formation. Dev. Cell **4,** 333–344 (2003).

512. Su, K.-C., Bement, W. M., Petronczki, M. & von Dassow, G. An astral simulacrum of the central spindle accounts for normal, spindle-less, and anucleate cytokinesis in echinoderm embryos. Mol. Biol. Cell **25,** 4049–62 (2014).

513. Piekny, A. J. & Maddox, A. S. The myriad roles of Anillin during cytokinesis. Semin. Cell Dev. Biol. **21,** 881–891 (2010).

514. Szafer-Glusman, E., Fuller, M. T. & Giansanti, M. G. Role of Survivin in cytokinesis revealed by a separation-of-function allele. Mol. Biol. Cell **22,** 3779–90 (2011).

515. Lewellyn, L., Carvalho, A., Desai, A., Maddox, A. S. & Oegema, K. The chromosomal passenger complex and centralspindlin independently contribute to contractile ring assembly. J. Cell Biol. **193,** 155–169 (2011).

516. Lekomtsev, S. et al. Centralspindlin links the mitotic spindle to the plasma membrane during cytokinesis. Nature **492,** 276–9 (2012).

517. Barr, F. A. & Gruneberg, U. Cytokinesis: Placing and Making the Final Cut. Cell **131,** 847–860 (2007).

518. Field, S. J. et al. PtdIns(4,5)P2 functions at the cleavage furrow during cytokinesis. Curr. Biol. **15,** 1407–1412 (2005).

519. Zhang, J. et al. Phosphatidylinositol polyphosphate binding to the mammalian septin H5 is modulated by GTP. Curr. Biol. **9,** 1458–1467 (1999).

520. Oegema, K., Savoian, M. S., Mitchison, T. J. & Field, C. M. Functional analysis of a human homologue of the Drosophila actin binding protein anillin suggests a role in cytokinesis. J. Cell Biol. **150,** 539–552 (2000).

521. Chalamalasetty, R. B., Hümmer, S., Nigg, E. A. & Silljé, H. H. W. Influence of human Ect2 depletion and overexpression on cleavage furrow formation and abscission. J. Cell Sci. **119,** 3008–3019 (2006).

522. Fackler, O. T. & Grosse, R. Cell motility through plasma membrane blebbing. J. Cell Biol. **181,** 879–884 (2008).

523. Ou, G., Stuurman, N., D'Ambrosio, M. & Vale, R. D. Polarized Myosin Produces Unequal-Size Daughters During Asymmetric Cell Division. Science (80-.). **330,** 677–680 (2010).

524. Guizetti, J. & Gerlich, D. W. ESCRT-III polymers in membrane neck constriction. Trends Cell Biol. **22,** 133–140 (2012).

525. Gruneberg, U., Neef, R., Honda, R., Nigg, E. A. & Barr, F. A. Relocation of Aurora B from centromeres to the central spindle at the metaphase to anaphase transition requires MKlp2. J. Cell Biol. **166,** 167–172 (2004).

526. Hu, C.-K., Coughlin, M. & Mitchison, T. J. Midbody assembly and its regulation during cytokinesis. Mol. Biol. Cell **23,** 1024–1034 (2012).

527. Gai, M. et al. Citron kinase controls abscission through RhoA and anillin. Mol. Biol. Cell **22,** 3768–78 (2011).

528. Kechad, A., Jananji, S., Ruella, Y. & Hickson, G. R. X. Anillin acts as a bifunctional linker coordinating midbody ring biogenesis during cytokinesis. Curr. Biol. **22,** 197–203 (2012).

529. Amine, N. El, Kechad, A., Jananji, S. & Hickson, G. R. X. Opposing actions of septins and Sticky on Anillin promote the transition from contractile to midbody ring. J. Cell Biol. **203,** 487–504 (2013).

530. Gruneberg, U. et al. KIF14 and citron kinase act together to promote efficient cytokinesis. J. Cell Biol. **172,** 363–372 (2006).

531. Bassi, Z. I., Audusseau, M., Riparbelli, M. G., Callaini, G. & D'Avino, P. P. Citron kinase controls a molecular network required for midbody formation in cytokinesis. Proc. Natl. Acad. Sci. U. S. A. **110,** 9782–7 (2013).

532. Watanabe, S., De Zan, T., Ishizaki, T. & Narumiya, S. Citron kinase mediates transition from constriction to abscission through its coiled-coil domain. J. Cell Sci. **126,** 1773–84 (2013).

533. Makyio, H. et al. Structural basis for Arf6–MKLP1 complex formation on the Flemming body responsible for cytokinesis. EMBO J. **31,** 2590–2603 (2012).

534. Joseph, N., Hutterer, A., Poser, I. & Mishima, M. ARF6 GTPase protects the post-mitotic midbody from 14-3-3-mediated disintegration. EMBO J. **31,** 2604–14 (2012).

535. Charras, G. T., Yarrow, J. C., Horton, M. A., Mahadevan, L. & Mitchison, T. J. Non-equilibration of hydrostatic pressure in blebbing cells. Nature **435,** 365–9 (2005).

536. Liu, J., Fairn, G. D., Ceccarelli, D. F., Sicheri, F. & Wilde, A. Cleavage furrow organization requires PIP 2-mediated recruitment of anillin. Curr. Biol. **22,** 64–69 (2012).

537. Sagona, A. P. et al. PtdIns(3)P controls cytokinesis through KIF13A-mediated recruitment of FYVE-CENT to the midbody. Nat. Cell Biol. **12,** 362–371 (2010).

538. Guizetti, J. et al. Cortical Constriction During Abscission Involves Helices of ESCRT-III–Dependent Filaments. Science (80-.). **331,** 1616–1620 (2011).

539. Saurin, A. T. et al. The regulated assembly of a PKCepsilon complex controls the completion of cytokinesis. Nat. Cell Biol. **10,** 891–901 (2008).

540. Dambournet, D. et al. Rab35 GTPase and OCRL phosphatase remodel lipids and F-actin for successful cytokinesis. Nat. Cell Biol. **13,** 981–988 (2011).

541. Schiel, J. A. et al. FIP3-endosome-dependent formation of the secondary ingression mediates ESCRT-III recruitment during cytokinesis. Nat. Cell Biol. **14,** 1068–78 (2012).

542. Yang, D. et al. Structural basis for midbody targeting of spastin by the ESCRT- III protein CHMP1B. Nat. Struct. Mol. Biol. **15,** 1278–1286 (2008).

543. Connell, J. W., Lindon, C., Luzio, J. P. & Reid, E. Spastin couples microtubule severing to membrane traffic in completion of cytokinesis and secretion. Traffic **10,** 42–56 (2009).

544. Elia, N., Sougrat, R., Spurlin, T. A., Hurley, J. H. & Lippincott-Schwartz, J. Dynamics of endosomal sorting complex required for transport (ESCRT) machinery during cytokinesis and its role in abscission. Proc. Natl. Acad. Sci. U. S. A. **108,** 4846–51 (2011).

545. Bastos, R. N. & Barr, F. A. Plk1 negatively regulates Cep55 recruitment to the midbody to ensure orderly abscission. J. Cell Biol. **191,** 751–760 (2010).

546. Carlton, J. G., Caballe, A., Agromayor, M., Kloc, M. & Martin-Serrano, J. ESCRT-III Governs the Aurora B–Mediated Abscission Checkpoint Through CHMP4C Jeremy. Science (80-.). **336,** 220–225 (2012).

547. Mathieu, J. et al. Aurora B and Cyclin B have opposite effects on the timing of cytokinesis abscission in drosophila germ cells and in vertebrate somatic cells. Dev. Cell **26,** 250–265 (2013).

548. Matias, N. R., Mathieu, J. & Huynh, J. R. Abscission Is Regulated by the ESCRT-III Protein Shrub in Drosophila Germline Stem Cells. PLoS Genet. **11,** 1–20 (2015).

549. Lafaurie-Janvore, J. et al. ESCRT-III Assembly and Cytokinetic Abscission Are Induced by Tension Release in the Intercellular Bridge. Science (80-.). **339,** 1625–1629 (2013).

550. Jinguji, Y. & Ishikawa, H. Electron microscopic observations on the maintenance of the tight junction during cell division in the epithelium of the mouse small intestine. Cell Struct. Funct. **17,** 27–37 (1992).

551. Reinsch, S. & Karsenti, E. Orientation of spindle axis and distribution of plasma membrane proteins during cell division in polarized MDCK II cells. J. Cell Biol. **126,** 1509–1526 (1994).

552. Kojima, T. et al. Occludin and claudin-1 concentrate in the midbody of immortalized mouse hepatocytes during cell division. J. Histochem. Cytochem. **49,** 333–40 (2001).

553. Guillot, C. & Lencuit, T. Mechanics of Epithelial Tissue Homeostasis and Morphogenesis. Science (80-.). **340,** 1185–1189 (2013).

554. Kosodo, Y. et al. Asymmetric distribution of the apical plasma membrane during neurogenic divisions of mammalian neuroepithelial cells. EMBO J. **23,** 2314–24 (2004).

555. Dubreuil, V., Marzesco, A. M., Corbeil, D., Huttner, W. B. & Wilsch-Brauninger, M. Midbody and

primary cilium of neural progenitors release extracellular membrane particles enriched in the stem cell marker prominin-1. J. Cell Biol. **176,** 483–495 (2007).

556. Kosodo, Y. et al. Cytokinesis of neuroepithelial cells can divide their basal process before anaphase. EMBO J. **27,** 3151–63 (2008).

557. Maddox, A. S., Lewellyn, L., Desai, A. & Oegema, K. Anillin and the Septins Promote Asymmetric Ingression of the Cytokinetic Furrow. Dev. Cell **12,** 827–835 (2007).

558. Herszterg, S., Pinheiro, D. & Bellaïche, Y. A multicellular view of cytokinesis in epithelial tissue. Trends Cell Biol. **24,** 285–293 (2014).

559. Gibson, M. C., Patel, A. B., Nagpal, R. & Perrimon, N. The emergence of geometric order in proliferating metazoan epithelia. Nature **442,** 1038–41 (2006).

560. Lau, K. et al. Anisotropic stress orients remodelling of mammalian limb bud ectoderm. Nat. Cell Biol. **17,** 569–579 (2015).

561. Grusche, F. a et al. Sds22, a PP1 phosphatase regulatory subunit, regulates epithelial cell polarity and shape. BMC Dev. Biol. **9,** (2009).

562. Fehon, R. G., McClatchey, A. I. & Bretscher, A. Organizing the cell cortex: the role of ERM proteins. Nat. Rev. Mol. Cell Biol. **11,** 276–287 (2010).

563. Verma, S. et al. A WAVE2-Arp2/3 actin nucleator apparatus supports junctional tension at the epithelial zonula adherens. Mol. Biol. Cell **23,** 4601–10 (2012).

564. Priya, R., Yap, A. S. & Gomez, G. A. E-cadherin supports steady-state Rho signaling at the epithelial zonula adherens. Differentiation **86,** 133–140 (2013).

565. Callan-Jones, A. C. & Voituriez, R. Active gel model of amoeboid cell motility. New J. Phys. **111,** 108102 (2013).

566. Recho, P., Putelat, T. & Truskinovsky, L. Contraction-driven cell motility. Phys. Rev. Lett. **111,** 2–6 (2013).

567. Hancock, J. F., Cadwallader, K., Paterson, H. & Marshall, C. J. A CAAX or a CAAL motif and a second signal are sufficient for plasma membrane targeting of ras proteins. EMBO J. **10,** 4033–4039 (1991).

568. Antunes, M., Pereira, T., Cordeiro, J. V., Almeida, L. & Jacinto, A. Coordinated waves of actomyosin flow and apical cell constriction immediately after wounding. J. Cell Biol. **202,** 365–379 (2013).

569. Pickering, K., Alves-Silva, J., Goberdhan, D. & Millard, T. H. Par3/Bazooka and phosphoinositides regulate actin protrusion formation during Drosophila dorsal closure and wound healing. Development **140,** 800–9 (2013).

570. Hunter, M. V., Lee, D. M., Harris, T. J. C. & Fernandez-Gonzalez, R. Polarized E-cadherin endocytosis directs actomyosin remodeling during embryonic wound repair. J. Cell Biol. **210,** 801–816 (2015).

571. Finer, J. T., Simmons, R. M. & Spudich, J. A. Single myosin molecule mechanics: piconewton forces and nanometre steps. Nature **368,** 113–9 (1994).

572. Guglielmi, G., Barry, J. D., Huber, W. & De Renzis, S. An Optogenetic Method to Modulate Cell Contractility during Tissue Morphogenesis. Dev. Cell **35,** 1–15 (2015).

573. Sugimura, K. & Ishihara, S. The mechanical anisotropy in a tissue promotes ordering in hexagonal cell packing. Development **140,** 4091–101 (2013).

574. Paluch, E., Sykes, C., Prost, J. & Bornens, M. Dynamic modes of the cortical actomyosin gel during cell locomotion and division. Trends Cell Biol. **16,** 5–10 (2006).

575. Charras, G., Hu, C.-K., Coughlin, M. & Mitchison, T. J. Reassembly of contractile actin cortex in cell blebs. J. Cell Biol. **175,** 477–90 (2006).

576. Burke, T. A. et al. Homeostatic actin cytoskeleton networks are regulated by assembly factor competition for monomers. Curr. Biol. **24,** 579–585 (2014).

577. Suarez, C. et al. Profilin regulates F-Actin network homeostasis by favoring formin over Arp2/3 complex. Dev. Cell **32,** 43–53 (2015).

578. Rotty, J. D. et al. Profilin-1 Serves as a gatekeeper for actin assembly by Arp2/3-Dependent and -Independent pathways. Dev. Cell **32,** 54–67 (2015).

579. Yarmola, E. G., Parikh, S. & Bubb, M. R. Formation and Implications of a Ternary Complex of Profilin, Thymosin β4, and Actin. J. Biol. Chem. **276,** 45555–45563 (2001).

580. Lee, C. W. et al. Dynamic localization of G-actin during membrane protrusion in neuronal motility. Curr. Biol. **23,** 1046–1056 (2013).

581. Ahuja, R. et al. Cordon-Bleu Is an Actin Nucleation Factor and Controls Neuronal Morphology. Cell **131,** 337–350 (2007).

582. Ravanelli, A. M. & Klingensmith, J. The actin nucleator Cordon-bleu is required for development of motile cilia in zebrafish. Dev. Biol. **350,** 101–111 (2011).

583. Zuchero, J. B., Coutts, A. S., Quinlan, M. E., Thangue, N. B. La & Mullins, R. D. p53-cofactor JMY is a multifunctional actin nucleation factor. Nat. Cell Biol. **11,** 451–459 (2009).

584. Rottner, K., Hänisch, J. & Campellone, K. G. WASH, WHAMM and JMY: Regulation of Arp2/3 complex and beyond. Trends Cell Biol. **20,** 650–661 (2010).

585. Webb, R. L., Zhou, M.-N. & McCartney, B. M. A novel role for an APC2-Diaphanous complex in regulating actin organization in Drosophila. Development **136,** 1283–1293 (2009).

586. Okada, K. et al. Adenomatous polyposis coli protein nucleates actin assembly and synergizes with the formin mDia1. J. Cell Biol. **189,** 1087–1096 (2010).

587. Breitsprecher, D. et al. Rocket Launcher Mechanism of Collaborative Actin Assembly Defined by Single-Molecule Imaging. Science (80-.). **336,** 1164–1168 (2012).

588. Jaiswal, R. et al. Drosophila homologues of adenomatous polyposis coli (APC) and the formin diaphanous collaborate by a conserved mechanism to stimulate actin filament assembly. J. Biol. Chem. **288,** 13897–13905 (2013).

589. Chereau, D. et al. Leiomodin Is an Actin Filament Nucleator in Muscle Cells. Science (80-.). **1,** 239–244 (2008).

590. Chen, X., Ni, F., Kondrashkina, E., Ma, J. & Wang, Q. Mechanisms of leiomodin 2-mediated regulation of actin filament in muscle cells. Proc. Natl. Acad. Sci. **112,** 12687–12692 (2015).

591. Cooper, J. A. & Sept, D. New Insights into Mechanism and Regulation of Actin Capping Protein. Int. Rev. Cell Mol. Biol. **267,** 183–206 (2008).

592. Edwards, M. et al. Capping protein regulators fine-tune actin assembly dynamics. Nat. Rev. Mol. Cell Biol. **15,** 677–89 (2014).

593. Ono, S. Mechanism of Depolymerization and Severing of Actin Filaments and Its Significance in Cytoskeletal Dynamics. Int. Rev. Cytol. **258,** 1–82 (2007).

594. Lo, S. H., Yu, Q. C., Degenstein, L., Chen, L. B. & Fuchs, E. Progressive kidney degeneration in

mice lacking tensin. J. Cell Biol. **136,** 1349–1361 (1997).

595. Lee, S. B., Cho, K. S., Kim, E. & Chung, J. blistery encodes Drosophila tensin protein and interacts with integrin and the JNK signaling pathway during wing development. Development **130,** 4001–4010 (2003).

596. Torgler, C. N. et al. Tensin Stabilizes Integrin Adhesive Contacts in Drosophila. Dev. Cell **6,** 357–369 (2004).

597. Tian, M. & Martin, S. G. Reduced phosphotyrosine binding by the v-Src SH2 domain is compatible with wild-type transformation. Oncogene **12,** 727–34 (1996).

598. Chen, H. & Lo, S. H. Regulation of tensin-promoted cell migration by its focal adhesion binding and Src homology domain 2. Biochem. J. **370,** 1039–1045 (2003).

599. Nag, S., Larsson, M., Robinson, R. C. & Burtnick, L. D. Gelsolin: The tail of a molecular gymnast. Cytoskeleton **70,** 360–384 (2013).

600. Logue, J. S. et al. Erk regulation of actin capping and bundling by Eps8 promotes cortex tension and leader bleb-based migration. Elife **4,** 1–31 (2015).

601. Otey, C. A. & Carpen, O. Alpha-actinin revisited: a fresh look at an old player. Cell Motil. Cytoskeleton **58,** 104–111 (2004).

602. Murphy, A. C. H. & Young, P. W. The actinin family of actin cross-linking proteins - a genetic perspective. Cell Biosci. **5,** 1–9 (2015).

603. Tseng, Y. et al. How actin crosslinking and bundling proteins cooperate to generate an enhanced cell mechanical response. Biochem. Biophys. Res. Commun. **334,** 183–192 (2005).

604. Esue, O., Tseng, Y. & Wirtz, D. α-Actinin and Filamin Cooperatively Enhance the Stiffness of Actin Filament Networks. PLoS One **4,** 1–6 (2009).

605. Bretscher, A. & Weber, K. Fimbrin, a new microfilament-associated protein present in microvilli and other cell surface structures. J. Cell Biol. **86,** 335–340 (1980).

606. Bretscher, A. Fimbrin is a cytoskeletal protein that crosslinks F-actin in vitro. PNAS **78,** 6849–6853 (1981).

607. Arruda, M. V. de, Watson, S., Lin, C. S., Leavitt, J. & Matsudaira, P. Fimbrin is a homologue of the cytoplasmic phosphoprotein plastin and has domains homologous with calmodulin and actin gelation proteins. J. Cell Biol. **111,** 1069–1079 (1990).

608. Stossel, T. P. et al. Filamins as integrators of cell mechanics and signalling. Nat. Rev. Mol. Cell Biol. **2,** 138–145 (2001).

609. Luo, T., Mohan, K., Iglesias, P. A. & Robinson, D. N. Molecular mechanisms of cellular mechanosensing. Nat. Mater. **12,** 1064–71 (2013).

610. Jansen, S. et al. Mechanism of actin filament bundling by fascin. J. Biol. Chem. **286,** 30087–30096 (2011).

611. Yamashiro, S., Yamakita, Y., Ono, S. & Matsumura, F. Fascin, an actin-bundling protein, induces membrane protrusions and increases cell motility of epithelial cells. Mol. Biol. Cell **9,** 993–1006 (1998).

612. Tseng, Y., Fedorov, E., McCaffery, J. M., Almo, S. C. & Wirtz, D. Micromechanics and ultrastructure of actin filament networks crosslinked by human fascin: a comparison with alpha-actinin. J. Mol. Biol. **310,** 351–366 (2001).

613. Seema, K. & George, S. P. Regulation of cell structure and function by actin-binding proteins:

villin's perspective. FEBS Lett. **582,** 2128–2139 (2009).

614. Breitsprecher, D. et al. Molecular mechanism of Ena/VASP-mediated actin-filament elongation. EMBO J. **30,** 456–467 (2011).

615. Bearer, E. L., Prakash, J. M., Manchester, R. D. & Allen, P. G. VASP protects actin filaments from gelsolin: An in vitro study with implications for platelet actin reorganizations. Cell Motil. Cytoskeleton **47,** 351–364 (2000).

616. Winkelman, J. D., Bilancia, C. G., Peifer, M. & Kovar, D. R. Ena/VASP Enabled is a highly processive actin polymerase tailored to self-assemble parallel-bundled F-actin networks with Fascin. Proc Natl Acad Sci U S A **111,** 4121–4126 (2014).

617. Amano, M. et al. Phosphorylation and Activation of Myosin by Rho-associated. J. Biol. Chem. **271,** 20246–20249 (1996).

618. Kimura, K. et al. Regulation of myosin phosphatase by Rho and Rho-associated kinase (Rho-kinase). Science (80-.). **273,** 245–248 (1996).

619. Amano, M. et al. The COOH Terminus of Rho-kinase Negatively Regulates Rho-kinase Activity. J. Biol. Chem. **274,** 32418–32424 (1999).

620. Feng, J. et al. Rho-associated kinase of chicken gizzard smooth muscle. J. Biol. Chem. **274,** 3744–3752 (1999).

621. Riento, K. & Ridley, A. J. Rocks: multifunctional kinases in cell behaviour. Nat. Rev. Mol. Cell Biol. **4,** 446–56 (2003).

622. Truebestein, L., Elsner, D. J., Fuchs, E. & Leonard, T. A. A molecular ruler regulates cytoskeletal remodelling by the Rho kinases. Nat. Commun. **6,** 10029 (2015).

623. Madaule, P. et al. Role of citron kinase as a target of the small GTPase Rho in cytokinesis. Nature **394,** 491–494 (1998).

624. Yamashiro, S. et al. Citron Kinase, a Rho-dependent Kinase, Induces Di-phosphorylation of Regulatory Light Chain of Myosin II. Mol. Biol. Cell **14,** 1745–1756 (2003).

625. Mckenzie, C. et al. Cross-regulation between Aurora B and Citron kinase controls midbody architecture in cytokinesis. Open Biol. **6,** 160019 (2016).

626. Unbekandt, M. & Olson, M. F. The actin-myosin regulatory MRCK kinases: Regulation, biological functions and associations with human cancer. J. Mol. Med. **92,** 217–225 (2014).

627. Litchfield, D. W. Protein kinase CK2: structure, regulation and role in cellular decisions of life and death. Biochem. J. **369,** 1–15 (2003).

628. Fricke, R. et al. Drosophila Cip4/Toca-1 integrates membrane trafficking and actin dynamics through WASP and SCAR/WAVE. Curr. Biol. **19,** 1429–37 (2009).

629. Rotty, J. D., Wu, C. & Bear, J. E. New insights into the regulation and cellular functions of the ARP2/3 complex. Nat. Rev. Mol. cell Biol. **14,** 7–12 (2013).

630. Steffen, A. et al. Sra-1 and Nap1 link Rac to actin assembly driving lamellipodia formation. EMBO J. **23,** 749–759 (2004).

631. Matsubayashi, Y., Coulson-Gilmer, C. & Millard, T. H. Endocytosis-dependent coordination of multiple actin regulators is required for wound healing. J. Cell Biol. **210,** (2015).

632. Lee, N. K. et al. Neogenin recruitment of the WAVE regulatory complex maintains adherens junction stability and tension. Nat. Commun. **7,** 11082 (2016).

633. Kast, D. J., Zajac, A. L., Holzbaur, E. L. F., Ostap, E. M. & Dominguez, R. WHAMM Directs the

Arp2/3 Complex to the ER for Autophagosome Biogenesis through an Actin Comet Tail Mechanism. Curr. Biol. **25,** 1791–1797 (2015).

634. Helwani, F. M. et al. Cortactin is necessary for E-cadherin-mediated contact formation and actin reorganization. J. Cell Biol. **164,** 899–910 (2004).

635. Sroka, R. et al. Cortactin is a scaffolding platform for the E-Cadherin adhesion complex controlled by Protein Kinase D1 phosphorylation. J. Cell Sci. **13,** (2016).

636. Kowalski, J. R. et al. Cortactin regulates cell migration through activation of N-WASP. J. Cell Sci. **118,** 79–87 (2005).

637. Schöenichen, A. & Geyer, M. Fifteen formins for an actin filament: A molecular view on the regulation of human formins. Biochim. Biophys. Acta - Mol. Cell Res. **1803,** 152–163 (2010).

638. Takeya, R., Taniguchi, K., Narumiya, S. & Sumimoto, H. The mammalian formin FHOD1 is activated through phosphorylation by ROCK and mediates thrombin-induced stress fibre formation in endothelial cells. EMBO J. **27,** 618–628 (2008).

639. Lammel, U. et al. The Drosophila FHOD1-like formin Knittrig acts through Rok to promote stress fiber formation and directed macrophage migration during the cellular immune response. Development **141,** 1366–80 (2014).

640. Leader, B. et al. Formin-2, polyploidy, hypofertility and positioning of the meiotic spindle in mouse oocytes. Nat. Cell Biol. **4,** 921–928 (2002).

641. Dettenhofer, M., Zhou, F. & Leder, P. Formin 1-isoform IV deficient cells exhibit defects in cell spreading and focal adhesion formation. PLoS One **3,** e2497 (2008).

642. Sotillos, S., Díaz-Meco, M. T., Caminero, E., Moscat, J. & Campuzano, S. DaPKC-dependent phosphorylation of Crumbs is required for epithelial cell polarity in Drosophila. J. Cell Biol. **166,** 549–557 (2004).

643. Huang, J., Zhou, W., Dong, W., Watson, A. M. & Hong, Y. Directed, efficient, and versatile modifications of the Drosophila genome by genomic engineering. Proc. Natl. Acad. Sci. U. S. A. **106,** 8284–8289 (2009).

644. Laprise, P. & Tepass, U. Novel insights into epithelial polarity proteins in Drosophila. Trends Cell Biol. **21,** 401–408 (2011).

645. McKinley, R. F. A. & Harris, T. J. C. Displacement of basolateral Bazooka/PAR-3 by regulated transport and dispersion during epithelial polarization in Drosophila. Mol. Biol. Cell **23,** 4465–71 (2012).

646. Kim, S. et al. Kinase-activity-independent functions of atypical protein kinase C in Drosophila. J. Cell Sci. **122,** 3759–71 (2009).

647. Walther, R. F. & Pichaud, F. Crumbs/DaPKC-dependent apical exclusion of bazooka promotes photoreceptor polarity remodeling. Curr. Biol. **20,** 1065–1074 (2010).

648. Morais-de-Sá, E., Mirouse, V. & St Johnston, D. aPKC Phosphorylation of Bazooka Defines the Apical/Lateral Border in Drosophila Epithelial Cells. Cell **141,** 509–523 (2010).

649. Krahn, M. P., Bückers, J., Kastrup, L. & Wodarz, A. Formation of a Bazooka-Stardust complex is essential for plasma membrane polarity in epithelia. J. Cell Biol. **190,** 751–760 (2010).